

Seismic Response of Transmission Line Guyed Towers without and with the Interaction of  
Tower Conductor Coupling

Rodrigo Freire De Macêdo

A Thesis  
in  
The Department  
of  
Building, Civil and Environmental Engineering

Presented in the Partial Fulfillment of the Requirements for the Degree of Master of Applied  
Science (Civil Engineering) at Concordia University  
Montreal, Quebec, Canada

September 2016

© Rodrigo Freire De Macedo, 2016

CONCORDIA UNIVERSITY  
School of Graduate Studies

This is to certify that the thesis prepared

By: Rodrigo Freire De Macedo

Entitled: Seismic Response of Transmission Line Guyed Towers With and Without the Interaction of Tower Conductor Coupling

and submitted in partial fulfillment of the requirements for the degree of

Master of Applied Science (Civil Engineering)

complies with the regulations of the University and meets the accepted standards with respect to originality and quality.

Signed by the final examining committee:

Dr. Ashutosh Bagchi Chair

Dr. Ramin Sedaghati Examiner

Dr. Ferawati Gani Examiner

Dr. Lucia Tirca Supervisor

Approved by \_\_\_\_\_  
Chair of Department or Graduate Program Director

\_\_\_\_\_  
Dean of Faculty

Date August 24, 2016

## ABSTRACT

### Seismic Response of Transmission Line Guyed towers without and with the Interaction of Tower Conductor Coupling

Rodrigo Freire De Macêdo

Steel lattice transmission line towers (TL) are widely used as supporting structures for overhead powerlines. According to their supporting configuration, these free-standing tower structures are classified as: Self-supporting towers and guyed towers. In general, they are designed for conductors' weight and environmental loads such as ice accretion and wind gustiness. Other exceptional loads, such as cable rupture and ice-shedding effects, are also considered. Due to an overall perception that these structures have a relatively low vulnerability to earthquake loads, the earthquakes effects are usually not considered in TL tower design. The current standards, for instance, do not require a design check for earthquake loads, although a significant percentage of transmission line infrastructure is located on Western and Eastern Canada where the seismic risk is considered high and moderate-to-high.

The main objectives of this research are: i) to assess the sensitivity of typical TL towers to earthquake loads, ii) to propose a simplified static method able to approximate the seismic response of TL guyed towers and iii) to study the dynamic interaction between the overhead powerlines and their supporting guyed towers.

In this study, two guyed towers (37.7 m and 53.1 m height) and two Self-supporting towers (36.7 m and 57.1 m height) designed according to current standard provisions were selected for investigation. Detailed three-dimensional finite element models developed in ANSYS-APDL software were subjected to nonlinear time-history analyses. To study the sensitivity of these TL towers to earthquake loads, two sets of ten seismic ground motions were selected as representative for Western Canada. The first set corresponds to site Class "C" and the second to site Class "D". It is important to note that the frequency content of these records is close to the natural frequency of the studied towers. Each tower was subjected to the aforementioned sets of seismic ground motions and the responses in term of axial forces triggered in tower members were compared with those resulted from standard load cases used in design. It was found that guyed towers are the most sensitive to seismic ground motions.

To reduce the computation time, an equivalent static method is proposed herein in order to approximate the seismic response of the free-standing guyed towers.

Finally, the dynamic interaction between the overhead powerlines and their supporting guyed towers is evaluated. This is done by carrying out detailed nonlinear transient simulations of the coupled tower-conductor system for a set of earthquake ground motion records of different frequency contents and by comparing the results of these simulations with the ones carried out for the free-standing towers.

## ACKNOWLEDGEMENTS

I would first like to thank my thesis advisor Dr. Lucia Tirca for her valuable suggestions, long discussions and advice. The door to Prof. Lucia Tirca office was always open whenever I ran into a trouble spot or had a question about my research or writing. She consistently allowed this thesis to be my own work, but steered me in the right the direction whenever she thought I needed it.

The author appreciates the contribution of the colleagues and engineers of SNC-Lavalin Inc. in this work by providing technical data, advise and tools used in this study.

Finally, I must express my very profound gratitude to my family for providing me with unfailing support and continuous encouragement throughout my years of study and through the process of researching and writing this thesis. This accomplishment would not have been possible without them. Thank you.

## TABLE OF CONTENTS

<b>LIST OF FIGURES</b>	<b>ix</b>
<b>LIST OF TABLES</b>	<b>xxii</b>
<b>LIST OF SYMSBOLS</b>	<b>xxiv</b>
<b>ACRONYMS</b>	<b>xxvii</b>
<b>CHAPTER I: INTRODUCTION</b>	<b>1</b>
1.1.    Introduction	1
1.2.    Motivation for Research	3
1.3.    Objectives	3
1.4.    Thesis Organization	4
<b>CHAPTER II: LITERATURE REVIEW</b>	<b>6</b>
2.1    Introduction	6
2.2    Overview of High-Voltage Lattice Transmission Line Towers	6
2.3    Design of TL Lattice Towers	10
2.3.1    Load Cases and Load Combinations	13
2.3.2    Load Strength Requirements	15
2.3.3    Design Strength Checks	15
2.3.4    Structural Analysis	16
2.3.5    Full-Scale Prototype Tests	18
2.4    Experience from past Earthquakes	19
2.5    Current practices in the Seismic Analysis of Transmission Lines	20
2.6    Learning from Previous Studies	21
2.7    Seismic Response of TL Structures	26
2.8    Earthquake Ground Motion	27
2.8.1    Seismic Hazard in Canada	29
2.9    Static and Dynamic Properties of Guy Cables	30
2.10    Natural Frequencies of Vibration of Lattice TL Towers	32
2.11    Research Background and Literature Review	34

## TABLE OF CONTENTS (cont'd)

<b>CHAPTER III: METHODOLOGY</b>	<b>36</b>
3.1 General	36
3.2 Towers used in the Study	39
3.3 Numerical Modelling	45
3.4 Transient Dynamic Analysis	47
3.5 Selection and scaling of Earthquake Records	48
<b>CHAPTER IV: STATIC AND DYNAMIC BEHAVIOR OF GUYED TOWERS AND ITS CABLES</b>	<b>56</b>
4.1. Introduction	56
4.2. Validation of Numerical Model against Experimental Test Results based on Pushover Analyses	56
4.3. Mode Shapes and Frequencies of Vibration	62
4.4. Pushover Analysis and Load Distribution Pattern	67
4.5. Static and Dynamic Properties of Guy Tower Cables	72
4.5.1. Static Properties	72
4.5.2. Dynamic Properties	74
4.5.3. Impulse Forces from Guy Cable Dynamics	75
4.5.3.1. <i>Nonlinear Dynamic Analysis</i>	76
4.5.3.2. <i>Analytical Formulation</i>	78
4.6. Horizontal Base Reaction from Harmonic Excitation	82
4.6.1. Steady-State Response	82
4.6.2. Total Response	88
<b>CHAPTER V: SENSITIVITY OF TL FREE-STANDING AND GUYED TOWERS TO EARTHQUAKE LOADS</b>	<b>95</b>
5.1. Introduction	95
5.2. Comparison between the Tower Response Resulted from Modal Response Spectrum Method vs. Nonlinear Time-History Method	95
5.3. Sensitivity of TL Towers to Earthquake Ground motion	97

## TABLE OF CONTENTS (cont'd)

5.4.	Seismic Base Reaction	103
5.4.1.	Assessment of Horizontal Base Shear under Earthquake Excitations	104
5.4.2.	Vertical Earthquake Excitation	107
5.5.	Approximate Static Method and Base Shear Check	108
<b>CHAPTER VI: SEISMIC RESPONSE OF THE COUPLED GUYED TOWER-CONDUCTOR SYSTEM</b>		<b>114</b>
6.1.	Introduction	114
6.2.	Description of the Coupled Tower-Conductor System	114
6.3.	Analysis of the Seismic Response of Free-Standing Towers	117
6.4.	Free-Vibration Characteristics of Overhead Cables	121
6.5.	Seismic Response of Overhead Cables	123
6.6.	Seismic Response of the Coupled Guyed tower-Conductor System	131
6.6.1.	Seismic Responses of Delta Guyed Tower under Ground Motions Applied in the Longitudinal and Transversal Directions	131
6.6.2.	Seismic Responses of Delta Guyed Tower under Ground Motions Applied in the Vertical Direction	133
<b>CHAPTER VII: CONCLUSIONS AND FUTURE WORK</b>		<b>140</b>
7.1	Conclusions	140
7.2	Recommendations for Future Work	143
<b>REFERENCES</b>		<b>145</b>
<b>APPENDIX I.</b>		<b>150</b>
<b>APPENDIX II.</b>		<b>170</b>
<b>APPENDIX III.</b>		<b>185</b>
<b>APPENDIX IV.</b>		<b>198</b>

## LIST OF FIGURES

	<b>Page</b>
Figure 2.1. Examples of TL towers. (a) 85 meters tall vertical self-supported double-circuit tower used for river-crossing span; (b) 30 meters tall vertical self-supported double-circuit tower; (c) flat self-supported single-circuit tower; (d) vertical self-supported double-circuit tower; (e) single-circuit guyed mast tower; (f) single-circuit lattice guyed delta tower; (g) single-circuit flat internally guyed portal tower; (h) single-circuit cross-rope suspension tower.	9
Figure 2.2. Example of a self-supported TL tower, its members and segments.	11
Figure 2.3. Standard orthogonal directions definition. Tower design.	12
Figure 2.4. Transmission line design methodology (CAN/CSA-C22.3 NO. 60826-10).	13
Figure 2.5. Locations of significant Earthquakes recorded between 1627 and 2012 (NRC).	29
Figure 2.6. Profile of a suspended guy cable.	30
Figure 3.1. Flowchart illustrating the proposed methodology.	37
Figure 3.2. Delta Guyed tower. General layout. (all units in millimetres)	41
Figure 3.3. Mast Guyed tower. General layout. (all unit in millimetres)	42
Figure 3.4. Delta Self-Supported Strain Tower. General layout. (all unit in millimetres)	43
Figure 3.5. Self-supported Dead End Tower. General layout. (all unit in millimetres)	44
Figure 3.6. Oblique view of Finite Element Models developed in ANSYS-APDL environment. (a) Delta Guyed tower; (b) Delta Self-supporting tower; (c) Mast Guyed tower; (d) Mast Self-supporting tower.	46
Figure 3.7 Design response spectrum for Bamfield, B.C. for 5% damping, site Class C (NBCC 2010) and the response spectra of selected scaled records.	55
Figure 3.8 Design response spectrum for Bamfield B.C. for 5% damping, site Class D (NBCC 2010) and the response spectra of selected scaled records.	55
Figure 4.1. Delta guyed tower layout and location of strain-gauges on members.	58
Figure 4.2. Deflection of the vertical axis of symmetry in the transversal direction under test load case number #1 (left) and longitudinal direction under test load case number #2 (right).	60
Figure 4.3. Member capacity usage percentage associated to test load case number #3.	62

## LIST OF FIGURES (cont'd)

	<b>Page</b>
Figure 4.4. Mode shapes. a) cable vibration. b) cable vibration. c) 1 <sup>st</sup> flexural mode of vibration in the transversal direction. d) tower rotation about vertical axis. e) 1 <sup>st</sup> flexural mode of vibration in the longitudinal direction. f) 2 <sup>nd</sup> flexural mode of vibration in the transversal direction.	65
Figure 4.5. Collection of unscaled ground motion records elastic response spectra.	66
Figure 4.6. Force distribution patterns over the height of Delta guyed tower. Transversal direction.	69
Figure 4.7. Capacity curves of Delta guyed tower. Transversal and longitudinal directions.	70
Figure 4.8. Force distribution patterns over the height of Mast guyed tower. Longitudinal direction.	70
Figure 4.9. Capacity curves of Mast guyed tower. Transversal and longitudinal directions.	71
Figure 4.10. Guy cable upper support displacement (left) and horizontal stiffness of guy cables (right).	73
Figure 4.11. Frequency-response relationship for guy cable. Harmonic excitation in the longitudinal direction.	75
Figure 4.12. Dynamic response (reactive horizontal force) of guy cable to step force with finite rise time. Static solution is show by dashed line. $t/T_{1st} = 0.50$ (upper left). $t/T_{1st} = 0.27$ (upper right). $t/T_{1st} = 0.21$ (lower left). $t/T_{1st} = 0.10$ (lower right).	78
Figure 4.13. Response spectra of base shear to forced harmonic excitation. Real component (top) and imaginary component (bottom).	84
Figure 4.14. Base shear response to horizontal harmonic forces. Base shear reacting in-phase with harmonic forces (left). Base shear out of phase with horizontal forces (center). Guy cable out of phase with mast motion (right).	85
Figure 4.15. MDOF and SDOF systems response spectra of base shear to forced harmonic excitation.	87
Figure 4.16. Steady-state and total response to harmonic excitation.	88
Figure 4.17. Fourier spectrum of the total and steady-state responses for a forcing frequency of 0.5 Hz (top) and 2.5 Hz (bottom).	90
Figure 4.18. Steady-state and total peak base shear response of SDOF and MDOF systems.	91

## LIST OF FIGURES (cont'd)

	<b>Page</b>
Figure 4.19. Variation of peak base shear response with the number of sustained harmonic cycles.	92
Figure 5.1. Dispersion diagram comparing the results of transient dynamic analysis with the results of response spectrum analysis for the axial force in each member of the Delta guyed tower subjected to NGA 15 record in the transversal direction.	97
Figure 5.2. Percentage of members with seismic axial forces higher than in design load cases. Earthquake ground motion acting on the transversal direction of TL tower.	100
Figure 5.3. Dispersion diagram for the base shear response from SDOF and MDOF systems. Delta guyed tower.	105
Figure 5.4. Mast guyed tower. Surface representation of base shear function (left). Dispersion diagram (right). Transversal calculation direction.	106
Figure 5.5. Mast guyed tower. Surface representation of base shear function (left). Dispersion diagram (right). Longitudinal calculation direction.	106
Figure 5.6. Delta guyed tower. Surface representation of base shear function (left). Dispersion diagram (right). Transversal calculation direction.	107
Figure 5.7. Delta guyed tower. Surface representation of base shear function (left). Dispersion diagram (right). Longitudinal calculation direction.	107
Figure 5.8. Dispersion diagrams for Mast Guyed tower (left) and Delta Guyed tower (right) for earthquake base reaction in the vertical direction.	108
Figure 5.9. Seismic force distribution patterns over the height of Delta guyed tower. Transversal calculation direction.	110
Figure 5.10. Dispersion diagrams comparing member axial forces obtained from nonlinear transient analysis and from the proposed approximate static method. Modal distribution of forces (left). Inverted triangular distribution of forces (right). Delta guyed tower analysed under NGA 953 applied in the transversal direction.	110
Figure 5.11. Force distributions over the height of Mast guyed tower. Longitudinal calculation direction.	111
Figure 5.12. Dispersion diagrams comparing member axial forces obtained from nonlinear transient analysis and from the proposed approximate static method. Modal distribution of forces (left). Inverted triangular distribution of forces (right). Mast guyed tower analysed under NGA 953 applied in the longitudinal direction.	111

## LIST OF FIGURES (cont'd)

	<b>Page</b>
Figure 5.13. Dispersion diagrams comparing member axial forces obtained from nonlinear transient simulations and from the proposed approximate static method. Transversal direction (left). Longitudinal direction (right). Modal distribution of forces. Delta guyed tower analysed under NGA 739.	112
Figure 6.1. Coupled guyed tower conductor system layout.	115
Figure 6.2. Supporting guyed tower and overhead conductors.	116
Figure 6.3. Envelope curves of Fourier response spectra of conductor support displacement of delta Self-supporting tower (top) and earthquake ground motion base displacement (bottom).	119
Figure 6.4. Fourier response spectra of conductor support displacement in the longitudinal direction of delta Self-supporting tower (top) and in the transversal direction of delta Self-supporting tower (bottom) for all studied earthquake ground motions.	119
Figure 6.5. Envelope curves of Fourier response spectra of conductor support displacement of delta guyed tower (top) and earthquake ground motion base displacement (bottom).	120
Figure 6.6. Fourier response spectra of conductor support displacement in the longitudinal direction of delta guyed tower (top) and in the transversal direction of delta guyed tower (bottom) for all studied earthquake ground motions.	120
Figure 6.7. Frequency-response relationship for conductor cable. Harmonic excitation in the longitudinal direction (top). Harmonic excitation in the vertical direction (middle). Harmonic excitation in the transversal direction (bottom).	122
Figure 6.8. Time-history of conductor cable tension ratio and ground motion accelerogram ( NGA 953 – low frequency content) applied in the longitudinal direction. Scenario “A”: seismic motion at one of the supporting nodes.	127
Figure 6.9. Fourier response spectra of conductor cable tension under NGA 953 (low frequency content ) applied in longitudinal direction. Scenario “A”: seismic motion at one of the supporting nodes.	127
Figure 6.10. Time-history of conductor cable tension ratio and ground motion accelerogram ( NGA 739 - medium frequency content) applied in the longitudinal direction. Scenario “A”: seismic motion at one of the supporting nodes.	128

## LIST OF FIGURES (cont'd)

	<b>Page</b>
Figure 6.11. Fourier response spectra of conductor cable tension under NGA 739 (medium frequency content) applied in the longitudinal direction. Scenario “A”: seismic motion at one of the supporting nodes.	128
Figure 6.12. Time-history of conductor cable tension ratio and ground motion accelerogram (NGA 57- high frequency content) applied in the longitudinal direction. Scenario “A”: seismic motion at one of the supporting nodes.	129
Figure 6.13. Fourier response spectra of conductor cable tension under NGA 57 (high frequency content) applied in the longitudinal direction. Scenario “A”: seismic motion at one of the supporting nodes.	129
Figure 6.14. Time-history of conductor cable tension ratio and ground motion accelerogram (NGA 953) applied in the longitudinal direction. Scenario “B”: synchronous seismic motion on both supporting end nodes.	130
Figure 6.15. Fourier response spectra of conductor cable tension under NGA 953 applied in the longitudinal direction. Scenario “B”: synchronous seismic motion on both supporting end nodes.	130
Figure 6.16. Time-history of horizontal base shear of Free-Standing Delta Guyed Tower and Coupled Delta Guyed Tower-Conductor System under NGA 953 record (low frequency content) applied in the longitudinal direction.	135
Figure 6.17. Persistence curve of horizontal base shear time-history of Free-Standing Delta Guyed Tower and Coupled Delta Guyed Tower-Conductor System under NGA 953 record (low frequency content) applied in the longitudinal direction.	135
Figure 6.18. Time-history of horizontal base shear of Free-Standing Delta Guyed Tower and Coupled Delta Guyed Tower-Conductor System under NGA 57 record (intermediate frequency content) applied in the longitudinal direction.	136
Figure 6.19. Persistence curve of horizontal base shear time-history of Free-Standing Delta Guyed Tower and Coupled Delta Guyed Tower-Conductor System under NGA 57 record (intermediate frequency content) applied in the longitudinal direction.	136
Figure 6.20. Time-history of horizontal base shear of Free-Standing Delta Guyed Tower and Coupled Delta Guyed Tower-Conductor System under NGA 739 record (high frequency content) Applied in the longitudinal direction.	137
Figure 6.21. Persistence curve of horizontal base shear time-history of Free-Standing Delta Guyed Tower and Coupled Delta Guyed Tower-Conductor System under NGA 739 record (high frequency content) applied in longitudinal direction	137

## LIST OF FIGURES (cont'd)

	<b>Page</b>
Figure 6.22. Time-history of horizontal base shear of Free-Standing Delta Guyed Tower and Coupled Delta Guyed Tower-Conductor System under NGA 953 applied in transversal direction.	138
Figure 6.23. Persistence curve of horizontal base shear time-history of Free-Standing Delta Guyed Tower and Coupled Delta Guyed Tower-Conductor System under NGA 953 record applied in transversal direction	138
Figure 6.24. Time-history of horizontal base shear of Free-Standing Delta Guyed Tower and Coupled Delta Guyed Tower-Conductor System under NGA 739 record applied in vertical direction.	139
Figure 6.25. Persistence curve of horizontal base shear time-history of Free-Standing Delta Guyed Tower and Coupled Delta Guyed Tower-Conductor System under NGA 739 record applied in transversal direction.	139
Figure I.1 NGA n° 953. Accelerogram. Horizontal component.	150
Figure I.2 NGA n° 953. 5% damping response spectra. Horizontal component.	150
Figure I.3 NGA n° 963. Accelerogram. Horizontal component.	151
Figure I.4 NGA n° 963. 5% damping response spectra. Horizontal component.	151
Figure I.5 NGA n° 986. Accelerogram. Horizontal component.	152
Figure I.6 NGA n° 986. 5% damping response spectra. Horizontal component.	152
Figure I.7 NGA n° 1005. Accelerogram. Horizontal component.	153
Figure I.8 NGA n° 1005. 5% damping response spectra. Horizontal component.	153
Figure I.9 NGA n° 1006. Accelerogram. Horizontal component.	154
Figure I.10 NGA n° 1006. 5% damping response spectra. Horizontal component.	154
Figure I.11 NGA n° 1039. Accelerogram. Horizontal component.	155
Figure I.12 NGA n° 1039. 5% damping response spectra. Horizontal component.	155
Figure I.13 NGA n° 1049. Accelerogram. Horizontal component.	156
Figure I.14 NGA n° 1049. 5% damping response spectra. Horizontal component.	156
Figure I.15 NGA n° 57. Accelerogram. Horizontal component.	157
Figure I.16 NGA n° 57. 5% damping response spectra. Horizontal component.	157
Figure I.17 NGA n° 735. Accelerogram. Horizontal component.	158

## LIST OF FIGURES (cont'd)

	<b>Page</b>
Figure I.18 NGA n° 735. 5% damping response spectra. Horizontal component.	158
Figure I.19 NGA n° 767. Accelerogram. Horizontal component.	159
Figure I.20 NGA n° 767. 5% damping response spectra. Horizontal component.	159
Figure I.21 NGA n° 776. Accelerogram. Horizontal component.	160
Figure I.22 NGA n° 776. 5% damping response spectra. Horizontal component.	160
Figure I.23 NGA n° 900. Accelerogram. Horizontal component.	161
Figure I.24 NGA n° 900. 5% damping response spectra. Horizontal component.	161
Figure I.25 NGA n° 1787. Accelerogram. Horizontal component.	162
Figure I.26 NGA n° 1787. 5% damping response spectra. Horizontal component.	162
Figure I.27 NGA n° 1794. Accelerogram. Horizontal component.	163
Figure I.28 NGA n° 1794. 5% damping response spectra. Horizontal component.	163
Figure I.29 NGA n° 15. Accelerogram. Horizontal component.	164
Figure I.30 NGA n° 15. 5% damping response spectra. Horizontal component.	164
Figure I.31 NGA n° 739. Accelerogram. Horizontal component.	165
Figure I.32 NGA n° 739. 5% damping response spectra. Horizontal component.	165
Figure I.33 NGA n° 848. Accelerogram. Horizontal component.	166
Figure I.34 NGA n° 848. 5% damping response spectra. Horizontal component.	166
Figure I.35 NGA n° 766. Accelerogram. Horizontal component.	167
Figure I.36 NGA n° 766. 5% damping response spectra. Horizontal component.	167
Figure I.37 NGA n° 721. Accelerogram. Horizontal component.	168
Figure I.38 NGA n° 721. 5% damping response spectra. Horizontal component.	168
Figure I.39 NGA n° 174. Accelerogram. Horizontal component.	169
Figure I.40 NGA n° 174. 5% damping response spectra. Horizontal component.	169
Figure II.1. Loading tree for Test 1.	170
Figure II.2. Loading tree for Test 2.	171

## LIST OF FIGURES (cont'd)

	<b>Page</b>
Figure II.3. Loading tree for Test 3.	172
Figure II.4. Deflection of the vertical axis of symmetry in the transversal direction for test case number 2.	173
Figure II.5. Deflection of the vertical axis of symmetry in the longitudinal direction for test case number 3 (right).	174
Figure II.6. Dispersion diagram – axial forces in leg members on the delta guyed tower's mast – analytical versus full-scale prototype results.	175
Figure II.7. Simulations' relative errors for the measured forces in the leg members on the delta guyed tower's mast.	176
Figure II.8. Dispersion diagram – axial forces in members at bottom segment – analytical versus full-scale prototype results.	177
Figure II.9. Dispersion diagram – axial forces in cross-arm members – analytical versus full-scale prototype results.	178
Figure II.10. Mode shapes. a) and b) cable vibration. c) 1 <sup>st</sup> flexural mode of vibration in the transversal direction. d) 1 <sup>st</sup> flexural mode of vibration in the longitudinal direction. e) 2 <sup>nd</sup> flexural mode of vibration in the transversal direction. f) 2 <sup>nd</sup> flexural mode of vibration in the longitudinal direction.	179
Figure II.11. Mode shapes. a) 1 <sup>st</sup> flexural mode of vibration in the transversal direction. b) 1 <sup>st</sup> flexural mode of vibration in the longitudinal direction. c) tower rotation about vertical axis. d) 2 <sup>nd</sup> flexural mode of vibration in the transversal direction. e) 2 <sup>nd</sup> flexural mode of vibration in the longitudinal direction. f) substructure vibration – ground-wire peak and beam.	181
Figure II.12. Mode shapes. a) tower rotation about vertical axis. b) 1 <sup>st</sup> flexural mode of vibration in the longitudinal direction. c) 1 <sup>st</sup> flexural mode of vibration in the transversal direction. d) 2 <sup>nd</sup> flexural mode of vibration in the transversal direction. e) 2 <sup>nd</sup> flexural mode of vibration in the longitudinal direction. f) substructure vibration.	183
Figure III.1. Dispersion diagrams comparing member axial forces of delta guyed tower obtained from nonlinear transient analysis and from the proposed approximate static method under NGA 57 record applied in transversal direction (left) and longitudinal direction (right).	189
Figure III.2. Dispersion diagrams comparing member axial forces of delta guyed tower obtained from nonlinear transient analysis and from the proposed approximate static method Under NGA 174 record applied in transversal direction (left) and longitudinal direction (right).	189

## LIST OF FIGURES (cont'd)

	<b>Page</b>
Figure III.3. Dispersion diagrams comparing member axial forces of delta guyed tower obtained from nonlinear transient analysis and from the proposed approximate static method under NGA 721 record applied in transversal direction (left) and longitudinal direction (right).	190
Figure III.4. Dispersion diagrams comparing member axial forces of delta guyed tower obtained from nonlinear transient analysis and from the proposed approximate static method under NGA 766 record applied in transversal direction (left) and longitudinal direction (right).	190
Figure III.5. Dispersion diagrams comparing member axial forces of delta guyed tower obtained from nonlinear transient analysis and from the proposed approximate static method under NGA 776 record applied in transversal direction (left) and longitudinal direction (right).	191
Figure III.6. Dispersion diagrams comparing member axial forces of delta guyed tower obtained from nonlinear transient analysis and from the proposed approximate static method under NGA 848 record applied in transversal direction (left) and longitudinal direction (right).	191
Figure III.7. Dispersion diagrams comparing member axial forces of delta guyed tower obtained from nonlinear transient analysis and from the proposed approximate static method under NGA 1006 record applied in transversal direction (left) and longitudinal direction (right).	192
Figure III.8. Dispersion diagrams comparing member axial forces of delta guyed tower obtained from nonlinear transient analysis and from the proposed approximate static method under NGA 1787 record applied in transversal direction (left) and longitudinal direction (right).	192
Figure III.9. Dispersion diagrams comparing member axial forces of delta guyed tower obtained from nonlinear transient analysis and from the proposed approximate static method under NGA 1794 applied in transversal direction (left) and longitudinal direction (right).	193
Figure III.10. Dispersion diagrams comparing member axial forces of mast guyed tower obtained from nonlinear transient analysis and from the proposed approximate static method under NGA 57 applied in transversal direction (left) and longitudinal direction (right).	193
Figure III.11. Dispersion diagrams comparing member axial forces of mast guyed tower obtained from nonlinear transient analysis and from the proposed approximate static method under NGA 174 record applied in transversal direction (left) and longitudinal direction (right).	194

## LIST OF FIGURES (cont'd)

	<b>Page</b>
Figure III.12. Dispersion diagrams comparing member axial forces of mast guyed tower obtained from nonlinear transient analysis and from the proposed approximate static method under NGA 721 record applied in transversal direction (left) and longitudinal direction (right).	194
Figure III.13. Dispersion diagrams comparing member axial forces of mast guyed tower obtained from nonlinear transient analysis and from the proposed approximate static method under NGA 766 record applied in transversal direction (left) and longitudinal direction (right).	195
Figure III.14. Dispersion diagrams comparing member axial forces of mast guyed tower obtained from nonlinear transient analysis and from the proposed approximate static method under NGA 776 record applied in transversal direction (left) and longitudinal direction (right).	195
Figure III.15. Dispersion diagrams comparing member axial forces of mast guyed tower obtained from nonlinear transient analysis and from the proposed approximate static method under NGA 848 record applied in transversal direction (left) and longitudinal direction (right).	196
Figure III.16. Dispersion diagrams comparing member axial forces of mast guyed tower obtained from nonlinear transient analysis and from the proposed approximate static method under NGA 1006 record applied in transversal direction (left) and longitudinal direction (right).	196
Figure III.17. Dispersion diagrams comparing member axial forces of mast guyed tower obtained from nonlinear transient analysis and from the proposed approximate static method under NGA 1787 record applied in transversal direction (left) and longitudinal direction (right).	197
Figure III.18. Dispersion diagrams comparing member axial forces of mast guyed tower obtained from nonlinear transient analysis and from the proposed approximate static method under NGA 1794 record applied in transversal direction (left) and longitudinal direction (right).	197
Figure IV.1. Fourier response spectra of conductor support displacement in the vertical direction for all studied earthquake ground motions. Delta Self-supporting tower.	198
Figure IV.2. Fourier response spectra of conductor support displacement in the vertical direction for all studied earthquake ground motions. Delta guyed tower.	199
Figure IV.3. Envelope curves of Fourier response spectra of conductor support displacement (top) and earthquake ground motion base displacement (bottom). Mast guyed tower.	199

## LIST OF FIGURES (cont'd)

	<b>Page</b>
Figure IV.4. Fourier response spectra of conductor support displacement in the longitudinal direction (top) and in the transversal direction (bottom) for all studied earthquake ground motions. Mast guyed tower.	200
Figure IV.5. FOURIER response spectra of conductor support displacement in the vertical direction for all studied earthquake ground motions. Mast guyed tower.	200
Figure IV.6. Time-history of conductor cable tension ratio under NGA 953 applied in vertical direction. Scenario "A": seismic motion at one of the supporting nodes.	201
Figure IV.7. Fourier response spectra of conductor cable tension under NGA 953 applied in vertical direction. Scenario "A": seismic motion at one of the supporting nodes.	201
Figure IV.8. Time-history of conductor cable tension ratio under NGA 57 applied in vertical direction. Scenario "A": seismic motion at one of the supporting nodes.	202
Figure IV.9. Fourier response spectra of conductor cable tension under NGA 57 applied in vertical direction. Scenario "A": seismic motion at one of the supporting nodes.	202
Figure IV.10. Time-history of conductor cable tension ratio under NGA 739 applied in vertical direction. Scenario "A": seismic motion at one of the supporting nodes.	203
Figure IV.11. Fourier response spectra of conductor cable tension under NGA 739 applied in vertical direction. Scenario "A": seismic motion at one of the supporting nodes.	203
Figure IV.12. Time-history of conductor cable tension ratio and NGA 57 record accelerogram in longitudinal direction. Scenario "B": synchronous seismic motion on both supporting end nodes.	204
Figure IV.13. Fourier response spectra of conductor cable tension under NGA 57 applied in longitudinal direction. Scenario "B": synchronous seismic motion on both supporting end nodes.	204
Figure IV.14. Time-history of conductor cable tension ratio and NGA 739 record accelerogram in longitudinal direction. Scenario "B": synchronous seismic motion on both supporting end nodes.	205
Figure IV.15. Fourier response spectra of conductor cable tension under NGA 739 applied in longitudinal direction. Scenario "B": synchronous seismic motion on both supporting end nodes.	205

## LIST OF FIGURES (cont'd)

	<b>Page</b>
Figure IV.16. Time-history of conductor cable tension ratio under NGA 953 record applied in vertical direction. Scenario “B”: synchronous seismic motion on both supporting end nodes.	206
Figure IV.17. Fourier response spectra of conductor cable tension under NGA 953 applied in vertical direction. Scenario “B”: synchronous seismic motion on both supporting end nodes.	206
Figure IV.18. Time-history of conductor cable tension ratio under NGA 57 applied in vertical direction. Scenario “B”: synchronous seismic motion on both supporting end nodes.	207
Figure IV.19. Fourier response spectra of conductor cable tension under NGA 57 applied in vertical direction. Scenario “B”: synchronous seismic motion on both supporting end nodes.	207
Figure IV.20. Time-history of conductor cable tension ratio under NGA 739 applied in the vertical direction. Scenario “B”: synchronous seismic motion on both supporting end nodes.	208
Figure IV.21. Fourier response spectra of conductor cable tension under NGA 739 applied in the vertical direction. Scenario “B”: synchronous seismic motion on both supporting end nodes.	208
Figure IV.22. Time-history of horizontal base shear of Free-Standing Delta Guyed Tower and Coupled Delta Guyed Tower-Conductor System. under NGA 57 applied in the transversal direction.	209
Figure IV.23. Persistence curve of horizontal base shear time-history of Free-Standing Delta Guyed Tower and Coupled Delta Guyed Tower-Conductor System under NGA 57 applied in transversal direction.	209
Figure IV.24. Time-history of horizontal base shear of Free-Standing Delta Guyed Tower and Coupled Delta Guyed Tower-Conductor System under NGA 739 applied in transversal direction.	210
Figure IV.25. Persistence curve of horizontal base shear time-history of Free-Standing Delta Guyed Tower and Coupled Delta Guyed Tower-Conductor System under NGA 739 applied in transversal direction.	210
Figure IV.26. Time-history of horizontal base shear of Free-Standing Delta Guyed Tower and Coupled Delta Guyed Tower-Conductor System under NGA 953 applied in vertical direction.	211

**LIST OF FIGURES (cont'd)**

	<b>Page</b>
Figure IV.27. Persistence curve of horizontal base shear time-history of Free-Standing Delta Guyed Tower and Coupled Delta Guyed Tower-Conductor System under NGA 953 applied in transversal direction.	211
Figure IV.28. Time-history of horizontal base shear of Free-Standing Delta Guyed Tower and Coupled Delta Guyed Tower-Conductor System under NGA 57 applied in vertical direction.	212
Figure IV.29. Persistence curve of horizontal base shear time-history of Free-Standing Delta Guyed Tower and Coupled Delta Guyed Tower-Conductor System under NGA 57 applied in transversal direction.	212

## LIST OF TABLES

	<b>Page</b>
Table 2.1. Typical load cases and combinations used in TL tower design.	14
Table 2.2. Load factors for adjustment of climatic loads in relation to a return period 1:50-years. (extracted from CAN/CSA C22.3 No. 60826-10)	15
Table 2.3. Summary of natural frequencies of vibration for tower structures and members reported in the literature.	33
Table 3.1. Characteristics of the transmission towers studied	40
Table 3.2. Towers used in the present study and their wind design parameters.	48
Table 3.3. Identified locations and their respective seismic spectral values as per NBCC (2010) (site Class C).	51
Table 3.4. Coefficients $F_a$ and $F_v$ specified in NBCC (2010) for site Class D.	52
Table 3.5. Earthquake records selected – horizontal component.	53
Table 3.6. Earthquake records selected – vertical component.	54
Table 4.1. The overall numerical model accuracy with reference to test results – Member axial forces.	61
Table 4.2. Modal properties of Delta Guyed tower.	64
Table 4.3. Comparisons between peak responses obtained from nonlinear dynamic analyses and results obtained with the analytical approach.	81
Table 4.4. Coefficients $a$ and $b$ derived for Eq. (4.21).	92
Table 5.1. Percentage of members with seismic axial forces higher than those resulted from typical design load cases. Earthquake ground motions scaled for Bamfield B.C. were applied in the transversal direction.	98
Table 5.2. Percentage of members with seismic axial forces higher than in design load cases. Statistics per direction of earthquake incidence.	101
Table 5.3. Number of members with capacity exceeded and maximum capacity usage of guy cables. Transversal direction of seismic load incidence.	102
Table 5.4. Number of members with capacity exceeded. Statistics per direction of earthquake incidence.	103
Table 5.5. Coefficients for Eqs. (5.1a) and (5.1b).	105
Table 5.6. Coefficients for equation 5.2.	108

### LIST OF TABLES (cont'd)

	<b>Page</b>
Table 5.7. Comparison of seismic base shear values calculated using Eq. 5.1 and the NBCC (2010) expression for the Mast guyed tower with earthquake ground motion incidence in the transversal direction.	113
Table 6.1 Main characteristics of the overhead cables.	115
Table 6.2 Peak dynamic tension to static tension ratio in overhead conductor. Scenario “A”: seismic motion at one of the supporting node, only.	126
Table 6.3 Peak dynamic tension to static tension ratio in overhead conductor. Scenario “B”: synchronous seismic motion on both end supporting nodes.	126
Table 6.4 Percentage of members with seismic axial forces higher than in design load cases.	134
Table II.1. Modal properties of Mast Guyed tower.	180
Table II.2. Modal properties of Delta Self-supporting Tower.	182
Table II.3. Modal properties of Mast Self-supporting Tower.	184
Table III.1. Percentage of members with seismic axial forces higher than in design load cases. Earthquake ground motions acting on longitudinal direction.	185
Table III.2. Percentage of members with seismic axial forces higher than in design load cases. Earthquake ground motions acting on vertical direction.	186
Table III.3. Number of members with capacity exceeded and maximum capacity usage of guy cables. Earthquake ground motions applied in longitudinal direction.	187
Table III.4. Number of members with capacity exceeded and maximum capacity usage of guy cables. Earthquake ground motions applied in vertical direction.	188

## LIST OF SYMBOLS

$A$	peak ground motion acceleration
$A_y$	value of the mode shape corresponding to tower section $y$
$A_i$	value of the mode shape corresponding to tower section $i$
$a_{max}$	peak ground acceleration
$a_{RMS}$	root mean square acceleration
$E$	modulus of elasticity
$F$	seismic inertia force
$F_0$	initial force
$F_a$	acceleration-based site coefficient
$F_e$	horizontal force function of the elastic stretching of the guy-cable
$F_g$	horizontal force function of the guy-cable's catenary stiffness
$F_v$	velocity-based site coefficient
$F_y$	seismic inertia force distributed over the height of the tower
$F(t)$	time-varying force
$h_i$	height of tower sections $i$
$h_y$	height of tower sections $y$
$i$	imaginary unit
$k_e$	horizontal stiffness of a perfectly taut cable
$k_{h-effec}$	effective stiffness of cluster of guy cables
$k_g$	horizontal stiffness of guy provided by the gravitational effects
$k_h$	horizontal stiffness of the guy cable
$L$	length of the chord line of guy cable
$m$	mass of a SDOF system
$M_n$	modal mass
$M_{eff-i}$	effective mass for the $i^{th}$ mode
$Q_T$	effect of the limit load on a given member of the structure
$R_C$	characteristic strength of the member
$S_a(T_n)$	response spectral acceleration for a period $T_n$

### LIST OF SYMBOLS (cont'd)

$t$	time variable
$t_r$	time of rise of the step force
$T$	average cable tension
$T_{mean}$	ground motion mean period
$T_n$	natural period of the structure
$T_{pred}$	ground motion predominant period
$u(t)$	displacement as function of time
$V$	base shear
$V(t)$	base shear as a function of time
$V(t)$	base shear as a function of time
$V(t)_{steady}$	steady-state component of base shear (harmonic excitation)
$V(t)_{transient}$	transient component of base shear (harmonic excitation)
$V(t)_{total}$	total base shear response (harmonic excitation)
$W_G$	unit weight of a guy cable
$W_y$	seismic weight of tower section y
$W_i$	seismic weight of tower section i
$\alpha$	angle between the guy chord line and the horizontal axis of reference
$\beta$	angle measured in the horizontal plan between the guy and the direction of the mast displacement
$\Delta q(t)_n$	displacement of the nodal coordinate
$\Delta q(t)''_n$	acceleration term of the nodal coordinate
$\Delta t$	time-step
$\Delta x(t)$	guy-cable displacement as a function of time
$\Delta x(t)_{max}$	maximum displacement of guy-cable
$(\Delta x_{st})_0$	static displacement of guy-cable
$\gamma$	load factors for adjustment of climatic loads
$\gamma_i$	participation factor for base excitation
$\varphi$	strength factor

### LIST OF SYMBOLS (cont'd)

$\vartheta$	displacement phase shift
$\delta$	maximum sag of a guy cable
$\omega$	circular frequency of vibration
$\{a\}$	nodal acceleration vector
$[C]$	damping matrix
$\{D\}$	vector describing the excitation direction
$\{F\}$	force vector
$\{F_1\}$	real component of the force
$\{F_2\}$	imaginary component of the force
$\{F(t)\}$	seismic inertia load vector
$[K]$	stiffness matrix
$[M]$	mass matrix of the structure
$\{u\}$	nodal displacement vector
$\{u_1\}$	real components of the displacement vector
$\{u_2\}$	imaginary component of the displacement vector
$\{v\}$	nodal velocity vector
$\{\varphi\}_i$	eigenvector

**ACRONYSMS**

APDL	ANSYS Parametric Design Language
BPA	Bonneville Power Administration
DDOF	Dynamic Degree of Freedom
DLT	Design Loading Tree
DAF	Dynamic Amplification Factor
DOF	Degree of Freedom
FEA	Finite Element Analysis
FEM	Finite Element Model
FFT	Fast Fourier Transform
GMR	Ground Motion Record
HVAC	High-Voltage Alternating Current
HVDC	High-Voltage Direct Current
MDOF	Multiple Degree of Freedom
NERC	North American Electric Reliability Corporation
PEER	Pacific Earthquake Engineering Research Center
RMSD	Root Mean Square Deviation
TL	Transmission Line
SI	International System of Units

## CHAPTER I

### INTRODUCTION

#### 1.1. Introduction

Steel lattice transmission line towers (TL) are widely used as supporting structures for overhead powerlines. They are classified in two main categories based on their supporting configuration: guyed towers and Self-supporting towers. The present study focuses on the seismic response of two guyed towers due to their sensitivity to earthquake loads. To emphasize this, the seismic response of guyed tower is compared with the response of Self-supporting towers with similar geometric configuration.

According to the current design practice, the main design loads considered for TL towers are conductors' weight and environmental loads originated from ice accretion and wind gustiness or some combination of both. Environment loads are usually the controlling load case in the design of these structures. Other exceptional loads, such as cable rupture and ice-shedding effects, are also considered. These dynamic loads are usually calculated using equivalent static load methods prescribed in the current TL Tower design standards. Earthquakes effects, however, are not usually considered in TL tower design. This neglect may be justified in areas of low seismicity as environment loads are likely to govern the design. However, in areas of high seismicity, forces in TL tower's members and connections resulted under earthquake loading may exceed those obtained from typical load cases considered in design.

In recent years, concerns about seismic activity and its effects on the built environment has increased. In Canada, this concern resulted in the development of ground motion maps, consecutive updating of seismic provisions of the National Building Code of Canada (NBCC) and inclusion of seismic analysis guidelines in the design standards of other nonbuilding structures such as telecommunication towers.

Most of electrical power generated in Canada comes from large hydropower and thermal power plants. For example, in British Columbia and Quebec, about 90% of the electrical power is generated by hydropower plants (Statistics Canada ,2013). Because large hydropower plants are located far from their main power delivery locations, transmission lines cover thousands of kilometres and cross various landscapes with different topographic and soil characteristics. It is noted that both aforementioned provinces are at high and medium-to-high seismic risk.

Given the size of the power transmission infrastructure in Canada, there has been some interest in adding a seismic load case for the design of transmission towers (Riley et al., 2005). However, because reported damages on TL towers from past earthquake events resulted in an overall perception that overhead TL tower structures have a relatively low vulnerability to earthquake ground motions, currently no code addresses this demand. Moreover, designers usually argue that loading caused by design cases generally exceeds the expected inertia loads from earthquake ground motions. Nonetheless, the number of post-earthquake reconnaissance reports is considered small (Pierre, 1995) and research carried out recently on the seismic analysis of TL towers highlights the relative importance of seismic effects in the performance of these structures, especially in regions of high seismicity and where design climatic loads may not be the controlling factor in design. Therefore, it remains relevant to understand the response of these structures under earthquake ground motions, especially if these lifeline systems are required to be fully operational in the earthquake aftermath.

Lattice telecommunication towers, which may be considered similar to TL towers in some aspects, have received more attention in recent years regarding their performance under seismic loads. In 1994, the Canadian Standard CSA S37 *Antennas, Towers and Antenna Supporting Structures* (CSA, 1994) introduced a new appendix entitled “Seismic Analysis of Towers”. The recommendation from this standard in regards to seismic effects is that the tower structure requires a design check for designated post-critical installations in regions of medium to high seismicity. This standard also refers to the National Building Code of Canada (NBCC, 2010) for the specification of seismic spectral accelerations. The latest edition of the CSA S37 standard (CSA, 2013) introduces mandatory seismic checks for all designated post-disaster structures that must remain serviceable immediately after an earthquake.

Finally, it should be mentioned that TL tower structures are constantly required by utilities to have their design optimized for the purpose of cost savings while meeting standard design requirements. This situation results in tower structures that have little to no reserve capacity to accommodate any extraordinary loading condition that may arise during the design lifetime of the structure.

## **1.2. Motivation for the Research**

In the case that a given TL is designated as a post-disaster structure, the designer is tempted to use simplified building code methods or to follow guidelines developed for telecommunication towers. However, as shown in previous studies, these structures respond to earthquake load in a different way than earthquake resistant concentrically braced frame buildings or telecommunication towers. For example, in the case of telecommunication towers, the geometry, structural configuration, the magnitude and nature of supported loads differ than those assigned to TL towers.

In the past, seismic analysis of TL towers has received little attention as compared with other similar nonbuilding structures as telecommunication towers. Although some research was conducted to analyse the seismic response of Self-supporting TL towers and the coupled dynamic behaviour of this type of tower with the overhead powerlines, no work addressed the response of guyed towers to earthquake loads.

Thus, it is a strong demand to analyse the response of guyed towers and the coupled guyed tower-conductor system to earthquake loads, especially when TL infrastructure is located in the high risk seismic zone of British Columbia. Although these TL towers were designed to carry conductors' weight and environmental loads such as ice accretion and wind gustiness, as well as exceptional loads such as cable rupture and ice-shedding effects, some load combinations including earthquake effects may govern the design. In addition, a motivation to develop a simplified equivalent static procedure to assess the sensitivity of these structures to seismic loads exists.

## **1.3. Objectives**

This research has the following objectives:

- To assess the sensitivity of typical TL towers to earthquake loads;
- To propose a simplified static method able to approximate the seismic response of TL guyed towers;
- To study the dynamic interaction between the overhead powerlines and their supporting guyed towers.

To reach these objectives, four existing free-standing TL Towers (two guyed towers and two Self-supporting towers), for which the controlling design case was the wind load, are subjected to two sets of earthquake ground motions. Detailed numerical models simulated in ANSYS-APDL software are developed and nonlinear time-history analysis is used to emphasise the differences in demand. From analysing the nonlinear seismic responses, a representative equivalent static method is proposed. Then, detailed nonlinear transient simulations of the coupled guyed tower-conductor system is carried out for a set of earthquake ground motions and the results are compared with those obtained for free-standing guyed towers.

#### **1.4. Thesis Organization**

Chapter One: The arguments, motivations and objectives of this study are presented.

Chapter Two: A literature review including the description of previous research work conducted on the dynamic response of TL towers subjected to seismic loads is presented.

Chapter Three: The general methodology used to carry out this research work is described, as well as the structural characteristics of the selected TL Towers. The selection of ground motion records and their characteristics are briefly discussed.

Chapter Four: Assessment of the static and dynamic properties of selected TL towers is presented. Nonlinear pushover analyses are carried out to assess the capacity of guyed towers to lateral load with different load distribution patterns. Static and dynamic properties of guy-cables are studied in particular and an analytical formulation is developed to estimate the impulse forces from guy-cable dynamics. A guyed tower structure is subjected to a harmonic excitation and expressions are derived in order to estimate the base shear.

Chapter Five: The results of nonlinear transient simulations are carried out for free-standing TL towers under two sets of 10 earthquake ground motion each. For each ground motion, two orthogonal and the vertical components were considered for investigations. The sensitivity of the studied towers to earthquake loads is assessed and comparisons are made between the seismic responses of these towers and the responses from governing design load cases. Earthquake base shear reactions are presented for both horizontal and vertical directions of ground motions. Expressions are derived from the results of these nonlinear transient simulations in order to propose an estimated base shear.

Chapter Six: The results of analyses carried out to assess the seismic response of a coupled guyed tower-conductor system are presented. First, analyses on the dynamic properties and seismic responses of each component of the system is carried out separately in order to evaluate whether dynamic interactions between the supporting guyed towers and overhead powerlines can be expected under earthquake loads. Then, the coupled guyed tower-conductor system is subjected to seismic excitation in order to emphasize the importance of considering the interaction of guyed tower and powerlines in the analysis.

Chapter Seven: In this chapter, conclusions are summarized as well as suggestions for future relevant research work.

## **CHAPTER II**

### **LITERATURE REVIEW**

#### **2.1. Introduction**

A high-voltage transmission line is generally composed of conductors and ground wires supported by towers. Nowadays, most of the transmission lines are supported by steel lattice towers. These towers are classified according to their support configuration as follow: Self-supporting free-standing towers and Self-supporting guyed towers.

Environmental loads, such as those originated from wind gustiness and ice accretion, are usually the controlling loads in the design of lattice tower structures. In the current design practice, earthquake effects are not considered in Transmission Line (TL) tower design, even though these are located in high risk seismic areas. This neglect is solely based on an overall perception that TL structures have a relatively low vulnerability to earthquake ground motions. However, this approach may be justified in areas of low seismicity, but not in areas of high seismicity where forces triggered in tower members and connections may exceed the design forces obtained from typical load cases considered in design practice.

Most of the published work on TL lattice towers is devoted to the analysis of these structures under environmental load conditions such as wind gustiness and ice accretion. Some exceptional load cases including dynamic loads originated from cable rupture, ice shedding and conductor galloping were also studied. Research in the seismic effects on TL towers has started only in recent years.

#### **2.2. Overview of High-Voltage Lattice Transmission Line Towers**

TL towers are designed to support conductors and ground wires. The geometric configuration of these towers depends on the type of high-voltage system, such as High-Voltage Alternating Current (HVAC) and Direct Current (HVDC), number of circuits and number of ground wires. Multi-circuit towers usually have a vertical configuration as illustrated in Figs. 2.1a, 2.1b and 2.1d, while single-circuit towers are either of vertical configuration (Fig. 2.1f) or horizontal or flat configurations illustrated in Figs. 2.1c, 2.1g and 2.1h.

The load cases required for the current design of TL towers are usually associated with minimum electrical clearances for conductors (which depend on voltage level), climatic conditions (such as wind pressure and loadings from ice accretion on the conductors and on the tower structure), and longitudinal load caused by broken conductors, tower failure or any other component failure.

As aforementioned, TL lattice towers can be classified according to geometric configuration and types of supports and their function in a transmission line system.

Galvanized steel angle members are usually used in the construction of steel lattice towers due to their acceptable trade-off between cost and durability. Structural steel for members of tower supports used in North America is usually steel grade 350 W (CSA G.41 21) or ASTM A572 Gr.50, with minimum yield strength of 345 MPa. For voltages exceeding 150 kV, steel lattice tower structures are usually the most viable solution.

Overhead powerline systems are supported by a family of towers, in which each tower performs a different function for the support of the same conductor. According to their function, TL towers can be classified into one of the following categories: **suspension** (or tangent), **strain**, **terminal**, **transposition** and **river-crossing structures**.

**Suspension towers** are used in relatively straight segments of the transmission line and are usually designed to accommodate small transmission line deviation angles (typically up to 3 degrees). They are designed with minimum cost as a priority making them light and very flexible structures. *Guyed towers are usually employed as suspension towers* because they are usually the most cost effective solution for straight segments of the TL system. In a suspension tower, the conductor phases pass through and are suspended from the insulator support points.

**Strain towers** are designed to accommodate various line deviations with angles up to 90°. These towers are designed to resist net tension from the conductors. The conductors are attached to the tower structure through strain insulators.

**Terminal towers** are the heaviest and strongest structures in a tower family. These towers are employed at the end of transmission lines and are designed to resist the full tension of all conductors and ground wires. *Self-supported towers, or a combination of self-supported and guy-supports, are usually employed as terminal tower structures* because they are the most laterally stiffer and stronger structures in a family of towers.

**Transposition towers** are usually required on longer segments of a transmission line and are used to perform a swap of the relative position of the phases.

**River-crossing towers** are usually the tallest structures in a tower family since they are used for relatively very long spans. These structures are generally tall self-supported suspension towers and they require specialized designs to suit specific ground conditions and spans.

TL towers can be designed to support single, double or multiple circuits and have a flat (Figs. 2.1c, 2.1g and 2.1h), delta (Fig. 2.1f) or vertical (Figs. 2.1a, 2.1b and 2.1d) geometric configurations. TL towers can also be classified according to their support systems, including conventional lattice Self-supporting (Figs. 2.1a to 2.1d), lattice guyed single masts (Figs. 2.1e and 2.1f) and lattice guyed frame and cross-rope suspension (Fig. 2.1h).

All these towers represent an evolution in conceptual design leading to cost savings. For suspension towers, used in relatively straight segments of the transmission line, guyed towers can represent a cost reduction up to 30% in regards to self-supported towers.

The choice of tower types extends also to available space dimensions, support footprints or aesthetics. While guyed tower structures are cheaper and easier to install, the compact design of self-supported towers requires smaller footprint dimensions, making it a better choice for urban settings where the price of the land represents a significant portion of the cost for a transmission line project.

The general shape of tower is defined in the design and is based on phase spacing, attachment height limits and line angles. These variables are defined in a tower outline drawing and conductor clearance diagram, which forms the basis of a detailed design.

A typical configuration of a TL tower is presented in Fig. 2.2. Structural members of a lattice tower are classified as: i) leg members, ii) primary bracing and iii) secondary bracing or redundant member. Insulators are usually present in lattice towers and their purpose is to transfer the loads from conductor and ground cables to the tower structure.

A leg member serves as the main corner support member of a tower structure, carrying the tower structure loads to the foundation. These members define the general outline of the tower structure. Leg members are presented in green color in the tower structure shown on Fig. 2.2.

Definition of orthogonal directions commonly used in tower design is presented in Fig. 2.3. The longitudinal direction is associated with the direction of the overhead cables alignment.

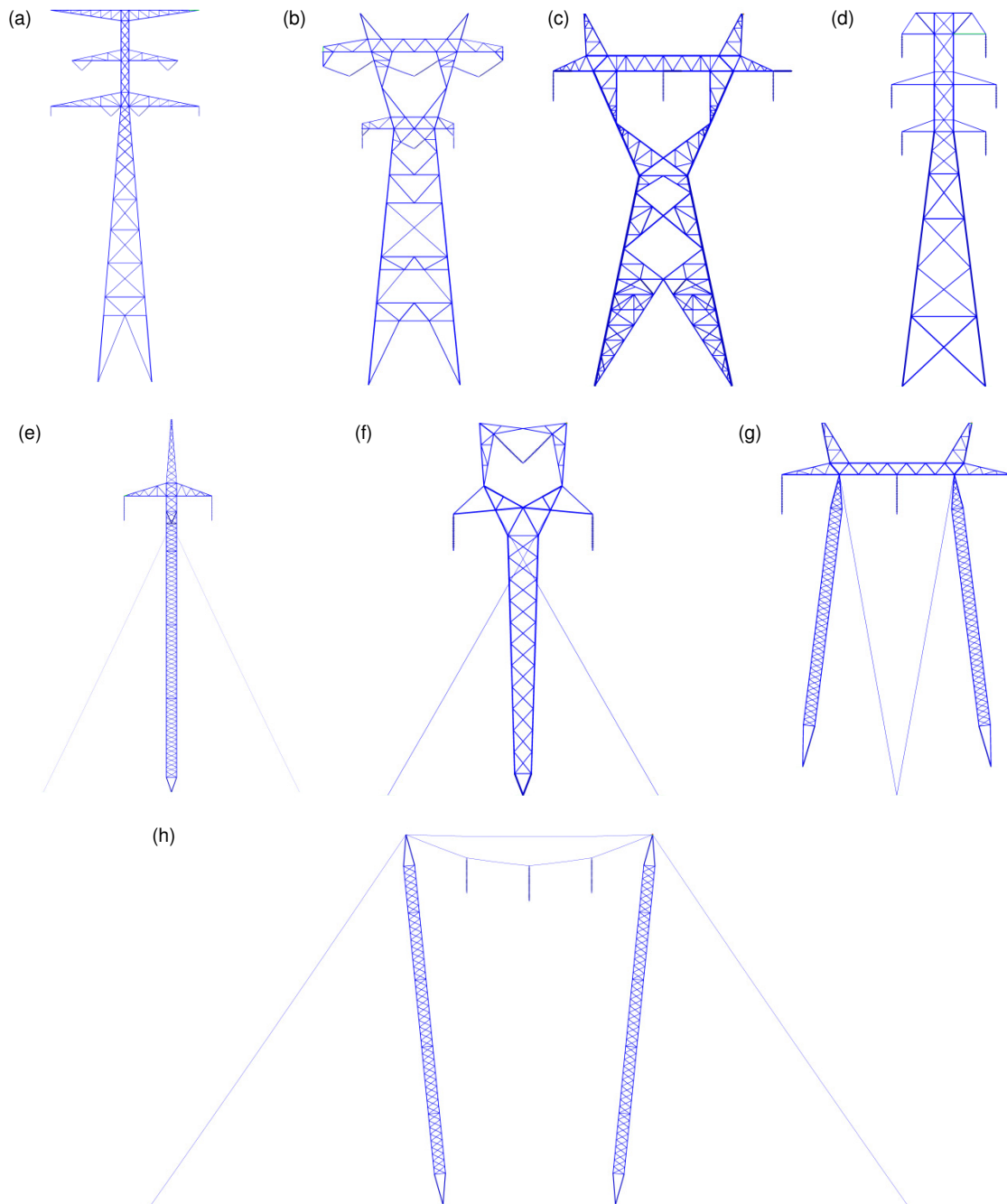


**Figure 2.1. Examples of TL towers. (a) 85 meters tall vertical self-supported double-circuit tower used for river-crossing span; (b) 30 meters tall vertical self-supported double-circuit tower; (c) flat self-supported single-circuit tower; (d) vertical self-supported double-circuit tower; (e) single-circuit guyed mast tower; (f) single-circuit lattice guyed delta tower; (g) single-circuit flat internally guyed portal tower; (h) single-circuit cross-ropes suspension tower.**

Primary bracings (in blue in Fig. 2.2) are members that support horizontal loads such as wind load and loads from conductors and ground wires. Horizontal brace members are required to distribute shear and torsional forces throughout the tower structure. Redundant members (in yellow in Fig. 2.2), are slightly loaded and their purpose is to reduce the unbraced length of load-carrying members (primary leg and primary bracing). Hence, by reducing the length of structural members, a substantial increase in their compression capacity is obtained. Tower segments are usually labelled in detailed design.

Because transmission lines are required to cross large extents of land with varying topography while maintaining the vertical and horizontal alignment of conductors as constant as possible, TL towers are usually designed to accommodate a modular composition in which their support members (tower legs, body extension and tower body) have a number of different heights used to accommodate variations in ground level along the TL alignment. The tower waist, which is the segment of the tower transitioning from the tower body to the tower upper body, is usually the part where the structural members are more demanded due to horizontal loading. The upper part of the tower (K-frame, cross-arms and ground-wire peaks) is designed according to the conductor clearances requirements and it supports the forces from the conductors.

### **2.3. Design of TL Lattice Towers**

TL structures in Canada are designed according to the requirements of the CAN/CSA-C22.3 NO. 60826-10 standard. This standard specifies loading and strength requirements derived from reliability based design principles. Reliability can be defined as the probability that a given structural system meets design requirements during a specified time. The general methodology proposed in the CAN/CSA-C22.3 NO. 60826-10 standard for the design of transmission line components is summarized in Fig. 2.4.

In the preliminary design phase, route selection and overhead cable configurations are defined, and available climatic data is collected. In Canada, CAN/CSA-C22.3 NO. 60826-10 gives climatic data, such as reference wind speed and ice thickness, with a 50-year return period. Security requirements (failure containment) and level of reliability for climatic limit loads in terms of return period are defined. Climatic loads and loads related to safety requirements based on these requirements are calculated and used for the structural design of the transmission line components.

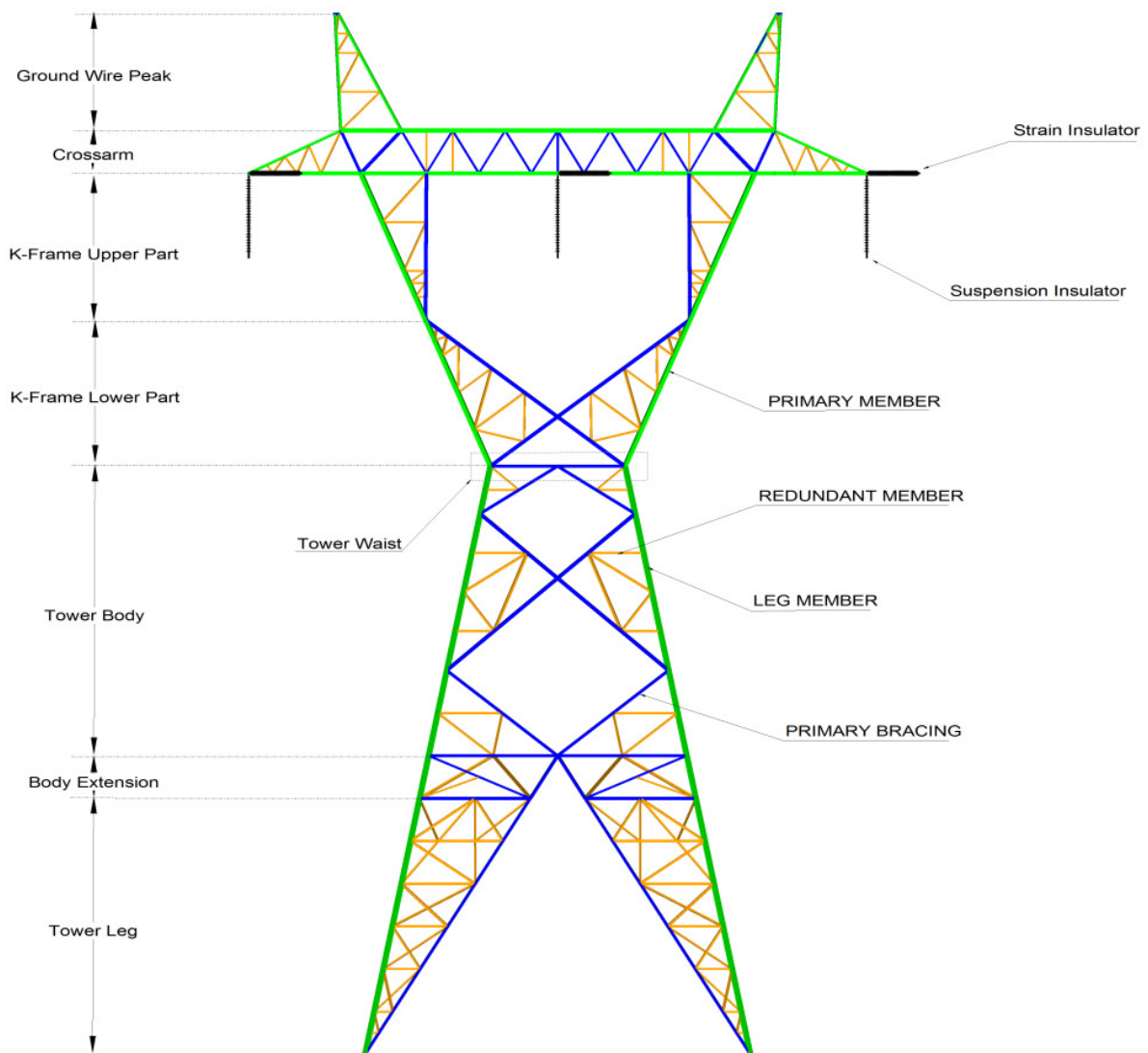


**Figure 2.2. Example of a self-supported TL tower, its members and segments.**

The design process of TL lattice towers usually follows the ensuing steps: tower selection, geometry definition and detailed structural design. The step of tower selection is characterized by the process of choosing the correct tower type for a specific transmission line system project. The basic geometry definition (or definition of the tower outline) is based on the transmission line design requirements such as phase spacing, attachment heights, maximum span limits and line angles. All these variables are considered in a tower outline drawing and conductor clearance diagram. These form the basis for a detailed structural analysis and design. The structural design process of latticed steel TL towers includes the definition of materials, load

cases and combinations, strength factors, effective slenderness and limiting conditions, minimum thickness and member connections. Common references used in the structural design of lattice towers in Canada are: CAN/CSA-C22.3 NO. 60826-10 - *Design criteria of overhead transmission lines*; CAN/CSA C22.3 No. 1-10 – *Overhead systems*; ASCE 10-15 – *Design of latticed steel transmission structures*; and IEC 60652 – *Loading tests on overhead line structures*.

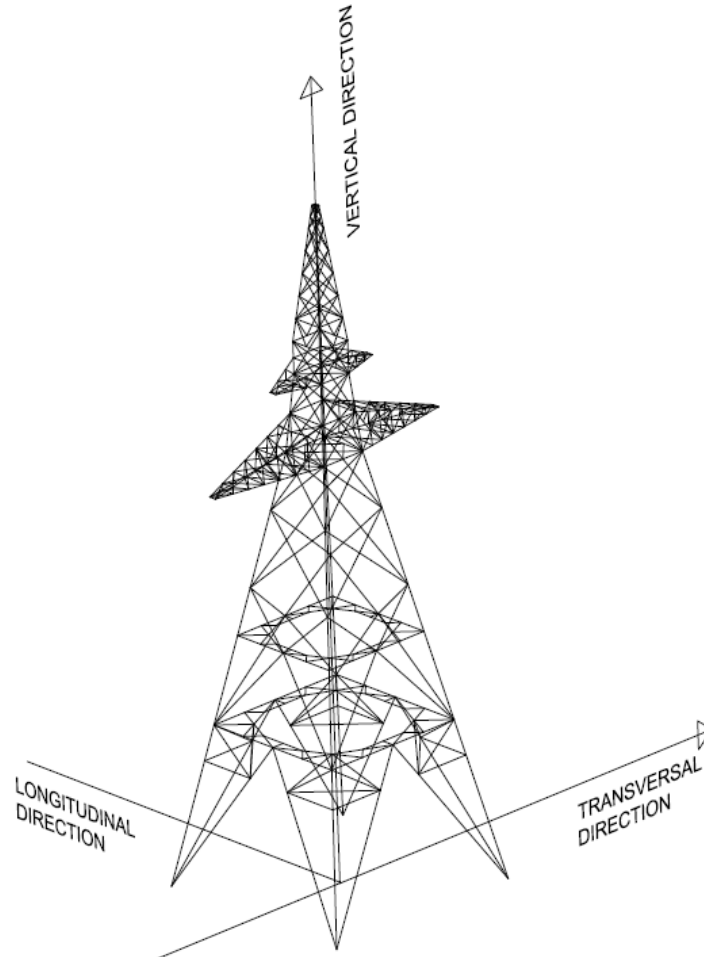


**Figure 2.3. Standard orthogonal directions definition. Tower design.**

### 2.3.1. Load Cases and Load Combinations

Load cases considered in tower design are used to provide a safe structure capable to withstand climatic loads (e.g. wind pressure and ice accretion) and failure containment loads (e.g. sudden broken conductors). In general, seismic loads are not considered in tower design. In fact, no seismic provision exists in the standards mentioned in the previous section. The loads considered in structural design can be divided into two main groups: loads acting on structure itself and loads acting on structure at the attachments of conductors and ground wires. Loads acting on the structure itself are usually due to tower self-weight, which includes the additional weight due to galvanization; sustained dead-loads from attached equipment (such as insulators), and ice accretion; and wind action on the structure members. Loads acting on the structure at the attachment points are from the tension of the conductors and ground wires due to their self-weight, broken wire and conductors, sustained dead-load from ice accretion and wind pressure.

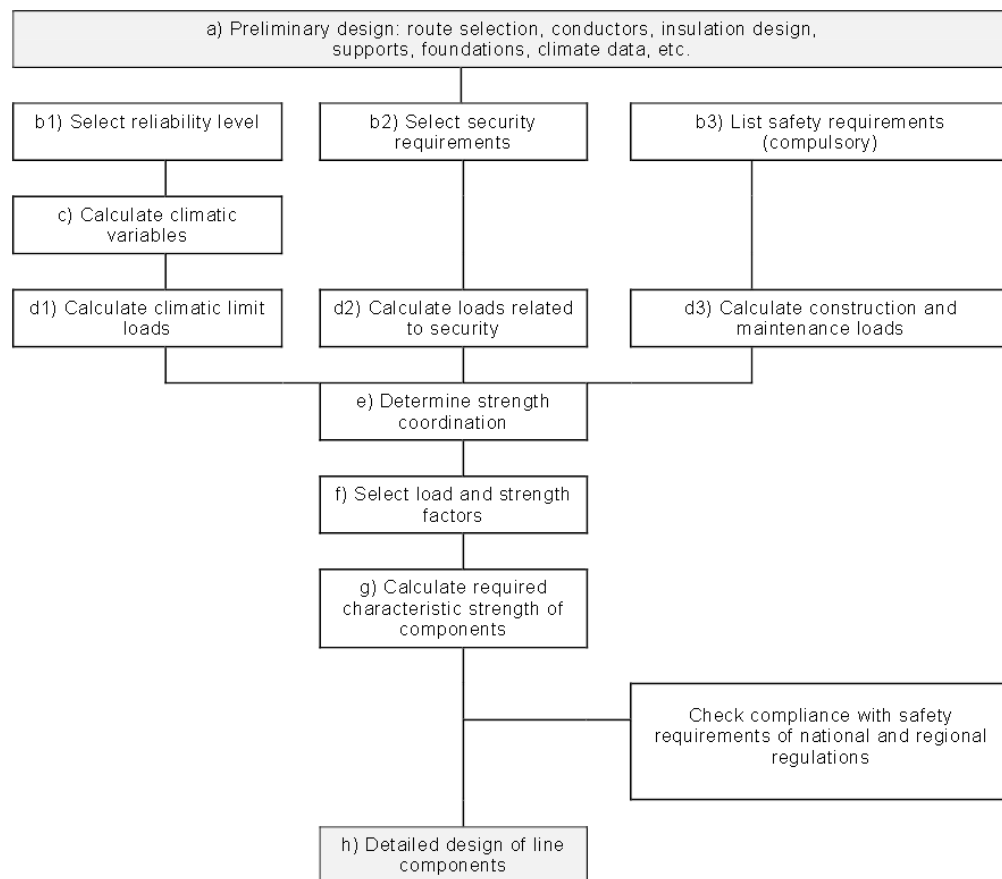


**Figure 2.4. Transmission line design methodology (CAN/CSA-C22.3 NO. 60826-10).**

As per CAN/CSA-C22.3 NO. 60826-10, load cases and combinations are categorized as follows:

- Climatic loads: loads due to environmental conditions imposed by action of wind and ice associated with coincident temperatures. The following load combinations are considered in design: Wind loads; Ice without wind; Ice with wind.
- Construction and maintenance loads: loads related to erection, stringing and maintenance;
- Failure containment loads: loads related to security requirements and associated with conductor failure or line component failure, sabotage or cascade failure.

These loads are applied to conductors and structures through a variety of load cases and combinations considering direction of load incidence, unbalanced loads from overhead conductors and different probabilistic combinations. These are generally based on the CAN/CSA C22.3 No. 1-10 deterministic approach, the CAN/CSA C22.3 No. 60826-10 reliability-based approach and/or specific project design requirements. Table 2.1 below presents typical parameters considered for main design load cases.

**Table 2.1. Typical load cases and combinations used in TL tower design.**

Load Cases and Combinations		Temp. (°C)	Radial Ice Thickness	Wind Pressure	Strength Factor ( $\phi$ )	Dynamic Amplific. Factor
Wind Load Cases	Max. Wind	-20	-	$W_{1:50}^{(1)}$	0.9	1.0
	Oblique Wind	-20	-	$W_{1:50}^{(1)}$	0.9	1.0
	Longitudinal Wind	-20	-	$W_{1:50}^{(1)}$	0.9	1.0
Ice Load Cases	Max. Ice	-5	$I_{1:50}^{(2)}$	-	0.9	1.0
	Wind and Ice	-5	$0.5 \times I_{1:50}^{(2)}$	$0.8 \times W_{1:50}^{(1)}$	0.9	1.0
	Ice shedding	-5	$I_{1:50}^{(2)}$	-	0.9	1.0
Broken wire	Broken wire without dynamic amplification	0	-	-	1.0	1.0
Construction and Maintenance	Tie down	-30°	-	$0.3 \times W_{1:50}^{(1)}$	0.5	1.0
	Maintenance	-30°	-	$0.3 \times W_{1:50}^{(1)}$	0.5	1.0
Failure Containment	Extreme broken wire with dynamic amplification	0	-		1.0	1.5

(1)  $W_{1:50}$  = 1:50 year return period wind pressure; (2)  $I_{1:50}$  = 1:50 year return period ice accretion;

Towers used in this study were designed in accordance with the CAN/CSA C22.3 No. 60826-10 reliability-based approach. In this approach, reliability requirements are used to ensure that TL can withstand climatic loads with a given return period during the life cycle of the project. For the CAN/CSA C22.3 No. 60826-10 standard, the reference reliability level is defined for a 50 year return period. For reliability levels of higher return periods, adjustments factors are applied to the 50-year return period climatic loads prescribed in this standard. The adjustment factors are presented in Table 2.2.

**Table 2.2. Load factors for adjustment of climatic loads in relation to a return period 1:50-years. (extracted from CAN/CSA C22.3 No. 60826-10)**

Return period	Wind Speed	Ice Variable	
		Ice Thickness	Ice Weight
50	1.00	1.00	1.00
150	1.10	1.15	1.20
500	1.20	1.30	1.45

### 2.3.2. Load Strength Requirements

In the reliability-based approach of the CAN/CSA C22.3 No. 60826-10 standard, the limit climatic design load defined for a given return period has to be checked for the following condition in the calculation process of each TL component:

$$\gamma \times Q_T < \varphi \times R_C \quad (2.1)$$

where  $\gamma$  is the load factor defined in table 2.2,  $Q_T$  is the effect of the limit load on a given member of the structure,  $\varphi$  is the strength factor and  $R_C$  is the characteristic strength of the member.

### 2.3.3. Design Strength Checks

Once the forces in members are calculated, design strength checks are carried out for members and connections. Design check for members is the process of comparing the axial compression and tension forces triggered in members and connections to the allowable capacity computed according to the given standard. Design checks for bolted connections are carried out in order to check the shear capacity, bearing capacity and tension capacity. Shear capacity is directly proportional to the number of bolts in the connection and the number of shear planes per bolt. Bearing capacity is directly proportional to the number of bolts and the number of bearing areas

per bolt. Tension capacity is related to the reduced cross-section area (net section), which in turn is a function of the number of holes.

The capacity in compression of a member depends on the following parameters:

- Member slenderness (controlled by the  $kL/r$  ratio) – controlling the overall buckling of the member and Cross-section slenderness (controlled by the  $b/t$  or  $w/t$  ratios) – defined as local buckling;
- Capacity of member ends bolted connections (e.g. buckling capacity of the attached gusset plate);
- Capacity of member ends bolted connections (e.g. shear capacity of bolts in the bolted connection);
- Capacity of member ends bolted connections (e.g. excessive bearing deformation at the bolt hole).

The capacity in tension of a member is determined by the minimum of the following:

- Tension capacity of the member based on net fracture;
- Capacity of tensile member ends bolted connections (e.g. block shear failure);
- Capacity of tensile member ends bolted connections (e.g. shear capacity of the bolts);
- Capacity of tensile member ends bolted connections (e.g. bearing capacity of the connected plates).
- Capacity of tensile member ends bolted connections (e.g. yielding capacity of gusset plate)

#### 2.3.4. Structural Analysis

Nowadays, the structural analysis procedure to determine design forces in the tower's members due to the applied design loads relies almost exclusively on Finite Element Analysis (FEA). Geometrically non-linear methods, which take into account secondary forces due to large displacements (i.e. P-Delta effects), are usually employed for the analysis of guyed towers; while stiffer self-supported towers are usually analyzed in a geometrically linear Finite Element Model (FEM). Material non-linearity (i.e. nonlinear stress-strain behavior of member's materials) is usually not considered in design practice because most standards and guidelines (such as the ones used in North America) assume that the tower shall be designed to withstand the design loads in the elastic range of the steel materials.

Nonlinear analysis, which considers both geometric and material nonlinearities, are usually done in connection with research projects, and it is usually used when the analyst wishes to study some structural complexities such as the effects of eccentricities of the connections or the effects of slippage of bolts, which usually occurs at high loads. Dynamic analyses are also employed in connection with research projects.

In numerical modeling, lattice TL towers are simulated as 3-dimensional truss structures during the design phase and tower's members are assumed to carry axial forces only. This assumption is based on the acknowledgement that the triangular arrangement of its members and characteristics of its connections will mainly result in axial forces throughout the structure's members, while flexural stresses are very small to be considered in design. Although steel lattice towers are modeled as pin-connected truss members, all design standards recognize the influence of end member conditions (i.e. actual rotational restraint of bolted connections and connection eccentricities) on the capacity of members. Therefore, design standards provide adjustments to scale down design stresses to account for these end conditions.

The design standard ASCE-10-15, for instance, recognizes that short members, defined in this standard as having a slenderness ratio less than or equal to 120, have their compressive force capacity influenced by the eccentricity of the end connections. It is noted that the magnitude of connection eccentricity is not taken into account. Rather than this, ASCE-10-15 standard considers whether eccentricities are present in one or both member ends in order to adjust the capacity of short member. For long members (defined as those with a slenderness ratio larger than 120), their compressive force capacity is influenced by the member end connection. Again, the design standard ASCE-10-15 only considers whether the restraints are present in one or both ends for adjusting the load capacity of the long member, ignoring the magnitude of the rotational restraining of the bolted connection.

A recurring problem with towers modeled as 3-dimensional truss structures is the problem of planar joints and mechanisms. The problem of planar joints in three dimensional truss models is that, mathematically, they have no stiffness in the direction perpendicular to the plane where all the connecting members are lying. Usually, the solution for the problem of planar joints is to use fictitious members, with very small stiffness, or to use beam elements to confer some stiffness in the direction perpendicular to the plane of the connecting members.

### 2.3.5. Full-Scale Prototype Tests

Full scale testing is mandatory and is carried out to most overhead power line towers before these towers are fabricated. Tower tests are set up to conform to design conditions and only static loads are applied to the full-scale tower prototype. The adequacy of the members and connections to withstand static design loads is verified under controlled conditions. There are a number of reasons that motivate full-scale tests in newly designed TL towers. Among them, the most relevant are:

- Because towers are designed to be as light as possible, the full member's capacity is used. The margin for error, therefore, becomes reduced;
- While FEM are reasonably accurate in predicting design forces in tower's members, these numerical models are typically approximations of the real structure. These numerical models usually do not include the complexity of structural member connections;
- The repeated use of a typical tower structure in a TL system, as well as the multitude of environments and different conditions which this tower structure may encounter, justifies a thorough assessment of its structural abilities.

Tower tests cannot confirm, however, how the tower will behave in the transmission line where the loads are dynamic in nature.

In recent years, research has been carried out to develop specialized numerical models for performing virtual tower tests. While such models represent a significant advance in the field of structural analysis, numerical modeling remains subject to the condition that input data accurately reflects the real structure.

#### **2.4. Experience from past Earthquakes**

Reports of recent earthquakes on damaged TL tower structures indicate that the major sources of damage are land sliding, foundation settlement and soil deformation. The EPRI (2009) summarizes some failure modes of TL tower structures due to earthquake events and their main causes. Post-earthquake reconnaissance reports after the 1994 Northridge earthquake mentioned 6 tower failures. The 1999 Chi.Chi earthquake in Taiwan reported 15 tower failures.

Main causes of tower's damage due to these events were reported to be land sliding and cascading following by conductor snapping. FEMA (1991) also indicates that the Kanto earthquake in Japan in 1923 and the Alaska earthquake in 1964 were responsible for destroying or damaging several transmission towers.

In other seismic events, no structural failure was reported. However, member damages were identified in several TL towers due to soil deformation resulting in foundation offsetting and tilting of the tower. Examples of earthquake events with a high number of damaged towers reported are the 1995 Kobe Earthquake in Japan (35 towers damaged) and the 1999 Kocaeli Earthquake in Turkey (EPRI, 2009). In addition to damages to supporting structures, snapping of conductors, as a result of additional tension or sag in the conductor, induced by large differential displacements between towers, are also reported.

It is recognized among researchers that the quantity of literature available reporting cases of damaged TL towers or failed towers in recent earthquakes does not reflect the actual magnitude and extents of damages to this infrastructure caused by earthquake events (Madugula et al. 2001). It is a fact that the publication of such information may result in legal issues and tower operators and designers are not inclined to share their experiences. It is also noted that the experience from earthquake effects on lattice TL towers reported in the literature refer mostly to the Self-supporting type. Guyed towers, which rely solely on its pretensioned guy cables for its lateral stability, may have a higher vulnerability to the effects of soil deformation and differential settlement after an earthquake event as some of its guy-anchors may be displaced relative to the tower base, resulting in either a slackened guy cable, without any function on the lateral stability of the mast, or a guy cable further stretched.

## **2.5. Current practices in the Seismic Analysis of Transmission Lines**

The small number of reported damages on TL towers from past earthquake events resulted in an overall perception among designers that overhead TL structures have a relatively low vulnerability to earthquake ground motion. Due to this perception, no code directly addresses seismic design for transmission lines. Some information on seismic analysis for overhead transmission structures can be found in CENELEC (2001), FEMA (1991 & 2003) and EPRI (2009), but common references used in the design of overhead transmission line structures in Canada, such as the CAN/CSA-C22.3 NO. 60826-10, ASCE 74 (2009) and ASCE 10 (1997 & 2015) standards, does not address seismic analysis and therefore these structures are usually not designed for seismic loading. ASCE 74 (2009), for instance, indicates that transmission structures are not typically designed for vibration caused by ground motion because these loads are generally exceeded by loading caused by wind and ice combinations or by broken wire effects. Therefore, by virtue of being designed to withstand the climatic and broken wire load combinations, transmission structures are perceived to be inherently capable of withstanding seismic induced forces.

This perception towards the seismic vulnerability of the components of the power transmission infrastructure is gradually changing among operators, however. Eidingen. et al. (2012) indicate that High-voltage transmission line networks throughout the world have failed during earthquakes and that some operators have recently developed a wide range of strategies for dealing with earthquake events. In North America, for instance, the Bonneville Power Administration (BPA) has modeled their networks to assess their performance under earthquake conditions.

In the power transmission infrastructure, the substations are perceived as the most vulnerable to seismic effects and have traditionally received more attention in the seismic design than transmission towers (EPRI, 2009). Some utilities take into account seismic loading in the design of long span crossings in high seismic zones. However, the seismic effects considered for these towers are usually restricted to the assessment of the vulnerability of these structures to the foundation soil deformation.

EPRI (2009) provides some information and references on the seismic analysis of overhead power lines, but it is limited to considerations of conductor motion and permanent differential displacement.

Lattice telecommunication towers, which may be considered similar to TL towers in some aspects, have received more attention in recent years regarding their performance under seismic loads. It is noted that the main difference between these 2 tower structures is the fact that TL towers carry overhead powerlines. In 1994, the Canadian Standard CSA S37 Antennas, Towers and Antenna Supporting Structures (CSA, 1994) introduced a new appendix entitled “Seismic Analysis of Towers”. The recommendation from this standard in regards to seismic effects is that the tower structure requires a design check for designated post-critical installations in regions of medium to high seismicity. The latest edition of the CSA S37 standard (CSA, 2013) introduces mandatory seismic checks for all designated post-critical structures that must remain serviceable immediately after an earthquake. This standard also refers to the National Building Code of Canada (NBCC, 2010) for the specification of seismic spectral accelerations.

In the case that a given TL is designated as an earthquake post-critical structure, the designer may be tempted to use simplified building code methods to design these structures or to follow guidelines developed for telecommunication towers. However, as shown in previous research reports found in the literature, these structures respond to earthquake load in a different way than that of earthquake-resistant buildings (e.g. concentrically braced frames) or telecommunication towers.

## **2.6. Learning from Previous Studies**

Although seismic analysis is currently not included in a standard practice used to design TL tower structures, previous studies highlights the relative importance of seismic effects on the performance of these structures, especially in locations characterised by high seismicity and where design climatic loads may not control the design. This section briefly describes the findings of these studies.

Due to significant nonlinearities of lattice tower members, especially for the guyed type of tower, the accurate assessment of the responses of these structures under dynamic loading conditions requires more sophisticated and time consuming nonlinear dynamic simulations that are not, in most cases, suitable for concept level design. This fact created a motivation among researchers to derive approximate static methods suitable for conceptual design. Most of these approximate static methods are devoted to the analysis of telecommunication and transmission towers under wind loading conditions, but some methods were also developed recently for the seismic analysis of lattice telecommunication towers.

Madugula et. al., (2001) summarizes a number of these static methods developed mostly for self-supported telecommunication towers. According to the author (Madugula et. al., 2001), no approximate method has been proposed yet for the seismic analysis of guyed masts. Madugula et al., (2001) cites the studies of Guevara (1993) and Amiri (1997) as a starting point for the seismic analysis of guyed towers, but these studies were based on tall telecommunication and antenna-supporting towers.

One of the major difficulties in the dynamic analysis of TL towers is the complex coupled behavior of the tower-cable system. This complex behavior was mostly investigated for wind loading conditions and conductor breakage. Most of the published work on the seismic analysis of transmission line structures considered either the free-standing tower alone or the overhead conductor alone without considering the dynamic interaction between the two. This could be explained by the significant computational effort that is required to simulate the dynamics of this system with significant nonlinearities arising from cable motion and interactions with the supporting towers. Only recently this coupled dynamic behavior has been the subject of more detailed numerical studies, although some previous work, such as the one of Long (1974), addressed this issue for Self-supporting lattice towers. Some examples of recently published work on this subject are the works of Li (2012); Li, T. and Li, H. (2010) and Li, H. et al. (2003). Long (1974) completed one of the first studies on the seismic response of TL towers. This study focused on the seismic effects on a Self-supporting free-standing tower, neglecting the effects of the overhead conductors. Later, this study was extended to evaluate the forces exerted by the conductor motion on the tower. A case study was first carried out for a rigid 43 meters tall free-standing tower with a natural frequency of 5 Hz. It was concluded that the entire structure moved rigidly and no amplification of structure response originated due to the frequency content of ground motion shaking. In the second part of the study, the forces exerted by conductors to the supporting tower due to earthquake excitation were also considered. The three orthogonal directions of ground motion incidence were considered and it was found that the resulting forces were very small and that could be resisted safely by the conductor and supports without cable breakage. The conclusions from this study are therefore aligned with the general consensus that stiff Self-supporting towers are not expected to induce a resonant vibration of the supported conductors.

Kotbuso et al. (1985) performed measurements of vibration properties on a Self-supporting 93 meters' tall suspension tower before and after the installation of overhead conductors. Natural frequencies, vibration modes and damping properties were derived from these measurements using Fast Fourier Transform analyses. Forced vibration tests were carried out after the installation of the overhead conductors and it was observed that there were no significant changes in the vibration properties of the tower, again indicating that the dynamic interactions between overhead conductors and Self-supporting towers are negligible.

Contradicting the conclusions reached by Long (1974) and Kotbuso et al. (1985), the study completed by Li et al. (1991) concluded that the effects of the overhead conductors on the seismic response of their Self-supporting towers are not negligible and should be taken into consideration. The study of Li et al. (1991) was, however, carried out for long-span transmission line systems. Three structural configurations were considered: a) the free-standing tower without the overhead conductors; b) the free-standing tower with the mass of the conductors lumped at the support joints; c) the coupled tower-conductor model. These configurations were subjected to dynamic seismic excitations for three earthquake records, namely El Centro (USA), Qian'an (China) and Ninghe (China), in all three orthogonal directions. It was found that, for vertical ground motion, the configuration "b" resulted in higher seismic response, whereas for the horizontal directions the configuration "c" (coupled tower-conductor model) resulted in the higher seismic responses.

Another numerical study published (Li et al., 1994) found that neglecting the presence of overhead cables in the seismic response of the Self-supporting tower could result in a significant underestimation in base shear forces. This study was carried out for 55 meters tall Self-supporting towers with overhead conductors spanning 400 meters and subjected to horizontal earthquake excitation. Three earthquake records were used in the simulations, namely El Centro (1940), San Fernando/Pacoima Dam (1971) and Olympia (1965). As in the previous study (Li et al., 1991), two structural configurations were considered: the free-standing tower with the mass of the conductors lumped at the support joints and the coupled tower-conductor model. It was found that the later configuration (coupled tower-conductor model) resulted in higher base shear values of up to 66% than the lumped model.

El Attar et al. (1995) studied the response of transmission lines under the action of earthquake ground motion in the horizontal and vertical directions. A relatively short and stiff Self-supporting tower was subjected to a harmonic horizontal ground acceleration of 0.28 g, representing the seismicity level of Victoria in British Columbia in accordance with the guidelines of the National Building Code of Canada (NBCC) available at the time. This study concluded that the displacement of tower at the top level resulted mainly from the contribution of the first mode of vibration. The overhead conductor alone was subjected to two earthquake ground motion records in the vertical direction and scaled to a peak ground acceleration of 0.21 g, equivalent to 75% of the horizontal peak ground-acceleration component prescribed for Victoria. It was found that earthquake ground motion records with low A/V ratio (i.e. peak ground acceleration to peak ground velocity ratio) resulted in displacement responses much higher than the response due to an earthquake ground motion record with high A/V ratio. The coupled dynamic behavior of the tower-cable system was not studied.

Ghobarah et al. (1995) studied the effect of multiple support excitations on the response of overhead power transmission lines by subjecting self-supported tower structures and their supported conductors to spatially incoherent seismic ground motions. The input ground motions were defined as displacement time histories. The critical damping ratio used in this analysis was 0.02 for all modes. The outcomes of this study indicated that the wave propagation velocity of the ground motion has a substantial effect on the response of the transmission line as compared with the responses from the assumption of spatially uniform ground motion. It was also concluded that the additional tension in transmission line cables due to lateral ground motion is relatively small.

Khedr, M (1998) studied the seismic response of six existing Self-supporting transmission towers with heights varying from 34.9 meters to 58.0 meters and used to support 120 kV to 450 kV overhead conductors. All these towers were modelled as three-dimensional lattice structures with their legs modeled as frame elements while primary and secondary bracing elements are modelled using truss elements. The objectives of this study were: to investigate the applicability of a proposed simplified static method that could approximate the response of the tower as determined by dynamic analysis and; to find an equivalent mass that could replace the mass of the overhead conductors in order to reflect the real behavior of the tower-conductor coupled system.

The study of Khedr, M (1998) found that Self-supporting suspensions towers with level and equal conductor spans presented no significant change in the frequency properties of the system with the changes in overhead cable tension. It was also found that only the mass of the overhead ground-wires affects the longitudinal seismic responses of the supporting towers and that 25% to 35% of the mass of the overhead ground-wires contributes to the longitudinal modes of vibration of the system. This study concluded that the response of the coupled tower-conductor system cannot be simplified in a way that would allow the use of simplified static equivalent methods to approximate the seismic response of the components of this system.

Riley et al. (2005) compared seismic effects with wind and ice effects on 500 kV towers using a scaled version of the measured ground motion of the 1998 Loma Prieta earthquake in California. This ground motion record was scaled to reproduce two earthquake events with return periods of 500-year and 2,500-year for Oregon. The outcome of this study was that seismic effects would be close to those from wind and ice when the 2,500-year return period ground motion is considered. Wind speed and ice loading used for comparison was not reported and authors mentioned that their study was preliminary and based on a limited number of ground motion records. The authors recommended that this line of study should be continued further to reach a comprehensive understanding of earthquake effects on transmission lines.

Lei and Chien (2009) investigated the dynamic behaviour of the coupled tower-conductor system when subjected to strong earthquake ground motion. A detailed FE model of the supporting towers and overhead cable was setup considering geometric nonlinearities. A soil-structure interaction model was also considered in the simulations. The authors indicated that ignoring the overhead cable contribution in the seismic response of the supporting towers would induce significant errors in predicting the ultimate strength of tower members.

Chen et al. (2014) presented a review of the state-of-the-art on the subject of dynamic responses and vibration control of transmission tower-line systems. In this article, research carried out on the dynamic responses of TL tower systems under wind, ice and earthquake conditions are reviewed and discussed. Regarding the seismic behaviour of TL tower systems, the authors layed out the following concluding remarks: a) the span of transmission lines is quite large in comparison with common civil engineering structures and therefore multl.excitation effects should be taken into account in detail; b) the widely reported failure of TL tower systems around the world indicates that loading patterns specified in codes do not depict the extreme loading

conditions, such as those originated from earthquake ground motions, and that design methods based on static analysis are limited and dynamic analysis on the interaction of tower-line systems should be used.

## **2.7. Seismic Response of TL Structures**

When seismic effects are considered in the design of TL towers, the primary concerns are usually related to conductor displacement (motion) and permanent differential displacements of tower foundation. Significant conductor motion during an earthquake event is expected to increase tension and displacement and generate additional forces in hardware, towers and foundations (EPRI, 2009). Differential displacement could cause detrimental effects in some members of the structure due to an unsymmetrical load distribution and enhanced P-delta effects from increased eccentric vertical loads. Considerations of the dynamic effects of ground motion inertia loads acting directly on the tower structure was not found to be reported in the literature.

The overall perception in regards to the coupled dynamic behavior of the tower-cable system is that the motion of the overhead conductor will have little to no effect on the seismic response of the supporting tower and, conversely, on additional tensions on the overhead cables. This perception is devoted to the Self-supporting type of towers and is backed up by some of the research carried out in the past, although other studies have concluded otherwise. It should be stretched that the understanding of the coupled dynamic behavior of the tower-cable system for Self-supporting towers is somehow developed, whereas for guyed towers no research has been carried out which leaves designers without any seismic design guidance.

Self-supporting lattice towers are usually stiffer than guyed towers and typically have a natural frequency of vibration ranging from 3 to 10 Hertz (i.e. period of vibration ranging from 0.1 to 0.33 seconds). Conductors and ground wires, on the other hand, typically have shorter natural frequency of vibration ranging from 0.1 to 0.3 Hertz (i.e. period of vibration ranging from 3 to 10 seconds). Therefore, the vibration of common Self-supporting towers is not expected to induce a resonant vibration on the supported conductors; conversely, the motion of the conductors can be approximated by considering the supporting towers as perfectly stiff since no dynamic interaction is expected. This coupled dynamic interaction should, however, be taken into consideration for tall Self-supporting towers, such as those used for river-crossing towers, that usually have lower natural frequencies than suspension type towers.

More flexible towers, such as guyed towers and tall towers used for long span crossings, typically have a natural frequency of vibration smaller than the traditional self-supported towers and thus closer to the natural frequencies of the supported cables. Therefore, it could be expected that the motion of the cables during ground motion will have an enhanced effect on these towers by means of resonant excitation.

## 2.8. Earthquake Ground Motion

Earthquakes are caused by fracture of rocks along fault lines which generates shear and surface waves that causes ground motion in the three orthogonal directions. The most common measure of ground motion is in the form of acceleration in unities of gravity ( $g = 9.81 \text{ m/s}^2$  in SI units). Peak ground acceleration values available in important earthquakes recorded in North America are in the range of 0.6 g to 2.0 g. Crustal earthquakes are relatively short events with strong motion restricted to a period of time no longer than 60 seconds. Typical frequency contents of ground motion cover the 1 Hz to 10.0 Hz range, with peak values in the range from 1.5 Hz to 5.0 Hz range (Madugula et. al, 2001).

According to Filiatrault et al. (2013) the response of a structure subjected to ground motion is mostly influenced by the following seismic parameters: amplitude, frequency content and duration of ground motion. The amplitude of the ground motion is usually expressed in terms of the peak ground acceleration ( $a_{max}$ ), which is used to define the maximum amplitude of a given accelerogram, or in terms of the root mean square acceleration ( $a_{RMS}$ ), which is a factored mean amplitude of the entire accelerogram, thus taking into account the damaging potential of the complete ground motion time-history.

The frequency content of a ground motion is usually expressed in terms of a single-degree-of-freedom (SDOF) response spectrum of the accelerogram or via a Fourier spectrum. Simpler indicators of the frequency content are the mean period ( $T_{mean}$ ) or the predominant period ( $T_{pred}$ ), which is defined as the period at which the maximum ordinate of a SDOF acceleration response spectrum occurs. The response spectrum is usually the choice of structural engineers for seismic analysis and design of structures, although in some cases time-history analyses are used. Earthquake response spectrum is developed by submitting the seismic ground motion to SDOF oscillators with a natural period  $T_n$  for a given range of frequencies of interest. Details about developing SDOF response spectrum can be found in relevant literature such as Clough, R.W.,

and J. Penzien. (1993). For structural systems that can be considered linear, the following expression, used to determine the maximum inertia force  $F$  applied to the mass  $m$  of a SDOF system of period  $T_n$ , is usually used to determine the peak seismic inertia forces on the structure.

$$F = S_a(T_n) \times m \quad (2.2)$$

where  $S_a(T_n)$  is the response spectral acceleration for a period  $T_n$ . In cases where the material and geometric properties of the structure vary significantly during the response to an earthquake ground motion, linear analysis are no longer appropriate and nonlinear transient analyses are required to obtain a more realistic seismic response.

For example, lattice transmission line towers are slender structures. These have axial loads acting on the tower's mast from tower's self-weight and conductor load and, during the seismic response, these loads will induce important second-order effects (i.e. P-Delta effects).

Because earthquakes are random in nature, the design and analyses of structures to seismic loading are usually based on a probable response spectrum for a given return period. Design response spectra are usually obtained from design codes containing seismic provisions such as NBCC (2010) which are all based on 5% damping and are determined for a return period of 2475 years, or a probability of exceedance of 2% in 50 years (Filiatrault et al., 2013).

Another measure of the frequency content of ground motion records used by several researchers is the  $A/V$  ratio, where  $A$  is the peak ground motion acceleration (in units of g) and  $V$  is the peak ground motion velocity (in units of m/s). According to El-Attar (1997), low  $A/V$  ground motion records represent low frequency content ground motion records associated with large earthquakes occurring at far epicentre distances. High  $A/V$  ground motion records represent high frequency content and is associated with small earthquakes at short epicentre distances. Low values of  $A/V$  (less than 0.8) represent low frequency content ground motion records while high values of  $A/V$  (more than 1.2) represent high frequency content ground motion records. The  $A/V$  values in the range of 0.8 to 1.2 are considered representative of ground motion records with intermediate frequency content.

### 2.8.1. Seismic Hazard in Canada

As mentioned in the Introduction section, most of the high-voltage transmission line infrastructure in Canada is located in British Columbia and Quebec, two of the provinces with the highest number of significant earthquakes recorded in the country. Fig. 2.5 depicts the locations of significant earthquakes recorded in Canada.

According to Adams and Atkinson (2003), about 25% and 14% of earthquakes recorded in Canada are in the western and eastern regions of the country, respectively. Among significant earthquakes, are those with magnitude 6 or greater. Lamontagne et al. (2008) showed that 60% of significant earthquakes have been recorded in western Canada (British Columbia) and 25% in eastern Canada.

This relatively higher level of seismicity in western and eastern Canada will affect the performance of high-voltage transmission line infrastructure. Thus, there is a need to consider seismic loading in the design or performance assessment of this type of infrastructure and its components.

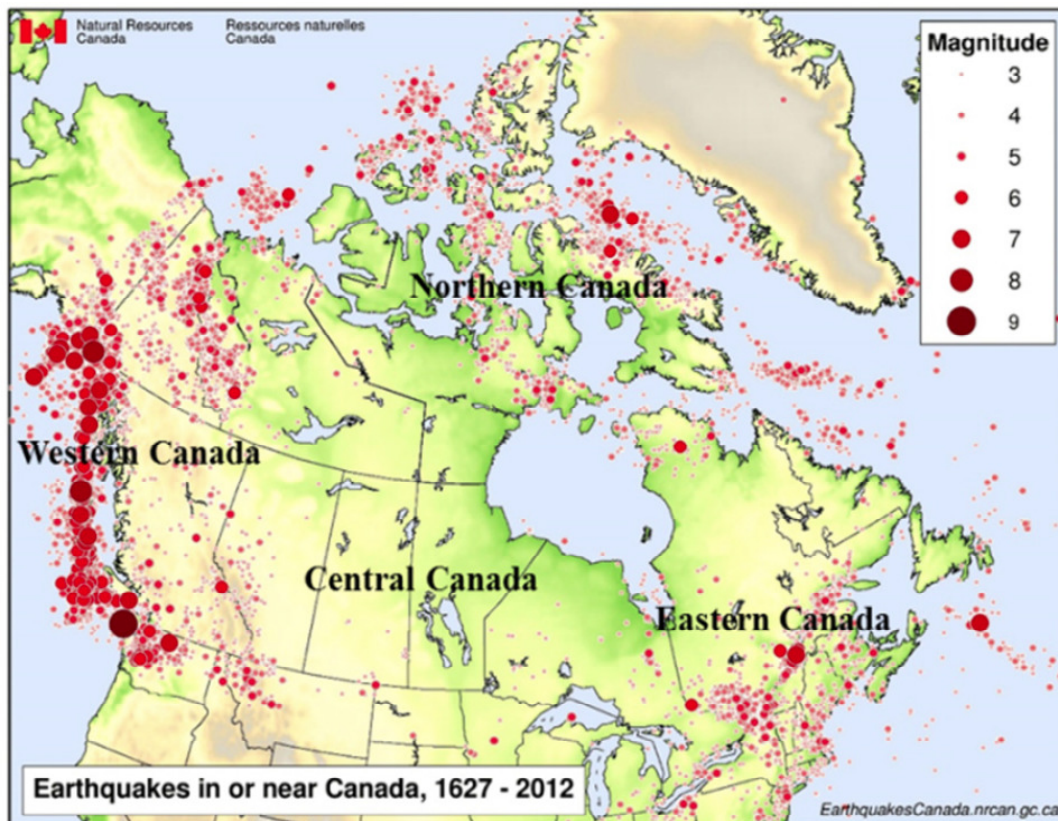


**Figure 2.5. Locations of significant Earthquakes recorded between 1627 and 2012 (NRC).**

## 2.9. Static and Dynamic Properties of Guy Cables

A suspended guy cable in a static position adopts a catenary profile in which the degree of sag of the cable, below a straight line joining its two ends as shown in Fig. 2.6, is a nonlinear function defined by its own weight and by the installed pretension in the guy cable. Guy tower cables are pre-tensioned to a certain percentage of its design tension capacity in order to provide enough lateral stability to the tower structure. This installed pretension is usually in the range of 6% to 8% of the guy's tensions capacity.

The resistance that a guy cable imposes to the horizontal movement of the tower mast is generated by two physical mechanisms: elastic stretching of the cable and changes of sag in the cable geometry (Madugula et. al, 2001). The relative contribution of these two mechanisms will vary according to the degree of tightness of the cable. Elastic stretching provides most of the resistance for a tight cable, whereas the amount of sag provides all the resistance for a slack cable.

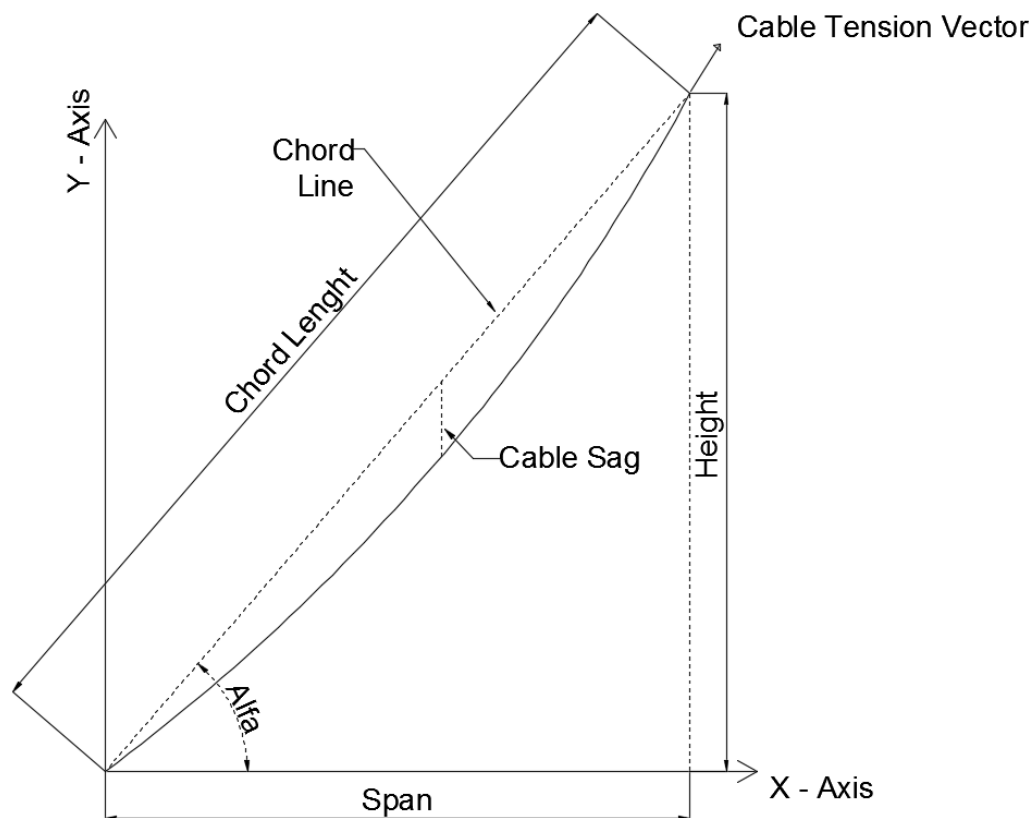


**Figure 2.6. Profile of a suspended guy cable.**

The analyst of a guyed tower has two choices for modelling the horizontal stiffness imposed by the guy cable to the displacement of the tower mast: a finite element approach, in which the cable is discretized into a series of tension-only elements; or an analytical expression that considers all parameters intervenient to the horizontal stiffness. Shears (1968) demonstrated that, if the sag is small relative to the cable length, the profile of the cable can be approximated by a parabolic curve and the horizontal stiffness  $k_h$  of the guy cable can be determined by the following expression:

$$k_h = k_e \times \left[ 1 + \frac{W_G \times L^3 \times k_e}{12 \times T^3 \times \left\{ 1 + 2.67 \times \left( \frac{\delta}{L} \right)^2 \right\}} \right]^{-1} \quad (2.3)$$

where  $L$  is the length of the chord line,  $\delta$  is the maximum sag,  $W_G$  is the unit weight of the cable and  $T$  is the average cable tension. The variable  $k_e$  represents the horizontal stiffness of a perfectly taut cable, and is given by the following expression:

$$k_e = \frac{A \times E}{L} \times \cos^2 \alpha \quad (2.4)$$

where  $\frac{A \times E}{L}$  represents the axial stiffness of the cable and  $\alpha$  is the angle between the chord line and the horizontal axis of reference (refer to Fig. 2.6). For a guy cable that is radiating from the direction of the applied load, the horizontal stiffness at the guy support level is adjusted by the following expression, where  $\beta$  is the angle measured in the horizontal plan between the guy and the direction of the mast displacement:

$$k_{h-efec} = k_h \times \cos^2 \beta \quad (2.5)$$

The expression of Eq. (2.3) proposed by Shears (1968) has limitations in determining the horizontal stiffness of the slackened cable as the mast deflects laterally under load. Because the sag rapidly increases in the slackened cable, the parabolic profile approximation used to derive Eq. (2.3) becomes less accurate. In this regard, Madugula et. al (2001) suggested that the horizontal stiffness of these slackened cables to be determined using a nonlinear catenary equation, or alternatively using the finite element method.

The above expressions are applicable for static analysis, only. For dynamic analysis, it is necessary to recognize that the restraint imposed by a guy cable to resist the horizontal displacement of the tower mast is also dependent on the frequency of the imposed motion. In addition, the phase shift between the amplitude of the mast displacement and the cable peak resisting force, caused by damping, is also frequency dependent (Madugula et. al, 2001). Davenport and Steels (1965) and Starossek (1991) proposed expressions for deriving the dynamic stiffness of taut cables based on the assumption of linear behavior. However, as observed by Madugula et. al (2001), the dynamic behaviour of guy cables can deviate significantly from predictions based on linear theory because of significant nonlinear behavior associated with cable curvature and variations in cable tension caused by vibratory movement.

### **2.10. Natural Frequencies of Vibration of Lattice TL Towers**

The dynamic loads transmitted to tower structures may become damaging when amplified by the effects of tower or member resonance. It is, therefore, important to know the natural frequencies of tower structures and its members. Towers have many different ways to vibrate, and the movements of a tower structure under dynamic forces can be discretized into the contribution of several natural modes of vibration. Modes of vibration can be considered for the overall structure, for parts of the tower structure (such as for guy cables) or for the tower members. The overall structure and substructure modes of vibration are generally obtainable with a standard numerical model, but modes of vibration for members requires very detailed analysis in which the members themselves are discretized in finite elements.

Table 2.3 lists the frequency for the first mode of vibration of guyed and self-supported TL towers found in the literature, including that of towers studied herein. It can be noted that the range of natural frequencies of guyed towers are different from those for typical self-supported lattice towers. Guyed towers are inherently more flexible than typical lattice Self-supporting towers. According to the information given in this table, guyed towers have their first natural frequency in the range of 1.7 Hz to 2.5 Hz whereas typical self-supported towers have their first natural frequencies in the range of 1.1 Hz to 4.9 Hz. From this table it can be also noted that the range of natural frequencies for TL lattice towers is approximately within the range of ground motion frequencies. In NBCC (2010), for instance, typical spectral response accelerations are in the range of period from 0.2 to 0.5 seconds (2.0 Hz to 5.0 Hz).

**Table 2.3. Summary of natural frequencies of vibration for tower structures and members reported in the literature.**

Study / Report	Tower Type and Characteristics	Natural Vibration Frequency
EPRI (2009).	Guyed Tower (single-circuit mast)	2.2 Hz (1 <sup>st</sup> structure mode); 12.4 Hz (substructure mode); 0.9 Hz (local Guy mode)
Gani and Légeron (2010)	Guyed Tower (single-circuit mast)	1.7 Hz (1 <sup>st</sup> structure mode - transversal)
Present study (2016)	Guyed Tower (single-circuit delta) <i>height = 37.7 meters; mass = 5,535 kg</i>	1.9 Hz (1 <sup>st</sup> flexural mode - transversal) 2.5 Hz (1 <sup>st</sup> flexural mode - longitudinal)
	Guyed Tower (single-circuit mast) <i>height = 53.1 meters; mass = 7,930 kg</i>	1.8 Hz (1 <sup>st</sup> flexural mode - transversal) 2.2 Hz (1 <sup>st</sup> flexural mode - longitudinal)
Long (1974)	Self-supporting Tower <i>height = 43.0 meters</i>	5.0 Hz (1 <sup>st</sup> structure mode of vibration)
El-Attar (1997)	Self-supporting Tower <i>height = 41.6 meters; mass = 11,100 kg</i>	1.8 Hz (1 <sup>st</sup> structure mode of vibration)
	Self-supporting Tower <i>height = 29.6 meters; mass = 7,000 kg</i>	3.5 Hz (1 <sup>st</sup> structure mode of vibration)
Ghobarah et al. (1995)	Self-supporting Tower <i>height = 41.6 meters</i>	1.8 Hz (1 <sup>st</sup> structure mode of vibration)
Yasui et al. (1999)	Self-supporting Tower <i>height = 71.0 meters</i>	1.3 Hz (1 <sup>st</sup> flexural mode - transversal) 1.3 Hz (1 <sup>st</sup> flexural mode - longitudinal)
Mara, T. G. (2013)	Self-supporting Tower <i>height = 46.9 meters</i>	1.1 Hz (1 <sup>st</sup> flexural mode - transversal) 1.2 Hz (1 <sup>st</sup> flexural mode - longitudinal)
Present study (2016)	Self-supporting Tower <i>height = 36.6 meters; mass = 23,680 kg</i>	3.9 Hz (1 <sup>st</sup> flexural mode - transversal) 4.9 Hz (1 <sup>st</sup> flexural mode - longitudinal)
	Self-supporting Tower <i>height = 57.1 meters; mass = 48,277 kg</i>	4.1 Hz (1 <sup>st</sup> flexural mode - transversal) 4.1 Hz (1 <sup>st</sup> flexural mode - longitudinal)
Khedr (1998)	Self-supporting Tower <i>height = 48.2 meters; mass = 13,500 kg</i>	3.4 Hz (1 <sup>st</sup> flexural mode - transversal) 3.5 Hz (1 <sup>st</sup> flexural mode - longitudinal)
	Self-supporting Tower <i>height = 41.6 meters; mass = 5,500 kg</i>	3.3 Hz (1 <sup>st</sup> flexural mode - transversal) 3.3 Hz (1 <sup>st</sup> flexural mode - longitudinal)
	Self-supporting Tower <i>height = 48.5 meters; mass = 6,500 kg</i>	2.4 Hz (1 <sup>st</sup> flexural mode - transversal) 2.4 Hz (1 <sup>st</sup> flexural mode - longitudinal)
	Self-supporting Tower <i>height = 34.9 meters; mass = 5,000 kg</i>	2.2 Hz (1 <sup>st</sup> flexural mode - transversal) 2.2 Hz (1 <sup>st</sup> flexural mode - longitudinal)
	Self-supporting Tower <i>height = 58.0 meters; mass = 13,000 kg</i>	2.1 Hz (1 <sup>st</sup> flexural mode - transversal) 2.2 Hz (1 <sup>st</sup> flexural mode - longitudinal)
	Self-supporting Tower <i>height = 36.5 meters; mass = 4,500 kg</i>	2.1 Hz (1 <sup>st</sup> flexural mode - transversal) 2.1 Hz (1 <sup>st</sup> flexural mode - longitudinal)

## **2.11. Research Background and Literature Review**

From the literature review it is shown that seismic analysis of TL towers has received little attention as compared with other similar non building structures such as telecommunication towers. While most of the research carried out so far on this subject was devoted to Self-supporting towers and the coupled dynamic behaviour of this type of tower with the overhead conductor motion, virtually no work addressed guyed towers specifically, or at least no published work on the seismic analysis of guyed towers was found. In general, researchers divided themselves in two groups in regards to their conclusions about the dynamic interaction between the supporting tower and overhead conductors. While one group concluded that the dynamic interactions between tower and overhead conductor are negligible, the other group recommended detail dynamic analysis in the case that a given TL tower needs to be checked for seismic loading. Again, it should be mentioned that most of the investigated studies on the seismic response of TLs were carried out for stiff Self-supporting towers, suspension Self-supporting towers with light overhead conductors and very tall Self-supporting towers used for long span applications such as river crossings.

The presented literature review also showed that there is a lack of research on seismic response of TL towers. Nowadays, concerns related to seismic performance of high-voltage transmission infrastructure has increased among operators. In addition, the standards currently used in Canada and in the US for the design of transmission lines do not address this concern. Also, the use of guyed towers as supporting structures for high-voltage transmission lines has increased in recent years and no experience on the seismic performance of these towers has been found in the literature. Finally, it should be mentioned that guyed towers are a relatively new application as supporting structures for transmission lines as compared with the Self-supporting type of tower that is a typical lattice configuration found in most of the existing or older transmission lines.

In the case that a seismic analysis of a TL guyed tower is required, designers are currently left with no guidance or choice of simplified or established method to be used in design. Because dynamic analysis is time consuming and, in many cases, no suitable for concept level design or analysis, designers may be tempted to use simplified static methods developed for earthquake-resistant buildings or other types of nonbuilding structures.

However, using the later systems is not applicable to TL towers design which show inherent nonlinear and complex dynamic behavior associated with coupled dynamic interaction of the tower-conductor system and, in the case of guyed towers, coupled dynamic interactions of the mast-guy system.

This situation serves as a motivation for this thesis to develop and propose simplified static equivalent methods capable of, at least, approximate the response given by detailed dynamic analysis. However, as indicated in previous research work, this is perceived as a difficult task since is not always possible to identify trends and develop parametric relationships suitable to be extended to other types of geometric and structural configurations.

## CHAPTER III METHODOLOGY

### 3.1. General

This section describes the general methodology used in this study to attain the objectives stated in Chapter I. To attain these objectives, the work described in the following paragraphs was carried out.. Hence, Fig. 3.1 depicts a flowchart of methodology applied to study the dynamic responses of studied TL towers without and with the consideration of the interaction between guyed tower and supported overhead conductors. All studied TL towers (two guyed towers and two Self-supporting towers) were subjected to seismic ground motions. These towers were designed, tested and built in Canada in accordance with the following standards: CAN/CSA C22.3 No. 1-10 – *Overhead systems* and ASCE 10-97 – *Design of latticed steel transmission structures*. The design of these towers was checked in this study to comply with the newest version the ASCE10-15 (2015) standard. It was found that they meet the requirements of this standard.

Based on the proposed methodology it was required to develop finite element numerical models (FEM) and determine the capacities of TL towers members according to the guidelines of design standards currently used in Canada. FEM models were developed in both PLS-TOWER and ANSYS-APDL software for each studied tower. PLS-TOWER software was used to simulate the static nonlinear response of the towers under design loading conditions and to determine tower member capacities based on the ASCE 10-15 design standard. Since the PLS-TOWER software used currently in design practice has no dynamic capabilities, the classical version of ANSYS Mechanical, namely ANSYS APDL, was used to assess the dynamic properties of these towers and to perform detailed nonlinear transient simulations for deriving the seismic responses. A program was developed using the FORTRAN programming language to translate PLS-TOWER model echo files containing data and information about the towers structure`s geometric configuration, member dimensions and cross-section properties, member connectivity and material properties, into input files for ANSYS-APDL, in order to ensure that both models have the same properties. The dynamic properties of these towers were then studied using ANSYS-APDL. Modal analyses were carried out for determining the mode shapes of vibration and their frequency. Harmonic excitation analyses were performed for deriving complete response spectra for a range of forced vibration frequencies.

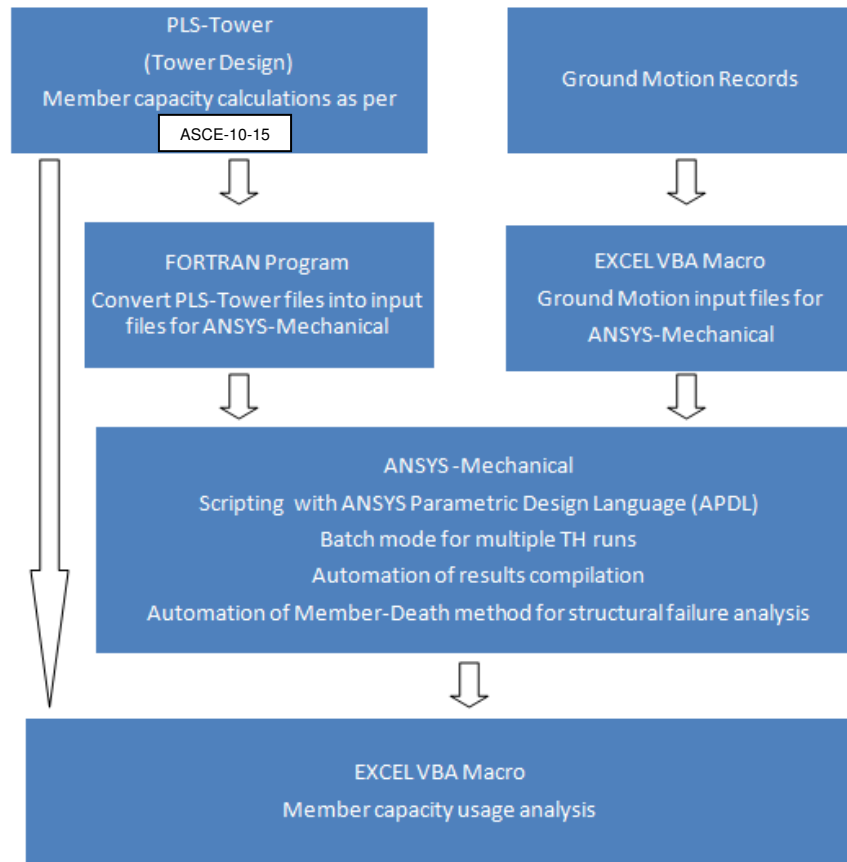


**Figure 3.1. Flowchart illustrating the proposed methodology.**

Twenty earthquake ground-acceleration records (i.e. accelerograms), with frequency content close to the natural frequencies of the studied towers, were selected and scaled to match the response acceleration design spectra given in NBCC (2010) for a given location and site class. Ten of these records are characteristic for site class C while the other ten records are characteristic for site class D. The studied TL towers were located in British Columbia in the vicinity of Vancouver. A scaling factor resulted from calculation was apply to these records such that the frequency content of these accelerograms was preserved. These ground motion records were taken from PEER Database and Excel spreadsheets were used to scale them to the target response design spectra. Excel VBA macros were developed to translate the scaled ground motion records into seismic input to be used in ANSYS-APDL for dynamic time-history analyses.

Detailed nonlinear dynamic analyses were performed for the towers studied herein. Each tower was subjected to 20 scaled ground motions (10 records were scaled for site class C and 10 for site class D). The free-standing towers were subjected to earthquake ground motions in three orthogonal directions of incidence (namely longitudinal, transversal and vertical) totalling 60 dynamic simulations for each tower.

Scripts were developed using the Parametric Design Language (PDL) available in ANSYS to allow ANSYS-APDL to perform multiple simulations in batch mode for the various ground motion scenarios studied herein and to finally compile the time-history results of each simulation into formats suitable for analyses of large amounts of data using Excel spreadsheets. Time-history outputs compiled from ANSYS-APDL are axial forces in each member, displacements of overhead conductor support and horizontal and vertical base shear reactions resulted from earthquake ground motion excitations. It is noted that these nonlinear transient simulations were performed in the elastic domain of the steel materials since, according to calculations performed with the PLS-TOWER software, the capacity of members are governed by their buckling strength or adjacent connection strength. It is also noted that the main forces in latticed structures are axial forces acting either on compression or tension, therefore only the time-history of axial forces are of interest for the present analyses.

Another Excel VBA macro was then developed to compare the peak axial force response for each member of studied tower with its capacity, as well as to identify the load case that triggers the maximum axial forces. These comparisons allowed the identification of the earthquake load cases where member failure or even structural instability resulting in structural failure could occur. In addition, from these comparisons it can be quantified the relevance of considering seismic forces in tower design in regards to other design load cases.

A second batch run of earthquake ground motion simulations was then performed only for the selected set of seismic cases where the capacity of at least one member was exceeded. In these simulations, however, the member-death method available in ANSYS-APDL, based on the EKILL command, was used to simulate the failure of a member when its capacity is exceeded. In this method, when a given response exceeds a limiting value, a zero value is attributed to the stiffness of this member, signifying that this member is no longer capable of transmitting forces to its adjacent nodes. In the case of the studied towers, the response in question is the axial force.

A script was developed within the APD Language environment, using the EKILL command, to compare, in every time-step of the transient simulations, the response axial forces for all tower members with their respective capacities. Structural instability, as consequence of sequential failure member, was assessed and the number of seismic cases with only damage to structural members or complete structural failure was determined for each tower. During these dynamic simulations, members with axial forces exceeding their respective capacities, as determined with the PLS-Tower software and based on the ASCE-10-15 standard, were turned off with the EKILL command.

Finally, detailed nonlinear transient seismic simulations considering the coupled tower-conductor system were performed only for the guyed tower identified as the most sensitive to seismic loading and for the three ground motion cases that resulted in higher seismic responses for this tower. In these simulations, four equal and level spans of overhead conductors and ground-wires supported by three delta guyed towers are considered. Details about the numerical models developed for the present study are presented in the subsequent sections of this chapter.

The results of analyses carried out in this research work were used to derive expressions for the estimation of horizontal seismic base shear forces for each tower. An equivalent static method is proposed for the guyed towers studied herein and its responses for each tower member are compared with the responses from detailed nonlinear transient simulations. An assessment of the accuracy of this simplified method is made and discussions concerning the difficulty of implementing this equivalent static method in the design process of these types of structures are conducted. The results of the simulations carried out for the free-standing delta guyed tower and for the coupled tower-conductor system are compared and an assessment is made on the relevance of considering the dynamic interactions between the tower and the overhead cables when subjected to earthquake excitations.

### **3.2. Towers used in the Study**

Four existing latticed high-voltage transmission line towers were used in the present study: two guyed towers and two Self-supporting towers. The guyed towers are suspensions towers of the delta and mast types with heights of 37.7 m and 53.1 m, respectively. The Self-supporting towers are strain or dead-end towers of the delta and mast types with heights of 36.6 m and 57.1 m, respectively. It is noted that both delta towers used in this study are components of the same transmission line project. These delta towers have about the same geometric configuration of

their upper sections, as determined by conductor motion clearances and required support height for conductors and ground-wires. These similarities provides the opportunity for comparing the responses of two towers differing mostly by their supporting configurations (guyed or Self-supporting). It is noted, however, that strain towers are usually stiffer and heavier than suspension towers since the former type is required to resist higher loads than the later, resulting in members with bigger dimensions and therefore heavier than their respective members in guyed towers. These lattice towers are typical TL towers used in North America for supporting high-voltage transmission lines. Some important characteristics of these towers, including their total mass and calculated natural frequencies corresponding to their fundamental flexural modes of vibration in both horizontal directions (transversal and longitudinal), are listed in Table 3.1. The geometric layouts of these towers are illustrated in Figs. 3.2 to 3.5.

Parameters presented in Table 3.1 lead to the following observation: a) guyed towers have lower natural frequency values than Self-supporting towers and b) fundamental flexural frequency of guyed towers are closer to the typical frequency content of ground motion records. The first observation is expected since guyed towers are inherently more flexible than Self-supporting towers of similar height and geometry.

**Table 3.1. Characteristics of the transmission towers studied**

Tower type	Height (m)	Base Width Leg-to-leg (m)	Top Width beam and cross-arm (m)	Total weight (kN)	First Mode Vibration Frequency (Hz)	
					Transversal Direction	Longitudinal Direction
Delta Guyed tower	37.7	-	19.8	54.3	1.93	2.51
Mast Guyed tower	53.1	-	15.6	77.8	1.82	2.20
Delta Self-supporting tower	36.6	13.6	21.8	232.3	3.88	4.94
Mast Self-supporting tower	57.1	18.4	24.0	473.6	4.09	4.07

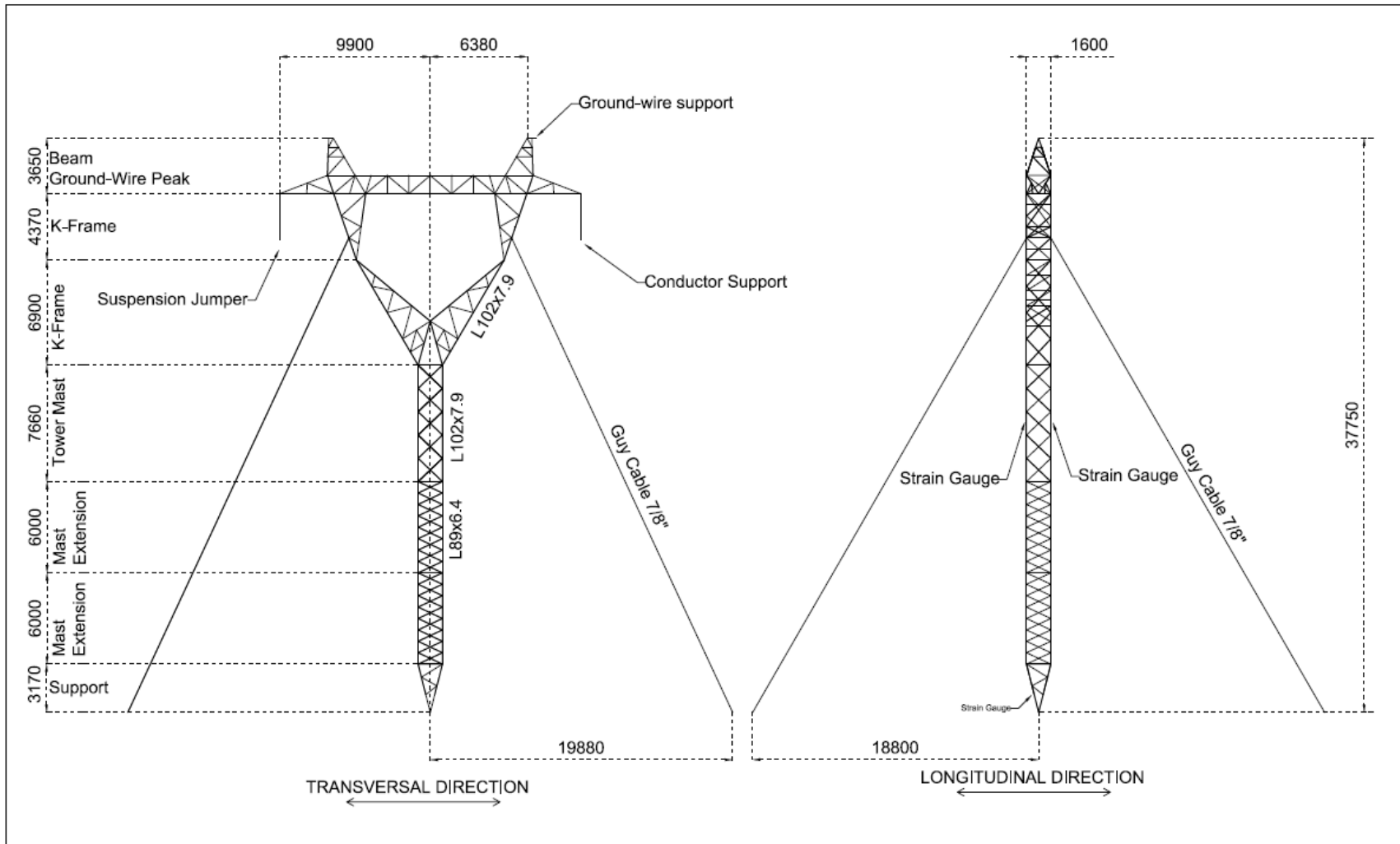


**Figure 3.2. Delta Guyed tower. General layout. (all units in millimetres)**

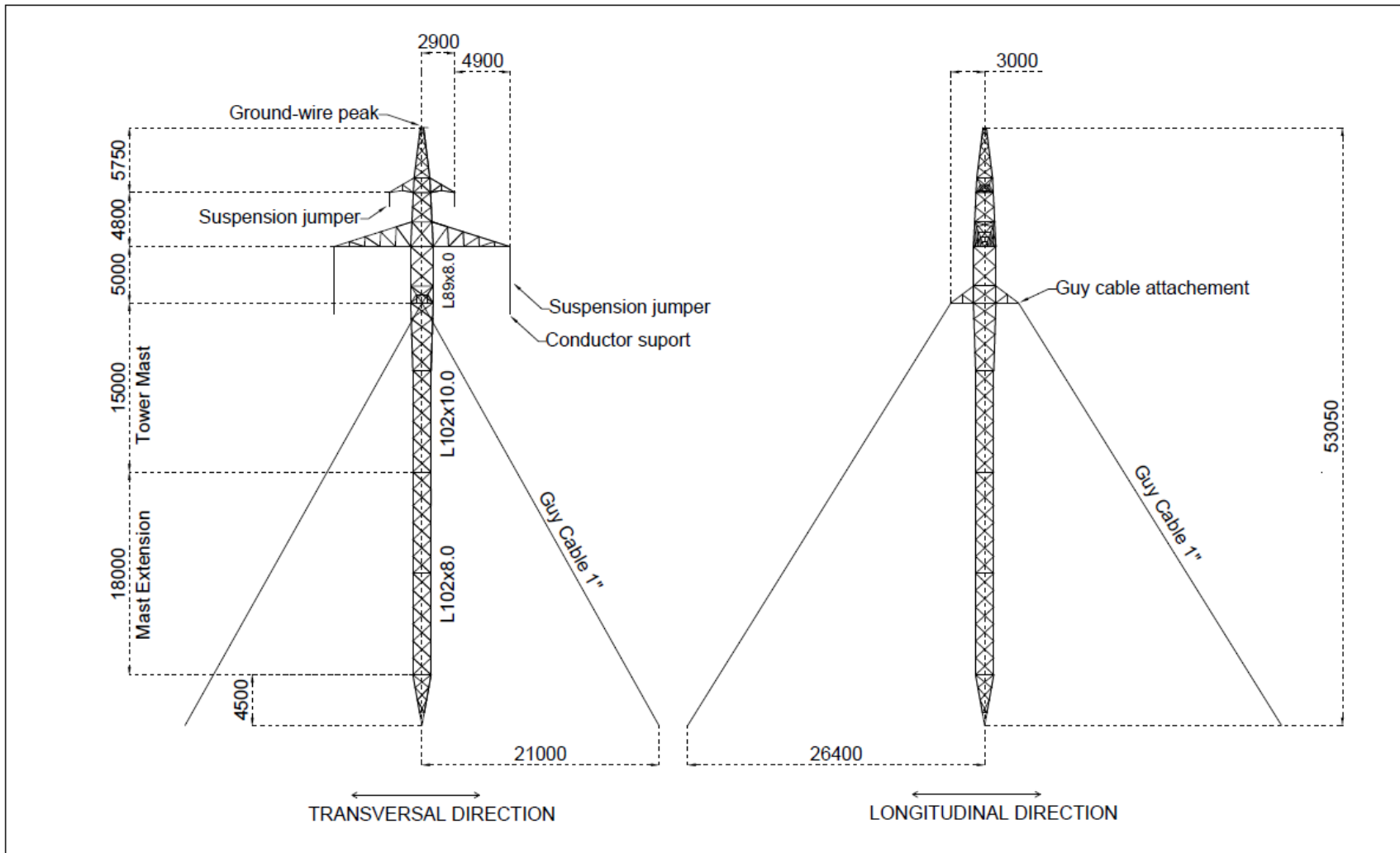


**Figure 3.3. Mast Guyed tower. General layout. (all unit in millimetres)**

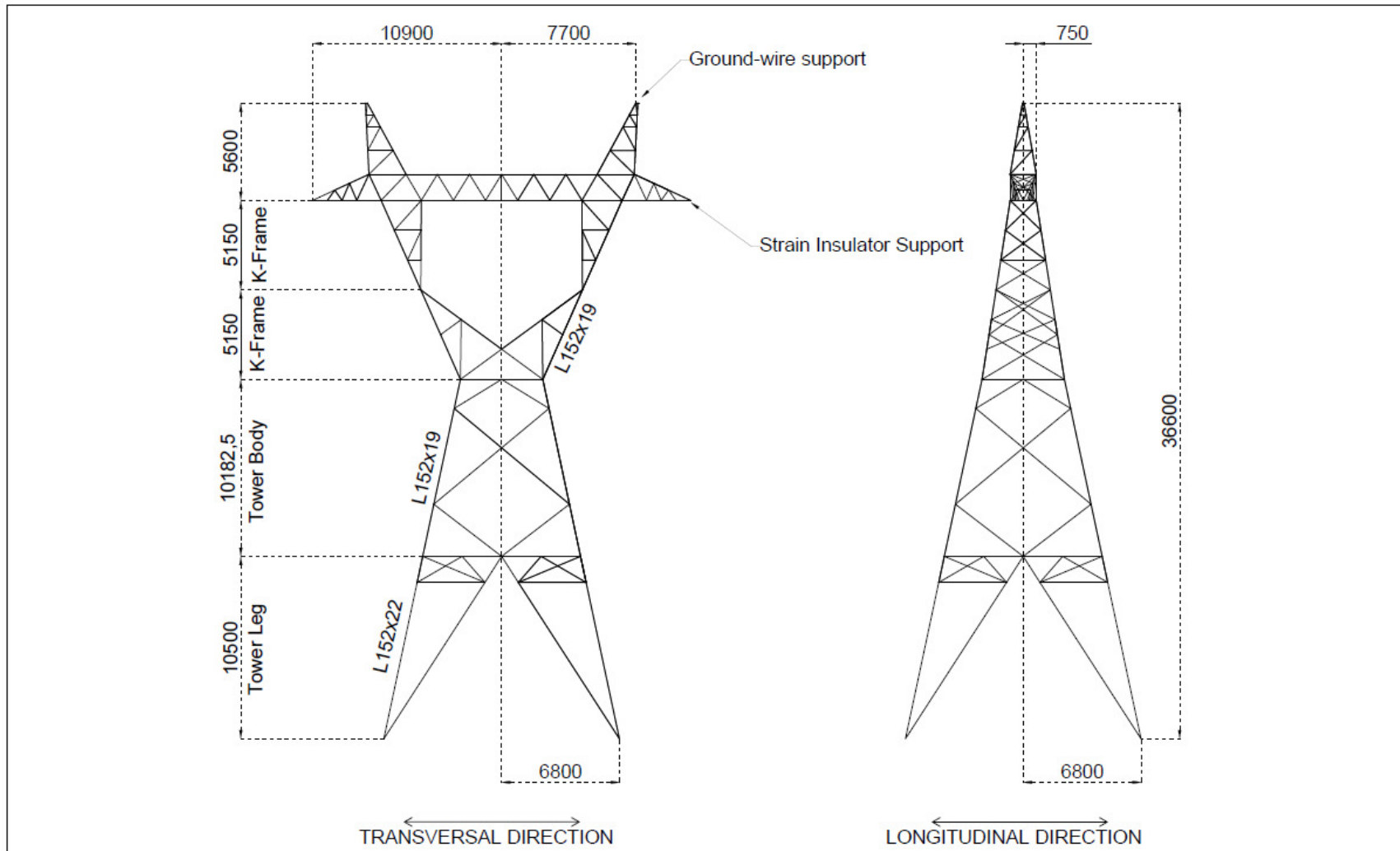


**Figure 3.4. Delta Self-Supported Strain Tower. General layout. (all unit in millimetres)**

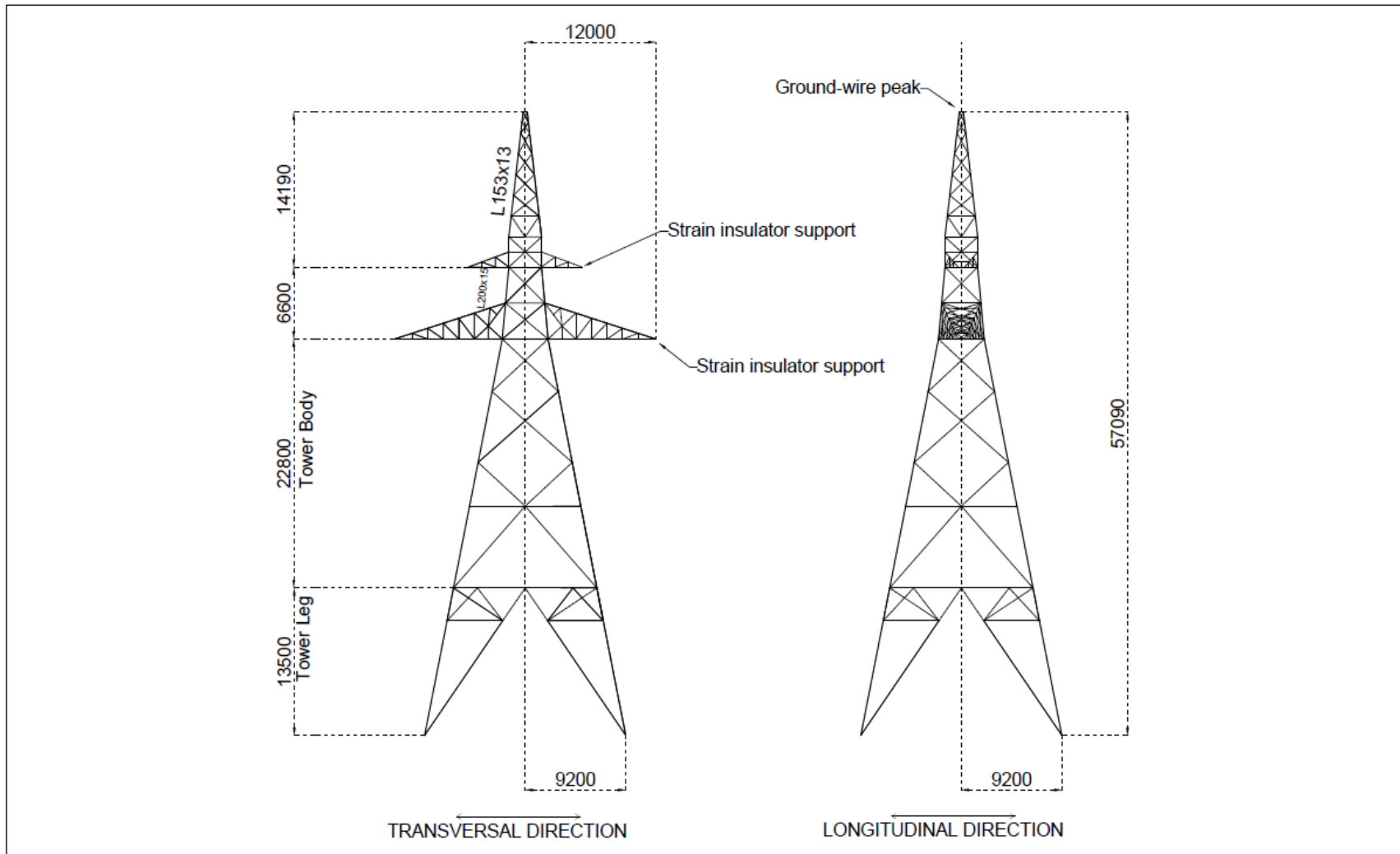


**Figure 3.5. Self-supported Dead End Tower. General layout. (all unit in millimetres)**

### 3.3. Numerical Modelling

All TL towers were modelled as linear elastic three-dimensional structures with frame elements for the main legs and truss elements for all other members such as primary and redundant bracing members. The supports are idealized as pinned on rigid foundations. In ANSYS-APDL, the frame-members are represented by BEAM188 elements and the truss-members are represented by LINK 180 elements. The BEAM188 element is suitable for analyzing slender to moderately stubby beam or frame members and it is based on Timoshenko beam theory which includes the shear-deformation effects (ANSYS, 2013). This element is a linear two-node element with six degrees of freedom: three translational and three rotational. The LINK180 element is suitable for modelling truss-members and sagging cables. This element is a uniaxial tension-compression element with three translational degrees of freedom at each node. The mass of the tower structures is scaled up by a factor of 1.1 to represent the addition of other non-structural elements attached to the tower structures and not directly represented in the model. This scaling is a standard practice in structural analysis carried out for tower design.

The cables are modelled as a sequence of two-node tension-only truss-elements using the LINK180 element available in ANSYS-APDL. Guy cables were modelled by a sequence of 40 tension-only truss-elements. The overhead conductors and ground-wires were modelled by 80 tension-only truss-elements. Prestressing in the guy cables are integrated in the LINK180 elements by using the INISTATE command available in ANSYS-APDL. It is noted that guy cables are usually prestressed when guyed towers are erected. This prestressing is usually in the order of 6% to 8% of the cable design tension force and is intended to enhance the lateral stability of these structures.

For modelling the overhead cables, a trial-and-error procedure involving the number of tension-only truss elements and coordinates of their end nodes was carried out in order to approximate the resulting profile and tensions along the modelled overhead cables to the design catenary profile and tension values. This was done interactively until the resulting profile and tensions are satisfactorily close to design values.

For simulation of free-standing towers, the mass of the overhead cables were calculated, divided equally, and lumped at their respective end nodes. Fig. 3.6 presents general layouts of the towers modelled in ANSYS-APDL environment.

The coupled tower-conductor system involves a significant level of geometric non-linearities due to large displacements of cable joints, therefore requiring significant computational effort. This fact alone suggests that dynamic methods based on linear theory, such as the modal superposition method, are not suitable for these types of structures and nonlinear transient analyses are required to correctly estimate their responses under dynamic loading conditions. Not only the coupled tower-conductor system was simulated using the nonlinear transient method, but also the free-standing towers because of their slenderness, flexibility, and dynamic effects associated with the interactions between the guy-cables and the tower mast.

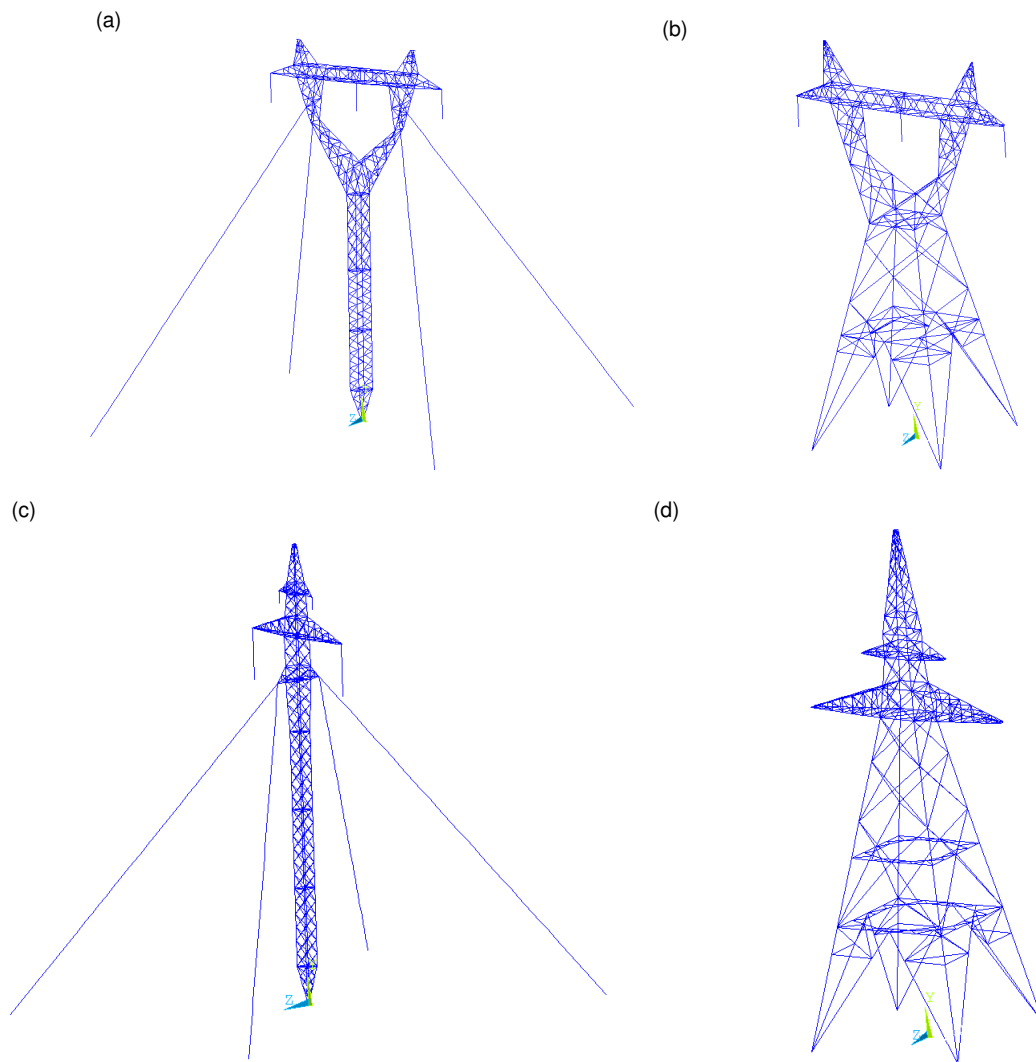


**Figure 3.6. Oblique view of Finite Element Models developed in ANSYS-APDL environment. (a) Delta Guyed tower; (b) Delta Self-supporting tower; (c) Mast Guyed tower; (d) Mast Self-supporting tower.**

### 3.4. Transient Dynamic Analysis

The dynamic response of towers subjected to base excitation from earthquake load is determined by solving the following equation of motion for a MDOF system.

$$[M] \times \{a\} + [C] \times \{v\} + [K] \times \{u\} = -\{F(t)\} \quad (3.1)$$

where  $[M]$  is the global mass matrix,  $\{a\}$  is the relative acceleration vector,  $[C]$  is the global damping matrix,  $\{v\}$  is the relative velocity vector,  $[K]$  is the global stiffness matrix,  $\{u\}$  is the relative displacement vector and  $\{F(t)\}$  is the dynamic (seismic) load vector. In this study, the Newmark time integration method was used to solve this equation of motion at discrete time-steps. These structures were treated as nonlinear systems. In nonlinear structural dynamic problems, the internal forces are not linearly proportional to the nodal displacement and the structural stiffness matrix is updated according to the current nodal displacement. The dynamic equation was solved using the Newmark- $\beta$  constant-average-acceleration method with coefficients  $\beta = 0.25$  and  $\gamma = 0.5$ . A detailed description of the Newmark method can be found in relevant literature, such as Chopra, A. K. (1995), Filiatrault et al. (2013) and on the Theory Reference Guide of ANSYS-APDL (2013).

To obtain reasonable accuracy for the nonlinear transient dynamic simulations, the first simulations were carried out with a time-step  $\Delta t$  corresponding to the following equation (Filiatrault et al., 2013):

$$\frac{\Delta t}{T_n} < 0.02 \quad (3.2)$$

where  $T_n$  is the shortest natural period of the structure. Following the recommendations of Filiatrault et al. (2013), additional simulations were carried out with time-steps half of the time-step established with the relationship expressed by Eq. (3.2). The results from these later simulations were virtually the same and all simulations were then performed with a time-step determined by Eq. (3.2).

The results of nonlinear 2<sup>nd</sup> order static simulations were used to establish the initial conditions for the transient dynamic simulations. These static simulations were based on self-weight loads and prestressing of guy cables and overhead conductors.

### 3.5. Selection and scaling of Earthquake Records

Governing load case for towers studied herein are related to wind loads acting on the latticed structure and on conductors and ground wires. These design wind loads were calculated as per the CSA C22.3 n° 60826-10 standard, and they are a function of the 10-minutes reference wind speed, with a return period of 50 years, for the sites where these towers were design for. Since wind pressures listed in Table C-2 of the NBCC (2010) (appendix C of division B) are calculated from reference wind speeds with a return period of 50 years as well, it is possible, from this table, to establish a set of locations where these towers could be also displaced. It is noted that the potential location should have the same ice loading conditions in addition to wind loading. After the selection of these similar locations in seismic areas, the design spectra are built for each location and the selected ground motions are scaled to match the design spectrum over the periods of interest.

Because the wind pressures listed in Table C-2 of the NBCC (2010) are based on wind speeds averaged on an hourly basis, it is necessary to associate the 10-minutes reference wind speeds used in the design with hourly wind speed values. This association was done using a ratio of probable maximum wind speed averaged over a period of 10-minutes to that averaged over one hour presented on Simiu and Scanlan (1996). The adopted ratio was 1.05. Wind velocity pressures listed in Table C-2 of the NBCC 2010 are then calculated using the following equation:

$$q = 0.5 \times \rho \times V^2 \quad (3.2)$$

where  $q$  is the design wind pressure in units of Pascal (NBCC, 2010),  $\rho$  is the average air density for the windy months of the year (unit of  $\text{kg/m}^3$ ) and  $V$  is the wind speed (unit of  $\text{m/s}$ ).

**Table 3.2. Towers used in the present study and their wind design parameters.**

Tower	10-minutes wind speed (km/h) <sup>(1)</sup>	hourly wind speed (m/s) <sup>(2)</sup>	hourly wind pressure (kPa) <sup>(2)</sup>
Delta Guyed tower	100.0	29.2	0.55
Delta Self-supporting tower			
Mast Guyed tower	120.0	35.0	0.80
Mast Self-supporting tower			

(1) reference wind speed used for design as per CSA C22.3 n° 60826-10 standard; (2) hourly wind speed and pressure as per appendix C of division B of NBCC (2010)

Table 3.2 lists the towers used in the present study, their respective 10-minutes reference wind speeds (used in their design as per CSA C22.3 n° 60826-10 standard) and their respective hourly wind speed and pressure (calculated as per NBCC, 2010). Table 3.3 lists a number of locations in Canada where these towers could have been designed for, and their respective seismic spectral data as per table C-2 of the NBCC (2010). Thirteen (13) locations, out of about 700 locations listed in table C-2 of the NBCC (2010), were identified.

It is noted that only one location with high spectral acceleration values was retained (e.g. Bamfield, B.C.) since one of the objectives of the present study is to assess the relevance of seismic loading in the design of transmission lattice towers in regards to other types of standard load cases. If these higher spectral acceleration values are shown not to be relevant for the structural response of the towers studied herein, than no further analyses would be required for lower spectral acceleration values. In the case that earthquake loads govern the tower design, then the outcomes of the present analyses would suggest that further analyses with lower values of spectral acceleration are necessary in order to somehow improve the quantification of the relevance of considering seismic loading in the structural analysis and design of transmission towers. The selected target spectral values used in the present studied are highlighted in Table 3.3.

Two sets of 10 ground motion records, obtained from PEER Ground Motion Database (2016), was used in the present study. These records contain time-series of ground motion acceleration (i.e. accelerograms), velocities and displacements in three orthogonal directions (two horizontal and one vertical). In the present study, only the vertical time-series and the time-series of the horizontal component with the highest peak ground acceleration value were considered. These ground motion records are listed in Tables 3.4 and 3.5 together with some of their parameters of interest for structural dynamic analyses.

Ten of these records are characteristic of site Class C (NBCC, 2010) while the other ten records are characteristic of site Class D (NBCC, 2010). Site Class C has a ground profile characterized by very dense soil and soft rock (Filiatrault et al., 2013) while site Class D has a ground profile characterized by stiff soil. The parameter that associates a given ground motion record to a given site Class is the shear wave average velocity. Shear wave average velocities in the range from 360 m/s to 760 m/s are associated with site Class C while shear wave average velocities in the range from 180 m/s to 360 m/s are associated with site Class D.

The design acceleration spectral values listed in Table 3.4 and taken from NBCC (2010) are determined for site Class C conditions. Acceleration-based and velocity-based site coefficients,  $F_a$  and  $F_v$ , respectively, are applied to obtain design spectral ordinates  $S(T_n)$  for other site conditions (Finn and Wightman, 2003). The design spectrum acceleration is therefore obtained from the following relationships (Filiatrault et al., 2013):

$$\begin{aligned}
 S(T_n) &= F_a \times S_a(0.2) \quad \text{for } T_n < 0.2 \text{ s} \\
 S(T_n) &= F_a \times S_a(0.2) \text{ or } F_v \times S_a(0.5) \quad \text{for } T_n = 0.2 \text{ s (whichever is lesser)} \\
 S(T_n) &= F_v \times S_a(1.0) \quad \text{for } T_n = 1.0 \text{ s} \\
 S(T_n) &= F_v \times S_a(2.0) \quad \text{for } T_n = 2.0 \text{ s} \\
 S(T_n) &= \frac{F_v \times S_a(2.0)}{2} \quad \text{for } T_n = 4.0 \text{ s}
 \end{aligned} \tag{3.3}$$

The  $F_a$  and  $F_v$  values for site Class D, extracted from NBCC (2010), are given in Table 3.5. Graphical representations of the 40 accelerograms used in the present study (20 in the horizontal direction and 20 in the vertical direction), together with their respective response spectra (evaluated for 5% damping), are presented in Appendix I. As mentioned previously, these accelerograms were scaled to design response spectra which are all based on 5% damping and are determined for a return period of 2475 years which corresponds to a probability of exceedance of 2% in 50 years. The scaling factors used for the vertical component of the accelerograms are the same ones used for scaling the horizontal component of the accelerograms to the target design spectra.

**Table 3.3. Identified locations and their respective seismic spectral values as per NBCC (2010) (site Class C).**

Province	Location	Hourly Wind Pressure (kPa) <sup>(1)</sup>	Seismic Data				
			S <sub>a</sub> (0.2) <sup>(2)</sup>	S <sub>a</sub> (0.5) <sup>(2)</sup>	S <sub>a</sub> (1.0) <sup>(2)</sup>	S <sub>a</sub> (2.0) <sup>(2)</sup>	PGA <sup>(3)</sup>
British Columbia	Bamfield	0.50	1.10	0.89	0.45	0.20	0.49
	Nanaimo	0.50	1.00	0.69	0.38	0.18	0.50
	Port Renfrew	0.52	1.00	0.81	0.41	0.18	0.45
	Jordan River	0.55	0.99	0.78	0.40	0.17	0.47
	Parksville	0.50	0.86	0.61	0.32	0.17	0.42
	Qualicum Beach	0.53	0.82	0.58	0.31	0.17	0.39
	Squamish	0.50	0.72	0.52	0.30	0.16	0.33
	Powell River	0.51	0.67	0.49	0.29	0.16	0.31
	Comox	0.52	0.66	0.49	0.29	0.16	0.30
	Campbell River	0.52	0.63	0.46	0.28	0.15	0.28
	Sandspit	0.78	0.56	0.48	0.40	0.20	0.29
Quebec	La Pocatière	0.50	2.00	1.00	0.46	0.14	1.10
	Rivière-du-Loup	0.50	1.00	0.56	0.24	0.08	0.49
	St-Georges-de-Cacouna	0.50	0.80	0.46	0.21	0.07	0.39

(1) hourly wind pressure with a return period of 1:50-year. Table C-2, appendix C of division B of NBCC (2010).  
(2) spectral acceleration values in units of g (m/s<sup>2</sup>); (3) peak ground acceleration

NBCC (2010) has no specific provisions regarding scaling of ground motion records. However, it is mentioned that all ground motion records considered in the analyses should be scaled to match the design spectrum (DS) at the fundamental period  $T_1$  of the structure. ASCE/SEI.7-10 (2013) provisions require that the mean of the 5% damped response spectra of at least 7 ground motion records should match or be above the target spectra over the interval of  $0.2T_1$  to  $1.5T_1$ . . This provision was adopted in the present study for scaling the selected ground motion records. Scaled acceleration response spectra for site Classes C and D are presented in Figs. 3.7 and 3.8. It is noted that only the ordinates of the acceleration response spectra were scaled, thus maintaining the frequency content of the original records.

**Table 3.4. Coefficients  $F_a$  and  $F_v$  specified in NBCC (2010) for site Class D.**

$F_a$				
$S_a(0.2) \leq 0.25$	$S_a(0.2) = 0.50$	$S_a(0.2) = 0.75$	$S_a(0.2) = 1.00$	$S_a(0.2) \geq 1.25$
1.3	1.2	1.1	1.1	1.0
$F_v$				
$S_a(1.0) \leq 0.10$	$S_a(1.0) = 0.20$	$S_a(1.0) = 0.30$	$S_a(1.0) = 0.40$	$S_a(1.0) \geq 0.50$
1.4	1.3	1.2	1.1	1.1

**Table 3.5. Earthquake records selected – horizontal component.**

Site Class	NGA n°	Event	Station	M <sub>w</sub> <sup>(1)</sup>	V <sub>s</sub> <sup>(2)</sup> (m/s)	T <sub>p</sub> <sup>(3)</sup> (sec)	T <sub>m</sub> <sup>(4)</sup> (sec)	A <sub>g</sub> <sup>(5)</sup> (g)	A/V <sup>(6)</sup> Ratio
<b>C</b>	963	Jan. 17, 1994 Northridge	Castaic, Old Ridge Route	6.7	450	0.26	0.54	0.63	1.10
	986	Jan. 17, 1994 Northridge	LA - Brentwood VA Hospital	6.7	417	0.24	0.63	0.41	0.77
	1005	Jan. 17, 1994 Northridge	LA - Temple & Hope	6.7	452	0.20	0.47	0.42	0.92
	1006	Jan. 17, 1994 Northridge	LA - UCLA Grounds	6.7	398	0.22	0.34	0.64	1.27
	57	Feb. 9, 1971 San Fernando	Castaic, Old Ridge Route	6.6	450	0.20	0.51	0.63	0.96
	735	Oct. 18, 1989 Loma Prieta	APEEL 7 - Pulgas	6.9	415	0.44	0.66	0.36	1.00
	1787	Oct. 16, 1999 Hector Mines	Hector	7.1	726	0.50	0.63	0.36	0.73
	1794	Oct. 16, 1999 Hector Mines	Joshua Tree	7.1	379	0.36	0.59	0.44	0.77
	15	July 21, 1952 Kern County	Taft Lincoln School	7.4	385	0.36	0.54	0.37	1.04
	739	Oct. 18, 1989 Loma Prieta	Anderson Dam (Downstream)	6.9	489	0.20	0.47	0.57	1.13
<b>D</b>	953	Jan. 17, 1994 Northridge	Beverly Hills - 14145 Mulhol	6.7	356	0.52	0.74	0.84	0.75
	1039	Jan. 17, 1994 Northridge	Moorpark - Fire Sta	6.7	342	0.26	0.47	0.67	1.43
	1049	Jan. 17, 1994 Northridge	Pacific Palisades-Sunset	6.7	191	0.24	0.34	0.47	1.42
	767	Oct. 18, 1989 Loma Prieta	Gilroy Array #3	6.9	350	0.20	0.37	0.62	1.54
	776	Oct. 18, 1989 Loma Prieta	Hollister - South & Pine	6.9	282	0.52	0.91	0.38	0.58
	900	June 28, 1992 Landers	Yermo Fire Station	7.3	354	0.68	0.91	0.42	0.48
	848	1992 Lander	Coolwater, TR	7.3	353	0.34	0.56	0.58	0.96
	766	1989 Loma Prieta	Gilroy Array 2	6.9	271	0.38	0.54	0.55	1.06
	721	1987 Superstition Hills-02	El Centro Imp. Co. Cent, 90°	6.5	192	0.22	0.66	0.68	0.74
	174	1979 Imperial Valley-06	El Centro Array 11, 230°	6.5	196	0.26	0.42	0.57	0.85
<b>Statistics</b>			<b>Max</b>	<b>7.4</b>	<b>726</b>	<b>0.68</b>	<b>0.91</b>	<b>0.84</b>	<b>1.54</b>
			<b>Min</b>	<b>6.5</b>	<b>191</b>	<b>0.20</b>	<b>0.34</b>	<b>0.36</b>	<b>0.48</b>
			<b>Mean</b>	<b>6.9</b>	<b>372</b>	<b>0.33</b>	<b>0.56</b>	<b>0.53</b>	<b>0.98</b>

(1) earthquake ground motion magnitude; (2) shear wave average velocity; (3) predominant period; (4) mean period; (5) peak earthquake ground motion acceleration; (6) ration of peak ground motion acceleration to peak velocity.

**Table 3.6. Earthquake records selected – vertical component.**

Site Class	NGA n°	Event	Station	M <sub>w</sub> <sup>(1)</sup>	V <sub>s</sub> <sup>(2)</sup> (m/s)	T <sub>p</sub> <sup>(3)</sup> (sec)	T <sub>m</sub> <sup>(4)</sup> (sec)	A <sub>g</sub> <sup>(5)</sup> (g)	A/V <sup>(6)</sup> Ratio
<b>C</b>	963	Jan. 17, 1994 Northridge	Castaic, Old Ridge Route	6.7	450	0.28	0.33	0.24	1.77
	986	Jan. 17, 1994 Northridge	LA - Brentwood VA Hospital	6.7	417	0.20	0.34	0.30	1.52
	1005	Jan. 17, 1994 Northridge	LA - Temple & Hope	6.7	452	0.08	0.31	0.22	2.12
	1006	Jan. 17, 1994 Northridge	LA - UCLA Grounds	6.7	398	0.22	0.31	0.61	2.60
	57	Feb. 9, 1971 San Fernando	Castaic, Old Ridge Route	6.6	450	0.20	0.26	0.38	2.08
	735	Oct. 18, 1989 Loma Prieta	APEEL 7 - Pulgas	6.9	415	0.92	0.61	0.14	1.00
	1787	Oct. 16, 1999 Hector Mines	Hector	7.1	726	0.28	0.39	0.16	1.25
	1794	Oct. 16, 1999 Hector Mines	Joshua Tree	7.1	379	0.52	0.47	0.28	1.15
	15	July 21, 1952 Kern County	Taft Lincoln School	7.4	385	0.34	0.44	0.25	1.63
	739	Oct. 18, 1989 Loma Prieta	Anderson Dam (Downstream)	6.9	489	0.06	0.37	0.36	1.50
<b>D</b>	953	Jan. 17, 1994 Northridge	Beverly Hills - 14145 Mulhol	6.7	356	0.22	0.34	0.62	1.60
	1039	Jan. 17, 1994 Northridge	Moorpark - Fire Sta	6.7	342	0.20	0.29	0.37	2.04
	1049	Jan. 17, 1994 Northridge	Pacific Palisades-Sunset	6.7	191	0.18	0.32	0.40	1.14
	767	Oct. 18, 1989 Loma Prieta	Gilroy Array #3	6.9	350	0.06	0.28	0.38	2.18
	776	Oct. 18, 1989 Loma Prieta	Hollister - South & Pine	6.9	282	0.14	0.70	0.41	1.29
	900	June 28, 1992 Landers	Yermo Fire Station	7.3	354	0.20	0.30	0.23	1.05
	848	1992 Lander	Coolwater, TR	7.3	353	0.10	0.23	0.25	1.77
	766	1989 Loma Prieta	Gilroy Array 2	6.9	271	0.08	0.24	0.44	1.79
	721	1987 Superstition Hills-02	El Centro Imp. Co. Cent, 90°	6.5	192	0.10	0.49	0.24	1.55
	174	1979 Imperial Valley-06	El Centro Array 11, 230°	6.5	196	0.14	0.45	0.22	1.24
<b>Statistics</b>			<b>Max</b>	<b>7.4</b>	<b>726</b>	<b>0.92</b>	<b>0.70</b>	<b>0.617</b>	<b>2.60</b>
			<b>Min</b>	<b>6.5</b>	<b>191</b>	<b>0.06</b>	<b>0.23</b>	<b>0.141</b>	<b>1.00</b>
			<b>Mean</b>	<b>6.9</b>	<b>372</b>	<b>0.23</b>	<b>0.37</b>	<b>0.326</b>	<b>1.61</b>

(1) earthquake ground motion magnitude; (2) shear wave average velocity; (3) predominant period; (4) mean period; (5) peak earthquake ground motion acceleration; (6) ration of peak ground motion acceleration to peak velocity.

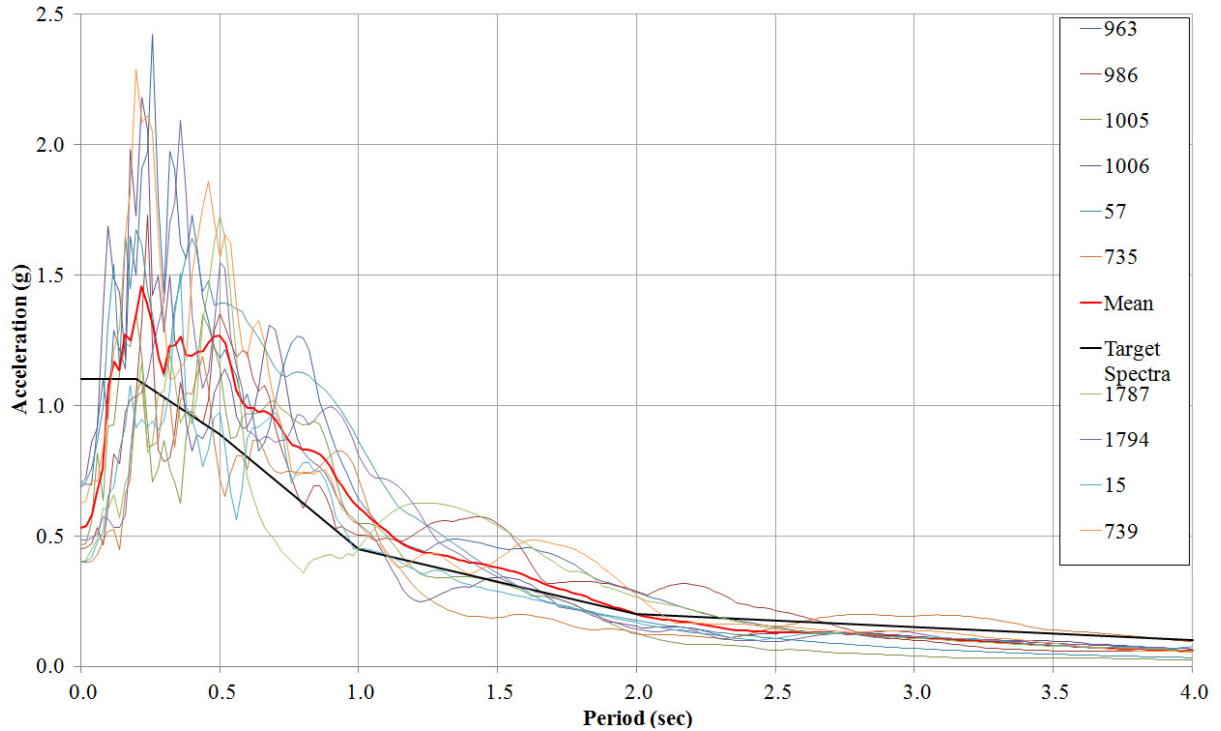


**Figure 3.7 Design response spectrum for Bamfield, B.C. for 5% damping, site Class C (NBCC 2010) and the response spectra of selected scaled records.**

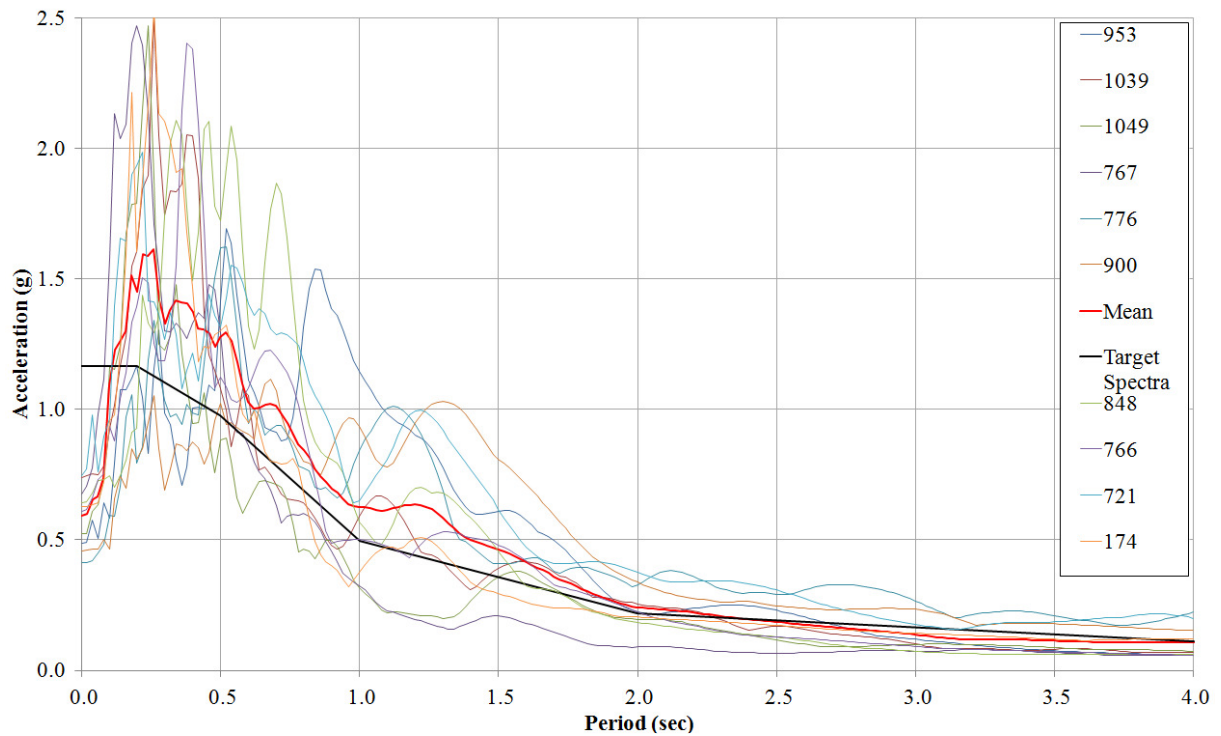


**Figure 3.8 Design response spectrum for Bamfield B.C. for 5% damping, site Class D (NBCC 2010) and the response spectra of selected scaled records.**

## CHAPTER IV

### STATIC AND DYNAMIC BEHAVIOR OF GUYED TOWERS AND ITS CABLES

#### 4.1. Introduction

This chapter is devoted to the understanding of static and dynamic properties of lattice TL guyed towers and how these properties could be used to estimate the response and assess the sensitivity of these structures to ground motion excitations. To simulate the static and dynamic response of delta guyed tower a numerical model is developed and validated against experimental test results. Modal analyses are carried out to determine the vibration properties of studied towers. Then, nonlinear pushover analyses are performed in order to assess the global capacity of guyed towers subjected to lateral static loads which have different distribution patterns.

Since the lateral stability of guyed towers is provided exclusively by the guy cables, static and dynamic properties of these elements are studied separately and an analytical formulation is developed to estimate the magnitude of impulse forces triggered in guy cables as a result of cable stretching due to tower mast displacement.

Finally, the guyed tower structure is subjected to harmonic excitation. From this response, expressions are derived to estimate the base shear reaction.

#### 4.2. Validation of Numerical Model against Experimental Test Results based on Pushover Analyses

A validation of numerical model developed with ANSYS-APDL software for the delta guyed tower studied herein was first completed before all other structural analyses pertaining to this study are carried out. This validation is done on the basis of comparison between the outcomes of numerical model and the results of full-scale prototype testing. It should be mentioned that this validation was only done for the delta guyed tower.

Pushover analyses were carried out based on the 2<sup>nd</sup> order linear analysis. These pushover analyses were based on the magnitude and direction of applied loads to a full-scale prototype tower. The purpose of experimental tests was to assess the accuracy of structural design under the critical loading conditions.

Outcomes from numerical simulations were compared with measurements of structure's displacement and members' strain-gauging taken during the tests. The objectives of these pushover analyses were to:

- Assess the accuracy of numerical methods in estimating the structure response and particularly the magnitude of forces triggered in tower's members when subjected to design static loading conditions;
- Evaluate the analytical idealization of tower structure's members (i.e. FE Truss-Model or FE Frame-Truss-Model) that best simulates the responses resulted during the full-scale prototype tests;
- Estimate which member(s) of the structures is(are) the most at risk under critical loading case.

These analyses present an opportunity to assess the uncertainties related to typical structural model build up in accordance with the current design practice, especially in what concerns the models for simulating the bolted connections which comes in a variety of configurations and are usually considered either hinges (with rotational degree of freedom) or rigid (without rotational degree of freedom). However, in construction practice, there is not a perfect pin connection or rigid connection. The assessment of connection model is important because, as indicated by several researchers, a significant number of lattice towers fail during physical tests when subjected to loads with magnitudes smaller than design loads and at locations different than that predicted from design.

The full-scale prototype of delta guyed tower was subjected to three different design load combinations (namely Test load cases number #1, #2 and #3) and it was later subjected to a destructive test under a load combination equal to 125% of the most critical design load combination corresponded to Test load case number #3. These three test load cases (#1, #2 and #3) are the most critical ones among thirty-six load cases considered during the design phase. Fig. 4.1 shows a general layout of the delta guyed tower and the locations of five members where strain-gauges were installed. Tower displacements were measured at 18 joints located in the Peak, Beam and K-Frame segments of the tower. According to standard CAN/CSA-C22.3 NO. 60826-10 (Design criteria of overhead transmission lines) requirements, the tower was subjected to incremental loads up to 100% of design loads and strain-gauging measurements were taken for all members identified in Fig. 4.1. Axial forces in the strain-measured members were then calculated based on the elastic properties of these members' materials.

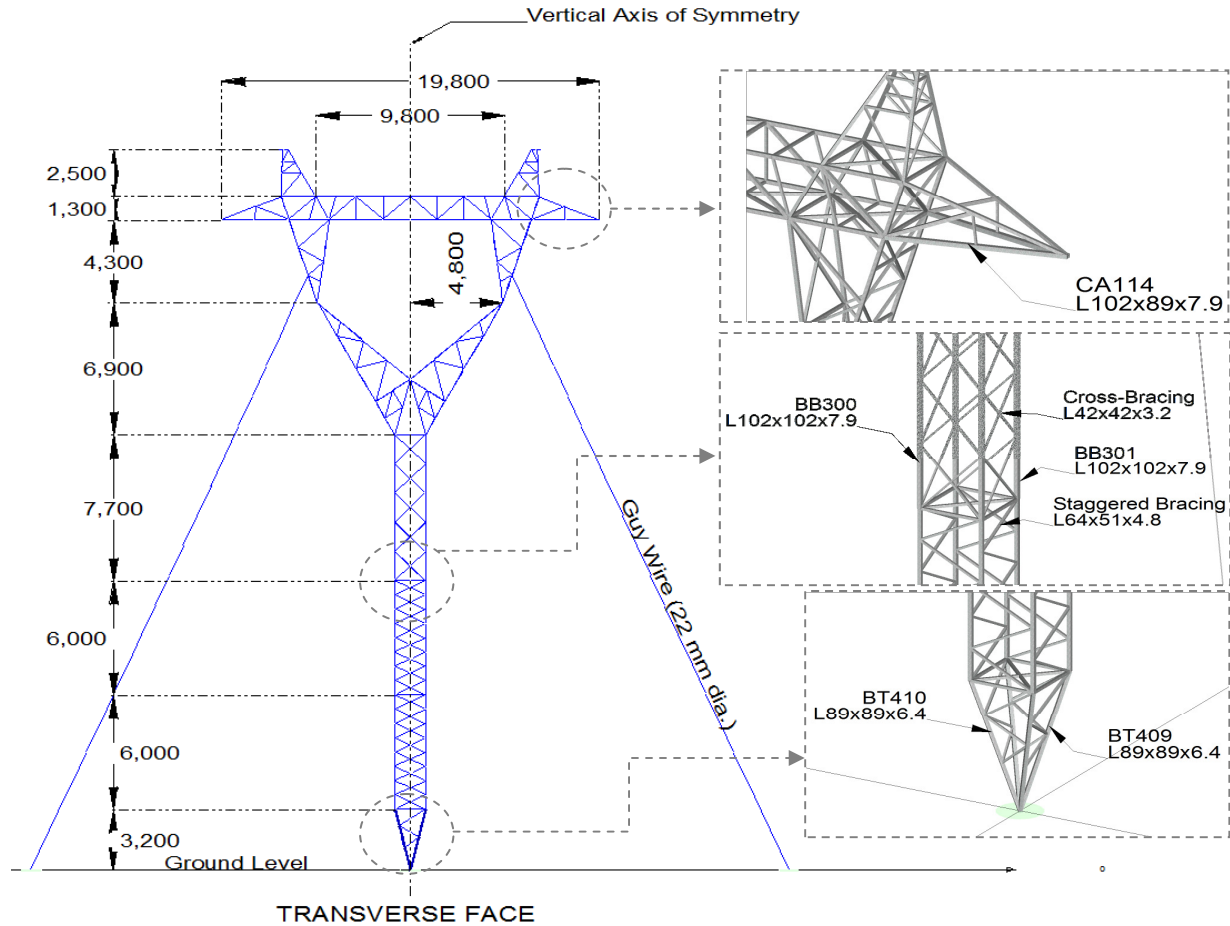


**Figure 4.1. Delta guyed tower layout and location of strain-gauges on members.**

During the application of Test load case number #3<sub>destructive</sub>, the tower was subjected to loads up to 125% of the design load associated to test load case number #3. Node displacement measurements were taken only for 100% of the corresponding design loads.

Figs. II.1 and II.2 (Appendix II) are loading trees, indicating the points on the structure where the loads were applied for each guyed tower test. In the tower tests, the design loads are applied to the tower structure by the action of pulling wires which are attached to certain connections. These wires pull the structure in the vertical and horizontal (transversal and longitudinal) directions.

For test load cases number #1 and #3, all loads are applied in the transversal and vertical directions. For test load case number #2, loads are applied in all three directions (transversal, longitudinal and vertical) and the tower is subjected to a torsional moment about its vertical axis of symmetry. Leg members in the body segment of the tower were chosen to be monitored

because, during the design phase, these members were identified as the most critical during loading. For the test load case number #3, which is the most critical design load case, numerical analyses indicated that the leg members in the tower body were targeted to be a potential failure location during the destructive test.

To replicate the full-scale delta guyed tower prototype, herein, two analytical idealization models for the tower structure members were used: a) all members are assigned the status of truss-elements using the FE Truss model which is able to transfer only axial loads and b) the main leg members are assigned the status of frame-elements using the FE Frame-Truss model (carrying both axial forces and bending moments) whereas all the other members such as: primary and secondary bracing members are assigned the status of truss-elements using the FE Truss model. The responses of guyed tower obtained from numerical analyses were compared with the prototype response where measured node displacements and member-forces were calculated based on member-strain measurements. Figs. 4.2 and II.3 (appendix II) presents comparisons between measured and simulated displacements of vertical axis of symmetry of the tower in the transversal and longitudinal directions. For test load cases number #1 and #3, for which all horizontal loads are applied in the transversal direction only, it can be seen from these figures that the performance of both numerical models (the FE Truss-Model and a combination of FE Frame-Truss and FE Truss model) are similar in simulating the displacement of the tower in the transversal direction. However, for test load case number #2, in which the tower is loaded in all 3 directions and is therefore subjected to a torsional moment about its vertical axis of symmetry, it can be seen from these figures that using the combination of FE Frame-Truss model for leg members and FE Truss model for the other members it presents a better simulation in terms of tower horizontal displacements in both transversal and longitudinal directions. This can be explained by the fact that in the stiffness matrix of the model some of the connections are rigid, which seems to be a more accurate representation of bolted connections with gusset plates connecting multiple members (e.g. leg and bracing members) This type of joint is more likely to present a rigid behavior when subjected to translational and rotational displacements at the same time.

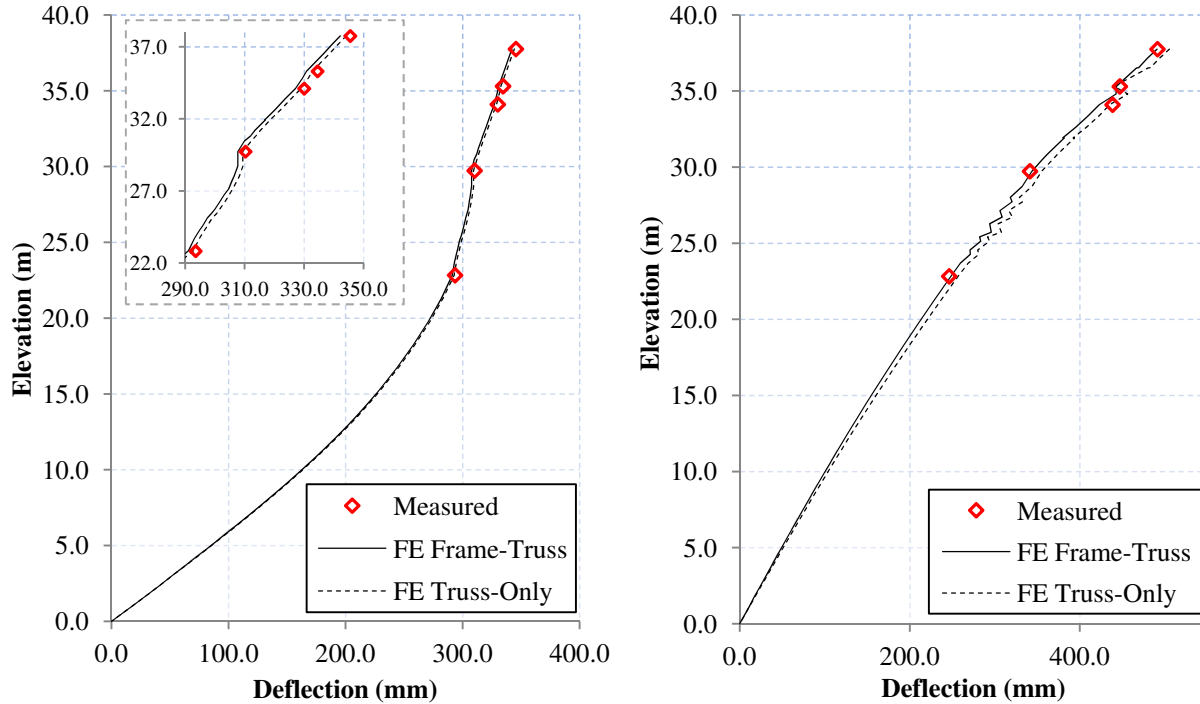


**Figure 4.2. Deflection of the vertical axis of symmetry in the transversal direction under test load case number #1 (left) and longitudinal direction under test load case number #2 (right).**

These suggest that using the FE Frame-Truss model to replicate the behaviour of tower leg members gives more accurate results when the tower is subject to longitudinal, transversal and torsional loading. Appropriate determination of the structure's stiffness properties is important for estimating the responses of lattice tower structures under dynamic loading. The dynamic property of guy cables usually governs the dynamic responses of the tower and influences the natural frequency of the tower itself. Thus, it plays an important role on the dynamic response of the structure because guyed towers, being slender and flexible, usually have many active modes of vibration associated with the tower mast vibration.

Figs. II.4, II.6 and II.7 (Appendix II) present dispersion diagrams for simulated and measured forces in the strain-gauged members (e.g. leg members, bottom segment members, cross-arm members), while Fig. II.5 presents a plot of the simulations' relative errors for the measured forces in the leg members. Further, Table 4.1 presents the overall performance parameters for the simulations in reproducing the axial forces measured by the strain-gages. Fig. 4.3 shows for all tower members their usage capacity in percentage depicted in color scale, when the structure is subjected to test load case number #3.

From the results given in Table 4.1 it can be seen that, overall, the two analytical idealization models considered herein show approximately the same accuracy in simulating the magnitude of forces measured in the gauged members. For example, for the leg members at the tower's basic-body segment identified as the most critical, the numerical model overestimates the ultimate compressive forces by about 5%, while the ultimate tensile forces are underestimated by about 5%.

**Table 4.1. The overall numerical model accuracy with reference to test results – Member axial forces.**

Member	Analytical Idealization	Performance Parameters			
		Compressive Force		Tension Force	
		<i>Mean Error</i>	<i>Standard Deviation</i>	<i>Mean Error</i>	<i>Standard Deviation</i>
Leg members	Truss	8.3%	6.5%	5.3%	4.6%
	Frame-Truss	8.5%	6.4%	5.3%	4.5%
Bottom members	Truss	7.2%	6.0%	n/a	n/a
	Frame-Truss	7.3%	5.9%		
Cross-arm member	Truss	5.3%	4.6%	8.4%	5.9%
	Frame-Truss	5.3%	4.5%	9.4%	6.0%

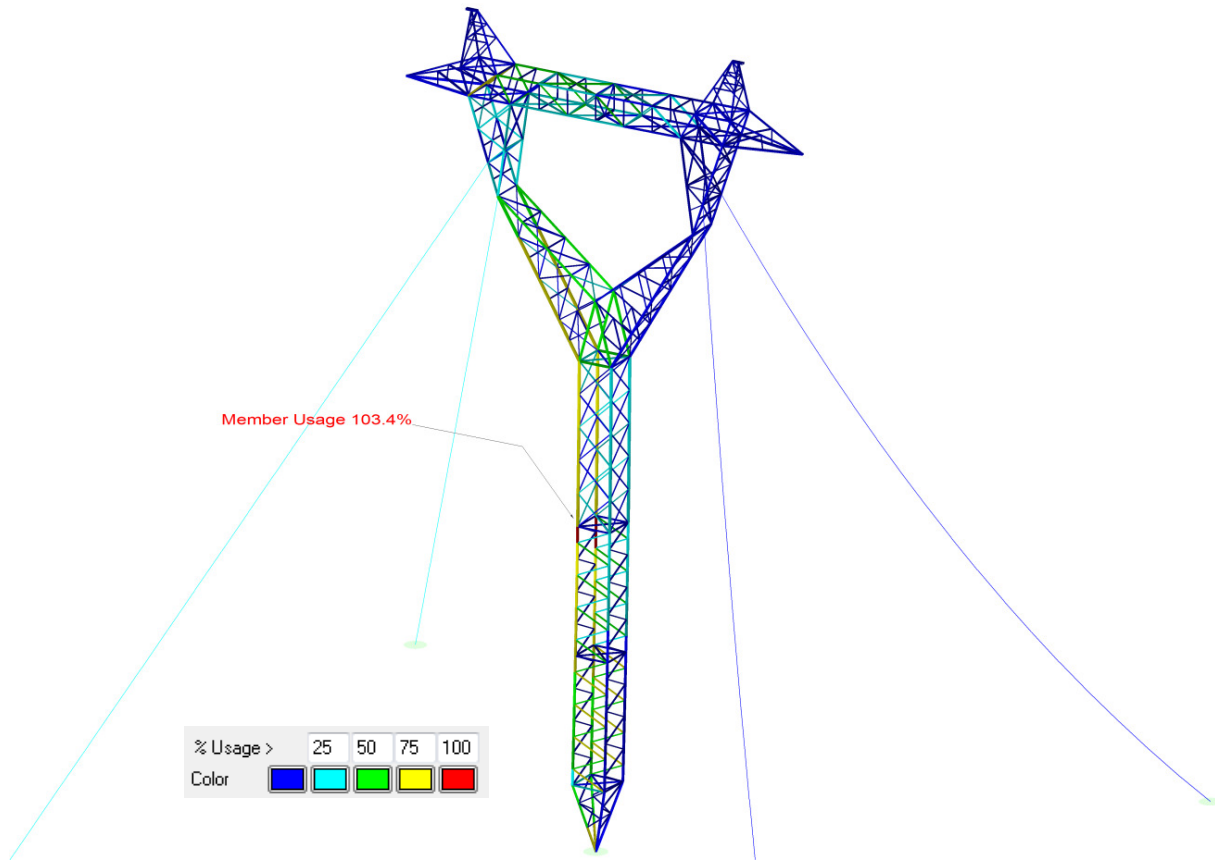


**Figure 4.3. Member capacity usage percentage associated to test load case number #3.**

### 4.3. Mode Shapes and Frequencies of Vibration

Modal analysis is a technique used to determine the vibration characteristics of a structure in terms of its natural frequencies, respective mode shapes and relevance of each mode shape in the vibration of the structure. Knowledge of the vibration characteristics of the structure is important for determining parameters for more detailed and computational intensive dynamic analysis, such as transient dynamic analysis, and for the design of structures expected to be subjected to dynamic loading.

Modal analyses were performed on the prestressed tower structures. A second order static analysis, considering the structures' self-weight, loads from prestressed guy cables and static loads from overhead cables, is first performed to update the stiffness matrix of the structure to the loaded conditions. A modal analysis is then performed considering the deformed shape of the structure from these static load conditions. Performing modal analyses on prestressed tower structures is necessary in order to predict more accurately their vibration characteristics. Lattice guyed towers are slender structures subjected to important structural nonlinearities associated

with P-Delta effects and cable-mast interactions. Hence, to analyse the guyed tower response, nonlinear structural dynamic techniques where the forces in the members are no longer linearly proportional to the nodal displacements and the stiffness matrix is dependent on the current displacement should be employed. Examples of transient dynamic analyses conducted on free-standing towers are shown in Chapter 5. In these analyses, the static loads and resulting P-Delta effects from their associated supported overhead cables are considered.

The Block Lanczos mode-extraction method available in ANSYS-APDL was used for the calculation of eigenvalues and eigenvectors. Enough modes of vibration were extracted in order to have a cumulative effective modal mass equal to or larger than 90% of the structure's mass.

Table 4.2 presents the results of modal analyses in terms of frequency of vibration of each mode and ratio of effective modal mass to total mass in each orthogonal direction of delta guyed tower. Mode shapes are illustrated in Fig. 4.4. Results of modal analyses for all other towers studied herein are presented in Appendix II.

The effective modal mass can be interpreted as the part of the total mass of the structure responding to earthquake excitation in each mode (Clough and Penzien, 1993). The effective modal mass gives a measurement of how much a given mode contributes to the base shear. The effective mass for the  $i^{th}$  mode is a function of the excitation direction and is determined using the following equation (Clough and Penzien, 1993):

$$M_{eff-i} = \frac{\gamma_i^2}{\{\varphi\}_i^T \times [M]_i \times \{\varphi\}_i} \quad (4.1)$$

where  $\{\varphi\}_i$  is the eigenvector,  $[M]_i$  is the mass matrix and  $\gamma_i$  is the participation factor for base excitation defined below.

$$\gamma_i = \{\varphi\}_i^T \times [M] \times \{D\} \quad (4.2)$$

In the above equation,  $\{D\}$  is the vector describing the excitation direction.

As it can be seen from Tables 4.2 and II.1 (Appendix II), guyed towers have several modes of vibration within the range of ground motion frequencies. It is noted that ground motion records considered in this study (refer to figures in Appendix I) show a predominant period of vibration in the horizontal direction in the range from 0.20 s to 0.74 s and that the mean period of vibration ranges from 0.34 s to 0.95 s. Within this ranges are the modes of vibration with the highest

effective modal mass of guyed tower, indicating that this type of tower is likely to have an important resonant base shear response during a typical earthquake event. In the vertical direction, the predominant period of vibration ranges from 0.06 s to 0.92 s. Fifteen modes of vibration were identified in the modal analyses for the delta guyed tower, totalling approximately 90% of the structure's mass. About half of these modes are characterized by the vibration of guy cables. In Fig. 4.4 is showed the deflected shape of delta guyed tower associated with different vibration modes.

**Table 4.2. Modal properties of Delta Guyed tower.**

Mode	Period (sec)	Freq. (Hz)	Ratio of Effective Modal Mass to Total Mass			Description
			Transv.	Long.	Vertical	
1	0.75	1.33	0.05	0.02	0.00	Cable vibration
2	0.73	1.37	0.00	0.00	0.02	Cable vibration
3	0.52	1.93	0.79	0.00	0.00	1 <sup>st</sup> flexural mode - Transversal
4	0.40	2.51	0.00	0.70	0.00	Tower rotation about vertical axis
5	0.37	2.69	0.01	0.14	0.00	Cable vibration
6	0.27	3.74	0.00	0.01	0.00	1 <sup>st</sup> flexural mode - Longitudinal
7	0.25	4.02	0.00	0.00	0.00	Cable vibration
8	0.22	4.54	0.04	0.00	0.00	2 <sup>nd</sup> flexural mode - Transversal
9	0.19	5.36	0.00	0.00	0.00	Cable vibration
10	0.15	6.72	0.00	0.00	0.00	Cable vibration
11	0.12	8.09	0.00	0.00	0.00	Cable vibration
12	0.12	8.65	0.00	0.00	0.00	Substructure vibration
13	0.12	8.66	0.00	0.00	0.00	Substructure vibration
14	0.11	9.47	0.00	0.00	0.00	Cable vibration
15	0.10	10.09	0.00	0.02	0.00	2 <sup>nd</sup> flexural mode - Longitudinal
<b>Total</b>			<b>0.89</b>	<b>0.90</b>	<b>0.03</b>	

(1) Green shading indicates the range of predominant period of vibration in the horizontal direction.

It should be mentioned that flexural modes of vibration are usually the most important ones to be investigated in vibration analyses of these types of structures. The slenderness of the tower mast results in important forces in the leg members due to bending and P-Delta effects. Nonetheless, the design of these towers is usually controlled by the capacity of the leg members in the mast. Results of modal analyses for the Self-supporting towers are also presented in Tables II.1, II.2 and II.3 of Appendixes II. For the Self-supporting delta tower, the first and second mode of vibration in the transversal direction has a period of 0.26 s and 0.08 s, respectively. For the Self-supporting mast tower, the first and second mode of vibration in the transversal direction has a period of 0.24 s and 0.20 s, respectively. These periods of vibration for the self-supported towers coincides or are close to the predominant period of some of the ground motion records considered in this study.

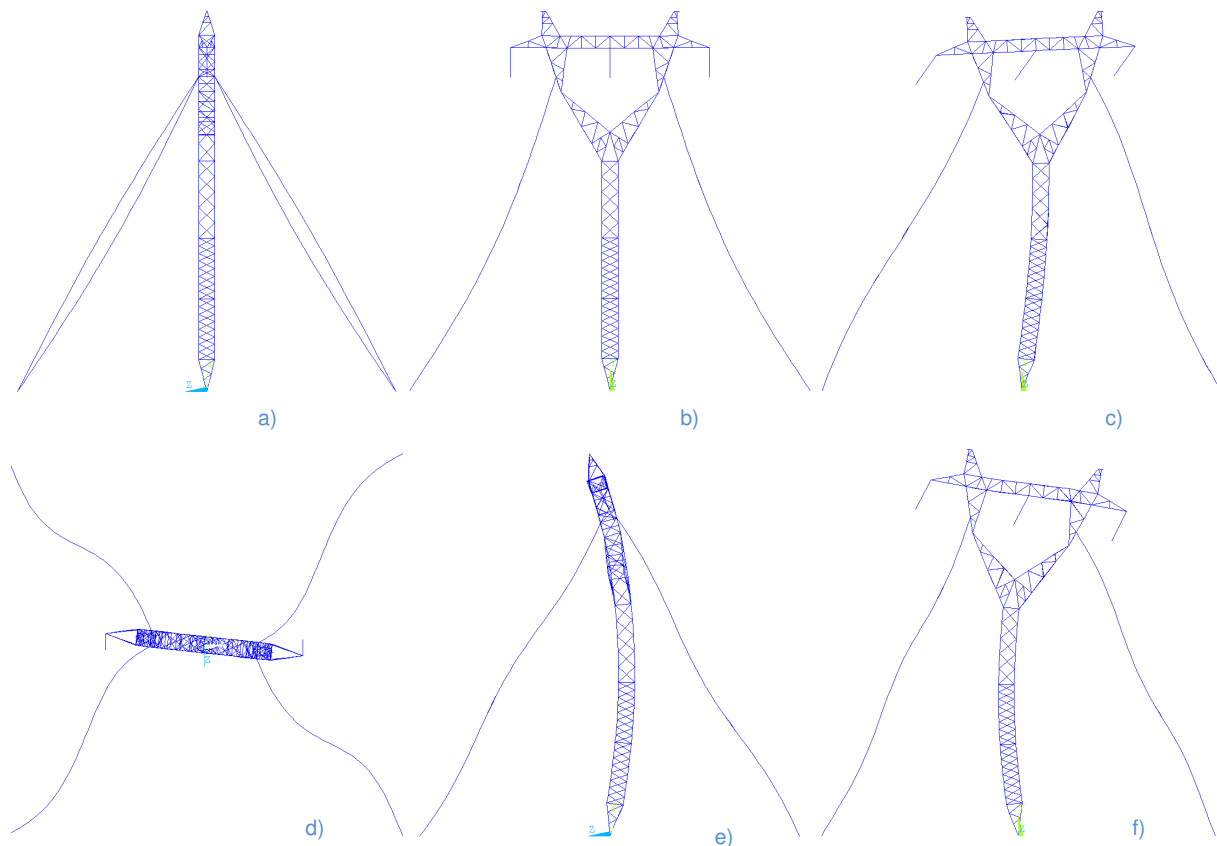


**Figure 4.4. Mode shapes. a) cable vibration. b) cable vibration. c) 1<sup>st</sup> flexural mode of vibration in the transversal direction. d) tower rotation about vertical axis. e) 1<sup>st</sup> flexural mode of vibration in the longitudinal direction. f) 2<sup>nd</sup> flexural mode of vibration in the transversal direction.**

Fig. 4.5 shows the elastic response spectra of 20 ground motion records used in this study. The range of natural periods fitting the main vibration periods of guyed towers and self-supported towers is also emphasised. As it can be seen from this figure, the range of natural periods for guyed and self-supported towers overlaps with a region of ground motion period content with higher response acceleration ordinates. This comparison indicates that these structures are likely to be subjected to resonant ground motion excitation. However, as presented in Table 4.2 and Tables II.1, II.2 and II.3 of Appendix II, guyed towers have a higher number of modes of vibration coinciding with the range of ground motions predominant periods than self-supported towers. This may suggest that guyed towers are more likely to be affected by earthquake loads than self-supported towers.

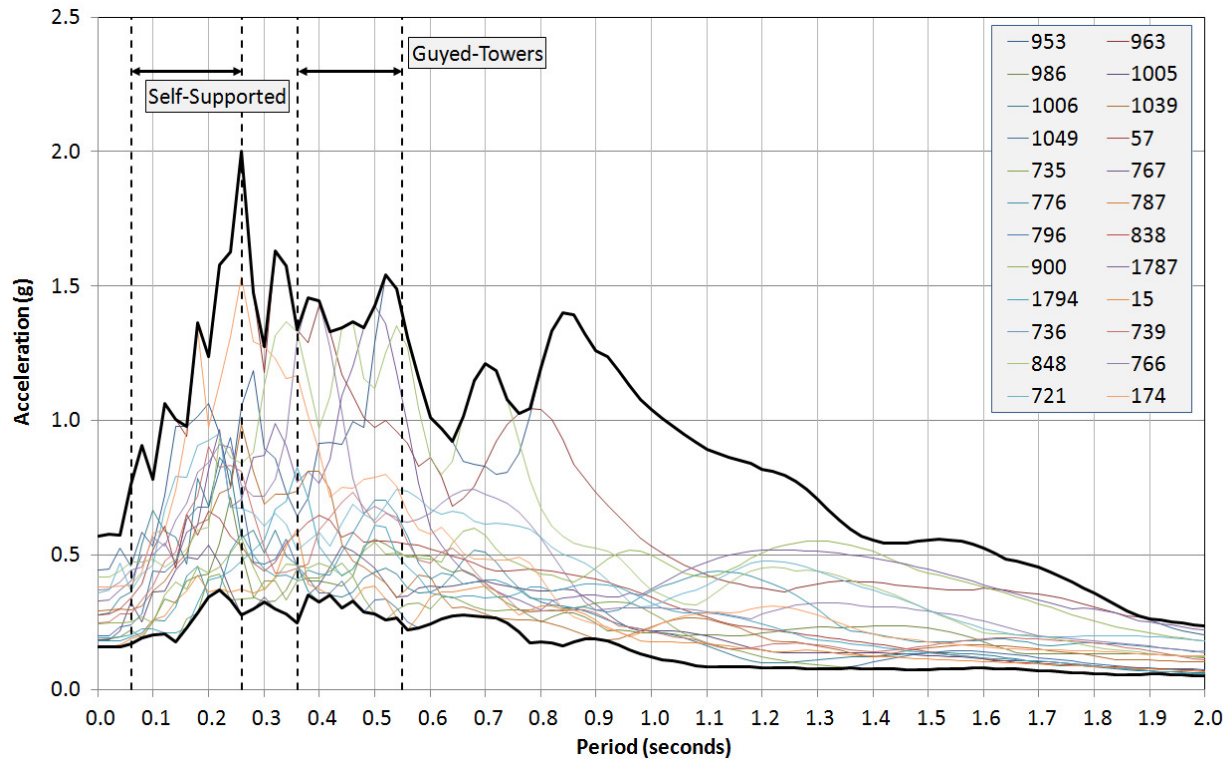


**Figure 4.5. Collection of unscaled ground motion records elastic response spectra.**

#### 4.4. Pushover Analysis and Load Distribution Pattern

Pushover analyses were carried out to predict the response of the TL guyed towers in terms of its deformation and damage anticipated in each member when subjected to lateral loads. A pushover analysis has the advantage of being less computational demanding than a dynamic time-history analysis and it provides a good estimate of the maximum seismic inertia load developed in a structure. The results of pushover analysis may also be used to derive an equivalent Single Degree-of-Freedom (SDOF) system that can be used to approximate the response of tower structure given by more complex Multi DOF (MDOF) system models.

A load distribution pattern must be defined for performing a pushover analysis. One approach that can be adapted for shear force distribution over the height of TL towers is that given in NBCC 2010 for the shear force distribution in the case of earthquake-resistant buildings. This pattern load is labelled inverted triangular distribution and the equation is given below:

$$F_y = V \times \frac{W_y \times h_y}{\sum_{i=1}^n W_i \times h_i} \quad (4.3)$$

where  $V$  is the seismic base shear,  $W_y$  and  $W_i$  are the seismic weights of tower sections  $y$  and  $i$ , respectively, and  $h_y$  and  $h_i$  are the height of tower sections  $y$  and  $i$ , respectively. Another approach is to distribute the loads proportional to the shape of the first flexural mode of the structure, as follows (Filiatrault et al., 2013):

$$F_y = V \times \frac{A_y \times m_y}{\sum_{i=1}^n A_i \times m_i} \quad (4.4)$$

where, for the case of a earthquake-resistant building,  $A_y$  and  $A_i$  are the values of the mode shape corresponding to floors  $y$  and  $i$ , respectively, and  $m_y$  and  $m_i$  are the values of the masses of floors  $y$  and  $i$ , respectively. For the case of a lattice TL tower, the mode shape vector can be calculated assuming that each section of the tower can be lumped to a single Dynamic Degree-of-Freedom (DDOF) located at the tower's sections center of mass and that the masses of each section can be lumped to their corresponding DDOF. Once the natural frequency corresponding to the 1<sup>st</sup> flexural mode of vibration of the analysed tower is determined, it can be used in Eq. (4.5) given below to solve for the corresponding mode shape vector.

$$[[k] - \omega^2 \times [m]] \times \{A\} = \{0\} \quad (4.5)$$

Herein,  $[k]$  is the stiffness matrix of the structure,  $\omega$  is the circular frequency of vibration for the first flexural mode of vibration,  $[m]$  is the mass matrix of the structure,  $\{A\}$  is the mode shape vector and  $\{0\}$  is the zero vector. The mode shape vector  $\{A\}$  contains the amplitude of vibration of each DDOF considered in the analysis and therefore represents the deformed shape of the structure when excited by a dynamic loading.

Pushover analyses carried out for the guyed tower structures herein studied were based on the vertical distribution of forces determined by Eqs. (4.3) and (4.4) for comparison purposes. Gravitational loads and loads from conductors and guy-cable pretension force were considered in these analyses in order to adequately capture the P-Delta effects. The lateral loads used in the pushover analyses were monotonically increased until global instability was reached. The conductor support displacement versus base shear is then plotted for analysis.

For each increment of the monotonically increase lateral loading, axial forces on each member of tower are computed and compared with its corresponding capacity. Once the capacity of a given member is exceeded, a zero value is attributed to the stiffness of this member and the pushover analysis continues until global instability is reached. Attribution of a zero value for the member stiffness is done using the EKILL command of the APDL (ANSYS, 2013).

As explained previously, most of the members in a latticed tower structure have their capacity controlled by either the elastic buckling strength or by the strength of member's connections. Yielding of steel material is rarely the controlling factor in the global response of these TL tower structures. In addition, all TL tower's members are expected to perform in the elastic domain until their capacity is reached. Attributing a zero value to the stiffness for the member with capacity exceeded it supposes that this member is no longer capable of transmitting forces. Post-buckling strength of members in compression was not considered in these simulations. The EKILL command simply disconnects the "failed" member from the structure's stiffness matrix.

Pushover analyses for guyed towers were performed in both horizontal directions (longitudinal and transversal) and with load distribution patterns defined by Eqs. (4.3) and (4.4) for comparison purposes, hence, totalling four pushover cases for each guyed tower. Figs. 4.6 and 4.8 show the load distribution patterns for the delta guyed tower and mast guyed tower in terms

of percentage of base shear. Then, Figs. 4.7 and 4.9 are plots of monotonic increase in base shear against conductor support displacement for the delta and mast guyed towers, respectively.

Comparing the force distribution patterns showed in Figs. 4.6 and 4.8, it can be seen that for the inverted triangle distribution pattern, a higher percentage of load is concentrated in the upper part of the tower where most of the structure's weight is located. The modal distribution pattern shifts part of the load to the tower mast where the critical design leg members are located. In Figs. 4.7 and 4.9, the base shear is presented in terms of a ratio to the structure's seismic weight. Capacity curves depicted in Figs. 4.7 and 4.9 indicate that structural instability occurs right after the first member reached failure. For all pushover analysis cases, structural failure occurs at the tower mast due to the failure of a leg member loaded in compression. These results show that the capacity of these structures is governed by the type of load distribution pattern.

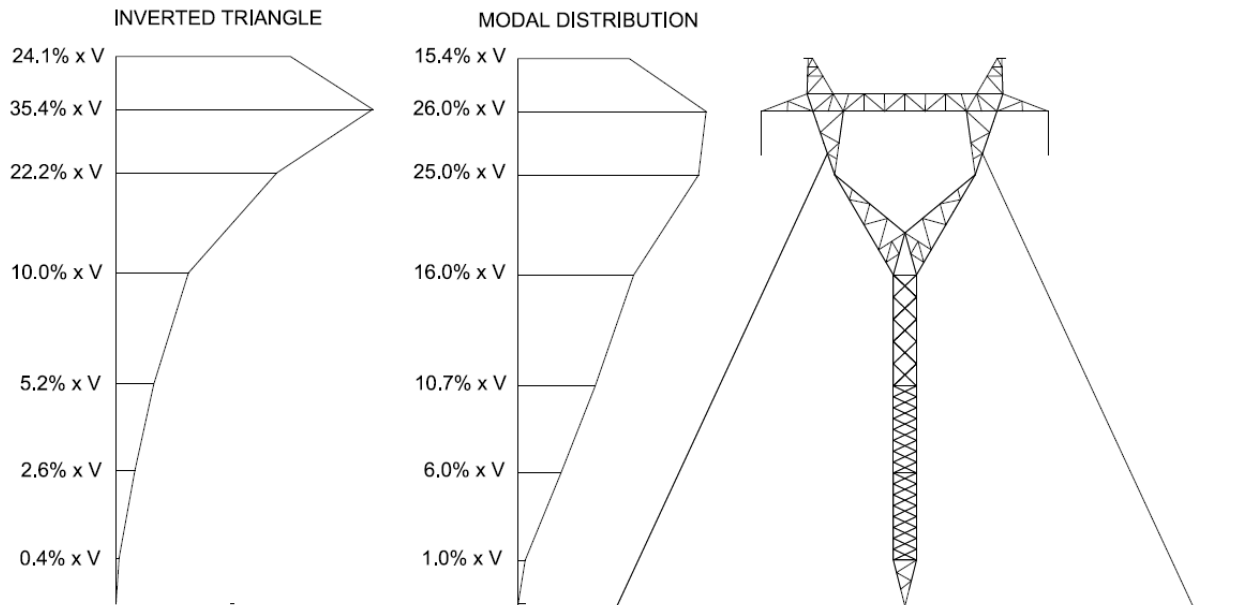


**Figure 4.6. Force distribution patterns over the height of Delta guyed tower. Transversal direction.**

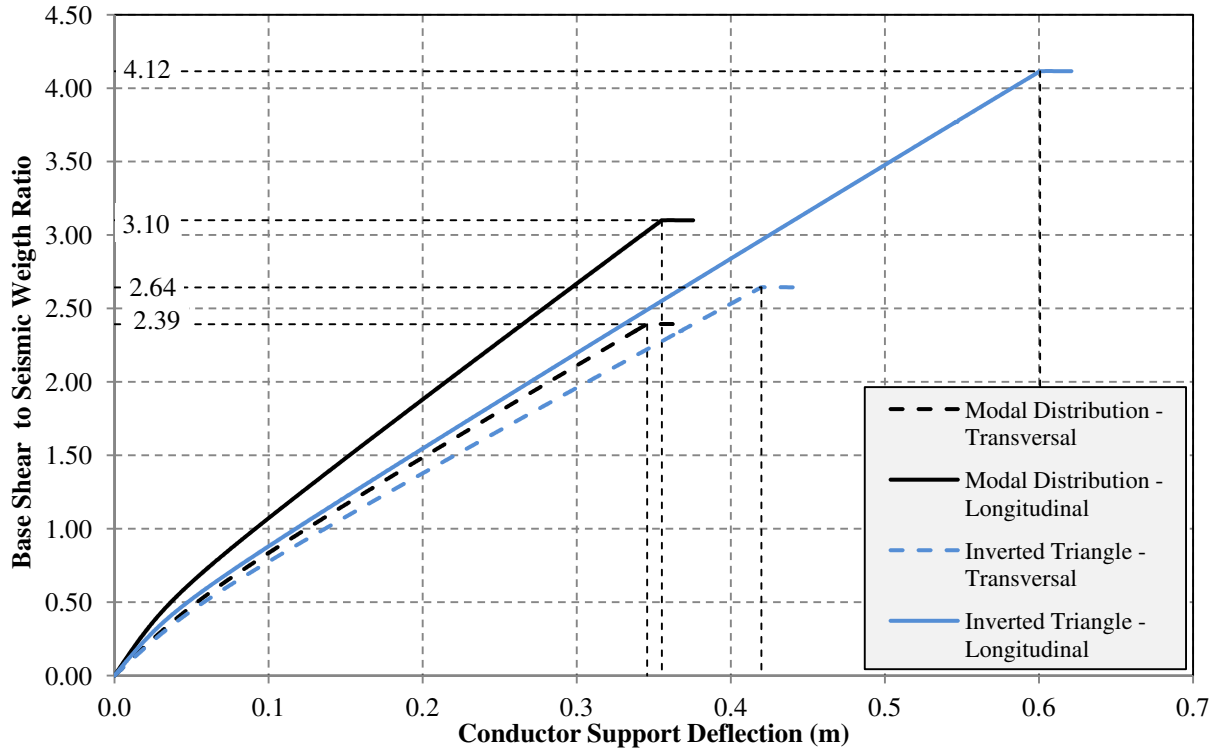


Figure 4.7. Capacity curves of Delta guyed tower. Transversal and longitudinal directions.

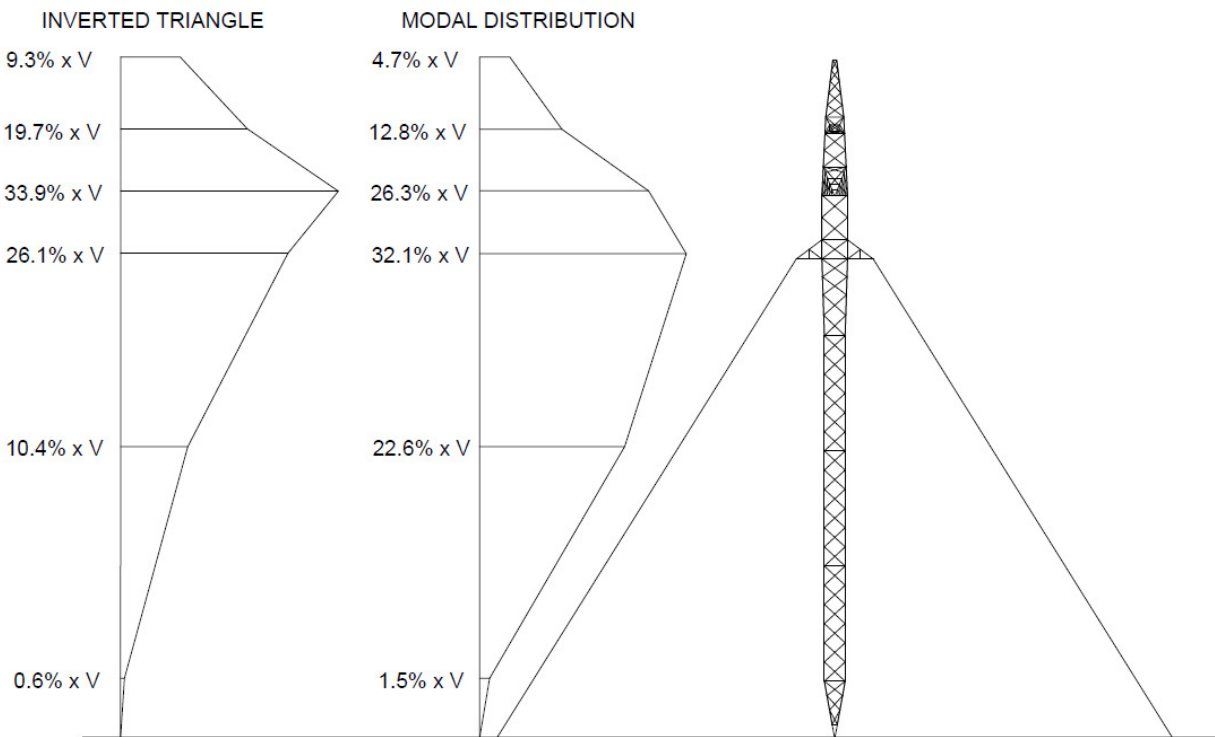
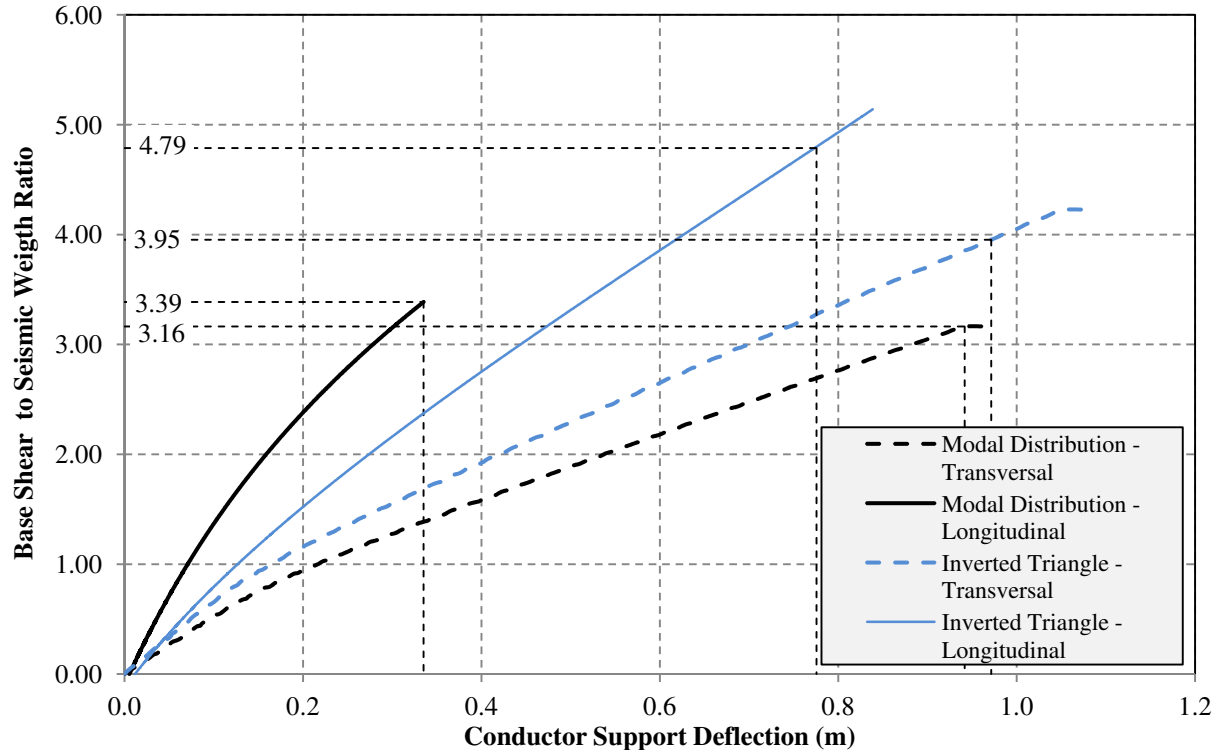


Figure 4.8. Force distribution patterns over the height of Mast guyed tower. Longitudinal direction.



**Figure 4.9. Capacity curves of Mast guyed tower. Transversal and longitudinal directions.**

Considering in pushover analysis the modal distribution pattern for distributing the static loads over the structure height, it results a lower capacity estimate, as presented in Figs. 4.7 and 4.9. Thus, the overall capacity of guyed towers as a result of the modal load distribution pattern is about 10% to 25% lower than the resulting capacity when the inverted triangular load distribution is considered. These comparisons also highlight the importance of considering P-Delta effects caused by the significant deformation that this type of flexible structure undergoes. Because the modal distribution takes into account the significant bending that the tower is expected to undergo when excited at a preferential frequency, P-Delta effects are increased by the enhanced deflection of the tower mast caused by the modal distribution of forces as compared with the inverted triangular distribution pattern. When vertical loads simulating the structure's self-weight and that of the overhead cables act on the laterally deformed tower structure, it leads to an additional overturning moment that is resisted by the lateral force-resisting system of the guyed tower, in this case the guy cables. This is an important observation not only for the seismic analysis of lattice guyed towers but also for the application of typical design controlling load cases such as wind. To summarize, the member that controls the design

of a lattice TL tower is a leg member located on the tower's mast and; in design practice wind pressure is usually uniformly distributed over the height of the structure or, in some cases, follows the vertical distribution pattern of an atmospheric boundary layer (Simiu, 1996).

Finally, it is noted that the pushover method has limitations in determining the capacity of guyed towers, in particular, because there are other failure mechanisms that are only evident when a time-history dynamic analysis is performed. As it will be shown later, an excessive bending of the tower mast may cause the guy-cable to become slack and to suddenly become tight as the tower mast reverses the bending movement towards its original position. This dynamic mechanism, characterized by the slacking and sudden tight of the guy cable, may result in an impulse force large enough to cause the rupture of the guy cable or to damage a member of the tower structure.

#### **4.5. Static and Dynamic Properties of Guy Tower Cables**

As mentioned previously, the lateral stability of guyed towers is mainly provided by the pre-tensioned guy cables. The usual analytical assumption for the structural behavior of this type of tower is that the base of the tower mast is constrained against translation but it is free to rotate and that the lateral displacement of the tower is mainly governed by the horizontal stiffness of the guy cables. Because of the inertial effects associated with cable vibration, the guy cable stiffness is dependent on the frequency of the imposed motion (Madugula et. al, 2001). For static loading conditions or slow motion of the tower mast, a nonlinear static analysis is considered appropriate for determining the stiffness of the cable. For dynamic loading conditions, a dynamic analysis is necessary to determine the action of the guy cable over the tower mast because of the complexities associated with the phase shift between mast displacement and resisting force from the cable. As it will be shown in this section, the resisting force from the cable depends on the frequency of vibration of the mast support.

##### **4.5.1. Static Properties**

The nonlinear stiffness of the guy cable of the delta guyed tower is analyzed using the finite element approach and the analytical equations proposed by Shears (1968) (see Section 2.9 of Chapter II). For the finite element approach, the guy cable was modeled as a sequence of 40 tension-only LINK180 truss-elements in ANSY-APDL. The variation in horizontal stiffness of the guy cable was analyzed by displacing the upper support in the horizontal direction, as

indicated in Fig. 4.10 - left. This guy cable is pretensioned to 7% of its design tension load and forms an angle of 55 degrees with the horizontal. This pretension is defined in the finite element model by using the INISTATE command of the APDL (ANSYS, 2013).

The resulting nonlinear horizontal stiffness of the guy cable is presented in Fig. 4.10. In this figure, the displacement of the cable support is shown as a percentage of the initial span of the guy (refer to Fig. 4.10 - left) and the varying stiffness is normalized by the initial stiffness of the guy cable. As shown, the prestressed cable is tight and has little sag, resulting in an initial stiffness close to the elastic stiffness defined by Eq. (2.4).

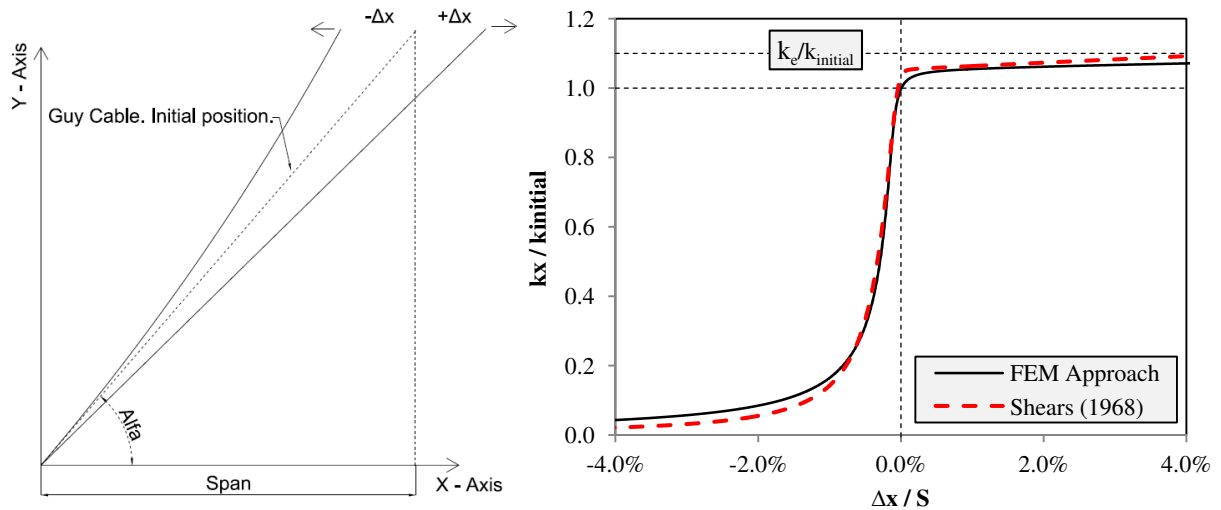


**Figure 4.10. Guy cable upper support displacement (left) and horizontal stiffness of guy cables (right).**

The limitation of Eq. (2.3) proposed by Shears (1968) and mentioned by Madugula et. al (2001), consists in determining the horizontal stiffness of the slackened cable. This limitation is highlighted when comparing its results with the results obtained from the FEM approach. Nevertheless, this equation yields satisfactorily approximate results to the FEM results and can be considered useful for concept design level. At a positive displacement, there is little sag remaining and the horizontal stiffness of the cable approaches an asymptotic value defined by the elastic stiffness of a perfect taut cable. Positive displacement is herein defined as the sense of displacement of the support that causes the cable to become taut. Conversely, negative displacement is defined as the sense of displacement of the support that causes the cable to become slack.

As the cable becomes slack, only its weight provides resistance to the mast motion. Similar to the positive displacement condition, the stiffness of the cable tends to an asymptotic value. An

expression for this asymptotic value can be derived from Eq. (2.3) by associating a very small value, or unit value, for simplification, to the elastic stiffness  $k_e$ . Therefore, Eq. (2.3) can be adapted to approximate the stiffness provided by the cable weight only, as follows:

$$k_g = \left[ 1 + \frac{W_G \times L^3}{12 \times T^3 \times \left\{ 1 + 2.67 \times \left( \frac{\delta}{L} \right)^2 \right\}} \right]^{-1} \quad (4.6)$$

where  $k_g$  is defined as the stiffness provided by the gravitational effects, only. As it will be shown later, both Eqs. (2.3) and (4.6) can be used to estimate an impulse force caused by an abrupt change in cable stiffness. This impulse force is originated when the cable passes from a slack condition to suddenly become taut as the tower mast is displaced.

#### 4.5.2. Dynamic Properties

Dynamic properties of interest for the guy cable were analyzed using the FEM approach. The guy cable was modeled as a sequence of 40 tension-only LINK180 truss-elements in ANSYS-APDL and it was subjected to harmonic acceleration with amplitude of 0.1 g in the longitudinal direction for various forcing frequencies ranging from 0.1 Hz to 10.0 Hz in steps of 0.1 Hz, thus totalling 100 nonlinear transient simulations. These simulations were carried out in ANSYS in batch mode using the APD Language. The maximum cable tension for each harmonic forcing frequency simulation was compiled and used to produce the response spectra presented in Fig. 4.11. A critical damping ratio of 0.1% was considered in these simulations. The objective of these simulations was to identify the frequencies in which the cable tension responses are amplified in regards to equivalent static tension. The ordinates in this response spectrum present the ratio of dynamic tension to static tension. These tension values are the mean of tension values obtained from the tension-only truss elements making up the cable model. The values in the abscissa axis represent the ratio of forcing frequency  $\omega$  to natural frequency  $\omega_n$ .

From this figure it can be observed that the tension force in the cable initially increases with increasing frequencies until it reaches a peak value at resonant frequency. An increase in the guy tension force is also observed when the forcing frequency attains the frequency of the second mode of vibration of the cable. The results of the harmonic analyses presented in Fig. 4.11 indicate that the stiffness of the cable can vary significantly with the forcing frequency.

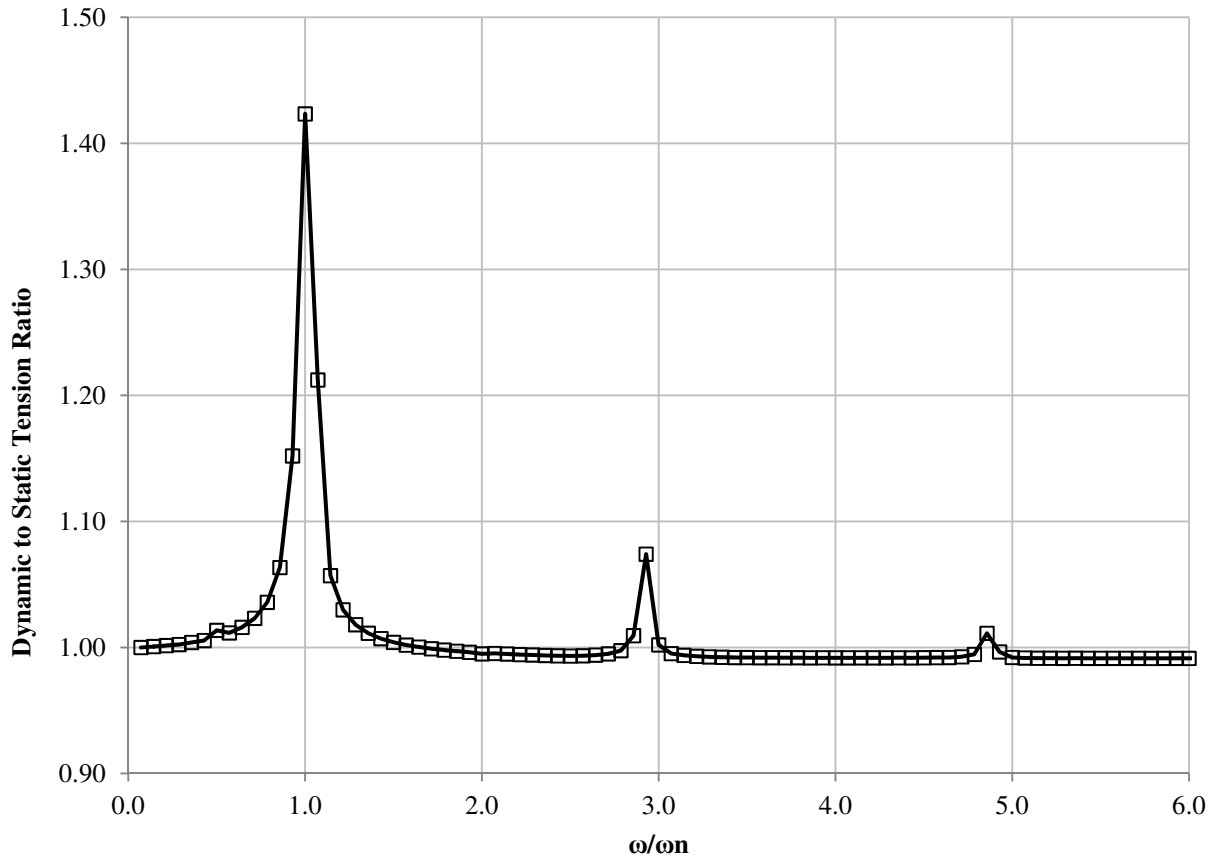


**Figure 4.11. Frequency-response relationship for guy cable. Harmonic excitation in the longitudinal direction.**

#### 4.5.3. Impulse Forces from Guy Cable Dynamics

As mentioned previously, an excessive bending of the tower mast during a ground motion shaking, may cause the guy-cable to become slack and to suddenly become taut as the tower mast reverses the bending movement towards its original position. This motion of the guy cable's upper support results in an impulse force that may be of important consideration for the analysis of guy cables and tower members. Naturally, this dynamic mechanism can be expected to occur when the tower is subjected to all types of dynamic loading conditions, such as gusty winds.

Current design standards used in U.S and Canada, such as ASCE 74 (ASCE, 2009) and CAN/CSA-C22.3 N°. 60826-10, describe failure containment longitudinal loads acting on the tower structure due to the failure of line components such as a broken conductor or ground wires, including their corresponding dynamic effects as a result of sudden unbalanced loads. Guy cable rupture is usually only considered in conjunction with other design load cases, such as wind

loading acting on an asymmetrically supported tower with one or more broken guy cables. Forces that guy cables directly exert to tower supports, as a result of the tower vibration, are not considered. Tension forces in the guy wires are usually calculated for static prestressed conditions, in which the static loads may be amplified for a given dynamic factor depending on the load case considered. In the scope of this study, it is questioned whether these impulse forces, originated from the slacking and tight dynamic mechanism of the guy cable during tower vibration, is relevant. This dynamic mechanism was studied herein using the FEM approach and an analytical expression is proposed for estimating the response to this impulse load.

#### *4.5.3.1. Nonlinear Dynamic Analysis*

Fig. 4.10 shows that the variation in static stiffness of guy cable is abrupt as the tower mast is displaced a small horizontal distance around its original position. When the guy cable is displaced to the left from its original position as per Fig. 4.10, the cable becomes slack and the tension force developed is mainly a function of the catenary stiffness; whereas when the cable is displaced to the right from its original position, the tension force developed in the guy cable is governed by the taut cable axial stiffness. As the mast transitions a small horizontal distance from the left to the right, the nonlinear stiffness relationships presented in Fig. 4.10 suggests that the guy cable will exert a step force on the tower mast with finite rise time due to an abrupt change in the guy cable stiffness.

Nonlinear dynamic FE simulations were carried out in order to assess the effects of this step force in the response of the guy cable. In these simulations, the upper support of the guy cable was subjected to a step force with rise time equal to half of the tower period of vibration for the 1<sup>st</sup> and 2<sup>nd</sup> flexural modes in the transversal and longitudinal directions (refer to Table 4.2). Since the period of vibration represents the time that the structure takes to complete one cycle, guy cables are expected to be subjected to a step force with a rise time equal to half of this period during vibration. The periods of vibration for the 1<sup>st</sup> and 2<sup>nd</sup> mode in the transversal direction for the delta guyed tower are 0.52 s and 0.22 s, respectively. For the longitudinal direction, the periods of vibration for the 1<sup>st</sup> and 2<sup>nd</sup> mode are 0.27 s and 0.10 s, respectively. The corresponding time of rise used in these simulations are, therefore, 0.26 s and 0.11 s in the transversal direction, and 0.14 s and 0.05 s in the longitudinal direction, respectively. The time varying force was applied to cause a displacement of the guy cable's upper support from -2% to 2% of  $S$ , where  $S$  is (refer to Figs. 2.5 and 4.10).

According to Chopra (1995), the excitation caused by a step force with finite rise time can be characterized by two phases: the rise phase and the constant phase. These two phases can be formulated in terms of the time-varying force as follows:

$$F(t) = F_g \quad t = 0 \quad (4.7.a)$$

$$F(t) = F_e \times \left(\frac{t}{t_r}\right) + F_g \quad t \leq t_r \quad (4.7.b)$$

$$F(t) = F_e \quad t > t_r \quad (4.7.c)$$

where  $F(t)$  is the value of the step force at time  $t$ ,  $t_r$  is the time of rise of the step force,  $F_e$  is the horizontal force function of the elastic stretching of the cable, and  $F_g$  is the horizontal force function of the cable's catenary stiffness. At the support position  $\Delta x/S$  equal to 2% (refer to Fig. 4.10), the step force is characteristically in the constant phase; little sag remains and the horizontal stiffness of the guy cable is mainly determined by its elastic stretching. In the constant phase,  $F(t)$  can be approximated to  $F_e$ , which in turn can be calculated using Eq. (2.4). Similarly, for the slack condition,  $F_g$  can be determined using Eq. (4.6).

In Fig. 4.12 is showed the horizontal reactive force  $R_H$  from the cable at the upper support normalized by the step-force  $F(t_r)$  plotted against  $t/T_{1st}$ , where  $T_{1st}$  is the period of vibration of the delta guyed tower in the 1<sup>st</sup> flexural mode in the transversal direction. The dotted line in Fig. 4.12 represents the step force acting on the guy support and the continuous line represents the horizontal reactive force from the guy cable. The results presented in this figure indicate that, when the tower vibrates in its 1<sup>st</sup> and 2<sup>nd</sup> flexural modes, the dynamic forces originated from the cable dynamics will have amplitude about 20% to 60% higher than the imposed force, respectively. It is noted that the amplitude of the upper support displacement considered in the FEM simulations was about 2% of  $S$  and the cable was initially at rest. These results permit the following observations: a) the smaller the value of the ratio  $t/T_{1st}$  is the higher is the amplitude of the dynamic response; b) for large values of  $t/T_{1st}$ , the dynamic response tends to approximate the static solution; c) the response attains its maximum value during the constant force phase of the response.

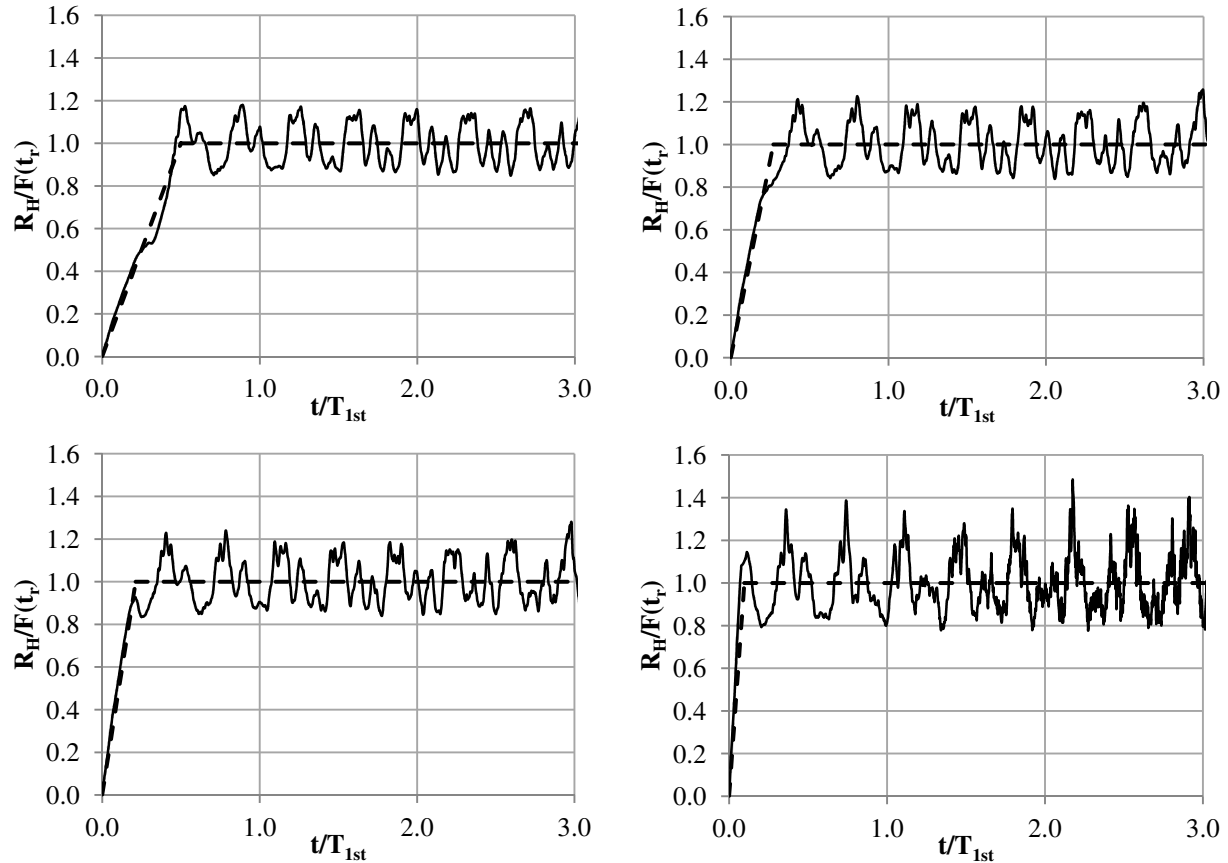


**Figure 4.12. Dynamic response (reactive horizontal force) of guy cable to step force with finite rise time. Static solution is show by dashed line.  $t_r/T_{1st} = 0.50$  (upper left).  $t_r/T_{1st} = 0.27$  (upper right).  $t_r/T_{1st} = 0.21$  (lower left).  $t_r/T_{1st} = 0.10$  (lower right).**

#### 4.5.3.2. Analytical Formulation

The excitation caused by a step force with finite rise time can be characterized by two phases: the rise phase and the constant phase. Since the damping for latticed tower structures and cables is known to be relatively small and the effects of damping for short duration dynamic loads usually has little significance in the initial transient response, for simplification, damping can be neglected and the response of an equivalent SDOF system can be obtained by applying the step force given in Eq. (4.7) and employing the Duhamel's integral for an undamped SDOF system. It is noted that Duhamel's integral is limited to determining the response of a linear system to an arbitrary time-varying load. The Duhamel's integral applied to the step force given by Eq. (4.7), has the following form:

$$\Delta x(t) = \frac{1}{m \times \omega} \times \int_0^t \frac{F_0}{t_r} \times \tau \times \sin \omega \times (t - \tau) \times d\tau \quad (4.8)$$

Simplifying the above integral and considering initial displacement  $\Delta x(0)$  and initial velocity  $\Delta x(0)'$ , gives the following expression:

$$\Delta x(t) = \left\{ (\Delta x_{st})_0 \times \left( \frac{t}{t_r} - \frac{\sin \omega \times t}{\omega \times t_r} \right) \right\} + \left\{ \Delta x(0) \times \cos \omega \times t + \frac{\Delta x(0)'}{\omega} \times \sin \omega \times t \right\} \quad (4.9)$$

where  $(\Delta x_{st})_0$  is the static displacement caused by the step force.

This static displacement can be computed by using equations presented previously for the calculation of the guy cable stiffness in the slack and taut conditions, respectively. The second term in Eq. (4.9) is the free-vibration response of the structure at the beginning of the ramp phase. If at rest the initial conditions are considered, then  $\Delta x(0) = 0$  and  $\Delta x(0)' = 0$ . It is noted that only the first term of Eq. (4.9) is considered for computing the response of the guy cable during the ramp phase. For the response during the constant phase, the following equation, proposed by Chopra (1995), is used:

$$\Delta x(t) = (\Delta x_{st})_0 \times \left\{ 1 - \frac{1}{\omega \times t_r} \times [\sin \omega \times t - \sin \omega \times (t - t_r)] \right\} \quad (4.10)$$

It is noted that the above equation accounts for the free-vibration of the SDOF system resulting from the displacement  $\Delta x(t_r)$  and velocity  $\Delta x(t_r)'$  at the end of the ramp phase. As mentioned previously, the maximum response occurs during the constant phase of the impulse loading. According to Chopra (1995), the maximum value of the response can be determined with the following equation:

$$\Delta x(t)_{max} = (\Delta x_{st})_0 \times \left\{ 1 + \frac{1}{\omega \times t_r} \times [(1 - \cos \omega \times t_r)^2 + (\sin \omega \times t_r)^2]^{0.5} \right\} \quad (4.11)$$

Eqs. (4.8) to (4.11) are applicable to SDOF systems. Because cables are flexible members with many active mode shapes, a MDOF system, modeled as a sequence of tension-only truss-elements, is usually the choice to estimate the responses of these members to dynamic loading. The dynamic response of a MDOF system can be determined by solving the following equation for each nodal coordinate  $\Delta q(t)_n$  specialized to an undamped system:

$$\Delta q(t)_n'' + \omega^2 \times \Delta q(t)_n = \frac{F(t)_n}{M_n} \quad (4.12)$$

where  $\Delta q(t)_n''$  is the acceleration term of the nodal coordinate,  $\Delta q(t)_n$  is the displacement of the nodal coordinate and  $M_n$  is the modal mass. The equation for the nodal coordinate is of the same form as the equation of motion for a SDOF system (Chopra, 1995), and the solution methods available for SDOF systems can be adapted to obtain solutions for  $\Delta q(t)_n$  for the modal equations. The maximum modal contribution of the  $n^{\text{th}}$  mode to the response of the cable is therefore:

$$\Delta x(t)_{max-n} = (\Delta q_{st})_0 \times \left\{ 1 + \frac{1}{\omega_n \times t_r} \times [(1 - \cos \omega_n \times t_r)^2 + (\sin \omega_n \times t_r)^2]^{0.5} \right\} \quad (4.13)$$

The combination of all the considered modes of vibration  $\Delta x(t)_n$  gives the total response of the cable. This combination is termed mode superposition method. Specialized to the response of a guy cable to an impulse load, it has the following form:

$$\Delta x(t)_{max} = \sum_{n=1}^N A_n \times (\Delta q_{st})_0 \times \left\{ 1 + \frac{1}{\omega_n \times t_r} \times [(1 - \cos \omega_n \times t_r)^2 + (\sin \omega_n \times t_r)^2]^{0.5} \right\} \quad (4.14)$$

Eq. (4.14) gives the maximum displacement response of the cable during the constant phase. This displacement response can be used to derive the cable tension using the equations presented in Chapter II for calculating the cable stiffness. Table 4.3 presents a comparison between the peak tension forces from the nonlinear dynamic analysis and those derived with the results obtained with Eq. (4.14). These peak tension forces are normalized using the equivalent static forces. The maximum difference between the results from the two methods is about 8%. This difference in results is apparently due to the fact that the mode superposition method does not take into account nonlinearities associated with the variation of guy stiffness and vibration properties (mode frequencies and modal amplitudes) with guy movement. This observation highlights the limitation of linear methods, such as spectral analysis methods based on modal superposition, in estimating the maximum response of structures with significant nonlinearities. Although these limitations are well known, the differences presented in Table 4.3 are relatively small and indicate that Eq. (4.14) can be considered useful for estimating the order of magnitude of the maximum dynamic response of a guy cable to an impulse load.

**Table 4.3. Comparisons between peak responses obtained from nonlinear dynamic analyses and results obtained with the analytical approach.**

$t_r/T_{1st}^{(1)}$	$R_{H-max}/F(t_r)^{(2)}$	
	FEM Nonlinear Dynamic Analysis	Analytical Approach (Eq. 4.14)
0.50	1.21	1.12
0.27	1.26	1.24
0.21	1.28	1.27
0.10	1.60	1.56

(1) Ratio of rise-time to period of vibration of the 1<sup>st</sup> flexural mode in the transversal direction. (2) ratio of peak dynamic force to equivalent static force.

By analysing the results of the FEM simulations and the form of Eq. (4.14), it can be seen that the ratio  $\Delta x(t)_{max}/(\Delta x_{st})_0$ , herein termed displacement response factor  $R_x$ , and consequently the ratio  $R_{H-max}/F(t_r)$ , depends on the magnitude of the cable displacement and on the ratio of rise-time to natural period  $t_r/T_{1st}$ . The smaller is the  $t_r/T_{1st}$  ratio the higher is the value of  $R_{H-max}/F(t_r)$ . The capacity curve presented in Fig. 4.7 indicates that the structure can deflect approximately 0.4 meters before the first member failure. At this deflected position, the tension in the tight guy cable is about 65% of its design tension capacity. To exceed the tensile capacity of guy cable, the static tension in the tight cable should be amplified by a factor of 1.55. Analyzing the results presented in Table 4.3, it can be seen that this level of dynamic amplification is reached for values of  $t_r/T_{1st} \leq 0.10$ , approximately. As mentioned previously,  $t_r/T_{1st} = 0.10$  corresponds to a rise-time of 0.05 seconds, which is linked to the period of vibration of 0.10 seconds of the 2<sup>nd</sup> flexural mode in the longitudinal direction.

The analyses presented in this section indicate that tight guy cables could be subjected to impulse forces potentially exceeding design limits in case the tower vibrates at higher mode frequencies. At higher vibration frequencies, tension forces in the guy cable could be amplified by a factor of 1.6 or more due to impulse forces originated from the mast vibratory motion. This level of dynamic amplification is in the range of dynamic amplification factors considered in typical design load cases. Typical dynamic coefficients used for broken conductor or ground wire load cases range from 1.5 to 2.0.

#### 4.6. Horizontal Base Reaction from Harmonic Excitation

The response of a structural system to harmonic excitation is a classical application of structural dynamics. Understanding the response of a structure to harmonic excitation it also provides information on the structure response to dynamic loads, such as inertia loads originated from ground motion excitations. In this study, harmonic excitation analyses were carried out to assess the dynamic amplification of the structures' responses for a given range of forcing frequencies. The free-standing delta guyed tower was subjected to a harmonic force with amplitude equal to the structure's weight and distributed along their height as per Eq.(4.3). The applied harmonic force has a sinusoidal time-varying pattern described by the following equation:

$$F(t) = F_0 \times \sin(\omega \times t) \quad (4.15)$$

where  $F_0$  is the amplitude of the harmonic force vector,  $\omega$  is the forcing frequency in units of radians/s and  $t$  is the time variable. Initially, only the steady-state response was studied. The complete response, including both the steady-state and transient responses, was studied after. Equations are proposed for estimating dynamic amplification factors for base shear response due to harmonic excitation.

##### 4.6.1. Steady-State Response

The harmonic analyses presented in this section were aimed at obtaining the steady-state response spectrum of base shear of the tower structures to harmonic horizontal forces. The transient response of the structure, which occurs at the beginning of the excitation and during the vibration of the structure caused by effects associated with mast and cable interactions, were considered in a subsequent phase of the analyses. In a steady-state harmonic analysis, the MDOF equation of motion has the following form (ANSYS, 2013):

$$\begin{aligned} ([K] - \omega^2 \times [M] + i \times \omega \times [C]) \times (\{u_1\} + i \times \{u_2\}) &= \{F_1\} + i \times \{F_2\} \\ \{F_1\} &= \{F_{max} \times \cos \varphi\}; \{F_2\} = \{F_{max} \times \sin \varphi\} \\ \{u_1\} &= \{u_{max} \times \cos \vartheta\}; \{u_2\} = \{u_{max} \times \sin \vartheta\} \end{aligned} \quad (4.16)$$

where  $[K]$  is the stiffness matrix,  $\omega$  is the forcing frequency in units of radians/s,  $i$  is the imaginary unit,  $[C]$  is the damping matrix,  $\{u\}$  is the nodal displacement vector,  $\{F\}$  is the force vector,  $\vartheta$  and  $\varphi$  are respectively the displacement and force phase shifts,  $u_{max}$  is the maximum displacement and  $F_{max}$  is the force amplitude. Herein,  $\{F_1\}$  and  $\{u_1\}$  are the real components of

the force and displacement vectors, respectively, whereas  $\{F_2\}$  and  $\{u_2\}$  are the imaginary components of the force and displacement vectors, respectively. The real components of  $\{F\}$  and  $\{u\}$  are associated with the in-phase component of the resisting forces that are available to restraint the tower against motion. The imaginary components of  $\{F\}$  and  $\{u\}$ , on the other hand, are associated with the out-of-phase resisting force component that does not contribute to the restraint but, instead, is associated with energy that is dissipated from the system. In the above equation, the time variable is not considered and the transient effects, which are time dependent, are removed from the analysis.

In Fig. 4.13 is showed the real and imaginary parts of the response spectra of base shear of the delta guyed tower for a steady-state harmonic analysis carried out with ANSYS APDL in the transversal direction. Values in the abscissa axis correspond to the ratio of forcing frequency  $\omega$  to natural frequency  $\omega_n$ . The natural frequency of this tower in the transversal direction is 1.93 Hz (refer to Table 4.2). Values in the ordinate axis corresponds to the ratio of response base shear to the amplitude of the harmonic force  $F_0$ . Base shear is defined as the resultant vector of reactions at the base of the tower mast and guy-anchors at the horizontal direction of the applied harmonic force. As mentioned previously, the amplitude of the harmonic force was taken to be equal to the weight of the tower structure. This ratio can be understood as the dynamic amplification of base shear for a given forcing frequency in terms of the structure's weight.

In the left part of Fig. 4.13 is presented the response base shear from the tower mast base (dashed red line), from one of the guy-anchors (dashed dark line) and the total base shear response (continuous dark line). The negative sign in Fig. 4.13 (left) signifies that the base shear is reacting in-phase with the applied harmonic force and that the guy-cables are offering restraint to the motion imposed by these horizontal forces. Conversely, for a positive sign, the base shear reaction is out-of-phase with the harmonic force, meaning that the guy-cables are pulling the tower mast in the same sense, or in-phase, with the horizontal forces.

Initially, the real component of base shear increases (in negative values) with increasing forcing frequencies until resonant frequency is attained. At this point, the sign of the real part reverses suddenly, becoming strongly positive. At resonant frequency, the imaginary part of base shear (Fig. 4.13 – right) suddenly takes on a large negative value, indicating that there is a sudden change in phase between the applied force and the base shear and that energy is being dissipated from the system.

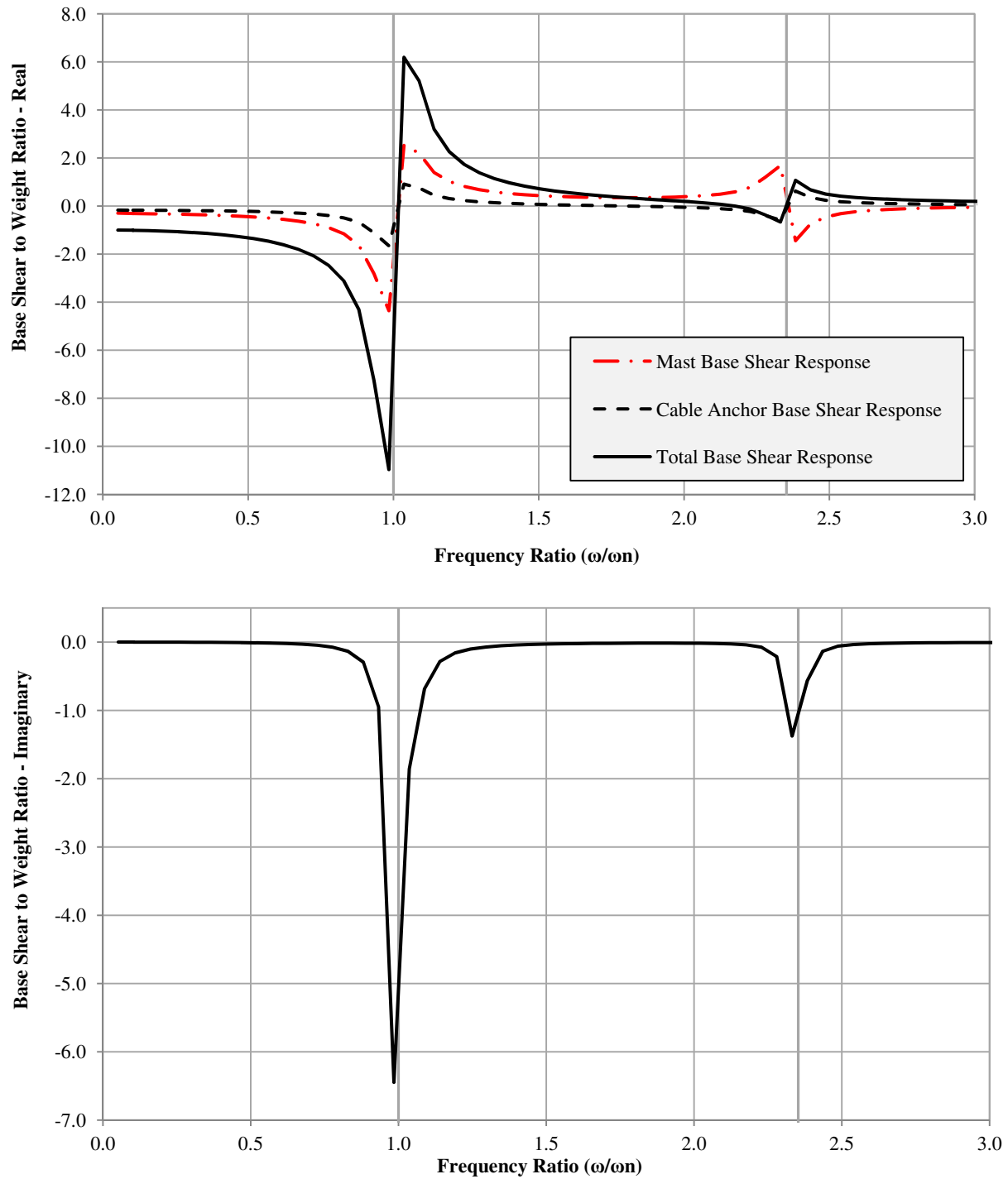


**Figure 4.13. Response spectra of base shear to forced harmonic excitation. Real component (top) and imaginary component (bottom).**

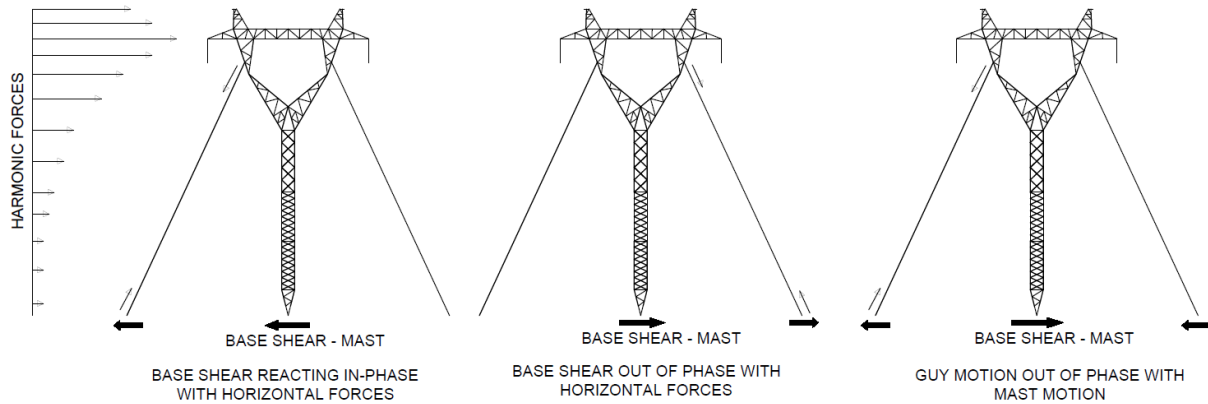


**Figure 4.14. Base shear response to horizontal harmonic forces. Base shear reacting in-phase with harmonic forces (left). Base shear out of phase with horizontal forces (center). Guy cable out of phase with mast motion (right).**

A second abrupt change in the base shear phase is also observed in Fig. 4.13 (right) when the forcing frequency attains the frequency of the second mode of vibration of the structural system. Before the frequency of the second mode of vibration is attained, the motion of both cables and mast are in phase. Approaching the frequency of the second mode of vibration, the motion of the cable takes on a sense contrary to the motion of the mast. This phase shift between the motion of the cable and the mast results in a discontinuity of the responses causing additional tension in the guy cable. In this situation, the cable is acting much like a damper due to a phase shift oscillation with respect to the mast. These above described situations are illustrated in Fig. 4.14. Finally, when the forcing frequency reaches the frequency of the second mode of vibration, another abrupt change is observed in both real and imaginary parts of the base shear response, signifying again a sudden change in the response phase and that energy is being dissipated from the system. It is noted herein that the response spectra of base shear presented in Fig. 4.13 (left) resembles the typical steady-state response spectra of a SDOF system subjected to harmonic excitation. The response spectra of base shear resulted for the MDOF system is given in Fig. 4.15. In addition, for the comparison purpose, the response spectra of base shear obtained for a SDOF system with the same natural frequency is also illustrated. For an undamped SDOF system, the steady-state response to a sinusoidal harmonic excitation is expressed as follows (Chopra, 1995):

$$u(t) \times k = F_0 \times \frac{1}{1 - (\omega/\omega_n)^2} \times \sin \omega \times t \quad (4.17)$$

where  $u(t)$  is the displacement and  $k$  is the stiffness of the SDOF, which can be derived from pushover curves (refer to Figs 4.7 and 4.9). The left term in the above equation can be understood as the steady-state response of base shear  $V(t)$ . The Eq. (4.17) can be rewritten as follows:

$$V(t)_{steady} = F_0 \times \left[ \frac{1}{1 - (\omega/\omega_n)^2} \right] \times \sin \omega \times t \quad (4.18)$$

Hence, Eq. (4.18) was used to derive the response spectrum of maximum base shear for various forcing frequencies  $\omega$  and the results are presented in Fig. 4.15 (red dashed line) where a comparison is made with the results of the MODF response spectra. The value of  $\omega_n$  considered in Eq. (4.18) is the frequency of the 1<sup>st</sup> flexural mode of vibration of the tower in the transversal direction.

This comparison indicates that the steady-state base shear response calculated with Eq. (4.18) for a SDOF system yields a good approximation to the results of the harmonic analysis based on a MDOF system. Thus, it is suggested that Eq. (4.18) can be used to estimate or approximate the maximum base shear response of this nonlinear MDOF structure to harmonic excitation. However, as it will be shown later, this equation needs to be adjusted to account for important transient effects caused by the structure's free-vibration and inherent nonlinearities.

Fig. 4.15 shows that the reactive base shear is amplified as the forcing frequency approaches the natural frequency of the structure. At resonant frequency (i.e.  $\omega = \omega_n$ ) the peak base shear response is several times greater than the applied load and the magnitude of this peak becomes dependant on the level of damping considered, which is usually small for these types of structures. In this study, the critical damping ratio was considered constant and equal to 2.0% for the tower structure and 0.1% for the guy cables. After the resonant peak, the base shear response tends to be smaller than the applied harmonic force amplitude due to a phase shifting between the applied force and the structure's response, as explained previously. Finally, a second peak appears in the response spectra where the response base shear is again amplified by the action of the second flexural mode of vibration in the transversal direction.

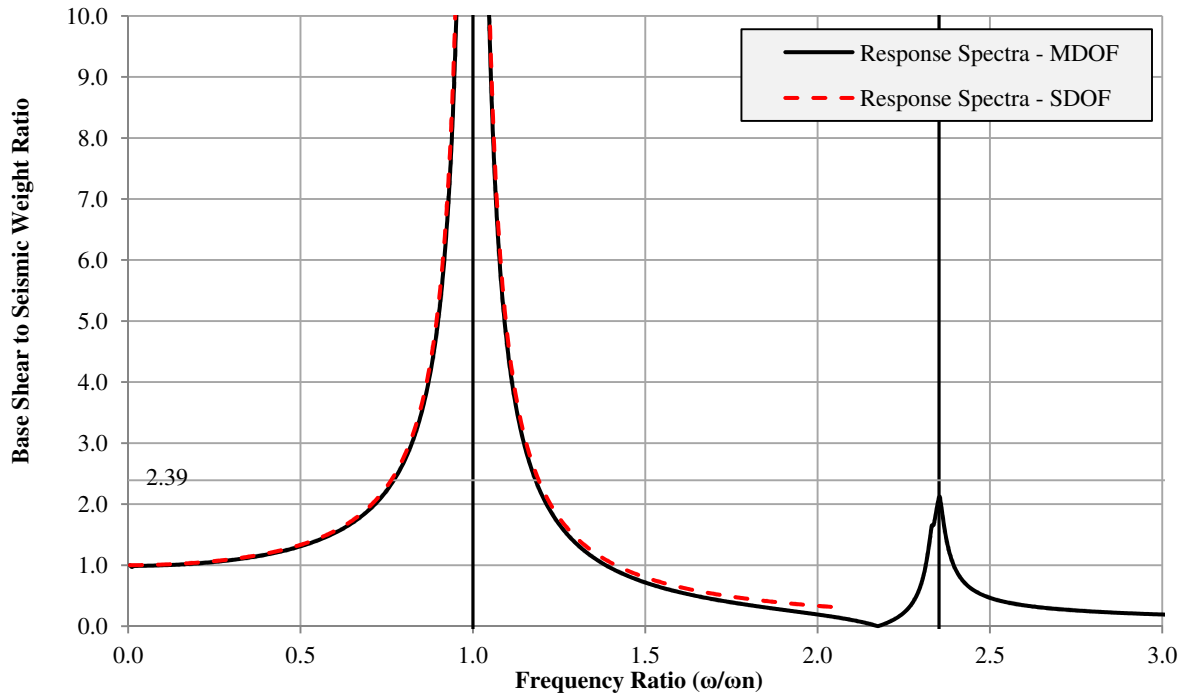


**Figure 4.15. MDOF and SDOF systems response spectra of base shear to forced harmonic excitation.**

Pushover analyses presented in Section 4.4 indicate that the flexural capacity of this delta guyed tower is attained for a base shear value of 2.39 times the weight of the structure. This limiting condition is also presented in Fig. 4.15 where is shown that the flexural capacity of the structure in the transversal direction is exceeded in case this structure is subjected to a harmonic force with amplitude equal to the structure's weight and with a forcing frequency ranging from 0.78 to 1.18 times the natural frequency of 1.93 Hz, that is, between 1.50 Hz and 2.28 Hz. As mentioned previously, the predominant period of ground motions considered herein ranges from 1.35 Hz to 5.00 Hz, therefore comprehending the above mentioned range of frequencies in which the tower's capacity would be exceeded by means of resonant excitation.

This analogy with a SDOF system permits the analysis of other aspects of the structure's response to harmonic excitation. Analyzing the term in brackets in Eq. (4.18), it can be seen that this term has a positive sign for  $\omega/\omega_n < 1$ , indicating that the response has the same sign as the harmonic force and that both are in phase. For  $\omega/\omega_n > 1$ , this term has a negative sign and the response is out of phase with the harmonic force. In the later case, the inertia forces due to tower vibration are in the contrary sense of the harmonic forces, thus resulting in a base shear response smaller than the applied harmonic force.

#### 4.6.2. Total Response

Harmonic analyses considering the total response of the structures were carried out based on nonlinear transient dynamic analysis for MDOF systems. As mentioned previously, in a transient dynamic analysis time-effects are account for and the calculated response of the structure to harmonic excitation includes both the steady-state and transient responses. These total response harmonic analyses were carried out for a set of forcing frequencies ranging from 0.25 Hz to 4.0 Hz, in steps of 0.25 Hz, in the transversal direction for the delta guyed tower.

An example of the base shear response of the delta guyed tower is presented in Fig. 4.16 for a harmonic force applied in the transversal direction and with a forcing frequency of 0.5 Hz. This figure shows that the base shear response contains two distinct vibration components: a steady-state response (dashed line) and a transient response, which is the difference between the total response (continuous black-line) and the steady-state response. The steady-state state response is the main component of the response and is represented by a harmonic curve defined by Eq. (4.18) and with a frequency equal to the forcing frequency  $\omega$ .

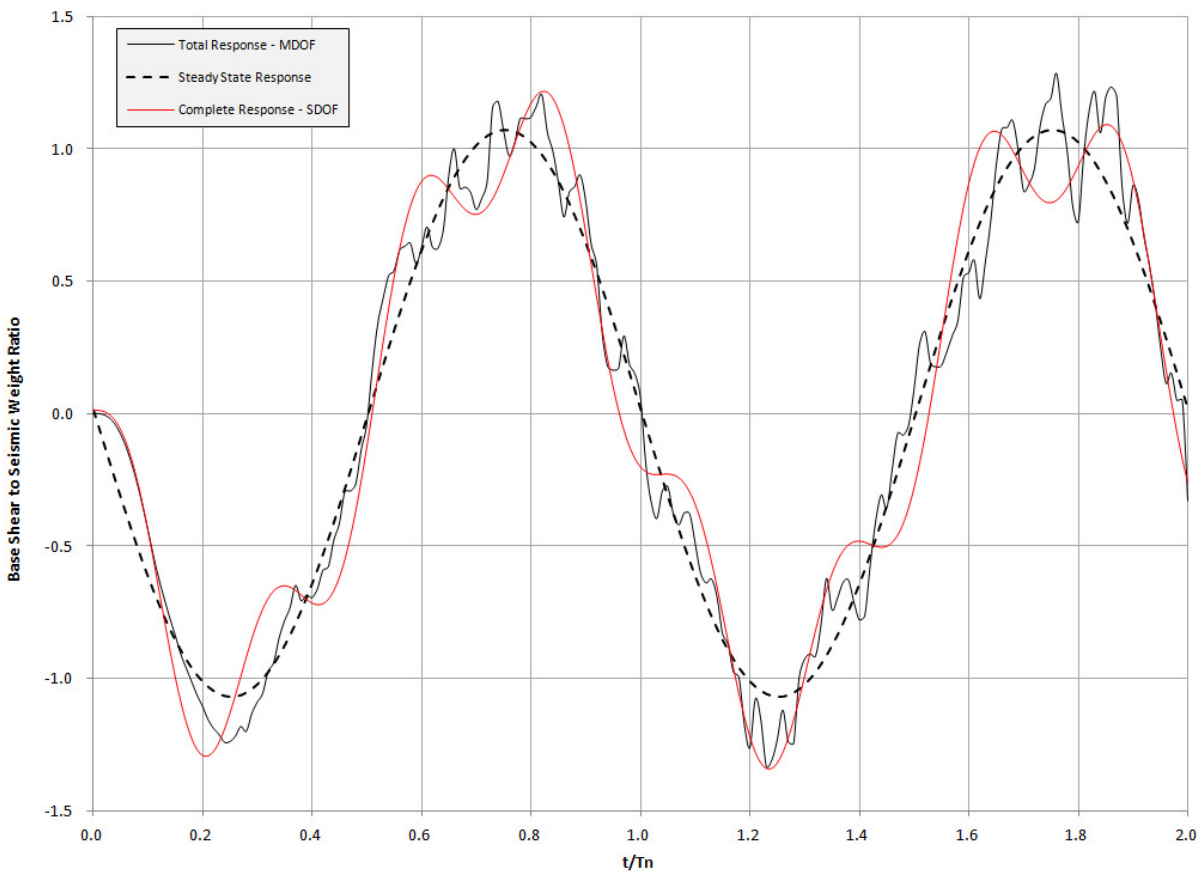


**Figure 4.16. Steady-state and total response to harmonic excitation.**

The transient component contains the resultant response of the structure defined by its several active modes of vibration and effects associated with cable-mast interactions. Fig. 4.16 shows that the transient component of the vibration significantly enhances the base shear response in regards to the steady-state response and should therefore be taken into account. Further, Fig. 4.17 shows an example of Fourier spectra of the total and steady-state responses of this tower for forcing frequencies of 0.5 Hz and 2.5 Hz. As indicated by the amplitude of the Fourier spectra, the transient response of the MDOF tower system is dominated by the natural frequency  $\omega_n$ . These response spectra suggest that the transient response of the MDOF tower system can also be approximated by the transient response of an equivalent SDOF system given by the following Eq. (4.19) for an undamped system (adapted from Chopra, 1995):

$$V(t)_{transient} = F_0 \times \frac{\omega/\omega_n}{1 - (\omega/\omega_n)^2} \times \sin \omega_n \times t \quad (4.19)$$

It is recalled herein that the level of damping for these lattice tower structures are usually considered small and does not significantly affect or attenuate the transient response of the structure at the beginning, or at the first cycles of the harmonic excitation.

The total base shear response of an equivalent SDOF is also plotted in Fig. 4.17 (red continuous line) for comparison purposes, and the steady-state and total response spectra of the delta guyed tower structure, based on Eqs. (4.18) and (4.19), are presented in Fig. 4.18 where a comparison is made with the MDOF base shear responses based on nonlinear transient analyses. From these comparisons, it can be seen that the complete base shear response of the equivalent SDOF system results in a good approximation of the base shear of the MDOF for forcing frequencies smaller than the natural frequency of the structure.

For forcing frequencies greater than the natural frequency, the base shear response of the MDOF is less than that of the SDOF system due to dampening effects caused by phase shift oscillations between cable and mast, as explained in the previous section, and a correction factor should be considered to estimate the base shear response of the MDOF system based on SDOF harmonic response equations. Hence, the following expression is proposed to estimate the total base shear response of TL guyed towers to harmonic excitation:

$$\text{for } \omega < \omega_n: \quad V(t)_{total} = V(t)_{steady} + V(t)_{transient} \quad (4.20a)$$

$$\text{for } \omega > \omega_n: \quad V(t)_{total} = 0.85 \times V(t)_{transient} + 0.40 \quad (4.20b)$$

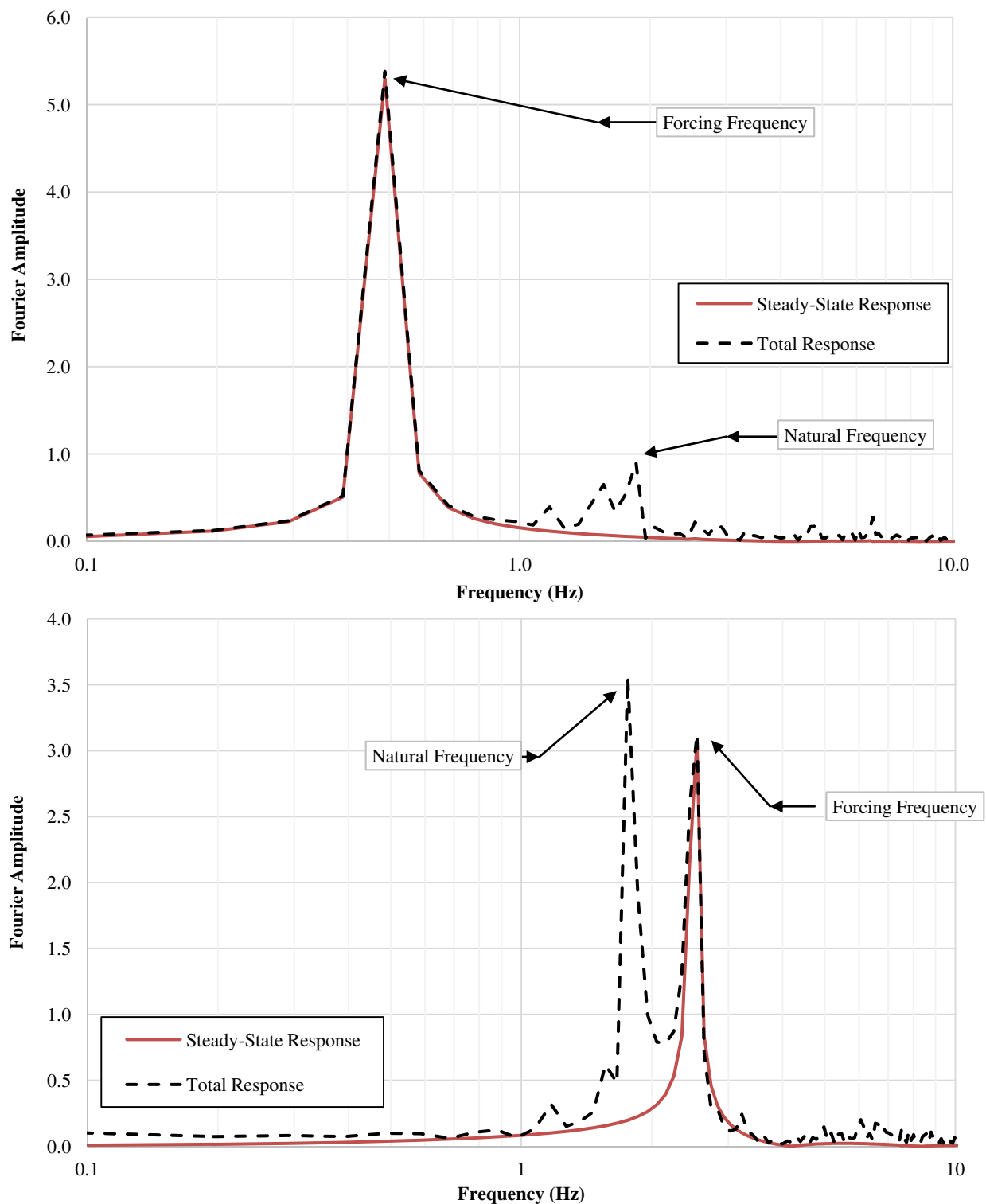


**Figure 4.17.** Fourier spectrum of the total and steady-state responses for a forcing frequency of 0.5 Hz (top) and 2.5 Hz (bottom).

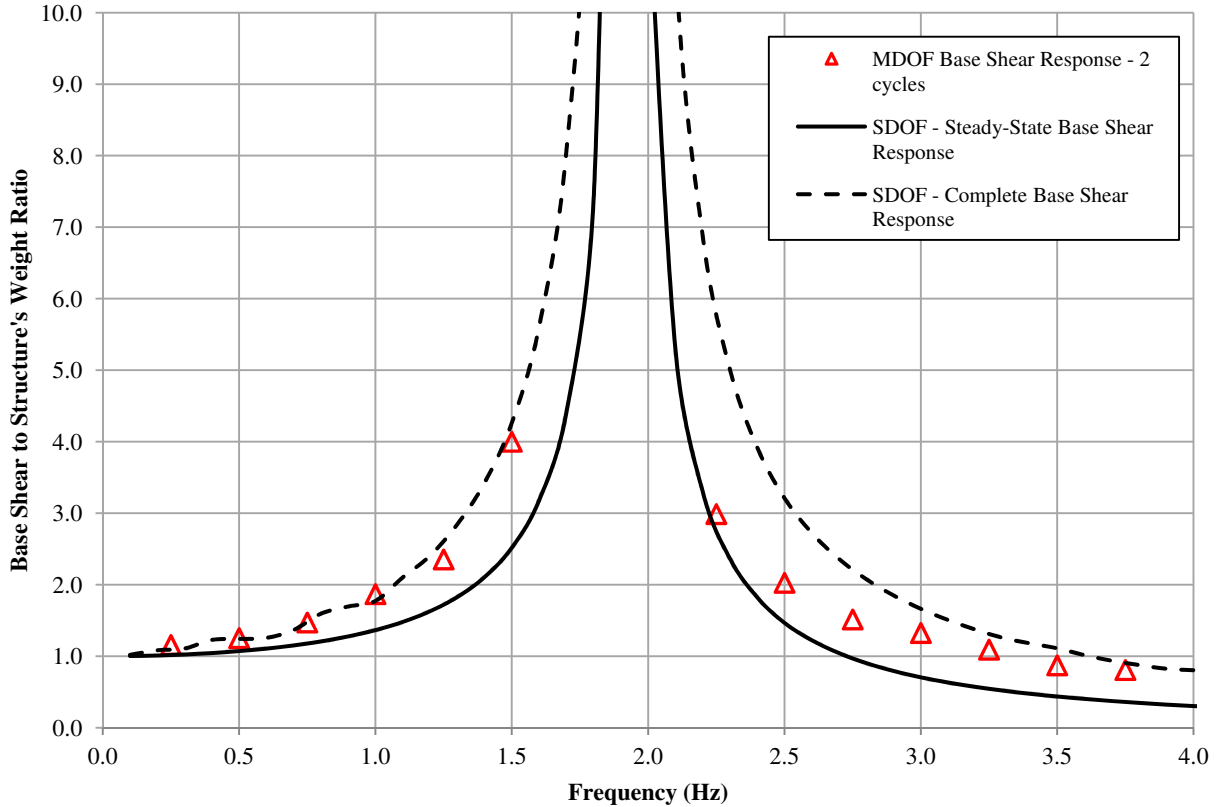


**Figure 4.18. Steady-state and total peak base shear response of SDOF and MDOF systems.**

For SDOF systems, the peak of the total response occurs when the peak steady-state and peak transient responses coincides or are in phase. Therefore, for the peak of the total response to occur, a number of sustained harmonic cycles may be necessary depending on the forcing frequency and damping, which introduces a time-lag between the two responses. This same principle applies to MDOF systems.

Further, in Fig. 4.19 is illustrated an example of the variation of peak base shear response with the number of sustained harmonic cycles for a forcing frequency of 0.5 Hz. As showed in this figure, the peak base shear response tends to increase with the number of sustained harmonic cycles but, as with SDOF systems, it also tends to an asymptotic limit. The proposed expression which correlates the number of sustained cycles with peak base shear response has the following form:

$$V(t)_{total} = (a + 1 - e^{-2 \times \pi \times \epsilon \times b \times j}) \times F_0 \quad (4.21)$$

where  $j$  is the number of sustained harmonic cycles and  $a$  and  $b$  are coefficients determined based on regression analyses of the above expression to the peak base shear responses from MDOF nonlinear transient analyses. Values for the coefficients  $a$  and  $b$  for various forcing frequencies are given in Table 4.4. In the above equation, the coefficient  $a$  gives a sense of the magnitude of the response for the first harmonic cycle and the magnitude of coefficient  $b$  gives a sense of the number of cycles necessary, or how fast, the peak response is attained. The higher the value of  $b$  the faster the response approximates to an asymptotic value.

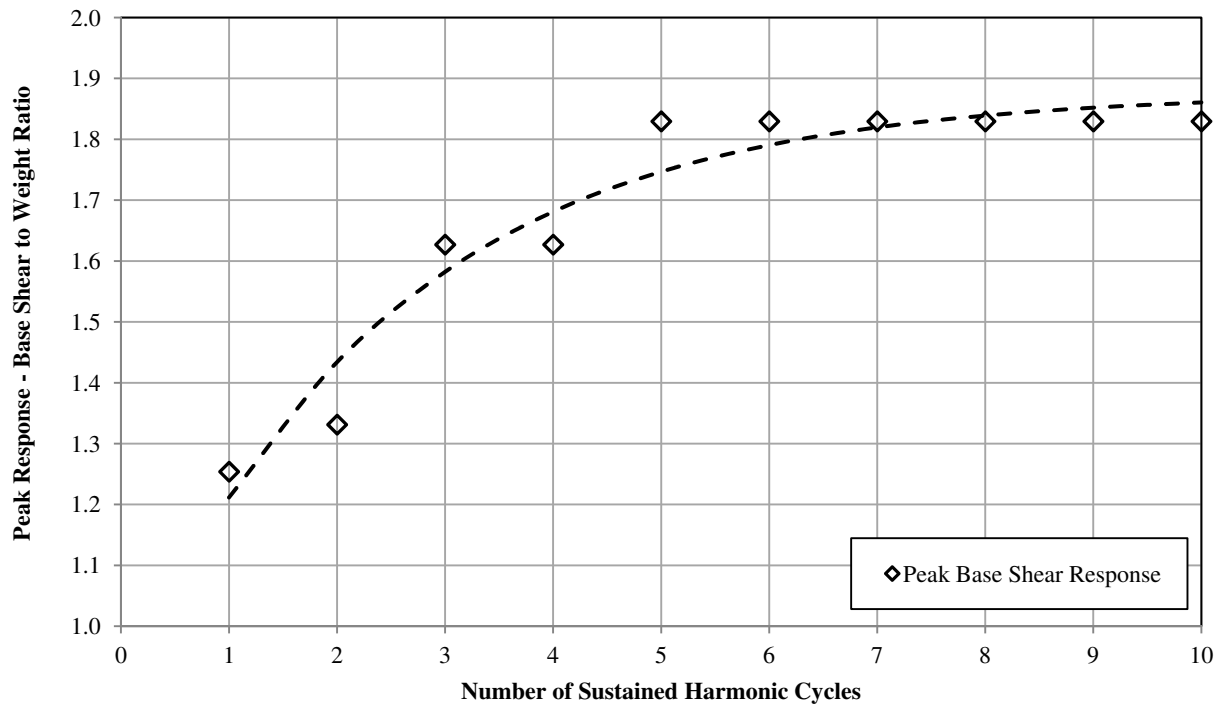


**Figure 4.19.** Variation of peak base shear response with the number of sustained harmonic cycles.

**Table 4.4.** Coefficients  $a$  and  $b$  derived for Eq. (4.21).

Forcing Frequency (Hz)	$a$	$b$	Forcing Frequency (Hz)	$a$	$b$
0.50	0.88	3.23	2.50	0.84	5.98
0.75	0.91	4.29	2.75	0.53	7.75
1.00	1.62	3.06	3.00	0.37	8.16
1.25	2.34	3.47	3.25	0.12	12.62
1.50	4.00	3.55	3.50	0.09	18.88
2.25	1.7	3.59	3.75	0.01	32.09

When the frequency of the harmonic force is equal to the natural frequency of the tower structure, the response attains its maximum and the magnitude of this peak is dependent on the damping ratio considered for the structure. This harmonic excitation is termed resonant excitation. For the peak resonant response to be attained, a number of sustained forcing cycles are necessary. Considering the forcing frequency equal to the natural frequency ( $\omega/\omega_n = 1$ ) and that the structure is at rest at the beginning of the harmonic excitation, the steady-state base shear response of the tower structure to harmonic excitation is given below in Eq. (4.22) which is adapted from Chopra (1995).

$$V(t)_{resonant} = F_0 \times (A \times \sin \omega \times t + B \times \cos \omega \times t)$$

$$A = \frac{1 - (\omega/\omega_n)^2}{[1 - (\omega/\omega_n)^2]^2 + [2 \times \varepsilon \times (\omega/\omega_n)]^2} \quad (4.22)$$

$$B = \frac{-2 \times \varepsilon \times (\omega/\omega_n)}{[1 - (\omega/\omega_n)^2]^2 + [2 \times \varepsilon \times (\omega/\omega_n)]^2}$$

Herein,  $\varepsilon$  is the viscous damping ratio defined as a fraction of critical damping. For a lightly damped structure, the maximum base shear response  $V(t)_{max}$  to a resonant harmonic excitation depends on the number of sustained harmonic cycles as defined by the following equation (adapted from Chopra, 1995):

$$V(t)_{max} = F_0 \times \frac{1}{2 \times \varepsilon} \times (\varepsilon^{-\varepsilon \times \omega_n \times t} - 1) \quad (4.23)$$

The analyses presented in this section have shown that, for the type of tower studied herein, SDOF equations can be used to derive dynamic amplification factors for dynamic loads that can be represented or approximated by harmonic functions. The use of equivalent and simpler SDOF systems for deriving parameters for use in design, such as base shear, is of particular interest for structural designers because the modeling of non-linearities and dynamic effects is usually a time-consuming task, requiring significant computational efforts, and therefore not suitable for concept level design.

Harmonic excitation analyses presented in this section also showed that the transient response of TL towers studied herein is mainly determined by the contribution of the first mode of vibration in direction of the analysis. For forcing frequencies smaller than the natural frequency of vibration, it was found that the vibration response is mainly characterized by the contribution of

the forcing frequency; whereas for forcing frequencies higher than the natural frequency, it was found the response is governed by both the forcing frequency and the frequency of the first flexural vibration mode and that the contribution of the first mode of vibration is higher than the contribution of the forcing frequency. Fourier response spectra presented in Fig. 4.17 indicates that other vibration modes also contribute to the transient response but the contribution of the first mode still predominates.

## **CHAPTER V**

### **SENSITIVITY OF TL FREE-STANDING AND GUYED TOWERS TO EARTHQUAKE LOADS**

#### **5.1. Introduction**

In this chapter, a comparison between the TL tower structure response resulted from linear dynamic analysis by the modal response spectrum method and that resulted from nonlinear dynamic analysis by the numerical integration time-history method is first completed. The purpose of this task is to determine whether the spectrum analysis method, which is less computationally-intensive than the transient time-history method, is suitable for determining the response of guyed tower structures subjected to seismic loads as ground motions. The relevance of considering seismic loads in the design of typical lattice high-voltage TL towers is evaluated by comparing the seismic response of towers studied herein and located in Bamfield, B.C. with the response from standard design load cases including wind and ice accretion. The sensitivity of these towers to earthquake ground motions is assessed by determining the number of members which capacity was exceeded and the number of seismic load cases where structural instability due to member failure was found. Expressions for determining the base shear response of free standing guyed towers were derived from the results of detailed nonlinear transient simulations carried out for 20 seismic ground motions in all orthogonal directions. Finally, an equivalent static method is proposed to approximate the seismic response obtained with nonlinear transient analyses for the free-standing guyed towers studied herein.

#### **5.2. Comparison between the Tower Response Resulted from Modal Response Spectrum Method vs. Nonlinear Time-History Method**

The use of modal response spectrum method has the advantage of replacing the lengthy nonlinear dynamic analysis applied to obtain the seismic response of tower structure systems. In the case where the material and geometric properties of the structure vary significantly during the response to earthquake ground motions, linear analysis are no longer appropriate and nonlinear transient analyses are necessary to obtain a more realistic seismic response. Because lattice TL towers are slender structures, axial loads in the masts from tower's self-weight and conductor load induce, during the seismic response, important second-order effects (i.e. P-Delta effects) which act toward decreasing the structure's stiffness.

It is noted that linear analysis methods, such as spectral analysis based on the mode superposition method, does not take into account important nonlinearities associated with the variation of guy tower stiffness and variation of vibration properties (mode frequencies and modal amplitudes) with guy tower movement. To highlight the limitation of the spectral analysis method in regards to the type of guyed tower structures studied herein, a comparison is made between the responses obtained with the spectral method and those obtained with detailed nonlinear transient simulations. The delta guyed tower was subjected to a nonlinear transient simulation and to a response spectrum analysis for the seismic case NGA 15 ( $A/V$  ratio of 1.04, intermediate frequency content) in the transversal directions. A comparison between the results of nonlinear transient simulations and response spectrum analysis is showed in Fig. 5.1 in terms of a dispersion diagram. This dispersion diagram plots the maximum axial forces for all members of the delta guyed tower obtained from both methods. When the responses for a given member are equal from both methods, the dot in the diagram corresponding to that member lies in the 45 degrees' line. Similarly, if the responses for a given member are different, this difference is presented in terms of deviation from the 45 degrees' line. The dispersion diagram in Fig. 5.1 shows that, for the members with axial forces in the range of 20 kN to 80 kN, both methods yield approximately the same axial forces. For members with axial forces higher than 80 kN, nonlinear transient simulations yield higher axial forces. It is noted that these members with higher axial forces are leg members located in the tower's mast and K-frame, and that the tower mast is subjected to important bending moments originated form P-Delta effects due to eccentricities of vertical loads from overhead cables and structure's self-weight during seismic induced motion. A greater dispersion in the results is also present for members with axial forces less than 20 kN. These members are generally secondary or redundant bracing members used in the tower design to confer higher buckling capacity to primary bracing members and leg members.

This comparison has shown that the response spectrum analysis may lead to significant differences in the response of these nonlinear tower structures, especially for the most demanded members. In addition, from this comparison resulted that the response spectrum analysis may not be appropriate for estimating the maximum responses of slender lattice towers such as the delta guyed tower studied herein.

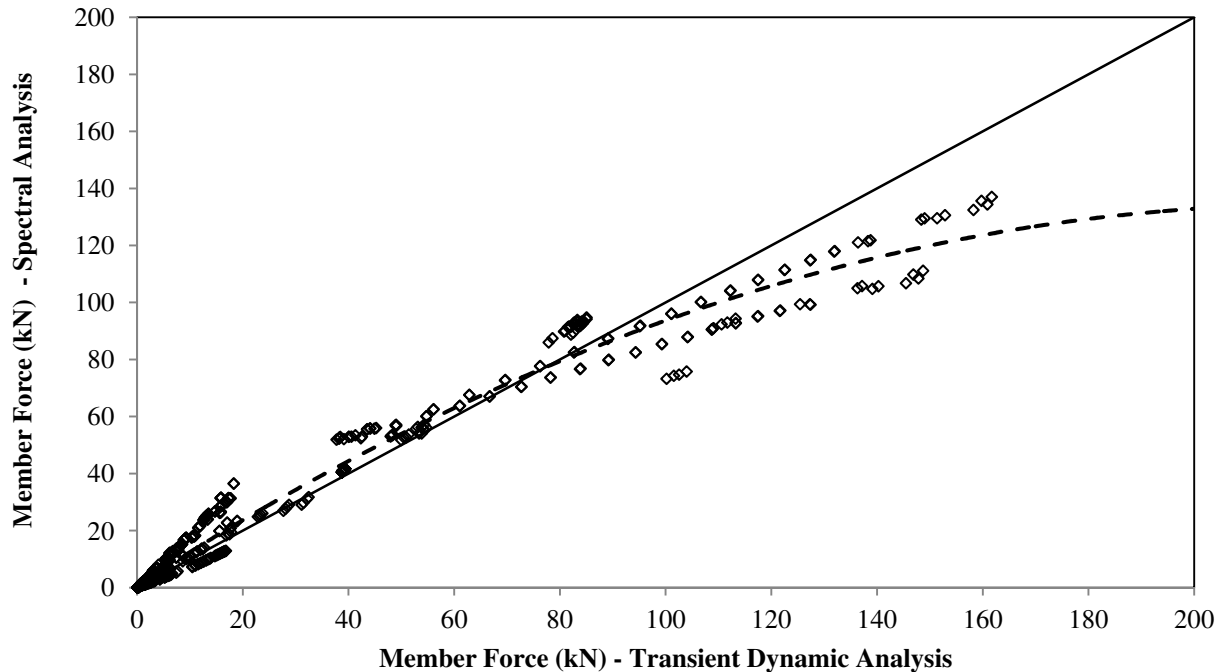


**Figure 5.1. Dispersion diagram comparing the results of transient dynamic analysis with the results of response spectrum analysis for the axial force in each member of the Delta guyed tower subjected to NGA 15 record in the transversal direction.**

### 5.3. Sensitivity of TL Towers to Earthquake Ground motion

As stated in Chapter I, one of the objectives of this study is to assess the relevance of considering seismic loads on the design of typical high-voltage TL towers. To attain this objective, the maximum axial forces on all members of the towers, derived from detailed nonlinear transient simulations under earthquake ground motion excitations, were compared with the maximum axial forces from the set of standard design load cases considered for the design of these towers. These towers were subjected to the set of 20 seismic ground motion records listed in Tables 3.5 and 3.6 (refer to Chapter III) in each one of the main horizontal directions (transversal and longitudinal direction) and in the vertical direction.

The percentage of TL tower's members in which seismic axial forces exceed the maximum axial forces from design load cases is presented in Table 5.1 for each ground motion case applied in the transversal direction. In Fig. 5.2 are depicted the results presented in Table 5.1. Results for seismic cases acting on the longitudinal and vertical directions are presented in Tables III.1 and III.2 in Appendix III. Further, the Table 5.2 presents the statistics of percentage of members with seismic axial forces exceeding maximum axial forces from design load cases for all directions analyzed.

**Table 5.1. Percentage of members with seismic axial forces higher than those resulted from typical design load cases. Earthquake ground motions scaled for Bamfield B.C. were applied in the transversal direction.**

NGA	Peak Ground Accel. (g)	Pred. Period (sec)	Tower			
			Guyed Towers		Self-supporting towers	
			Delta	Mast	Delta	Mast
			<i>Tower Weight (kN)</i>			
			54.3	77.8	232.3	473.6
			<i>Tower Height (m)</i>			
			37.7	53.1	36.6	57.1
Percentage of members with seismic axial forces higher than in design load cases						
1787	0.36	0.50	37%	8%	4%	1%
735	0.36	0.44	30%	14%	1%	2%
15	0.37	0.36	30%	23%	6%	4%
776	0.38	0.52	47%	25%	1%	4%
986	0.41	0.24	36%	12%	6%	3%
900	0.42	0.68	32%	11%	9%	2%
1005	0.42	0.20	29%	12%	8%	6%
1794	0.44	0.36	36%	17%	1%	1%
1049	0.47	0.24	43%	19%	13%	9%
766	0.55	0.38	7%	19%	8%	1%
739	0.57	0.20	59%	36%	5%	7%
174	0.57	0.26	32%	26%	8%	14%
848	0.58	0.34	60%	27%	7%	4%
767	0.62	0.20	31%	11%	8%	5%
963	0.63	0.26	60%	19%	9%	3%
57	0.63	0.20	37%	41%	13%	5%
1006	0.64	0.22	29%	10%	16%	9%
1039	0.67	0.26	28%	22%	15%	6%
721	0.68	0.22	35%	22%	6%	2%
953	0.84	0.52	82%	16%	15%	2%
		<b>Min.</b>	<b>7%</b>	<b>8%</b>	<b>1%</b>	<b>1%</b>
		<b>Max.</b>	<b>82%</b>	<b>41%</b>	<b>16%</b>	<b>14%</b>
		<b>Mean</b>	<b>39%</b>	<b>20%</b>	<b>8%</b>	<b>5%</b>

Overall, the results presented in these tables show that although the weight of Self-supporting towers studied herein is five to six times higher than the weight of similar guyed towers (similarity defined by approximately the same height and geometric configuration of the upper sections), the results from numerical simulations indicate that guyed towers are prone to a higher percentage of members with seismic axial forces higher than those resulted from typical design load cases. This remark shows that these towers are sensitive to seismic demand. The four selected towers listed in Table 5.1 for comparison purpose were designed to environmental loads

but not to earthquake load shaking. Scaling factors and other parameters characterizing the ground motions used herein are given in Tables 3.5 and 3.6 of Chapter III.

Although Self-supporting towers are heavier and therefore subjected to higher seismic inertia loads, members of guyed towers are more demanded due to dynamic effects induced by the frequency content of the seismic input and due to significant bending of their mast. It is also noted that these Self-supporting towers are strain towers (see definition in Chapter II) and are designed for higher tension loads from overhead cables than suspension guyed towers.

In Fig. 5.2 is showed that members of guyed towers are more sensitive to earthquake ground motions than members of Self-supporting towers. The results showed in Fig. 5.2 correspond to the application of seismic loads in transversal direction of TL towers. These TL towers studied herein were subjected to earthquake loads applied in the transversal direction of TL towers, longitudinal direction of TL towers and vertical direction. The results presented in Table 5.2 show that the effect of vertical component of seismic ground motion is more important in the response of heavier Self-supporting towers than in the case of flexible guyed towers.

The results presented in these figures and tables show that seismic loads are more relevant for the design of flexible guyed towers than for the design of Self-supporting towers. The delta type guyed tower is especially sensitive to ground motion excitation and present, on average, 39% of its members with seismic axial forces higher than the forces triggered from the governing design load case. It should be mentioned that previous studies carried out on the seismic analyses of lattice transmission towers also emphasized the relevance or importance of seismic loads in the design of these structures. As indicated by the literature review presented in Chapter II, these studied were mostly performed for Self-supporting towers however, and only telecommunication guyed towers were assessed for seismic loads.

Another objective stated in Chapter I was the assessment of the vulnerability of these towers to earthquake ground motion. To attain this objective, the element-death method available in ANSYS Mechanical, based on the EKILL command (ANSYS, 2013, was used to simulate the failure of a member when its capacity is exceeded. In this method, when a given response exceeds a limiting value, a zero value is attributed to the stiffness of this member, signifying that this member is no longer capable of transmitting forces to its adjacent nodes. In the case of the studied towers, the response in question is axial force. A script was developed within the APD Language environment to compare, in every time-step of the time-history simulations, the

response axial forces for all tower members with their respective capacities as determined by calculations performed with the PLS-TOWER software and based on the guidelines of ASCE (10-15). It is noted that in this study, the member capacity in compression is the buckling strength and the member capacity in tension is the tensile strength. Therefore, the post-buckling capacity of the member was not considered and herein, the definition of member failure is conservative.

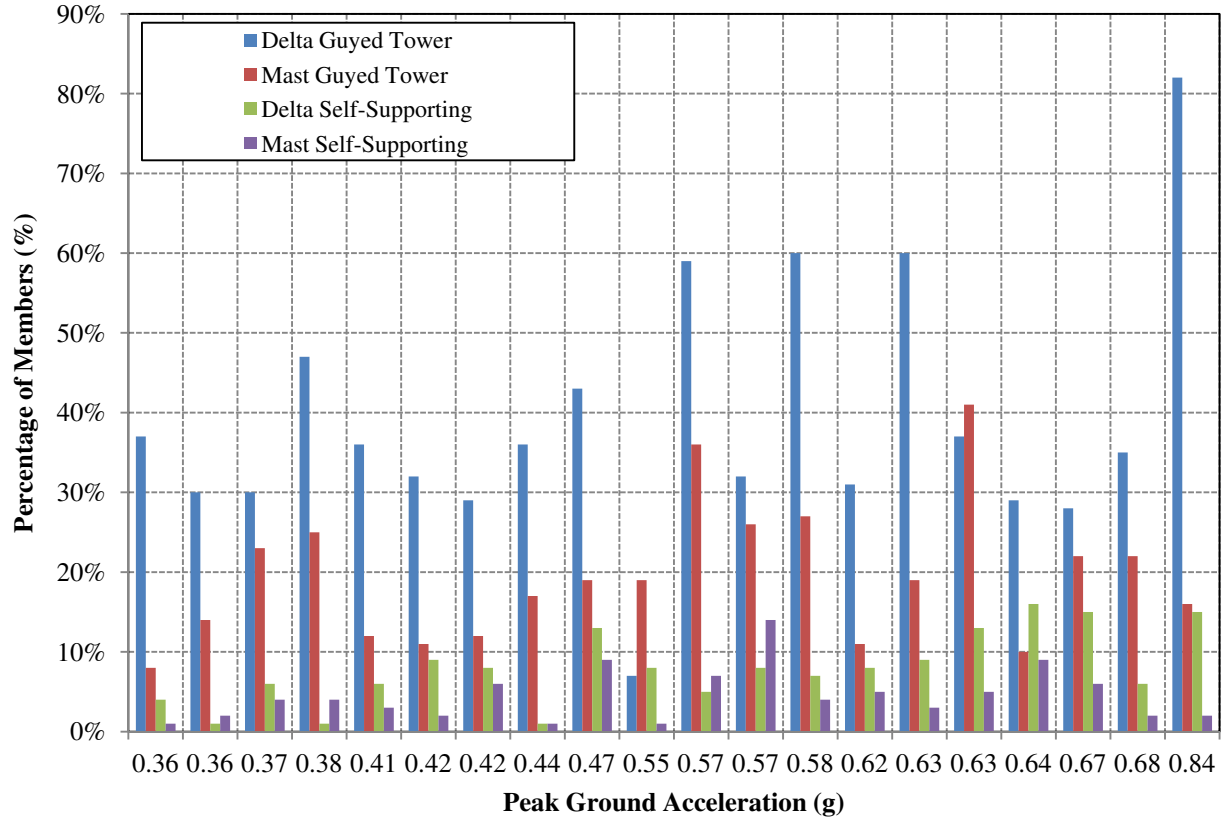


**Figure 5.2. Percentage of members with seismic axial forces higher than in design load cases. Earthquake ground motion acting on the transversal direction of TL tower.**

The number of members with capacity exceeded by the action of seismic forces acting on the transversal direction, for each seismic case and site class, is presented in Table 5.3. Results for all other directions of analyses (longitudinal and vertical) are presented in Tables III.3 and III.4 in Appendix III. In addition, Table 5.4 presents the statistics of number of members with capacity exceeded by the action of seismic forces acting on each one of the direction analyzed. As expected, delta guyed tower shows the highest number of failed members.

**Table 5.2. Percentage of members with seismic axial forces higher than in design load cases. Statistics per direction of earthquake incidence.**

Earthquake Incidence Direction	Statistics	Tower			
		Guyed Towers		Self-supporting towers	
		Delta	Mast	Delta	Mast
		<i>Tower Weight (kN)</i>			
		54.3	77.8	232.3	473.6
		<i>Tower Height (m)</i>			
		37.7	53.1	36.6	57.1
Percentage of members with seismic axial forces higher than in design load cases					
Transversal	Min.	7%	8%	1%	1%
	Max.	82%	41%	16%	14%
	Mean	39%	20%	8%	5%
Longitudinal	Min.	7%	4%	1%	1%
	Max.	62%	22%	23%	22%
	Mean	25%	12%	10%	7%
Vertical	Min.	1%	1%	8%	1%
	Max.	31%	4%	16%	8%
	Mean	2%	3%	11%	3%

For the mast guyed tower, only one seismic ground motion conducted to collapse of the tower whereas under three seismic ground motions only one member was damaged without causing a structural failure mechanism. In the context of these numerical simulations, a collapse is defined as the instability of the structure due to a mechanism formed by consecutive failures of members. In all these cases, it was found, that the first element to fail is located in a leg member in the part of the tower mast adjacent or close to the connections where the guy-cables are attached. In the case of two of these considered ground motions, time-history outputs from these simulations showed that the failure of the member occurred at or near to the time sequence when a discontinuity between the response of the mast and guy-cables took place.

For the delta guyed tower, six seismic cases resulted in the collapse of the tower. Similar to the mast guyed tower, the first elements to fail are leg members located either on the tower mast or on the K-frame and near the supporting node of guy-cables. In none of these simulations the tensions limit of the guy-cables was exceeded.

For the Self-supporting towers, only one case resulted in the structural failure of the mast type of tower. Similar to the guyed towers, this structural failure was preceded by the failure of a leg member located in the mast section of the tower.

**Table 5.3. Number of members with capacity exceeded and maximum capacity usage of guy cables. Transversal direction of seismic load incidence.**

NGA	$A_g^{(5)}$ (g)	$T_p^{(2)}$ (sec)	$S(T_a)^{(3)}$ (g)	Guyed tower				Self-supporting towers	
				Delta		Mast		Delta	Mast
				Number of Members	Guy Max. Usage	Number of Members	Guy Max. Usage	Number of Members	Number of Members
1787	0.36	0.50	1.64	4	33%	-	38%	-	-
735	0.36	0.44	0.65	35	15%	-	29%	-	-
15	0.37	0.36	0.85	8	17%	1	36%	-	-
776	0.38	0.52	1.62	4	36%	-	40%	-	-
986	0.41	0.24	1.30	43	19%	-	27%	-	-
900	0.42	0.68	0.94	7	20%	-	28%	-	-
1005	0.42	0.20	1.00	7	19%	-	26%	-	-
1794	0.44	0.36	1.52	4	31%	-	42%	-	-
1049	0.47	0.24	0.89	30	19%	-	31%	-	-
766	0.55	0.38	1.09	-	17%	-	36%	-	-
739	0.57	0.20	1.66	8	51%	1	45%	-	-
174	0.57	0.26	1.32	3	27%	-	41%	-	-
848	0.58	0.34	1.93	8	44%	1	53%	-	4
767	0.62	0.20	1.04	22	18%	-	31%	-	-
963	0.63	0.26	1.21	72	33%	-	34%	-	-
57	0.63	0.20	1.39	5	28%	12	51%	-	-
1006	0.64	0.22	1.14	3	23%	-	26%	-	-
1039	0.67	0.26	1.00	3	29%	-	31%	-	-
721	0.68	0.22	1.43	4	28%	-	38%	-	-
953	0.84	0.52	1.69	144	69%	-	57%	-	4
			<b>Min.</b>	-	<b>15%</b>	<b>1</b>	<b>26%</b>	-	<b>4</b>
			<b>Max.</b>	<b>144</b>	<b>69%</b>	<b>12</b>	<b>57%</b>	-	<b>4</b>

(1) peak earthquake ground motion acceleration; (2) predominant period; (3) spectral coordinate corresponding to 1<sup>st</sup> mode period.

**Table 5.4. Number of members with capacity exceeded. Statistics per direction of earthquake incidence.**

Earthquake Incidence Direction	Statistics	Tower			
		Guyed Towers		Self-supporting towers	
		Delta	Mast	Delta	Mast
		<i>Tower Weight (kN)</i>			
		54.3	77.8	232.3	473.6
		<i>Tower Height (m)</i>			
		37.7	53.1	36.6	57.1
Transversal	Min.	-	1	-	4
	Max.	144	12	-	4
Longitudinal	Min.	-	-	-	4
	Max.	21	-	-	25
Vertical	Min.	-	-	2	1
	Max.	17	-	6	4

#### 5.4. Seismic Base Reaction

Expressions for deriving seismic base shear for free-standing TL guyed towers are suggested based on the outcomes of the numerical simulations performed for the two guyed towers studied herein. These expressions are derived for each one of the orthogonal directions (transversal, longitudinal and vertical). In the present study, these expressions are presented as a percentage of structure's weight. The free-standing guyed towers studied herein were subject to detailed nonlinear transient simulations. In this analysis, 20 scaled ground motion records given in Chapter 3 were considered separately in each orthogonal direction (transversal, longitudinal and vertical directions). Then, the time-history series of base reactions were extracted and compiled. The type of seismic input considered in these simulations was synchronous ground motion applied at the tower base (tower mast base and guy-anchors). These ground motion were taken from the PEER Ground Motion Database (2016). A uniform damping of 2% of the critical viscous damping was considered for the tower's latticed structure. The choice for this damping value was based on the findings of Kotsubo et al. (1985) and El Attar et al. (1995). For the guy-cables, a damping ratio of 0.1% was considered. Based on the set of outcomes from these simulations, expressions were derived based on regression analyses.

#### 5.4.1. Assessment of Horizontal Base Shear under Earthquake Excitations

A first attempt was made to correlate the base shear responses from an equivalent SDOF system with those obtained from nonlinear transient simulations for the MDOF system. The base shear response for the equivalent SDOF system was obtained by solving the equation of motions of a SDOF system for all scaled seismic accelerograms considered in the present study for the horizontal direction. Fig. 5.3 shows a dispersion diagram of the results of both SDOF and MDOF systems. The dashed lines in this diagram represent an absolute error of 0.2. As shown in this diagram, some of the responses from SDOF and MDOF systems have a good correlation but the dispersion is considered high and, overall, the responses obtained by solving the equation motion for an equivalent SDOF system are not considered satisfactory for estimating the base reaction of these towers. This poor correlation indicates that the use of SDOF response acceleration spectra values for deriving seismic inertia forces is not considered suitable for these types of structures.

Then, regression analyses were performed on the results of nonlinear transient simulations in an attempt to derive expressions for estimating base shear response as a function of the tower's natural flexural period and ground motion parameters. It was observed that the magnitude of base shear not only had a direct proportional correlation with peak ground motion acceleration but also at resonant frequencies (i.e. ground motion predominant periods close to or coinciding with the natural period of the structure) the magnitude of the base shear response was amplified. A second order polynomial function with two independent variables was chosen and regression analyses were carried out to determine the values of the coefficients of this function that resulted in a best fit to the base shear responses obtained by the nonlinear transient simulations. This function is given in Eq. (5.1a) where the ratio of maximum base shear response to structure's weight is expressed in terms of the peak ground motion acceleration  $A$ , expressed in units of  $g$  (gravity), and the variable  $F$ , herein named frequency term and defined by Eq. (5.1b). From Eq. (5.1b) it can be seen that the frequency term introduces a relationship between natural period of vibration of the tower structure  $T_n$  and the predominant period of the ground motion record  $T_g$ . This variable  $F$  attains its maximum value when  $T_n = T_g$ , thus introducing the effect of dynamic resonance into the base shear response of Eq. (5.1a). All the other coefficients given in Eqs. (5.1a) and (5.1b) are given in Table 5.5 for each tower structure analyzed.

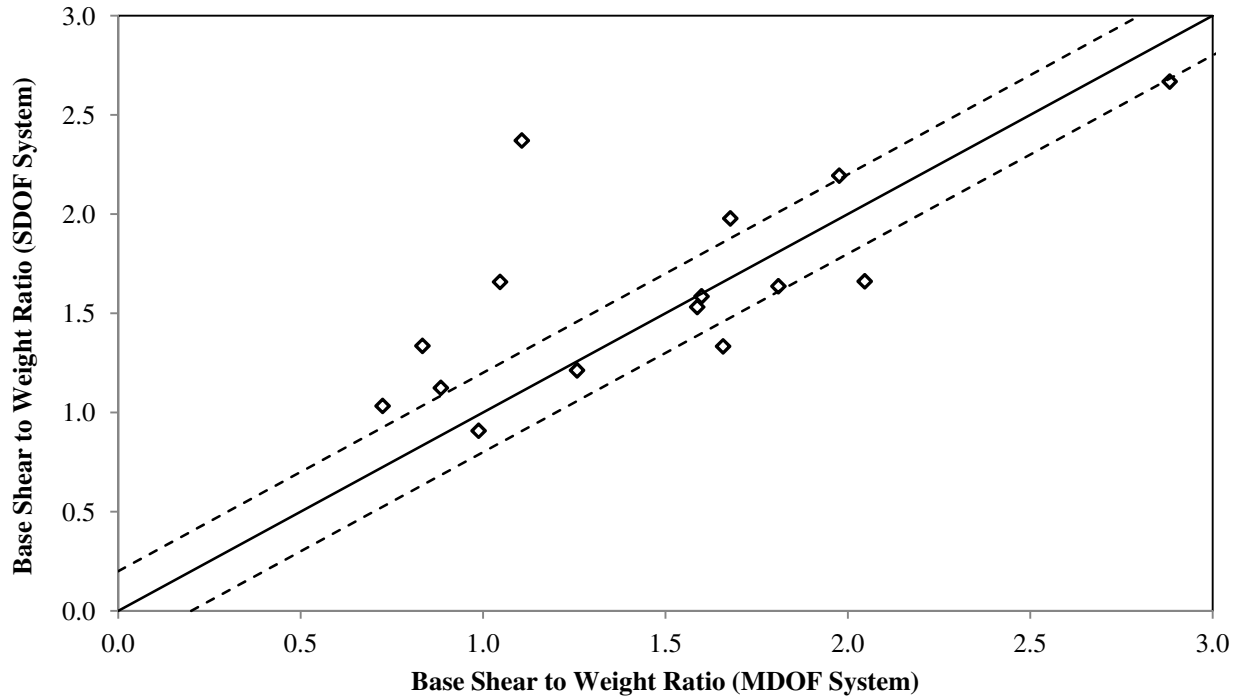


**Figure 5.3. Dispersion diagram for the base shear response from SDOF and MDOF systems. Delta guyed tower.**

$$\frac{V_{max}}{W} = a \times A^2 + b \times F^2 + c \times A \times F + d \times A + e \times F + f \quad (5.1.a)$$

$$F = \frac{1}{[1 - (T_n/T)^2]^2 + [g \times (T_n/T)]^2} \quad (5.1.b)$$

**Table 5.5. Coefficients for Eqs. (5.1a) and (5.1b).**

Coefficient	Tower			
	Delta guyed tower		Mast guyed tower	
	Transversal	Longitudinal	Transversal	Longitudinal
a	-0.79	-0.92	-0.50	-0.55
b	-1.03	-3.03	-3.39	-4.60
c	4.32	4.55	4.32	4.02
d	1.75	2.04	1.81	1.92
e	0.55	0.21	0.64	0.64
f	1.30	0.52	0.26	0.29
g	0.67	0.91	0.73	1.05

These fitted functions are depicted in the surface graphs of Figs. 5.4 to 5.7 for the guyed towers. The dispersion diagrams in these figures presents the absolute error of the fitted functions in regards to the base shear responses obtained with nonlinear transient simulations. The dashed lines in these diagrams represents the maximum absolute errors found between the base shear responses predicted with Eq. (5.1a) which included Eq. (5.1b) and those obtained with numerical simulations.

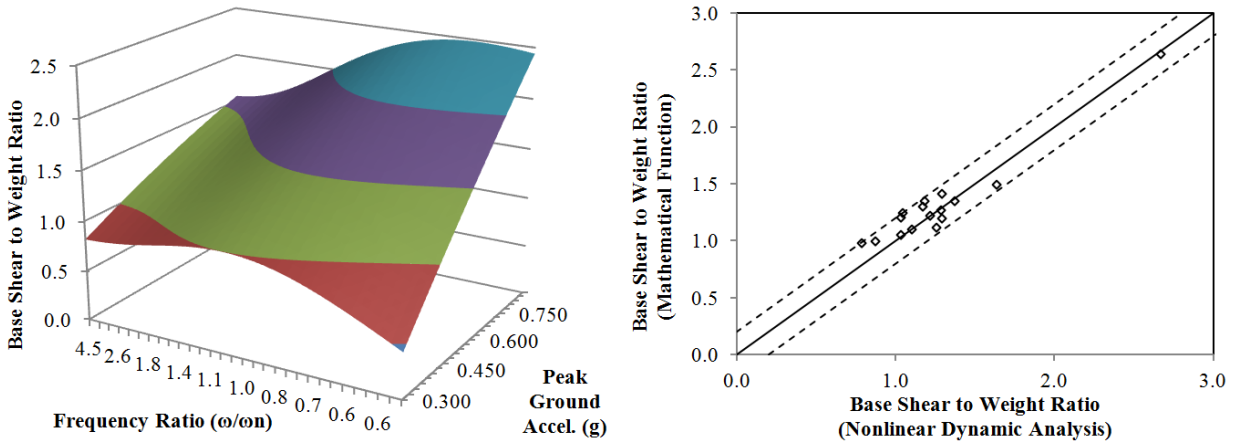


**Figure 5.4. Mast guyed tower. Surface representation of base shear function (left). Dispersion diagram (right). Transversal calculation direction.**

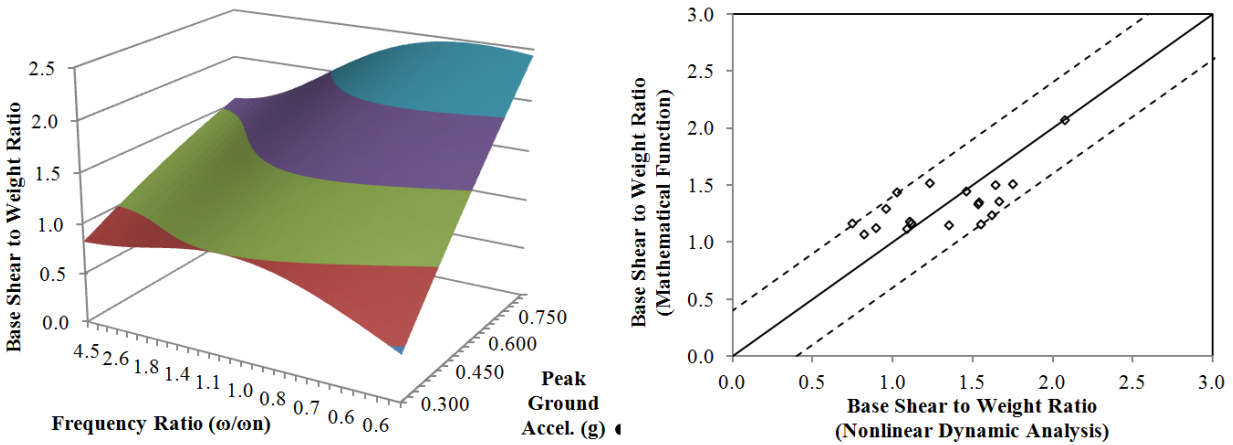


**Figure 5.5. Mast guyed tower. Surface representation of base shear function (left). Dispersion diagram (right). Longitudinal calculation direction.**

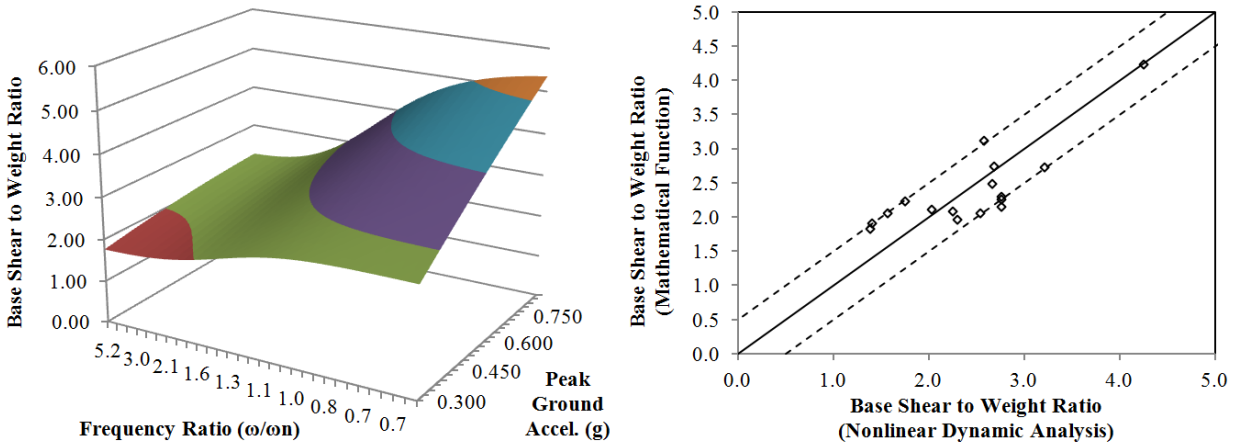


**Figure 5.6. Delta guyed tower. Surface representation of base shear function (left). Dispersion diagram (right). Transversal calculation direction.**

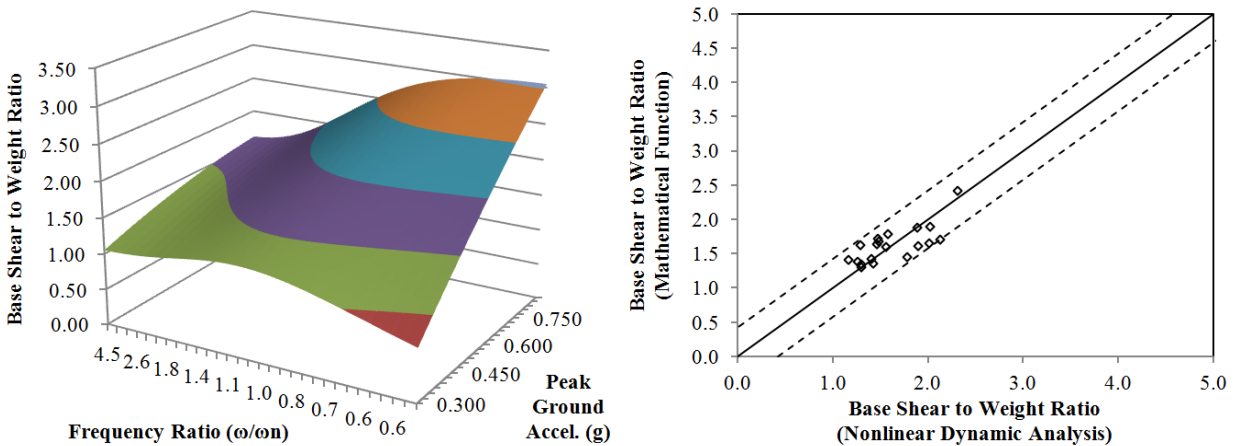


**Figure 5.7. Delta guyed tower. Surface representation of base shear function (left). Dispersion diagram (right). Longitudinal calculation direction.**

#### 5.4.2. Vertical Earthquake Excitation

The towers studied herein were also analyzed considering the 20 scaled earthquake ground motion records acting in the vertical direction. Similar to the horizontal component of earthquake excitation, an attempt was also made to derive an expression for the vertical base reaction based on regression analyses. By analyzing the results of the numerical simulations and comparing them with the parameters of each seismic case, it was observed that the vertical base reaction only had a reasonable correlation with peak ground motion acceleration. Therefore, a polynomial quadratic function with only one independent variable (in this case the vertical peak ground motion acceleration) was used for regression analyses. The adjusted coefficients of this function for both towers are presented in Table 5.6. In Fig. 5.8 is given the dispersions diagrams depicting the absolute errors of Eq. (5.2) in regards to the results of nonlinear transient simulations.

$$\frac{V_{\max}}{W} = a \times A^2 + b \times A + c \quad (5.2)$$

**Table 5.6. Coefficients for equation 5.2.**

Coefficient	Tower	
	Delta guyed tower	Mast guyed tower
a	-1.88	-3.89
b	3.16	6.47
c	1.45	1.77

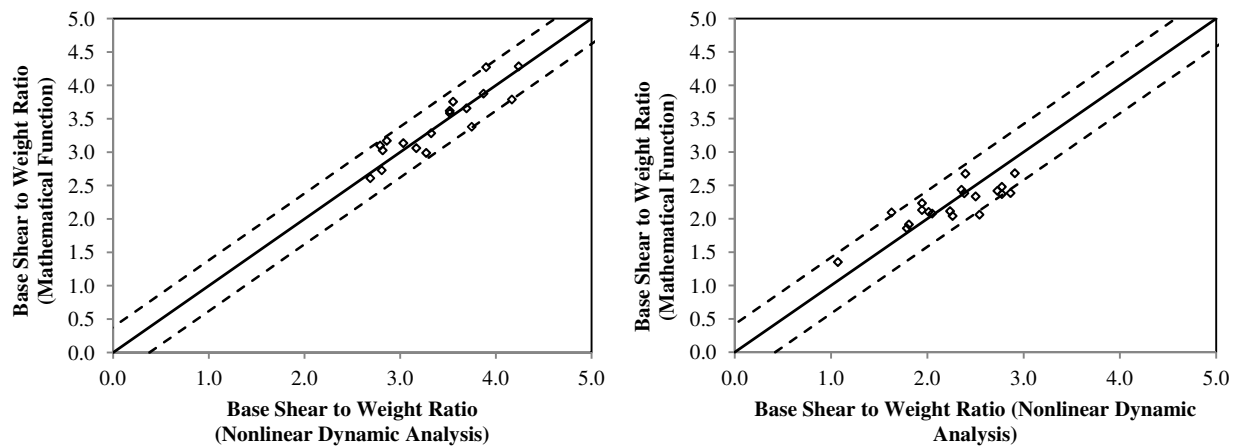


**Figure 5.8. Dispersion diagrams for Mast Guyed tower (left) and Delta Guyed tower (right) for earthquake base reaction in the vertical direction.**

### 5.5. Approximate Static Method and Base Shear Check

The static method proposed herein is based on the definition of a horizontal seismic load profile that can result in approximate responses (i.e. axial forces) at each tower member to the responses obtained from detailed nonlinear transient simulations. Two lateral distribution patterns of seismic forces were tested: the inverted triangular distribution (refer to Eq.(4.3)) and the modal distribution (refer to Eq. (4.4)). Graphical representations of these seismic load distribution patterns are presented in Figs. 5.9 and 5.11 for the delta guyed tower and mast guyed tower studied herein, respectively. It is noted that, as indicated by the Fourier response spectra presented in Chapter IV, for harmonic excitation in the horizontal direction, the transient response of the guyed towers studied herein is mainly characterized by the contribution of the first flexural mode of vibration in the direction of analysis. Therefore, the deflected shape of

these structures, when subjected to horizontal dynamic loading, is expected to be mainly characterized by the shape of the first mode of vibration in the direction of analysis.

In addition to the horizontal seismic load profile, this approximate static method also considers that forces on the guy-cables are amplified by a given dynamic factor to take into account the impulse forces originated from the cable-mast dynamic interactions described in Section 4.5.3 of Chapter IV. These dynamic amplification factors are determined using the relationships developed in this section.

This approximate static method is developed in two consecutive simulations. In the first simulation, the tower is subjected to the seismic load profile only and the tension on the stretched guy-cables are determined. The seismic load profile is calculated based on Eq. (4.4) and is a function of the seismic base shear determined using the expressions developed in section 5.4 of this chapter. A dynamic amplification factor is then applied to the resulting cable tension from the first simulation and the resulting incremental tension is added to the stretched guy-cables only by means of a prestressing force. In ANSYS-APDL, this prestressing force is implemented using the INISTATE command (ANSYS, 2013). A second pushover simulation is then carried out in both senses of the direction of analysis and the axial forces in each member are compiled.

In order to demonstrate the applicability of this proposed method in estimating the maximum axial forces originated from seismic excitation, its responses were compared with the responses obtained from detailed nonlinear transient simulations for each member of the guyed towers studied herein. The tower is then analyzed herein using the static method for 10 scaled ground motion records used for the transient analyses in the horizontal direction. The parameters of the mode shapes were calculated as described in Section 4.4 of Chapter IV. It is noted that these static simulations must consider important second order effects originated from large deflections. Figs. 5.10 and 5.12 presents dispersion diagrams comparing the axial forces at each member of the delta guyed tower and mast guyed tower, respectively, obtained from the proposed static method with the maximum axial forces obtained from nonlinear transient simulations for one seismic case. The dispersion diagram on the left of Figs. 5.10 and 5.12 is based on the modal distribution of seismic forces and the dispersion on the right is based on the inverted triangular distribution of seismic forces. By comparing these two diagrams, it is observed that the modal distribution of forces presents a better correlation with the responses from nonlinear dynamic simulations, especially for the most demanded leg members. The axial forces obtained with the

inverse triangular pattern are systemically lower than the axial forces resulting from nonlinear transient simulations. The modal pattern was then retained for this proposed static method as its responses better correlates with the responses obtained from dynamic simulations.

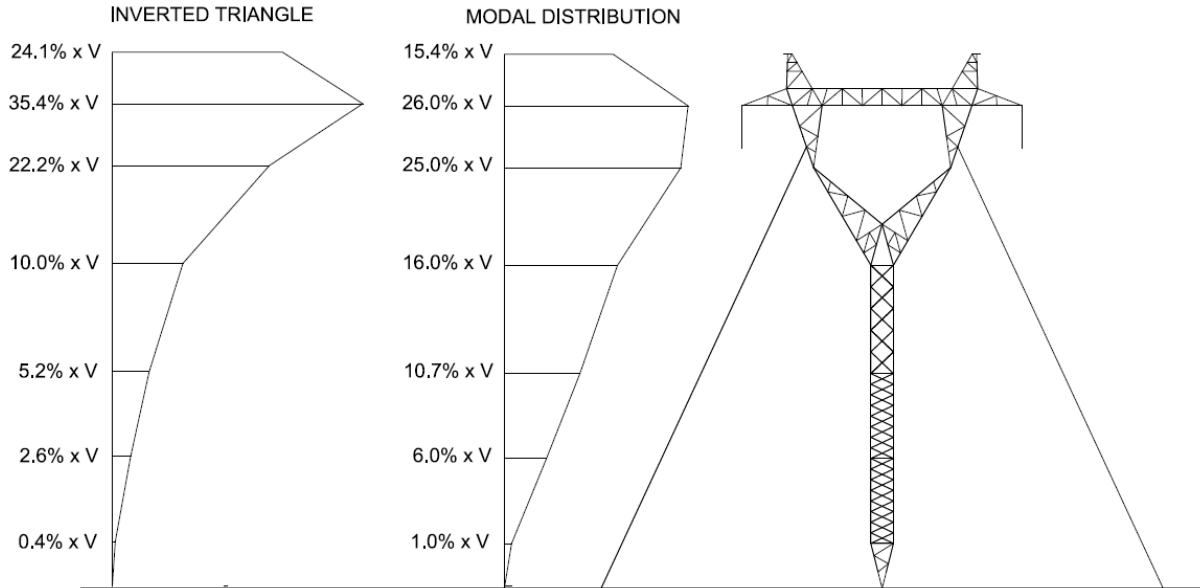


**Figure 5.9. Seismic force distribution patterns over the height of Delta guyed tower. Transversal calculation direction.**

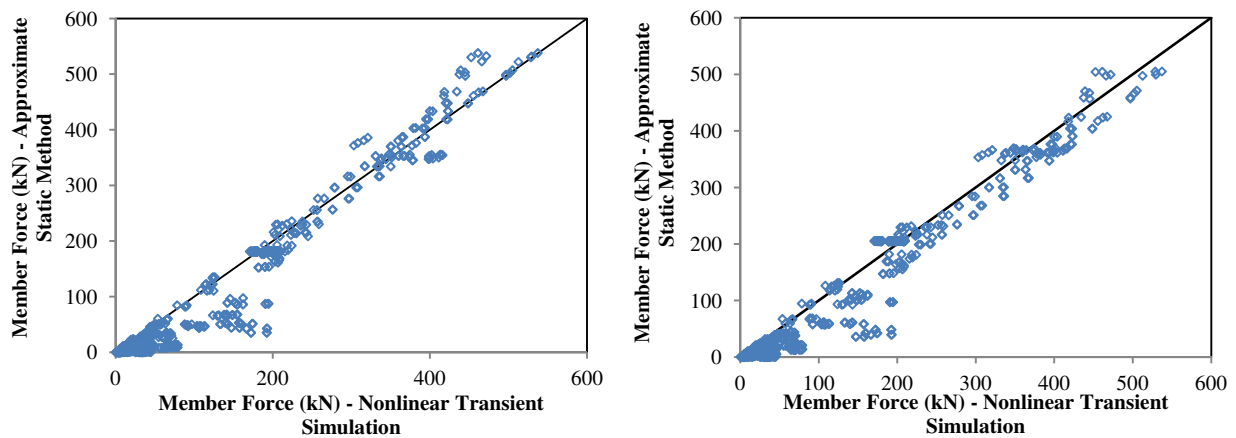


**Figure 5.10. Dispersion diagrams comparing member axial forces obtained from nonlinear transient analysis and from the proposed approximate static method. Modal distribution of forces (left). Inverted triangular distribution of forces (right). Delta guyed tower analysed under NGA 953 applied in the transversal direction.**

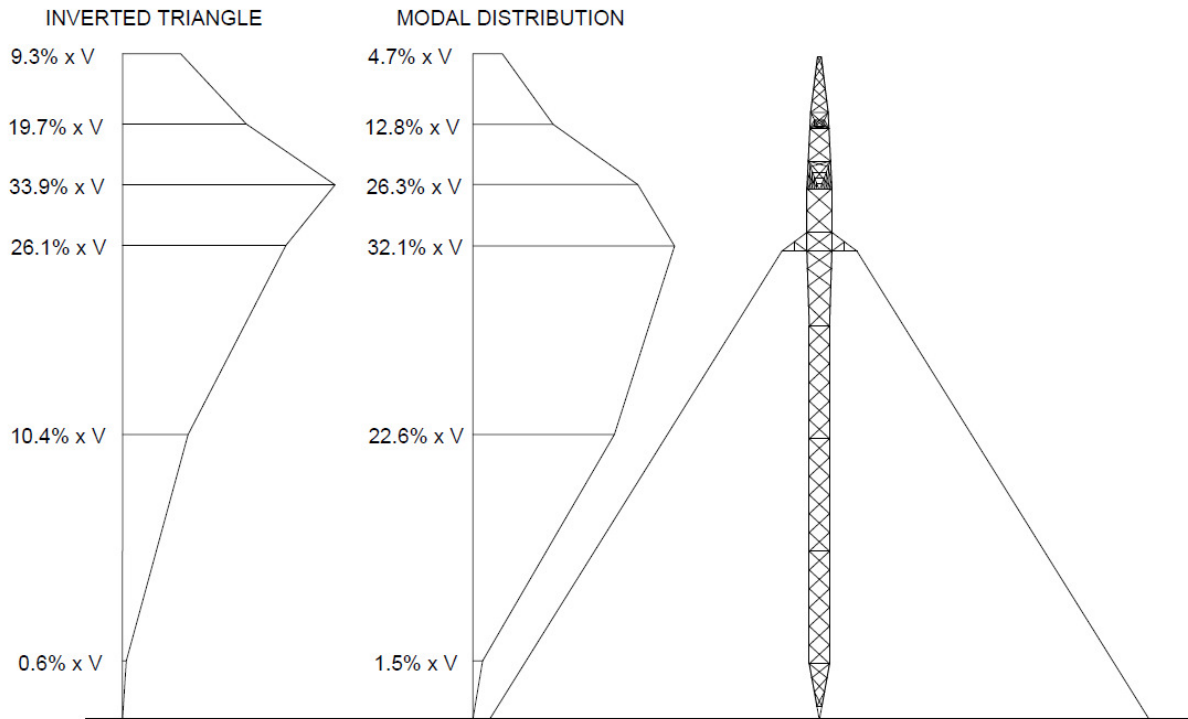


**Figure 5.11. Force distributions over the height of Mast guyed tower. Longitudinal calculation direction.**

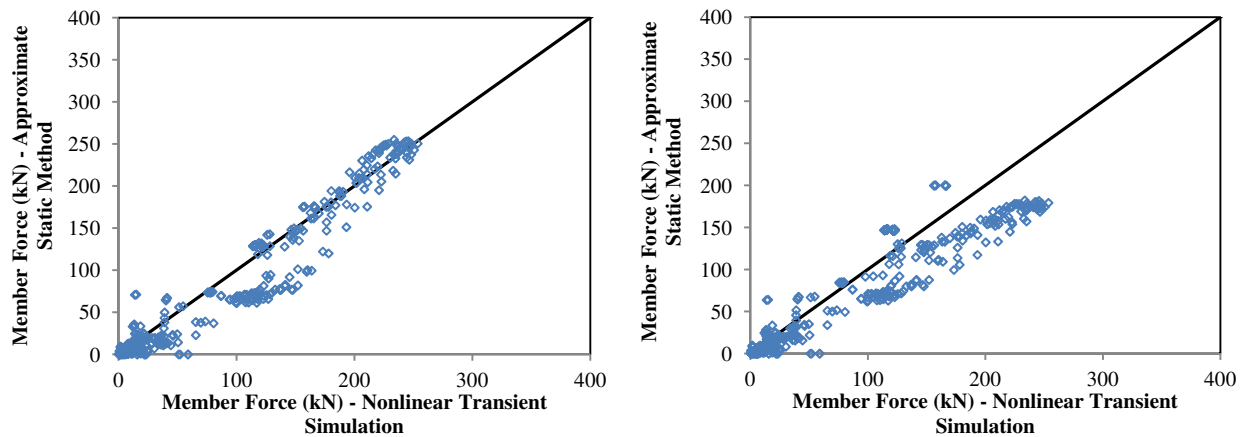


**Figure 5.12. Dispersion diagrams comparing member axial forces obtained from nonlinear transient analysis and from the proposed approximate static method. Modal distribution of forces (left). Inverted triangular distribution of forces (right). Mast guyed tower analysed under NGA 953 applied in the longitudinal direction.**

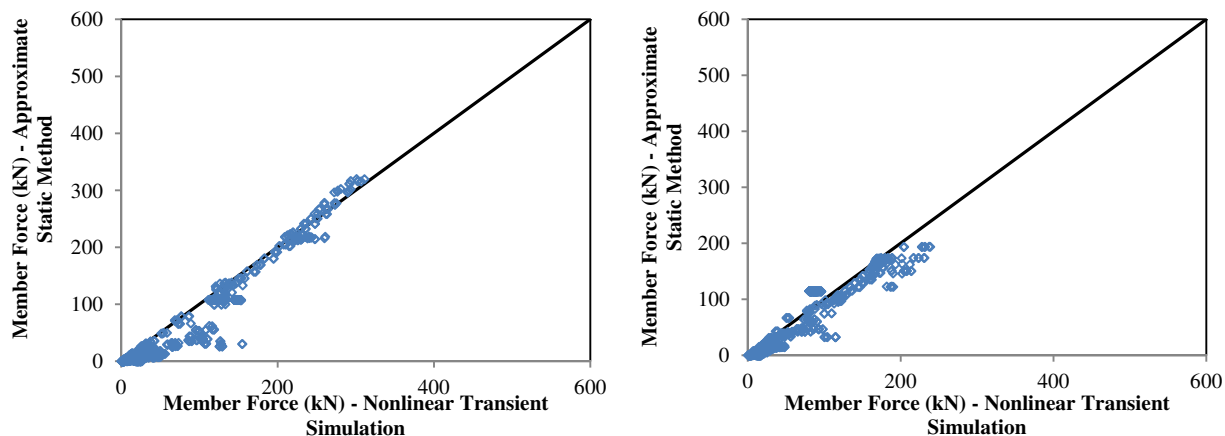


**Figure 5.13. Dispersion diagrams comparing member axial forces obtained from nonlinear transient simulations and from the proposed approximate static method. Transversal direction (left). Longitudinal direction (right). Modal distribution of forces. Delta guyed tower analysed under NGA 739.**

To validate the applicability of this method, nonlinear pushover simulations followed by the procedure described in the previous paragraphs were performed for 10 seismic ground motions applied separately in the transversal and longitudinal direction. Dispersion diagrams presented in Fig. 5.13 illustrate the performance of this proposed static method when subjected to seismic ground motion (NGA 739). Dispersion diagrams resulted when other seismic ground motions were employed are presented in Figs. III.1 to III.18 in Appendix III. Overall, the higher dispersion (or smaller correlation) between the responses obtained from the static method and those from dynamic simulations is observed in secondary members of the tower structure, such as secondary bracing and redundant members, while for the main members carrying higher axial forces the responses from the static method presents a good correlation with the responses from dynamic simulations. All these comparisons indicate that the static method proposed herein can be used as a preliminary design check for seismic load for the types of guyed tower studied herein.

A comparison between the proposed Eq. (5.1), presented in Section 5.4.1 of this chapter, and the expression given in NBCC (2010) for the calculation of seismic base shear is performed for the Mast guyed tower subjected to earthquake ground motions applied in the transversal direction. The purpose of this comparison is to evaluate whether the equation proposed in NBCC (2010) could be used to estimate seismic base shear for the type of structures studied herein. In NBCC (2010), the minimum design base shear  $V$  is obtained from the following expression:

$$V = \frac{S(T_a) \times M_v \times I_e \times W}{R_d \times R_0} \quad (5.3)$$

where  $S(T_a)$  is the design spectrum at the design period  $T_a$ ,  $M_v$  is the higher mode factor,  $I_e$  is the importance factor for a building,  $W$  is the seismic weight of the structure,  $R_d$  is the ductility related force modification factor and  $R_0$  is the overstrength-related force modification factor. For the Mast guyed tower studied herein, the following parameters were considered:  $T_a = 0.55$  sec (resulted from modal analyses);  $W = 77.8$  kN (in this example the seismic weight did not include the weight of the attached conductors);  $I_e = 1$ ;  $M_v=1$ ;  $R_d = 1$  and  $R_0 = 1$ . It is noted that for Bamfield, B.C (see Table 3.3), for  $T = 0.55$  s it results  $S(T_a) = 0.85$  g. Therefore,  $V = 65.8$  kN.

Comparison of seismic base shear values calculated using Eq. (5.1) and that given in NBCC (2010) is showed for the Mast guyed tower in Table 5.7. There were selected four records (#1005, # 735, #1039 and #1049) scaled to match the design spectrum for Bamfield, site class C. All scaled ground motions were applied in the tower's transversal direction. As shown in this table, there are differences between the base shear computed with the two expressions. These differences are in the range from 15% to 40%. By using the proposed equation, larger base shear is demanded. Further analyses are required in order to validate the proposed equation.

**Table 5.7. Comparison of seismic base shear values calculated using Eq. 5.1 and the NBCC (2010) expression for the Mast guyed tower with earthquake ground motion incidence in the transversal direction.**

NGA	$A_g^{(5)}$ (g)	$T_p^{(2)}$ (sec)	$S(T_a)^{(3)}$ (g)	Seismic Base Shear (kN)		
				Proposed Equation (A)	NBCC (2010) (B)	Dif. (%) [(B)-(A)]/(A)
1005	0.42	0.20	0.87	76.3	65.8	-14%
735	0.36	0.44	0.74	93.5		-30%
1039	0.67	0.26	0.86	110.0		-40%
1049	0.47	0.24	0.80	85.6		-23%

## CHAPTER VI

### SEISMIC RESPONSE OF THE COUPLED GUYED TOWER-CONDUCTOR SYSTEM

#### 6.1. Introduction

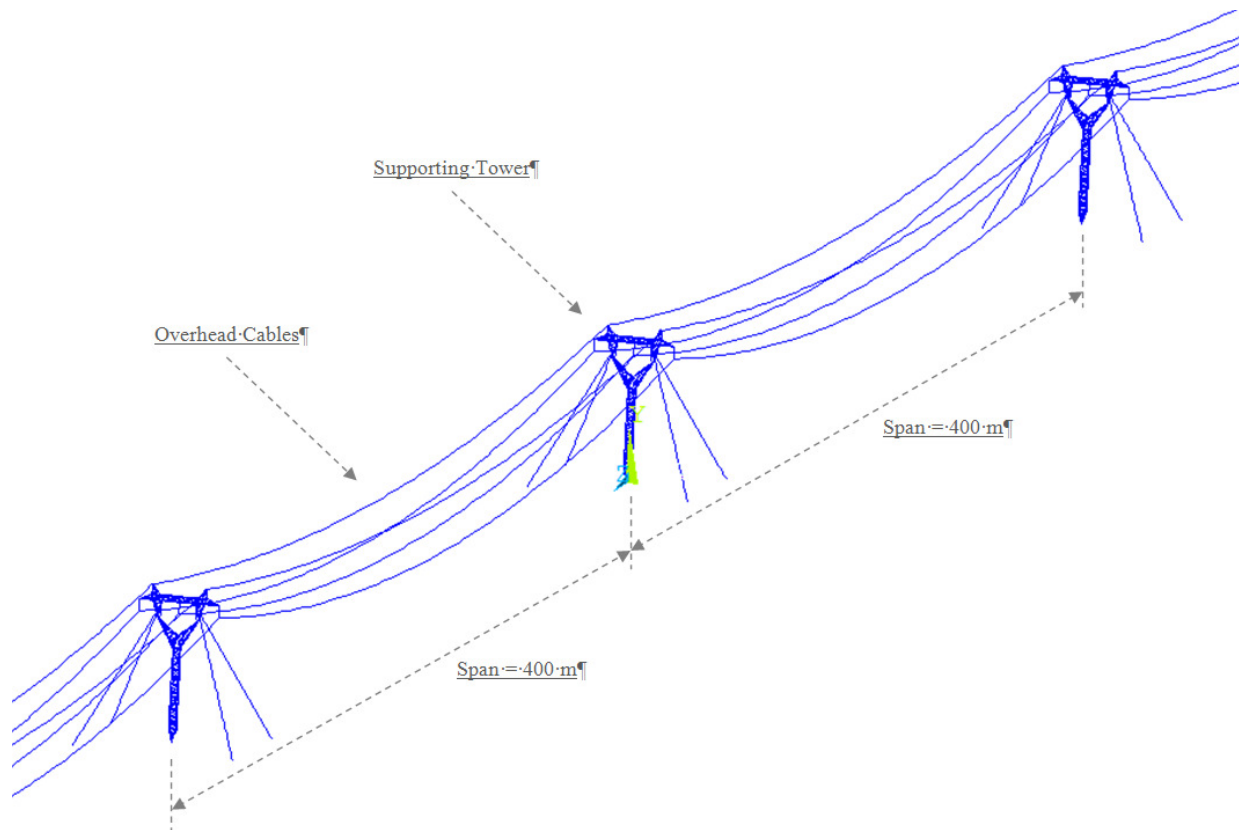
This chapter presents the results of analyses carried out to assess the response of a coupled guyed tower and conductor system to earthquake ground motions. A description of this system is first made. Analyses on the dynamic properties and seismic response of each component of the system (supporting guyed tower and supported conductors) is made separately in order to evaluate whether dynamic interactions between these components are likely to occur during an earthquake event. The frequency contents of the seismic responses of the free-standing towers considered herein are analyzed. The free-vibration characteristics of the overhead cables (conductors) are analyzed by imposing harmonic accelerations with a range of forcing frequencies in each of the three main orthogonal directions (transversal, longitudinal and vertical). The overhead cables are subjected to seismic excitation motion at their supports in each of the three main orthogonal directions separately. To analyse the response, three seismic ground motions with different level of frequency content (low, intermediate and high) given by  $A/V$  ratio were selected. Finally, the coupled guyed tower and conductor system is subjected to the three selected ground motions in each of the main orthogonal directions and discussions are made regarding the importance of considering the contribution of the overhead cables' mass in the seismic response of the supporting tower structures. It is noted that comparisons are made between the seismic responses of the supporting guyed tower (i.e. free-standing tower) and the guyed tower with overhead cables (i.e. coupled guyed tower conductor system).

#### 6.2. Description of the Coupled Guyed Tower Conductor System

The coupled guyed tower conductor system studied herein is based on a portion of a transmission line that is supported by suspension delta guyed towers presented and studied in the previous chapters. These towers support three conductor cables and two ground-wire cables spanning 400 meters between supports. The main characteristics of these overhead cables are given in Table 6.1. The layout of the studied system is showed in Fig. 6.1. This transmission line system was designed to support 315 kV HVac powerlines.

**Table 6.1 Main characteristics of the overhead cables.**

Parameter	Overhead Conductor	Ground-Wire
Configuration	Twin bundled ACSR Drake conductor	OPGW and OHSW
Cable span	400 m	400 m
Sag to span ratio	0.04	0.04
Cross-sectional area	470 mm <sup>2</sup>	96 mm <sup>2</sup> (OHSW); 158 mm <sup>2</sup> (OPGW)
Weight	16 daN/m	7.6 N/m (OHSW); 8.5 N/m (OPGW)
Damping ratio	0.1 %	0.1 %

**Figure 6.1. Coupled guyed tower conductor system layout.**

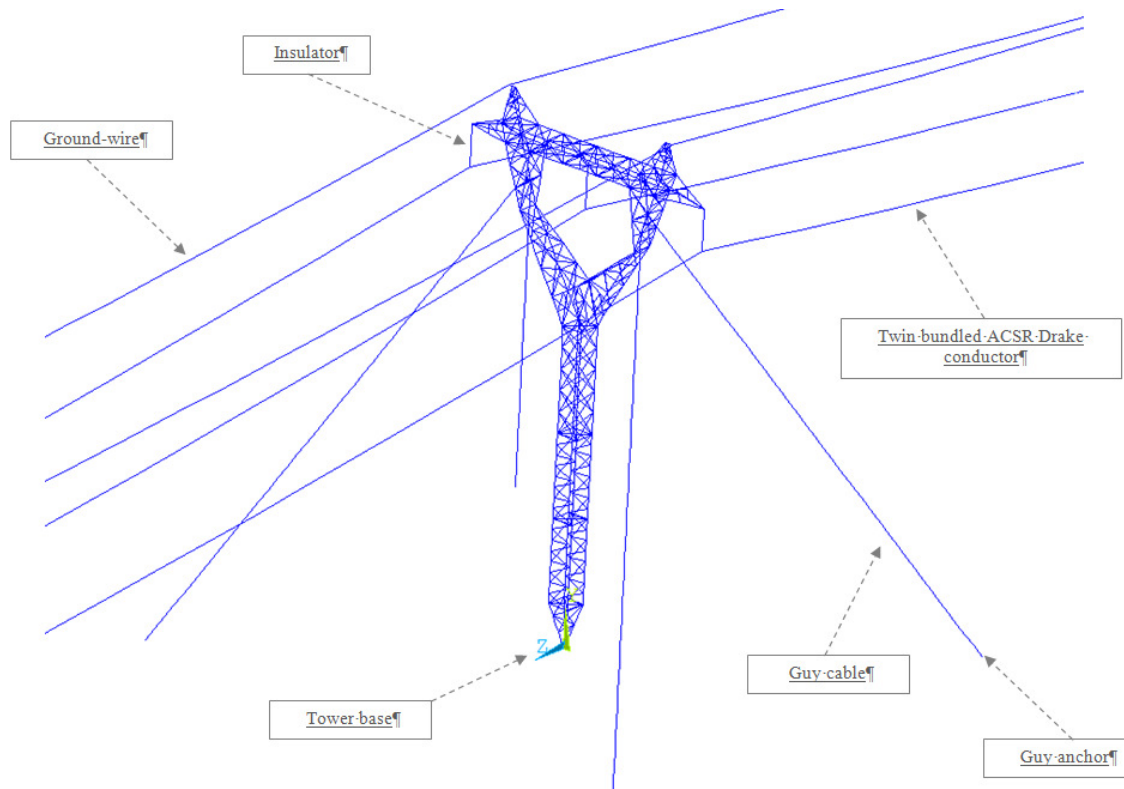


**Figure 6.2. Supporting guyed tower and overhead conductors.**

The coupled guyed tower conductor system studied herein is composed of 3 suspension delta guyed towers and 5 spans of overhead cables totalling 2,000 meters of transmission lines. Each span has 3 conductor cables and 2 ground-wire cables. Each overhead cable was modelled as a sequence of 80 tension-only truss elements using the LINK180 element of ANSYS-APDL. The layout of this system is depicted in Fig. 6-1 and details are given in Fig. 6.2. Springs were used as boundary conditions for the overhead cables located at the end's spans. The COMBIN39 element from ANSYS-APDL was used as boundary condition elements. The COMBIN39 is a unidirectional element with nonlinear generalized force-deflection capability and with up to three translational degrees-of-freedom (ANSYS, 2013). The force-displacement relationship used for this spring element was developed from pushover analyses for the free-standing tower. This configuration was chosen with the intent of limiting the effects of the assumptions made herein for the boundary conditions in the response of the coupled guyed tower-conductor system. Only the responses from the overhead cables in the middle spans and the supporting tower located at the middle of the system were considered for analyses. It is understood that the farther the boundary condition is from the mid tower being analyzed, the smaller will be the relevance of the assumptions made for the boundary conditions on the response of this tower.

### 6.3. Seismic Response of Free-Standing Towers

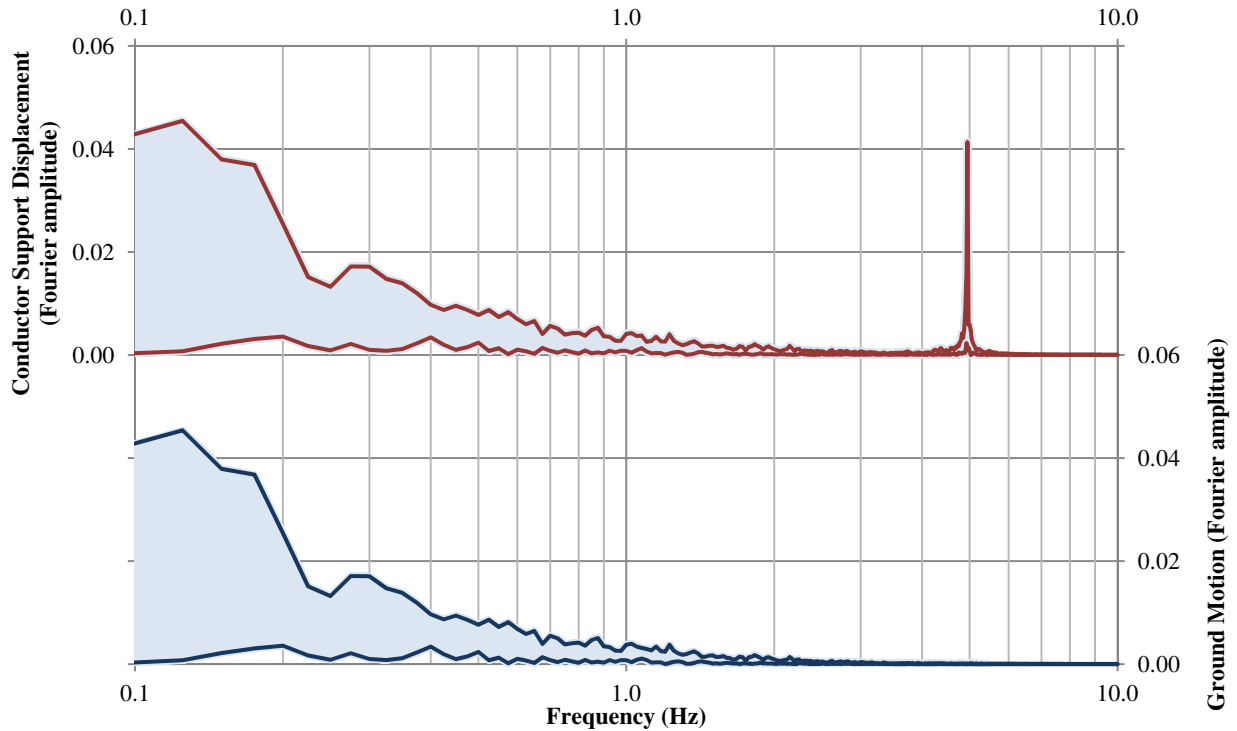
As mentioned in Chapter V, all four TL towers studied herein (Figs. 3.2 to 3.5) were subjected to earthquake ground motion excitations at their base in each of the three main orthogonal directions of analysis (longitudinal, transversal and vertical). The 20 seismic ground motions used in this study are listed in Tables 3.5 and 3.6 of Chapter III. The resulting displacements of the nodes where the overhead cables are attached to the supporting free-standing towers were compiled for each seismic ground motion and their frequency contents were analyzed by means of a Fourier response spectrum. The goal of these analyses was two-fold: a) to assess the vibration characteristics that are expected to be imposed to the overhead cables by the seismic ground motions applied at the base of the supporting towers and b) to evaluate whether dynamic interactions between the supporting towers and overhead cables are likely to occur. These dynamic interactions are characterized by resonant effects arising from frequencies associated with modes of vibration of the overhead cables coinciding with the frequency content of the supporting tower vibration; or modes of vibration of the overhead cables being activated by means of sub and/or super harmonic resonance, whereby the overhead cable may be induced to resonate at one of its natural frequencies by external excitation occurring at some multiple of natural frequency (Benedettini and Rega, 1989; Sparling, 1995; Madugula et al., 2001).

Fig. 6.3 shows a comparison between the envelope of Fourier response spectra of earthquake ground motion at the base of the delta Self-supporting tower (seismic input) and the envelope of Fourier response spectra of conductor support node displacement when the ground motion was applied in the longitudinal direction. In this case, only the horizontal component of each one of the selected 20 ground motions was applied in the longitudinal direction of TL towers. By comparing these two response spectra, it is observed that the seismic vibration of this free-standing Self-supporting tower is mainly characterized by two distinct frequency components: one associated with the ground motion imposed vibration to the tower base, and one associated with the natural frequency of vibration of the tower. Fig. 6.4 presents Fourier response spectra envelopes resulted for 20 seismic ground motions applied in the longitudinal and transversal directions. As shown in this figure, only the first mode of vibration in each direction is activated for this delta Self-supporting tower.

These response spectra indicate that the overhead cables will be subjected to an imposed motion at their end nodes with frequency contents equal to the frequency content of the seismic excitation and of the natural frequency of vibration of the tower structure. The same Fourier response spectra analyses were made for the vertical component of seismic ground motions as depicted in Fig. IV-1 of Appendix IV. It was found that the response of this tower subjected to vertical seismic excitation is mostly defined by the frequency content of the imposed vertical ground motion at its base. In other words, no mode of vibration is activated when this tower was subjected to vertical seismic excitation.

Figs. 6.5 and 6.6 present the Fourier response spectra for the delta guyed tower similar to the ones described for the delta Self-supporting tower. As shown in these figures, the frequency content associated with the modes of vibration of this guyed tower is closer to the frequency content of the ground motion excitation as compared with the frequency of the Self-supporting tower. Also, the Fourier response spectra presented in Figs. 6.5 and 6.6 shows that other modes of vibration participate in the seismic response of this tower and that the Fourier amplitude of the response for the natural mode of vibration in the transversal direction is approximately twice higher than the Fourier amplitudes of the Self-supporting type. Similarly to the findings for the Self-supporting tower, the Fourier response spectra of the vertical component of seismic excitation of the delta guyed tower (see Fig. IV-2 in Appendix IV) shows that the responses of this tower to vertical excitations are exclusively dominated by the frequency content of the imposed vertical ground motion at its base. Fourier response spectra for the mast guyed tower are also presented in Figs. IV-3 to IV-5 of Appendix IV and the same observations made for the delta guyed tower in the above paragraph are applicable to this tower.

These analyses indicate that overhead cables supported by relatively flexible guyed towers will be subjected to seismic excitations for a larger number or range of frequencies than overhead cables supported by relatively rigid Self-supporting towers. It was also observed that the magnitude of the imposed excitation displacement on the support end nodes of the cables will be higher for overhead cables supported by guyed towers than for overhead cables supported by Self-supporting towers.



**Figure 6.3. Envelope curves of Fourier response spectra of conductor support displacement of delta Self-supporting tower (top) and earthquake ground motion base displacement (bottom).**

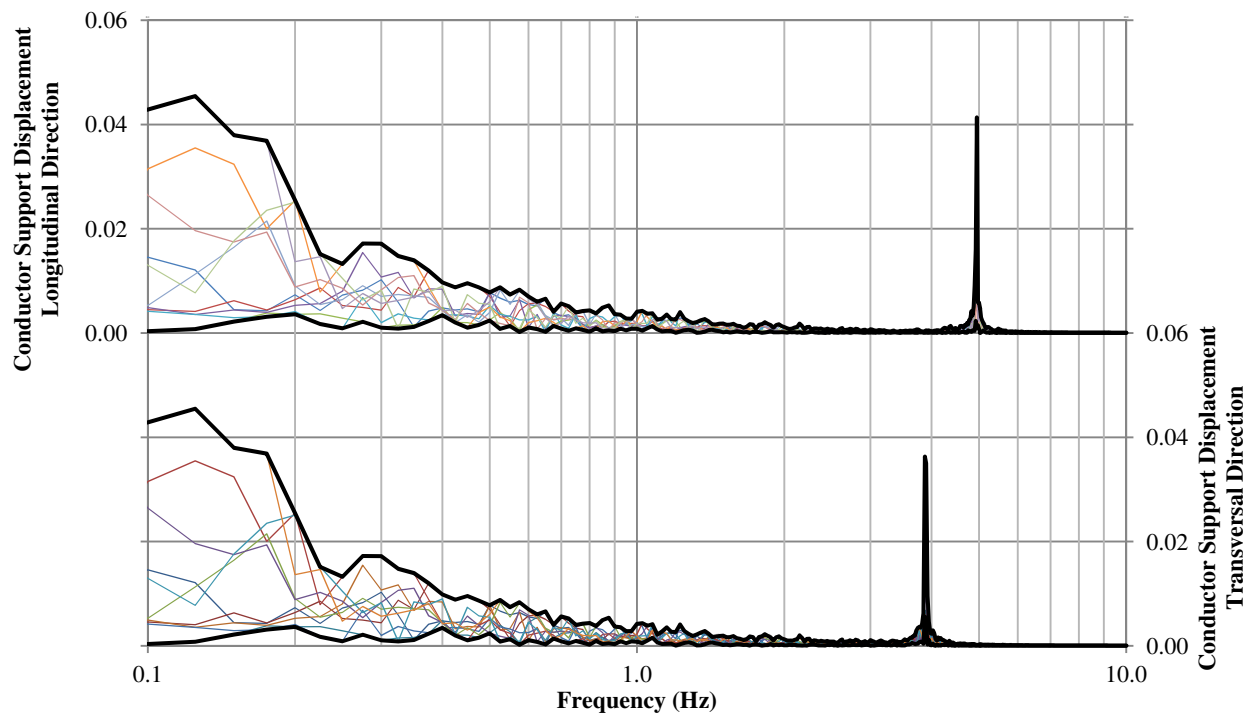


**Figure 6.4. Fourier response spectra of conductor support displacement in the longitudinal direction of delta Self-supporting tower (top) and in the transversal direction of delta Self-supporting tower (bottom) for all studied earthquake ground motions.**

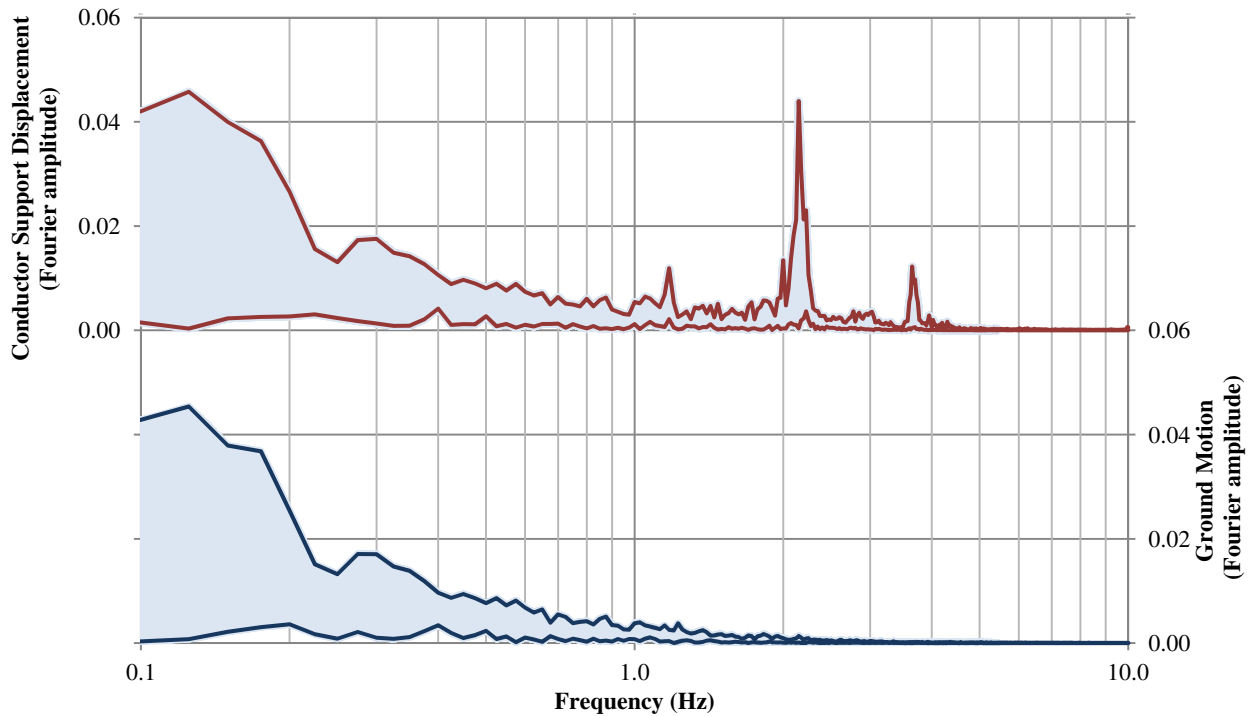


**Figure 6.5.** Envelope curves of Fourier response spectra of conductor support displacement of delta guyed tower (top) and earthquake ground motion base displacement (bottom).

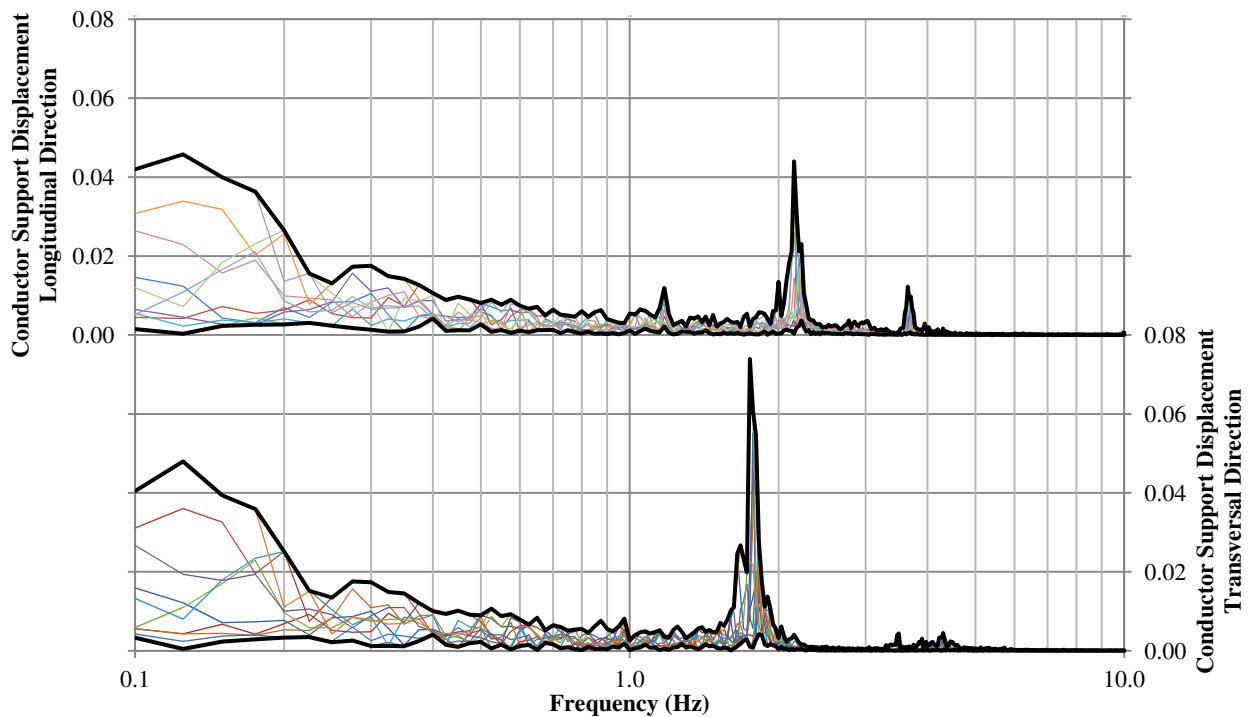


**Figure 6.6.** Fourier response spectra of conductor support displacement in the longitudinal direction of delta guyed tower (top) and in the transversal direction of delta guyed tower (bottom) for all studied earthquake ground motions.

#### 6.4. Free-Vibration Characteristics of Overhead Cables

To determine the free-vibration characteristics of the overhead cables studied herein, the overhead conductor was subjected to harmonic acceleration with amplitude of 0.1 g in each of the three main orthogonal directions separately for various forcing frequencies ranging from 0.1 Hz to 10.0 Hz in steps of 0.1 Hz, thus totalling 100 nonlinear transient simulations for each orthogonal direction. These simulations were carried out in ANSYS in batch mode using the APD Language. The maximum cable tension for each harmonic forcing frequency simulation was compiled and used to produce the response spectra presented in Fig. 6.7. A critical damping ratio of 0.1% was considered in these simulations. The objective of these simulations was to identify the frequencies in which the cable tension responses are amplified in regards to equivalent static tension. The ordinates in these response spectra present the ratio of dynamic tension to static tension. These tension values are the mean of tension values of the tension-only truss elements making up the modelled cables.

The following observations are made from the response spectra presented in Fig. 6.7: a) the cable tension response is mainly governed by the first or lower modes of vibration (in the range of 0.2 Hz to 0.5 Hz) for harmonic excitation in the vertical and transversal directions. This range of frequencies is closer to typical natural frequency values of flexible guyed towers than to typical natural frequency values of stiffer Self-supporting towers; b) for excitation in the longitudinal direction, the tension response in cable is governed by higher modes of vibration with peak dynamic amplification occurring at the forcing frequency of 4.8 Hz. It is noted that this frequency of vibration is close to the natural frequency of vibration of the Self-supporting towers studied herein; c) dynamic amplification is larger for harmonic excitation in the longitudinal direction and smaller for harmonic excitation in the transversal direction.

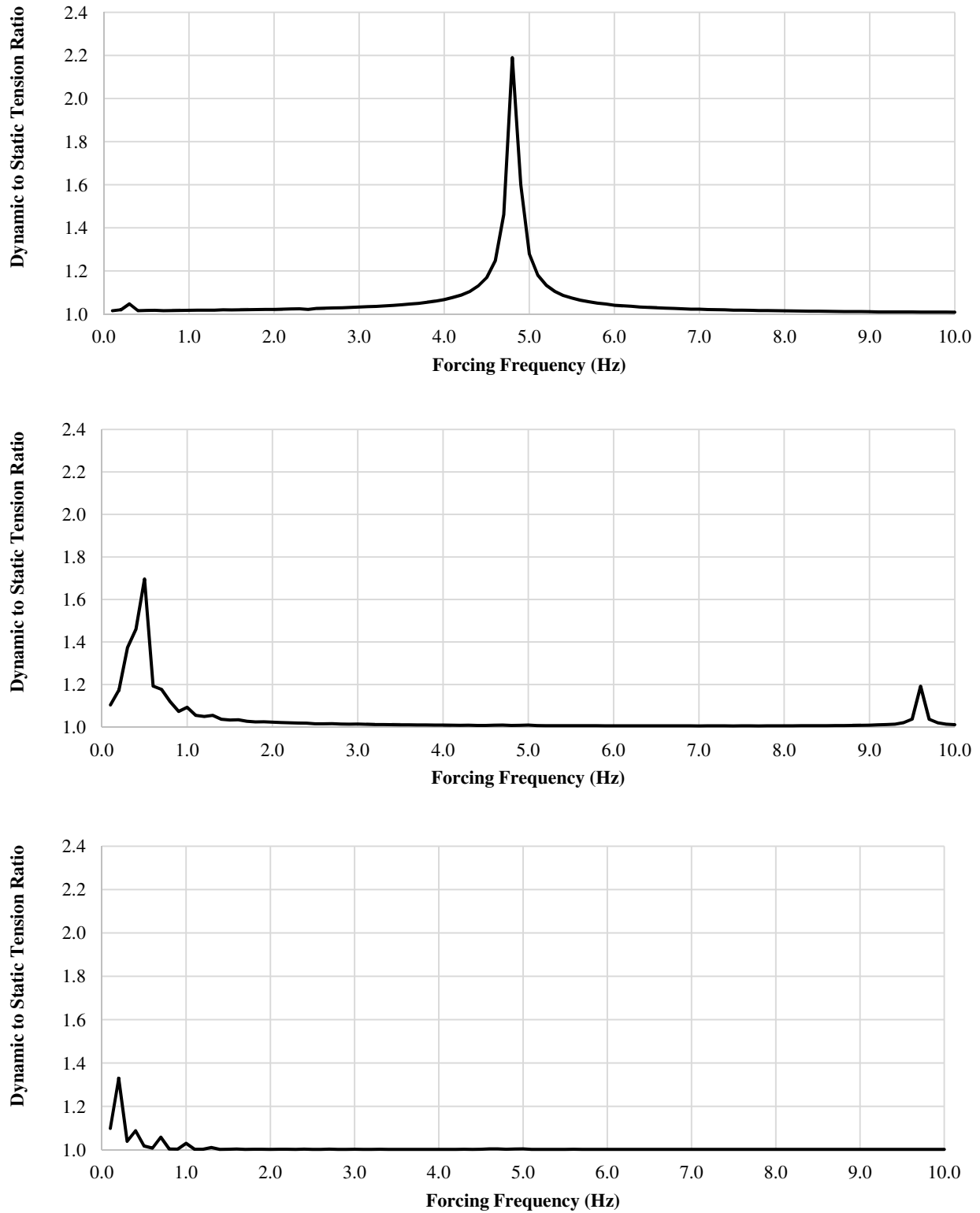


**Figure 6.7. Frequency-response relationship for conductor cable. Harmonic excitation in the longitudinal direction (top). Harmonic excitation in the vertical direction (middle). Harmonic excitation in the transversal direction (bottom).**

### 6.5. Seismic Response of Overhead Cables

The overhead conductor studied herein was subjected to seismic excitations at its end supporting nodes in each of the three main orthogonal directions of analyses (transversal, longitudinal and vertical separately). To analyse the response of the overhead conductor, three seismic ground motions with low, intermediate and high level of frequency content as determined by  $A/V$  ratio were employed. Two scenarios were considered: scenario “A”) seismic ground motion at only one of the supporting nodes; scenario “B”) synchronous seismic motion on both end node supports. For scenario “A”, seismic motion applied at one of the supporting node causes stretching of the cable. Then, the dynamic tension in the cable is caused by the inertia effects of the cable motion in the direction of the node displacement and by the elastic stretching and resulting inertia effects of the cable motion in the vertical direction. For the second scenario “B”, seismic motion on both end node supports is expected to result in dynamic tension of the cable mainly caused by the inertia effects of the cable motion in the direction of imposed motion. The first scenario “A” is more likely to occur during an earthquake event because it can be reasonably assumed that the seismic motion of the supporting towers will be asynchronous. This asynchronous motion of supporting towers may be due to a combination of causes such as ground motion shear wave velocity propagating on long spans, foundation soil heterogeneity, differences in topographic elevations and transmission line alignment deviations.

The ground motions selected for these simulations are the ones that resulted in the highest seismic responses for the free-standing delta guyed tower. The selected ground motion records were: NGA 57, NGA 953 and NGA 739. It is noted that NGA 57 has the  $A/V$  ratio equal to 0.96 (characteristics of intermediate frequency content), NGA 953 has the  $A/V$  ratio equal to 0.75 (characteristics of low frequency content) and NGA 739 has the  $A/V$  ratio equal to 1.12 (characteristics of high frequency content). The study of El Attar et al. (1995) found that earthquake ground motion records with low  $A/V$  ratio resulted in cable responses higher than the response due to an earthquake ground motion records with high  $A/V$  ratio. The present simulations results will be discussed against the conclusions reached by El Attar et al. (1995) for seismic excitation of the overhead conductor studied herein.

Time-history series of cable tension were compiled for all simulations and the ratios of peak dynamic tension to static tension were calculated. Static tension refers to the average tension along the cable due to its self-weight only. Peak dynamic tension refers to the maximum average tension along the modelled cable finite elements as a result of seismic excitation. Figs. 6.8, 6.10 and 6.12 present the time-history series of dynamic to static cable tension ratio for seismic records NGA 953, NGA 739 and NGA 57, respectively, for seismic motion imposed at only one end node (scenario “A”). Figs. 6.9, 6.11 and 6.13 present the corresponding Fourier response spectra. In Table 6.2 is showed the results of these simulations in terms of peak dynamic tension to static tension ratio according to scenario “A”.

The results presented in Figs. 6.8 to 6.13 and Table 6.2 lead to the following observations:

- when the low frequency content ground motion (NGA 953) was employed it resulted the highest tension values in the longitudinal direction. For all other directions considered under the effect of the same record (NGA 953), differences in results are insignificant for the three seismic records employed herein;
- seismic parameters and results presented in Table 6.2 suggest that there is a higher correlation between the cable tension response and the frequency content of the seismic excitation than between the cable tension response and the magnitude of the seismic acceleration;
- while the frequency content of the response obtained under the NGA 953 record is mainly determined by the contribution of the first modes (Fig. 6.9), the frequency content resulted when the other two seismic ground motions were employed are determined by the contribution of the first mode and of a higher mode in which its frequency coincides with the predominant frequency of these two seismic ground motions (Table 6.2);
- the first mode participation in the dynamic response of the cable tension is due to stretching of the cable in the longitudinal direction and the resulting cable motion in the vertical direction. Higher mode contributions are due to resonant effects;

- analyses of simulation results and time-history of cable tension responses to seismic ground motion of higher frequency content (NGA 739 and NGA 57) shows that the vibration of the cable has two distinct components: one component that is a quasi steady-state response of the cable motion in the vertical direction, and one component that can be interpreted as a resonant transient response with frequency equal to the predominant frequency of the seismic input.

Graphical results for scenario “B” simulations are presented in Figs. 6.14 and 6.15 and in Figs. IV.12 to IV.21 of Appendix IV. Results in numerical format are given in Table 6.3 All these results lead to the following observations:

- no correlation apparently exists between the frequency content of the seismic inputs, as determined by their respective  $A/V$  ratio, and the tension response of the cables;
- parameters and results presented in Table 6.3 indicate that the more relevant factor that affects the cable response is the resonant effect derived from the proximity of the predominant frequency of the seismic input with the frequency of the mode with the highest contribution in the direction of analysis (i.e. longitudinal direction);
- frequency content of the cable tension response is mainly determined by the frequency of the vibration mode that has the highest contribution in the direction of excitation.

Comparisons between the results of the simulations of scenarios “A” and “B” shows that, overall, seismic excitation from asynchronous motion of the cable’s end supports results in higher tension values than for the case of synchronous seismic motion of end supports. This is expected since for the case of asynchronous motion the cable will be stretched and the inertia effects due to the vertical motion of the cable will cause an increase in cable tension.

**Table 6.2 Peak dynamic tension to static tension ratio in overhead conductor. Scenario “A”: seismic motion at one of the supporting node, only.**

Seismic Case	$A_g^{(5)}$ (g)	A/V Ratio	$T_p^{(3)}$ (sec)	$T_m^{(4)}$ (sec)	Peak Dynamic Tension to Static Tension Ratio		
					Direction		
					Transversal	Longitudinal	Vertical
NGA 953	0.84 <sup>(1)</sup> 0.62 <sup>(2)</sup>	0.75 <sup>(1)</sup> 1.60 <sup>(2)</sup>	0.52 <sup>(1)</sup> 0.22 <sup>(2)</sup>	0.74 <sup>(1)</sup> 0.34 <sup>(2)</sup>	1.06	2.45	1.13
NGA 57	0.63 <sup>(1)</sup> 0.38 <sup>(2)</sup>	0.96 <sup>(1)</sup> 2.08 <sup>(2)</sup>	0.20 <sup>(1)</sup> 0.20 <sup>(2)</sup>	0.51 <sup>(1)</sup> 0.26 <sup>(2)</sup>	1.06	1.53	1.13
NGA 739	0.57 <sup>(1)</sup> 0.36 <sup>(2)</sup>	1.13 <sup>(1)</sup> 1.50 <sup>(2)</sup>	0.20 <sup>(1)</sup> 0.06 <sup>(2)</sup>	0.47 <sup>(1)</sup> 0.37 <sup>(2)</sup>	1.06	1.88	1.12

(1) Horizontal component of ground motion. (2) Vertical component of ground motion.

**Table 6.3 Peak dynamic tension to static tension ratio in overhead conductor. Scenario “B”: synchronous seismic motion on both end supporting nodes.**

Seismic Case	$A_g^{(5)}$ (g)	A/V Ratio	$T_p^{(3)}$ (sec)	$T_m^{(4)}$ (sec)	Peak Dynamic Tension to Static Tension Ratio		
					Direction		
					Transversal	Longitudinal	Vertical
NGA 953	0.84 <sup>(1)</sup> 0.62 <sup>(2)</sup>	0.75 <sup>(1)</sup> 1.60 <sup>(2)</sup>	0.52 <sup>(1)</sup> 0.22 <sup>(2)</sup>	0.74 <sup>(1)</sup> 0.34 <sup>(2)</sup>	1.03	1.34	1.10
NGA 57	0.63 <sup>(1)</sup> 0.38 <sup>(2)</sup>	0.96 <sup>(1)</sup> 2.08 <sup>(2)</sup>	0.20 <sup>(1)</sup> 0.20 <sup>(2)</sup>	0.51 <sup>(1)</sup> 0.26 <sup>(2)</sup>	1.01	1.48	1.05
NGA 739	0.57 <sup>(1)</sup> 0.36 <sup>(2)</sup>	1.13 <sup>(1)</sup> 1.50 <sup>(2)</sup>	0.20 <sup>(1)</sup> 0.06 <sup>(2)</sup>	0.47 <sup>(1)</sup> 0.37 <sup>(2)</sup>	1.02	1.41	1.10

(1) Horizontal component of ground motion. (2) Vertical component of ground motion.

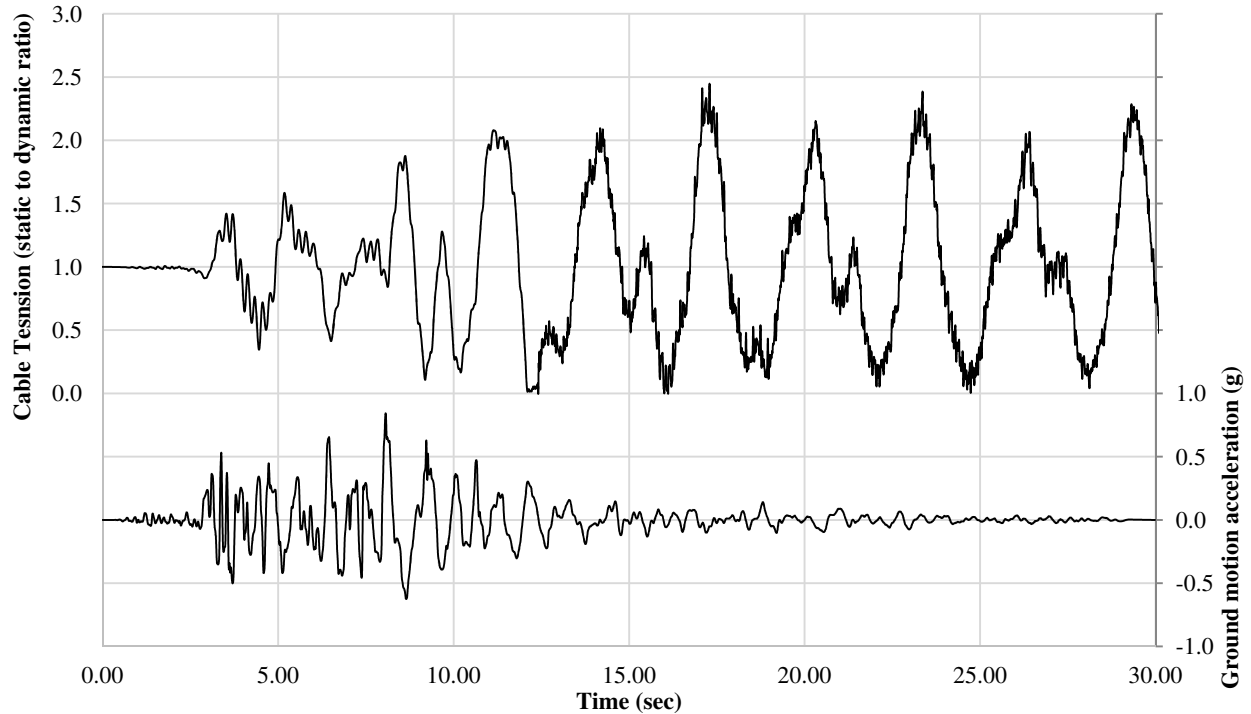


**Figure 6.8. Time-history of conductor cable tension ratio and ground motion accelerogram ( NGA 953 – low frequency content) applied in the longitudinal direction. Scenario “A”:** seismic motion at one of the supporting nodes.

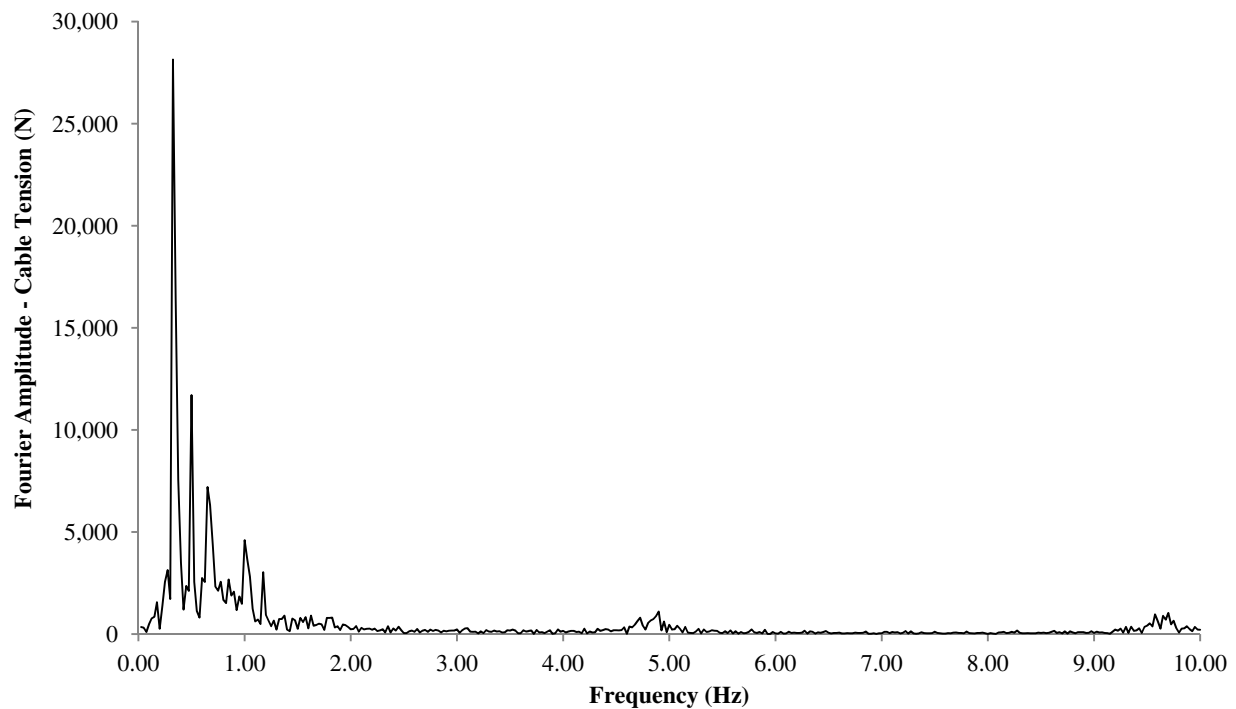


**Figure 6.9. Fourier response spectra of conductor cable tension under NGA 953 (low frequency content) applied in longitudinal direction. Scenario “A”:** seismic motion at one of the supporting nodes.

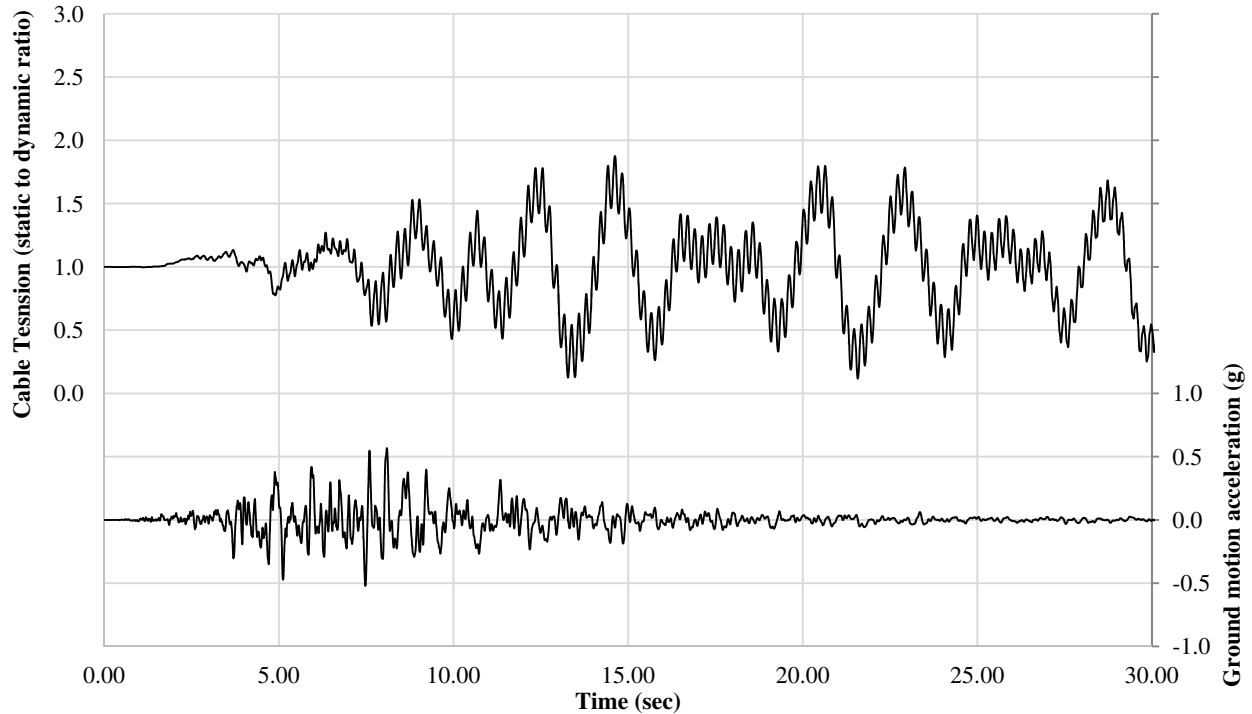


**Figure 6.10.** Time-history of conductor cable tension ratio and ground motion accelerogram ( NGA 739 - medium frequency content) applied in the longitudinal direction. Scenario “A”: seismic motion at one of the supporting nodes.

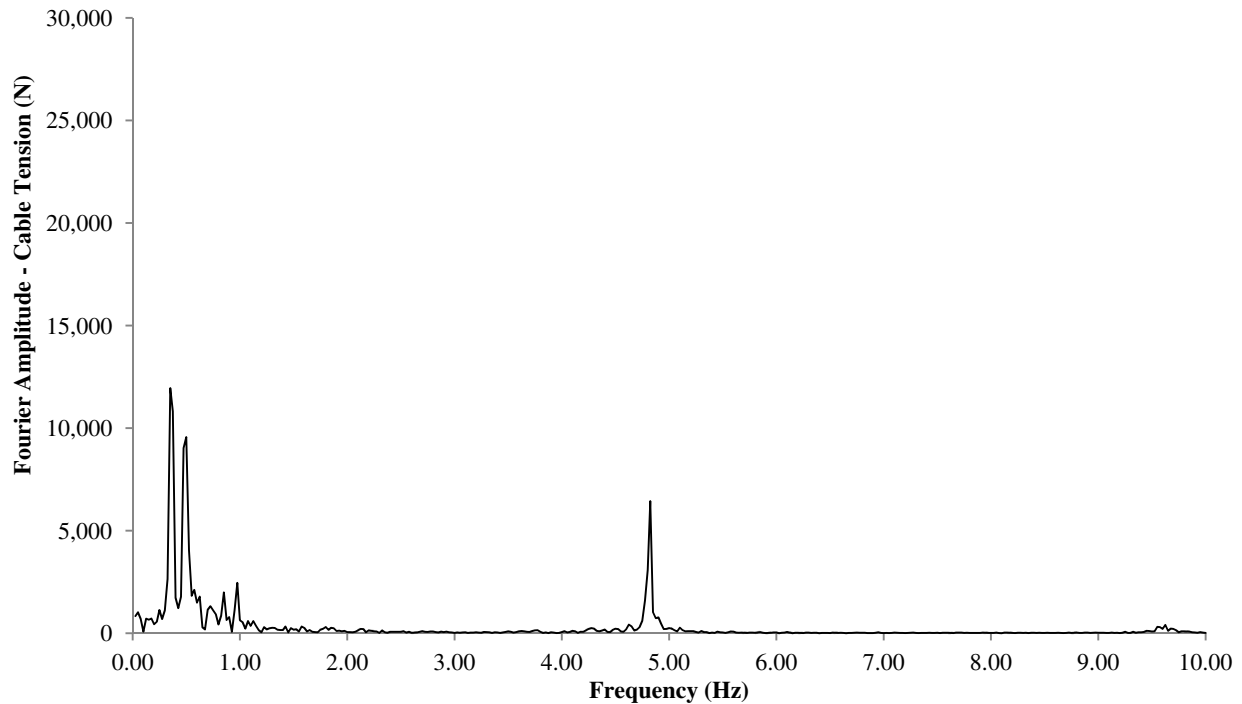


**Figure 6.11.** Fourier response spectra of conductor cable tension under NGA 739 (medium frequency content) applied in the longitudinal direction. Scenario “A”: seismic motion at one of the supporting nodes.

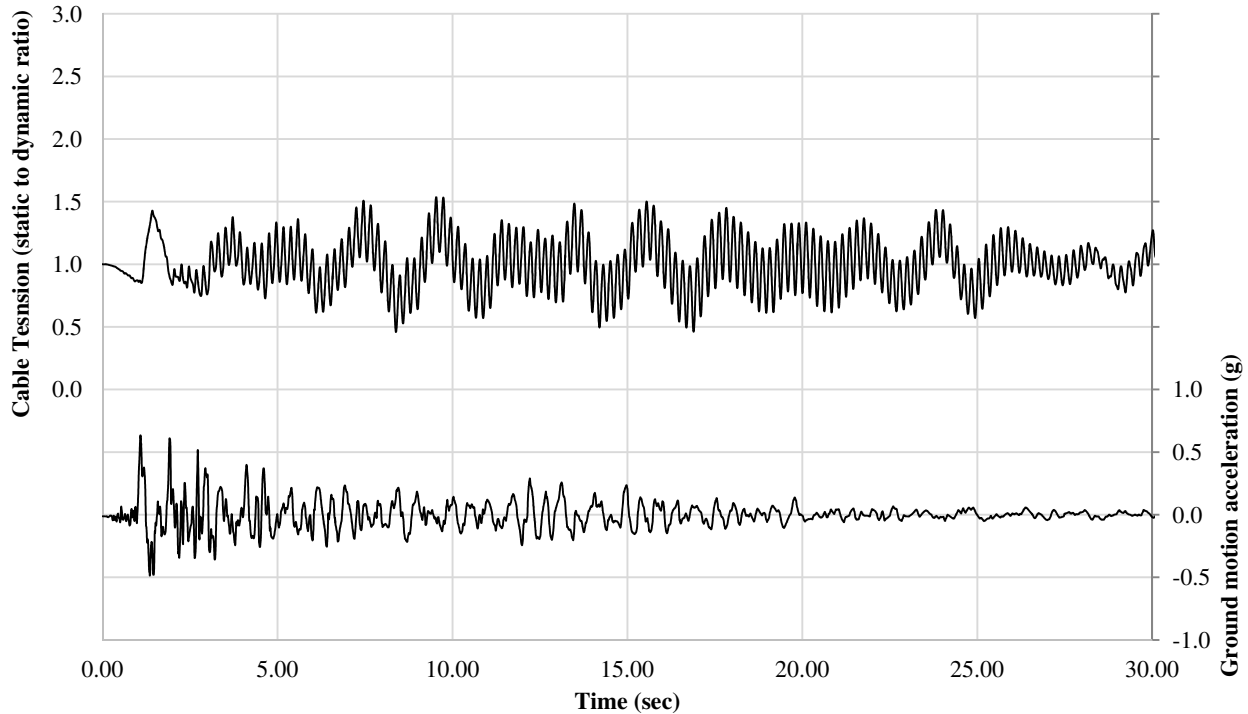


**Figure 6.12. Time-history of conductor cable tension ratio and ground motion accelerogram (NGA 57- high frequency content) applied in the longitudinal direction. Scenario “A”: seismic motion at one of the supporting nodes.**

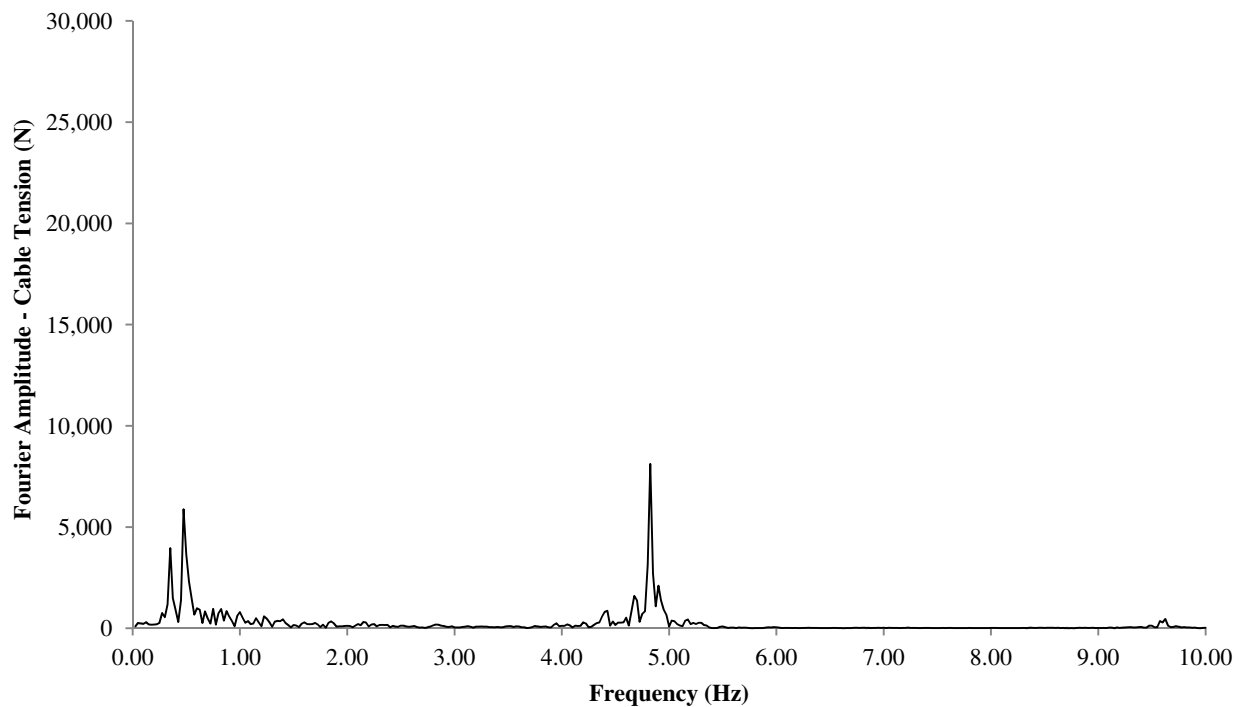


**Figure 6.13. Fourier response spectra of conductor cable tension under NGA 57 (high frequency content) applied in the longitudinal direction. Scenario “A”: seismic motion at one of the supporting nodes.**

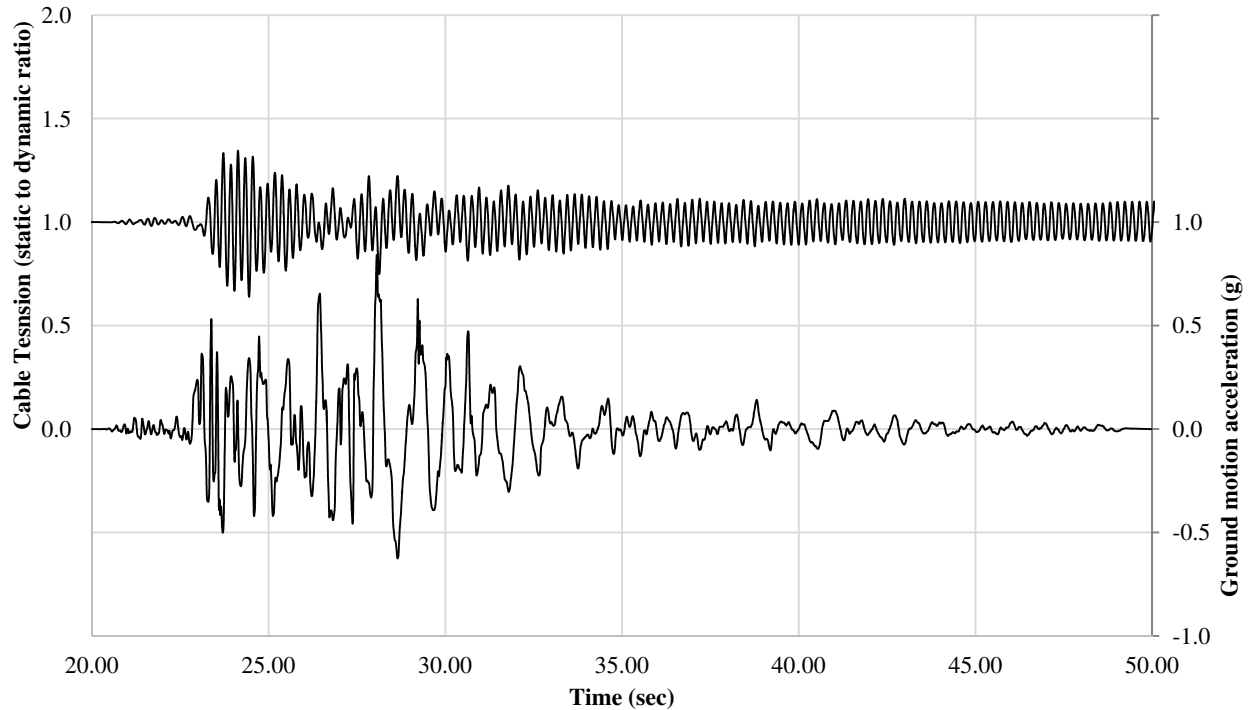


**Figure 6.14.** Time-history of conductor cable tension ratio and ground motion accelerogram (NGA 953) applied in the longitudinal direction. Scenario “B”: synchronous seismic motion on both supporting end nodes.

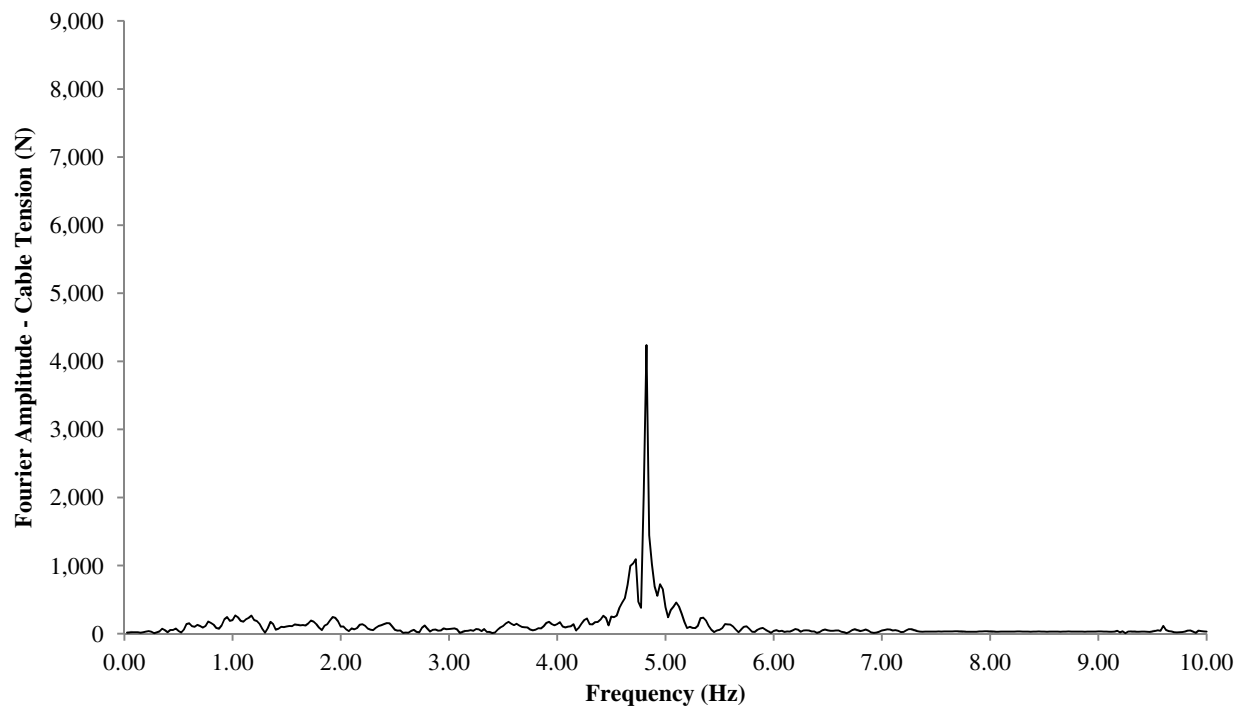


**Figure 6.15.** Fourier response spectra of conductor cable tension under NGA 953 applied in the longitudinal direction. Scenario “B”: synchronous seismic motion on both supporting end nodes.

## 6.6. Seismic Response of the Coupled Guyed tower-Conductor System

The same earthquake ground motion records used for the seismic analyses of the overhead cables were used for the seismic analyses of the coupled guyed tower conductor system described in Section 6.1. In the time-history analyses, all supporting towers were subjected to synchronous ground motions at their base. These ground motions were applied separately in the three main orthogonal directions (longitudinal, transversal and vertical). The study of El Attar et al. (1995) found that earthquake ground motion records with low  $A/V$  ratio resulted in displacement response of towers much higher than the response resulted under an earthquake ground motion with high  $A/V$  ratio. The coupled dynamic behavior of the guyed tower cable system was not studied by El Attar et al. (1995). The present simulations are used to discuss the findings obtained for overhead cables in the case of a coupled guyed tower conductor system against the conclusions reached by El Attar et al. (1995).

The effect of the overhead cables' mass to the response of the supporting towers is studied in this section by comparing the responses of the free-standing delta guyed towers with the responses of supporting delta guyed towers when the coupled-system is included in analysis. Table 6.4 shows a comparison of the responses of the delta guyed tower with the consideration of coupled-system versus the responses of free-standing delta guyed tower when subjected to earthquake ground motions applied separately in the three orthogonal directions.

### 6.6.1. Seismic Responses of Delta Guyed Tower under Ground Motions Applied in the Longitudinal and Transversal Directions

The results presented in Table 6.4 shows that for earthquake ground motions with low frequency content ( $A/V$  ratio less than 0.80) applied in the longitudinal direction, the inertia effects of the overhead cables enhance the responses resulted in the supporting delta guyed towers whereas under the effect of intermediate and high frequency content ground motions, the overhead cables attenuate the responses in the supporting delta guyed towers. in Figs. 6.16, 6.18 and 6.20 presents comparisons between the time-history series of horizontal base shear reactions of the free-standing delta guyed tower and coupled delta guyed tower conductor-system under NGA 953, NGA 57 and NGA 739 records applied in the longitudinal direction.

By comparing these time-history responses, it was observed that the motion of the overhead cables introduced a phase shift in the response of the supporting delta guyed towers for records of intermediate and high frequency content. This phase shift resulted in a damped oscillation of the system, thus attenuating the dynamic responses in the supporting delta guyed towers.

In that sense, the overhead cables acted to restrain the seismic motion of the supporting towers rather than contributing to the inertia seismic forces acting on the tower. Conversely, for the low frequency content record, the oscillatory inertia effects of the overhead cables enhanced the base shear reaction on the supporting towers.

Figs. 6.17, 6.19 and 6.21 present persistence curves of the base shear time-history series presented in Figs. 6.16, 6.18 and 6.20, respectively. These persistence curves give a measure of how much the base shear reaction in the supporting delta guyed tower is enhanced or attenuated by the inertia action of the overhead cables. The greater is the difference between the persistence curves of the free-standing delta guyed tower and the supporting delta guyed tower of the coupled-system, the greater is the influence of the mass of the overhead cables in the response of the supporting delta guyed tower. A comparison of the curves in these three figures suggests that the higher is the frequency content of an earthquake ground motions (as defined by its  $A/V$  ratio) the higher is the damped oscillation effect introduced by the overhead cables.

The results presented in Table 6.4 also show that for earthquake ground motions acting in the transversal direction, the inertia effects of the overhead cables tend to attenuate the maximum responses in the supporting tower. Fig. 6.23 and Figs. IV-23 and IV.25 in Appendix IV presents persistence curves of the base-shear time-histories presented in Fig. 6.22 and Figs. IV-22 and IV-24 of Appendix IV, respectively, for earthquake ground motions acting in the transversal direction. From these persistence curves it can be seen that while higher values of base-shear responses are attenuated by the induced motion of the overhead cables, lower values of base-shear responses are enhanced in all simulated seismic cases. For low frequency content earthquake, simulations indicate that the inertia effects of overhead cable motion reduce maximum base-shear response by about 30%. For intermediate and high frequency content earthquake, simulations indicate that the inertia effects of overhead cable motion reduce maximum base-shear response by about 20%.

### 6.6.2. Seismic Responses of Delta Guyed Tower under Ground Motions Applied in the Vertical Direction

The results presented in Table 6.4 show that for earthquake ground motions acting in the vertical direction, the inertia effects of the overhead cables tend to enhance the maximum responses in the supporting delta guyed tower. However, the differences between the responses of free-standing delta guyed towers and delta guyed towers supporting the cable elements are not significant. Fig. 6.25 and Figs. IV-27 and IV-29 in Appendix IV presents persistence curves of base-shear time-histories presented in Fig. 6.24 and Figs. IV-26 and IV-28 respectively for earthquake ground motions acting in the vertical direction. From these persistence curves it can be seen that while higher values of base-shear responses are enhanced by the induced displacement of the overhead cables, lower values of base-shear responses are attenuated in all simulated seismic cases. For high frequency content records, simulations indicate the inertia effects of overhead cable motion increase maximum vertical reaction response by about 30%. For intermediate and low frequency content records, simulations indicate the inertia effects of overhead cable motion increase maximum vertical reaction response by about 10%.

**Table 6.4 Percentage of members with seismic axial forces higher than in design load cases.**

Seismic Case	Configuration	Percentage of members with seismic axial forces higher than in design load cases	Number of members with capacity exceeded	Maximum capacity usage of guy cables
<b>Longitudinal Direction</b>				
NGA 953 <i>Low freq. content</i>	Free-Standing Delta Guyed Tower	60%	9	40%
	Coupled Delta Guyed Tower-Conductor syst.	<b>91%</b>	<b>100</b>	<b>86%</b>
NGA 57 <i>Intermediate freq. content</i>	Free-Standing Delta Guyed Tower	<b>62%</b>	<b>17</b>	<b>54%</b>
	Coupled Delta Guyed Tower-Conductor syst.	30%	4	34%
NGA 739 <i>High freq. content</i>	Free-Standing Delta Guyed Tower	<b>34%</b>	<b>5</b>	<b>32%</b>
	Coupled Delta Guyed Tower-Conductor syst.	21%	-	25%
<b>Transversal Direction</b>				
NGA 953 <i>Low freq. content</i>	Free-Standing Delta Guyed Tower	<b>82%</b>	<b>144</b>	<b>69%</b>
	Coupled Delta Guyed Tower-Conductor syst.	70%	11	65%
NGA 57 <i>Intermediate freq. content</i>	Free-Standing Delta Guyed Tower	<b>37%</b>	<b>5</b>	<b>28%</b>
	Coupled Delta Guyed Tower-Conductor syst.	31%	4	27%
NGA 739 <i>High freq. content</i>	Free-Standing Delta Guyed Tower	<b>59%</b>	<b>8</b>	<b>51%</b>
	Coupled Delta Guyed Tower-Conductor syst.	39%	4	38%
<b>Vertical Direction</b>				
NGA 953 <i>Low freq. content</i>	Free-Standing Delta Guyed Tower	-	-	10%
	Coupled Delta Guyed Tower-Conductor syst.	<b>2%</b>	-	<b>10%</b>
NGA 57 <i>Intermediate freq. content</i>	Free-Standing Delta Guyed Tower	-	-	8%
	Coupled Delta Guyed Tower-Conductor syst.	-	-	<b>9%</b>
NGA 739 <i>High freq. content</i>	Free-Standing Delta Guyed Tower	-	-	8%
	Coupled Delta Guyed Tower-Conductor syst.	<b>1%</b>	-	<b>9%</b>

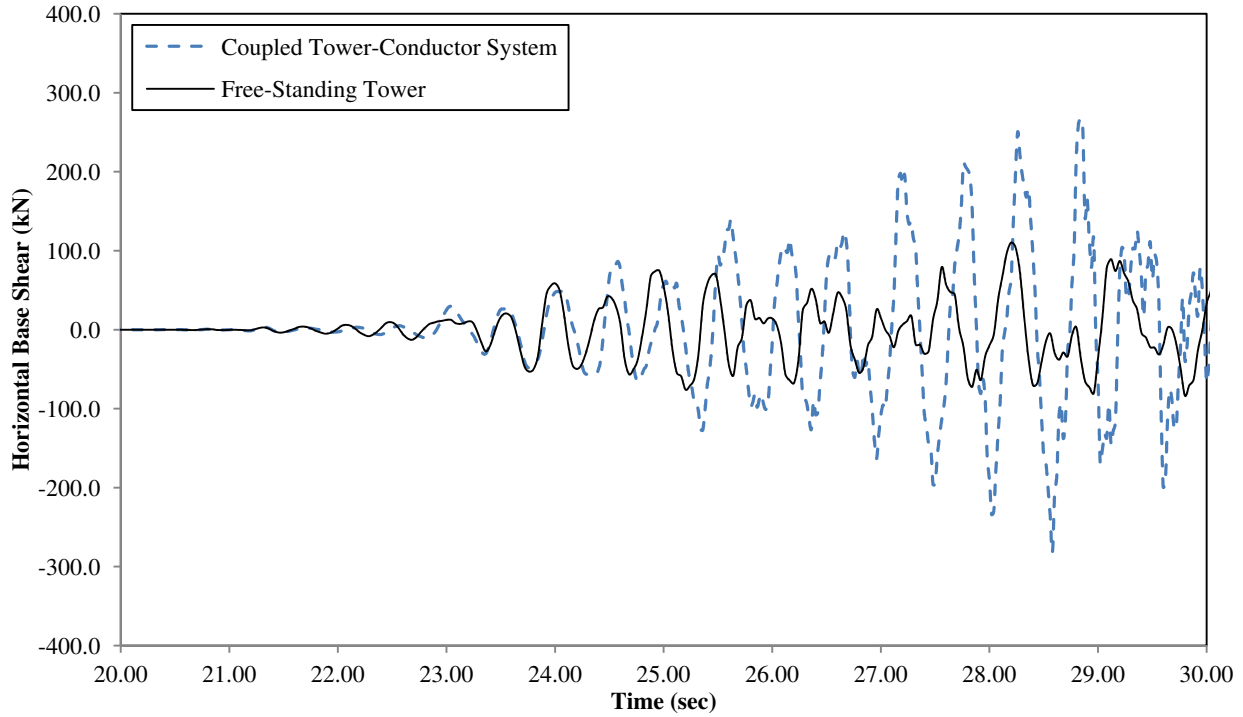


**Figure 6.16. Time-history of horizontal base shear of Free-Standing Delta Guyed Tower and Coupled Delta Guyed Tower-Conductor System under NGA 953 record (low frequency content) applied in the longitudinal direction.**

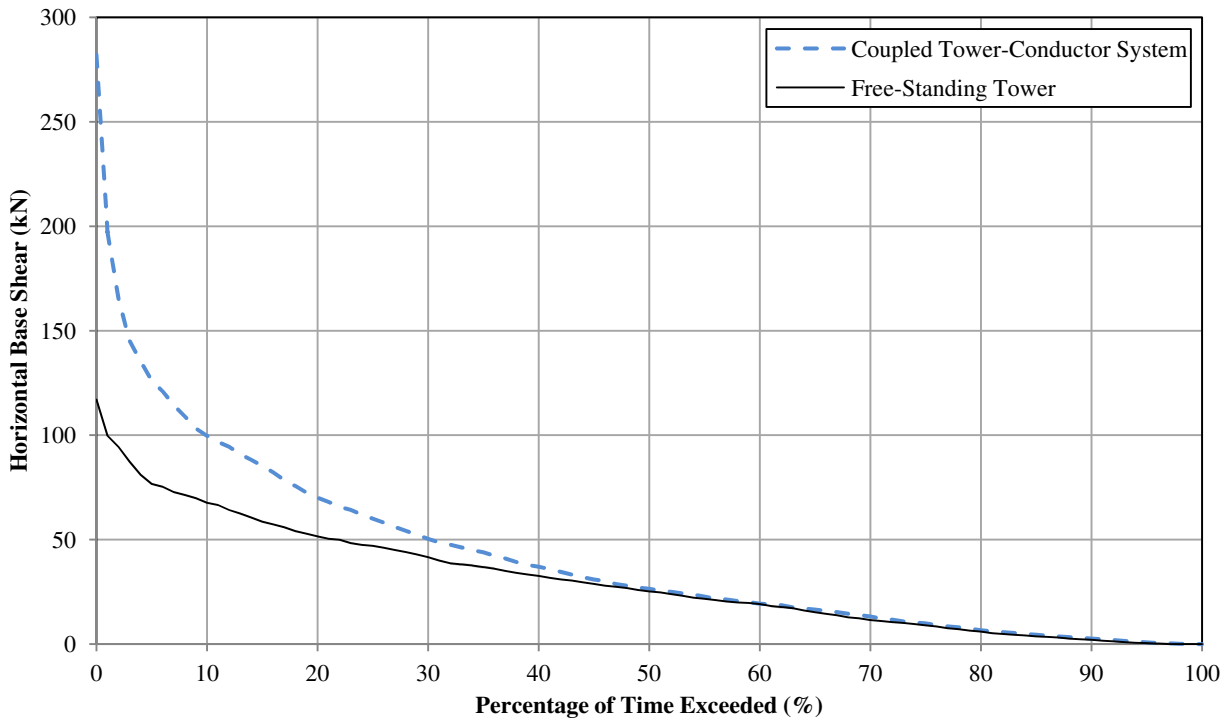


**Figure 6.17. Persistence curve of horizontal base shear time-history of Free-Standing Delta Guyed Tower and Coupled Delta Guyed Tower-Conductor System under NGA 953 record (low frequency content) applied in the longitudinal direction.**

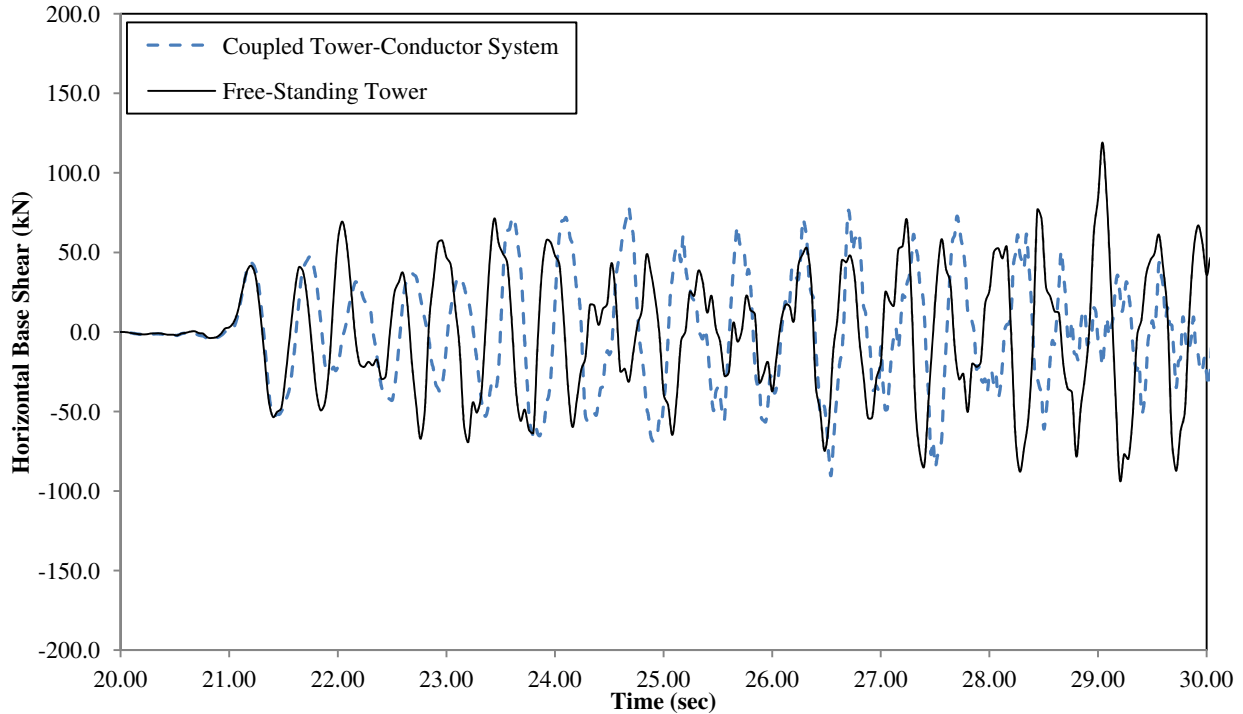


**Figure 6.18. Time-history of horizontal base shear of Free-Standing Delta Guyed Tower and Coupled Delta Guyed Tower-Conductor System under NGA 57 record (intermediate frequency content) applied in the longitudinal direction.**

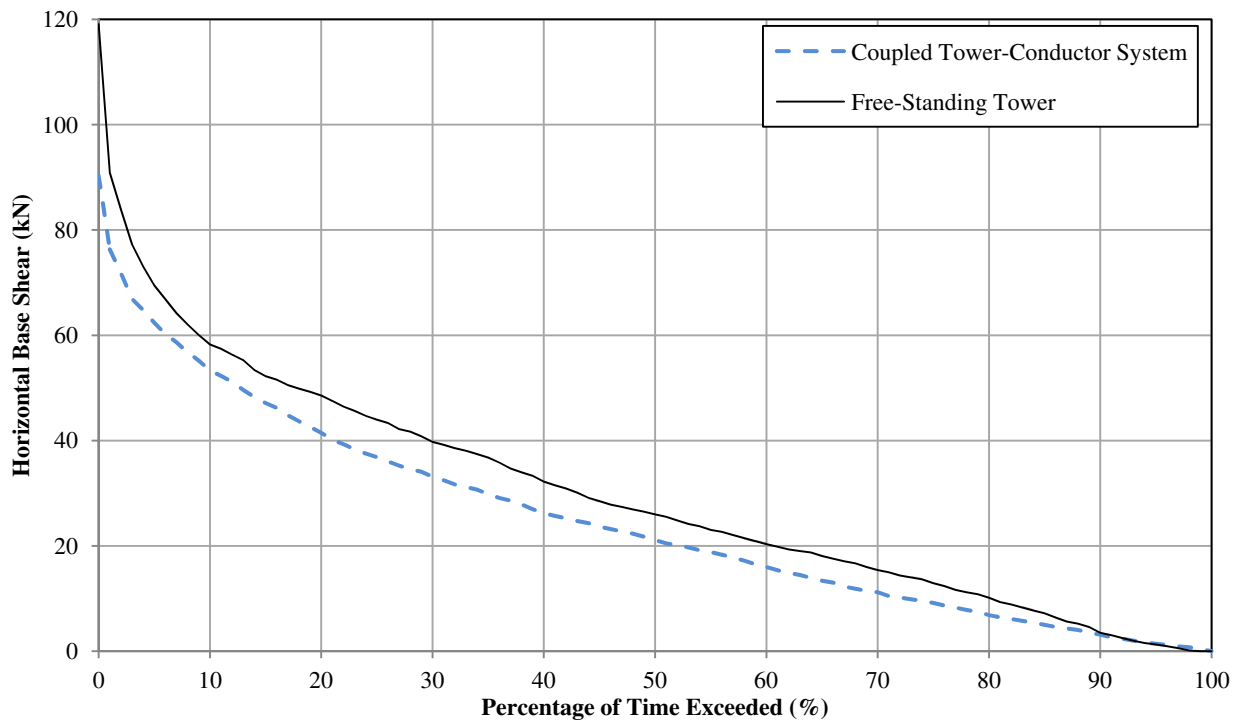


**Figure 6.19. Persistence curve of horizontal base shear time-history of Free-Standing Delta Guyed Tower and Coupled Delta Guyed Tower-Conductor System under NGA 57 record (intermediate frequency content) applied in the longitudinal direction.**

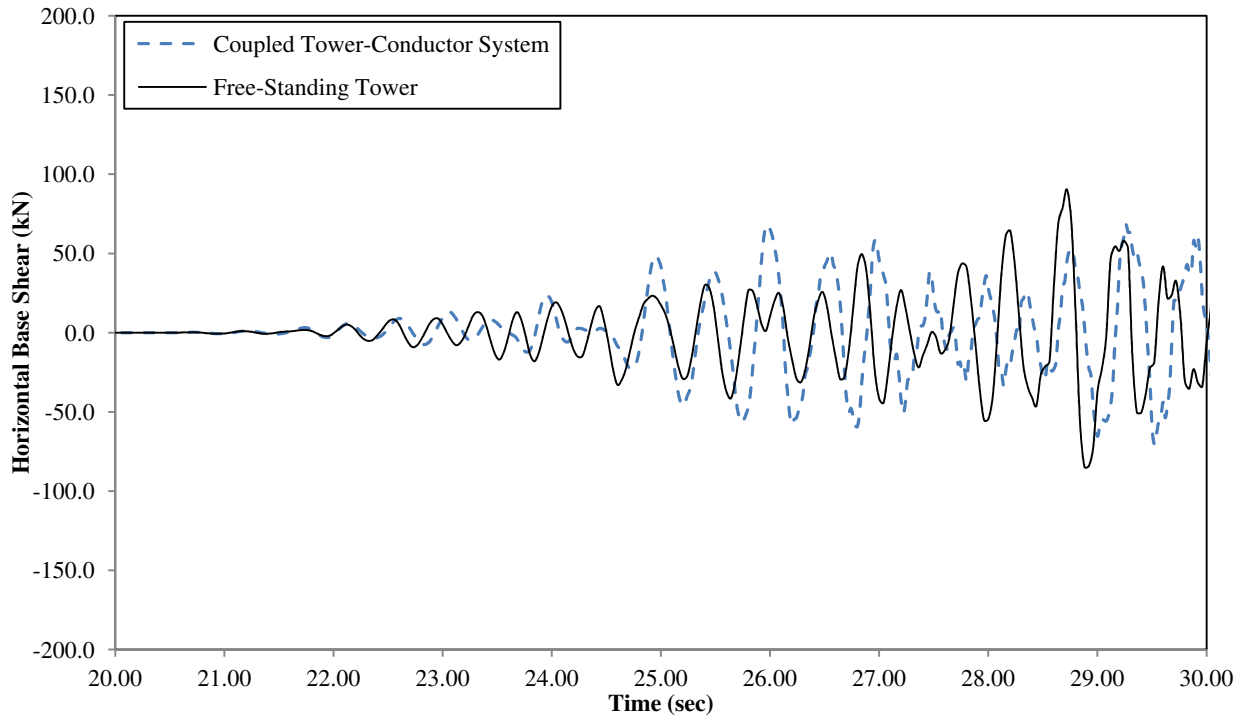


**Figure 6.20. Time-history of horizontal base shear of Free-Standing Delta Guyed Tower and Coupled Delta Guyed Tower-Conductor System under NGA 739 record (high frequency content) Applied in the longitudinal direction.**

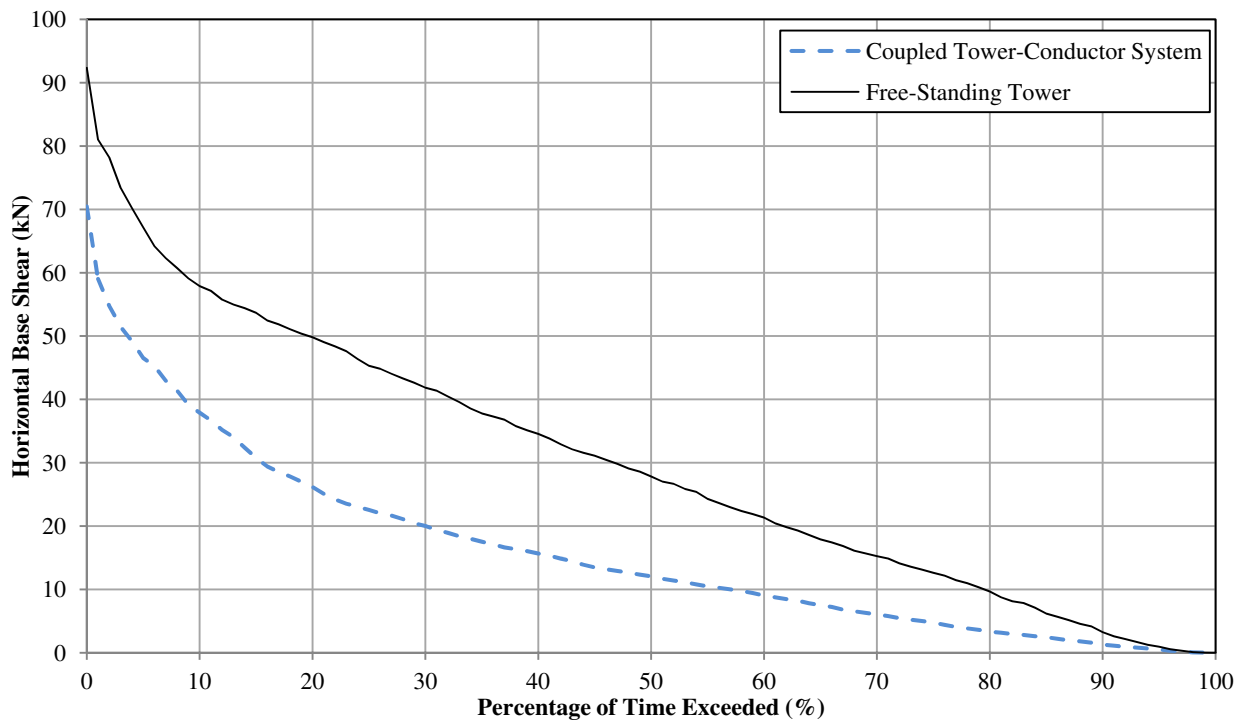


**Figure 6.21. Persistence curve of horizontal base shear time-history of Free-Standing Delta Guyed Tower and Coupled Delta Guyed Tower-Conductor System under NGA 739 record (high frequency content) applied in longitudinal direction**

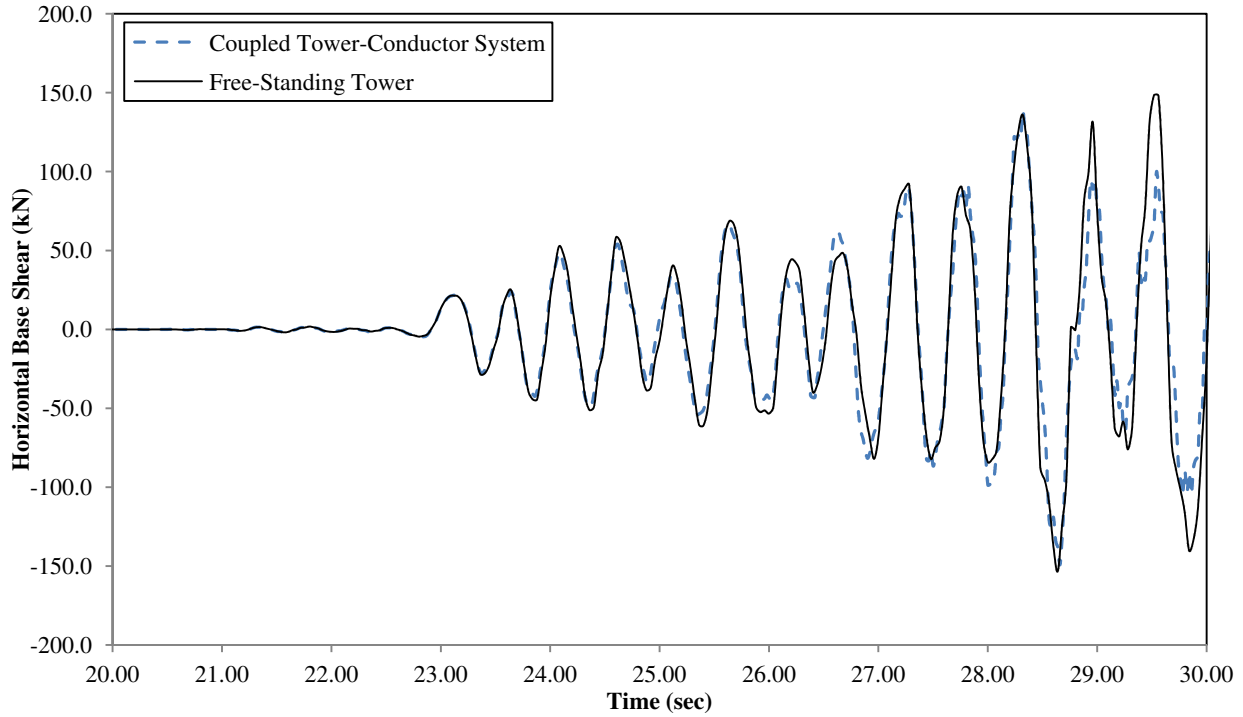


**Figure 6.22. Time-history of horizontal base shear of Free-Standing Delta Guyed Tower and Coupled Delta Guyed Tower-Conductor System under NGA 953 applied in transversal direction.**

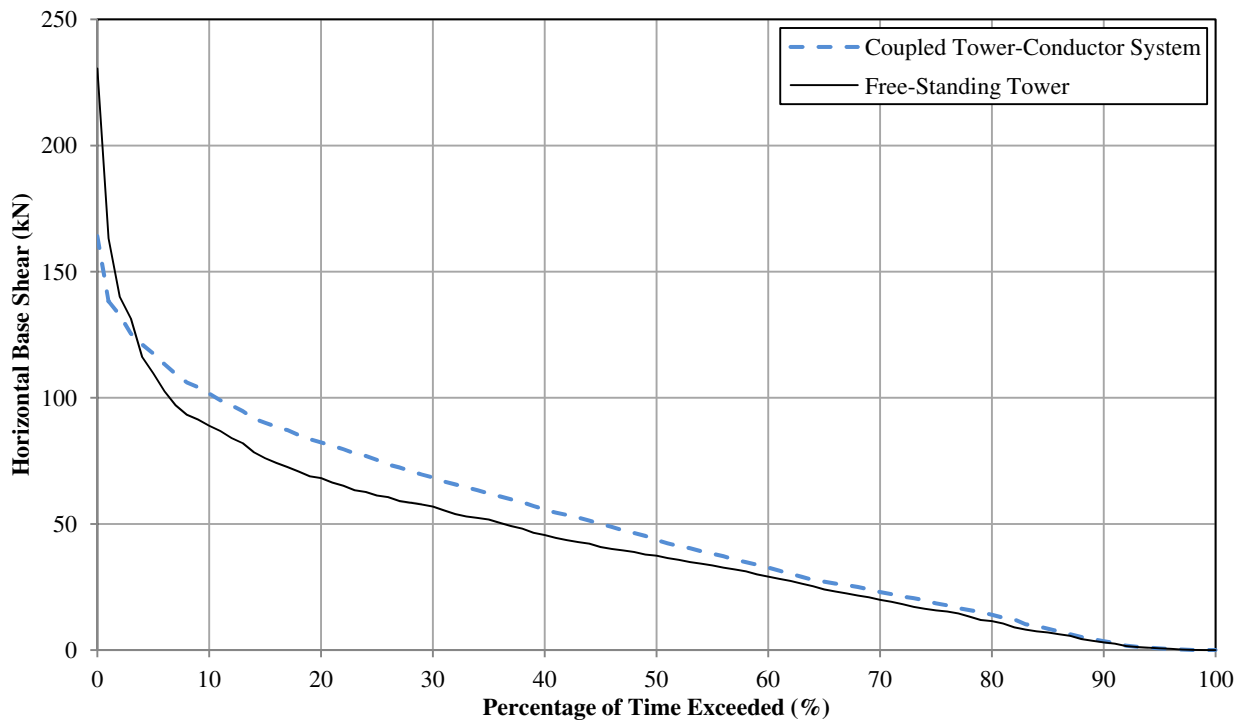


**Figure 6.23. Persistence curve of horizontal base shear time-history of Free-Standing Delta Guyed Tower and Coupled Delta Guyed Tower-Conductor System under NGA 953 record applied in transversal direction**

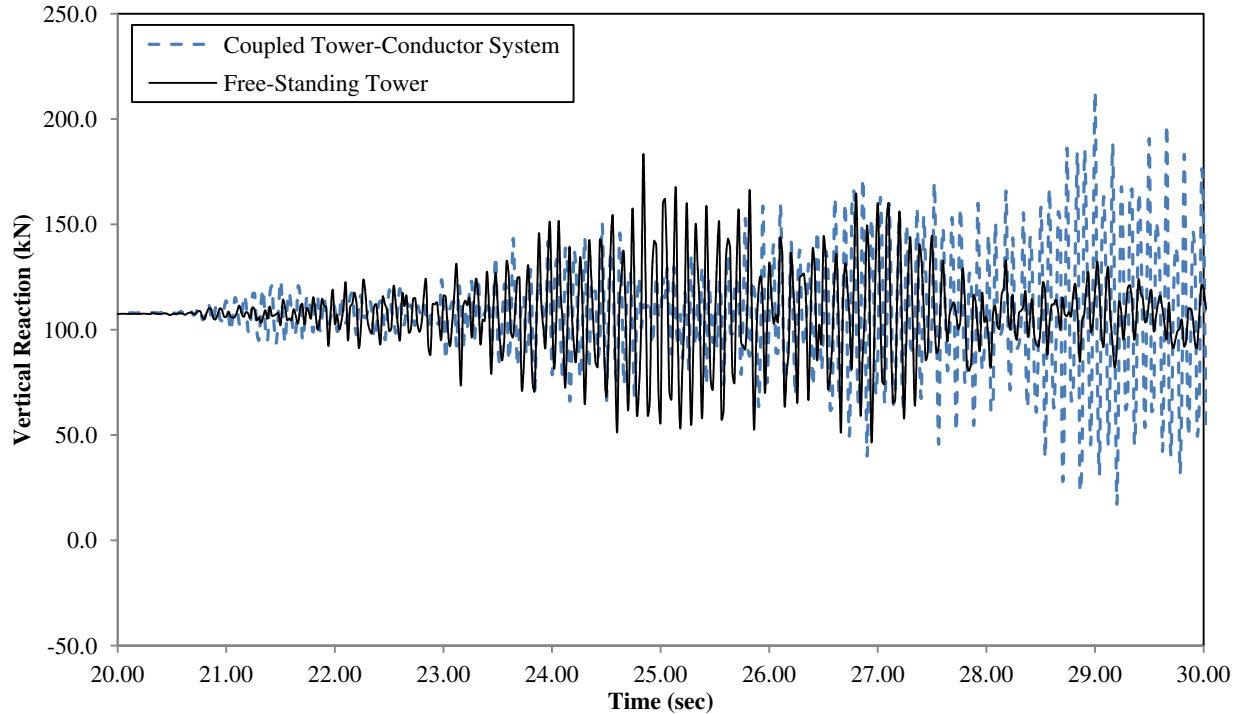


**Figure 6.24. Time-history of horizontal base shear of Free-Standing Delta Guyed Tower and Coupled Delta Guyed Tower-Conductor System under NGA 739 record applied in vertical direction.**

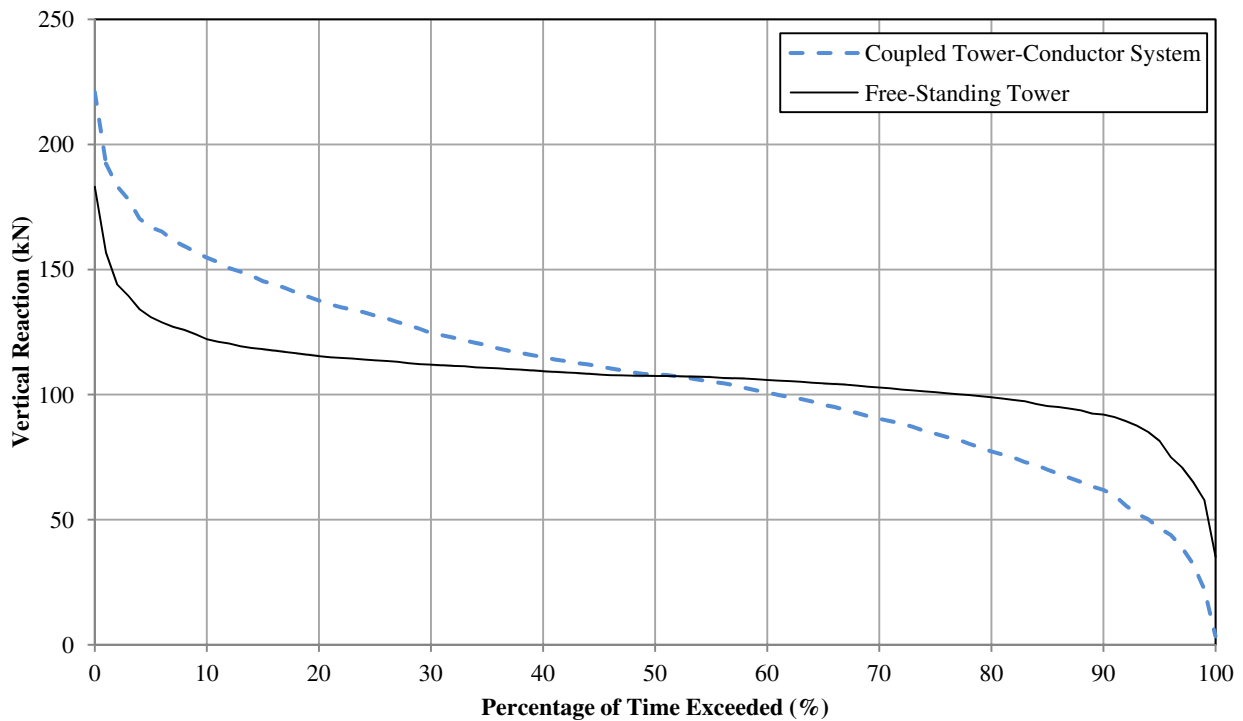


**Figure 6.25. Persistence curve of horizontal base shear time-history of Free-Standing Delta Guyed Tower and Coupled Delta Guyed Tower-Conductor System under NGA 739 record applied in transversal direction.**

## CHAPTER VII

### CONCLUSIONS AND FUTURE WORK

#### 7.1. Conclusions

Previous research work was mainly devoted to Self-supporting TL towers, while studies involving guyed towers were mainly devoted to telecommunication towers. The TL guyed towers studied herein were found to be more sensitive to seismic excitation than typical Self-supporting towers. Since these lattice guyed towers have become popular structures for supporting high-voltage transmission lines, they should receive more attention when employed in areas of high seismic risk.

In this study, four existing TL towers studied herein are investigated. These lattice towers were designed, built and tested in accordance with the requirements of the CAN/CSA C22.3 No. 60826-10 and ASCE-10-97 standard. The design of these towers was checked to fulfill the requirements of the current standard ASCE-10-15. It is noted that ASCE-10-97 is the previous edition of the current ASCE standard. The controlling design load cases for these towers were the wind load and a combination of ice and wind load.

To study the sensitivity of these TL towers to earthquake loads, they were relocated in high seismic risk area of British Columbia that matched the environmental conditions (e.g. wind, snow and ice) considered in design. Then, all four towers were modeled in ANSYS-APDL software and were subjected to nonlinear time-history analyses. Two sets of 10 ground motions each were selected and scaled to match the design spectrum over the period of interest from  $0.2T_1$  to  $1.5T_1$ . The three main orthogonal directions of selected ground motions were employed in this study. Due to high sensitivity of TL guyed towers to seismic input, the dynamic properties and seismic response of these free-standing guyed towers were studied in detail, as well as the seismic response of TL guyed towers when the coupled tower-conductor system is considered.

The main findings and contributions of this research are:

- To simulate the steel lattice guyed tower members, the FE Frame-Truss-Model selected from ANSYS-APDL library is more accurate than the FE Truss-Model when the leg members of towers are replicated. For all other tower's members, the use of FE Truss-Model is adequate. This finding was checked by validation of the FE numerical model with measurements from the full-scale prototype tests;

- Different load distribution patterns (e.g. inverse triangle and modal distribution) used in pushover analyses of slender and flexible TL guyed towers showed different axial forces triggered in the members of towers. Thus, when modal distribution pattern is used, the magnitude of forces triggered in members of guyed towers is 10% to 25% higher than in the case of inverse triangle loading pattern. When a uniform distribution pattern is used for wind loads in pushover analyses, the higher mode effects are neglected. In this study, by using different load distribution patterns across the structure height, an equivalent static force method is proposed in order to approximate the seismic base shear for the studied TL towers. This method was verified against nonlinear time-history results obtained from the simulated tower models. Impulse forces from the guy tower-cable sudden stretching, as a result of dynamic interactions between guyed tower-cables and tower-mast, were studied using a FE method and analytical equations. Results of these analyses indicate that the static tension forces in the guy tower-cables could be dynamically amplified by a factor as big as 1.6;
- The base shear response of delta-guyed tower to harmonic excitation can be approximated by using analytical expressions applied to an equivalent SDOF system;
- To estimate the values of seismic base shear and vertical reactions of free-standing TL guyed towers, analytical expressions are proposed to be used for the preliminary design of towers to seismic loads. These are based on the tower weight, fundamental period of the tower, peak ground motion acceleration and predominant period of ground motion. These expressions can be used for towers with similar geometry and dimensions.. Also, these expressions should be used with appropriate caution for seismic inputs with frequency content significantly different than the ones used in the present study;
- Response spectral analyses showed that for TL Self-supporting towers only one mode of vibration is activated during seismic excitation, whereas for the TL guyed tower many modes of vibration are activated. These response spectra also showed that the amplitudes of vibration associated with the activated modes are higher for TL guyed towers than for Self-supporting towers. It is also noted that the mode frequencies of vibration of TL guyed towers are closer to those of earthquake ground motions;

- Typical vibration frequencies of the overhead conductors studied herein, when harmonically excited in the vertical and transversal directions, are different than those of free-standing TL towers;
- To study the response of overhead conductors, two scenarios were considered: scenario “A” meaning that seismic excitations are applied at only one of the supporting nodes and scenario “B” when synchronous seismic excitations are applied at both end supporting nodes. It is noted that scenario “A” is more likely to occur during an earthquake event because it is expected that the seismic response of supporting towers to be asynchronous. When low frequency content ground motions are applied in the longitudinal direction of TL, there are expected higher axial tension forces in cables than in the case of seismic excitations of higher frequency content. For the other two orthogonal directions analyzed (vertical and transversal) there is no significant distinction observed in the response.;
- The comparisons made between the seismic responses of TL guyed towers and TL guyed towers coupled with overhead cables indicate that the inertia effects induced by cables tend to attenuate the response of the supporting guyed towers. However, for low frequency content earthquake, the analyses presented herein indicate that the response of supporting TL guyed towers is enhanced when the ground motion acts on longitudinal direction. It was also observed that the motion of the overhead cables induces a phase shift in the response of the supporting guyed towers for earthquakes of intermediate and high frequency content. This phase shift resulted in a damped oscillation of the system which attenuates the dynamic response of supporting guyed towers. Thus, the overhead cables act to restrain the seismic motion of supporting guyed towers rather than contributing to the increase of seismic inertia forces developed in tower.

## 7.2. Recommendations for Future Work

All conclusions presented above are associated to the types and dimensions of TL towers used herein. Applicability of these findings to other types of TL towers must be exerted with caution. The work developed in this research covered several aspects related to the understanding of the seismic response of lattice TL guyed towers. However, more research is recommended to further investigate the following topics:

- Further investigations in the development of load distribution patterns are required in order to assess the most fitted one. For solving this drawback, consideration of higher mode effects is required. Results of these investigations could conduct to important contributions to design practice and design standards for safer and more reliable structures;
- There could be other potentially damaging effects of ground motions to the integrity of TL structures that need to be considered: differential foundation settlement, support spreading and asynchronous ground motion effects, etc. TL guyed towers, which rely solely on its pretensioned guy cables for its lateral stability, may have a higher vulnerability to the effects of soil deformation and differential settlement after an earthquake event as some of its guy-anchors may be displaced relative to the tower base. This conducts to either a slackened guy cable which becomes non-functional to the lateral stability of the mast, or a guy cable further stretched;
- Asynchronous ground motion could be particularly damaging to guyed towers since the attachments of the guy cables to the ground are usually distanced apart by as much as 100 meters and the stability of this type of tower relies exclusively on the pre-tensioned guy cables. In addition, asynchronous ground motions could have a damaging effect to overhead conductors when the couple tower–conductor system is considered. It is noted that overhead conductors have long spans between supporting towers. Hence, the asynchronous ground motion effect on the response of TL structures should be studied more in detail;

- As it was shown by the comparisons made for the results of dynamic simulations carried out for the free-standing towers and for the coupled guyed tower-conductor system, the seismic response of the supporting guyed tower structure is significantly modified by its dynamic interactions with the overhead conductor motion. The results of these simulations indicated that the frequency content of the earthquake ground motions is relevant in determining the responses of the coupled system. Further investigations are suggested to ascertain the observations regarding the effect of the frequency content of ground motion on the response of these structures and to develop simplified methods capable to approximate the effects of the overhead cable motion on the response of the supporting towers. To solve this issue near field type ground motions and subduction ground motions need to be considered for investigations.

## REFERENCES

- Adams, J., and Atkinson, G.M. (2003). "Development of seismic hazard maps for the proposed 2005 edition of the National Building Code of Canada." *Can. J. Civ. Eng.*, 30, 255-271.
- American Society of Civil Engineers – ASCE-7 & SEI Standards (2013). Minimum design loads for buildings and other structures. Standards ASCE/SEI 7-10. 2013 / 636 pp.
- American Society of Civil Engineers – ASCE 74 (2009). Guidelines for electrical transmission line structural loading (3<sup>rd</sup> edition). Manual of practice (MOP 74). Wong, C. Jerry, and Miller, Michael D., eds. Reston, VA, USA: ASCE, 2009. ProQuest ebrary. Web. 15 January 2016.
- American Society of Civil Engineers – ASCE (10-97). Design of lattice steel transmission structures.
- American Society of Civil Engineers – ASCE/SEI (10-15). Design of lattice steel transmission structures.
- Amiri, G. G. (1997). Seismic sensitivity of tall guyed telecommunication towers. Ph.D. Thesis, Department of Civil Engineering and Applied Mechanics, McGill University, Montreal, Canada, 243 pp.
- ANSYS (2013). Mechanical APDL Command Reference. Release 15.0. November, 2013.
- ANSYS (2013). Mechanical APDL Theory Reference. Release 15.0. November, 2013.
- Atkinson, G. (2009). "Earthquake time histories compatible with the 2005 National Building Code of Canada uniform hazard spectrum." *Can. Journal of Civil Eng.*, 36(6), 991-1000.
- Benedettini, F., and Rega, G. (1989a). Planar non-linear oscillations of elastic cables under superharmonic resonance conditions. *J. Sound and Vibration*, 132(3), 353-366.
- Benedettini, F., and Rega, G. (1989b). Planar non-linear oscillations of elastic cables under subharmonic resonance conditions. *J. Sound and Vibration*, 132(3), 367-381.
- Blevins, R.D. 1995. *Formulas for Natural Frequency and Mode Shape*. Krieger Pub Co.
- Canadian Standards Association – CAN/CSA-S37-94 – *Antenna, Towers and Antenna-Supporting Structures* (1994).
- Canadian Standards Association – CAN/CSA-S37-13 – *Antenna, Towers and Antenna-Supporting Structures* (2013).
- Canadian Standards Association – CAN/CSA-C22.3 NO. 60826-10 (R2015) - *Design criteria of overhead transmission lines (Adopted CEI/IEC 60826:2003, third edition, 2003-10, with Canadian deviations)*.

Chen, B.; Guo, W.; Li, P.; Xie, W. (2014). Dynamic Responses and Vibration Control of the Transmission Tower-Line System: A State-of-the-Art Review. Hindawi Publishing Corporation. The Scientific World Journal. Volume 2014, Article ID 538457, 20 pages. <http://dx.doi.org/10.1155/2014/538457>

Chopra, A. K. (1995). Dynamic of Structures - Theory and Application to Earthquake Engineering, First Edition, Prentice-Hall International Series in Civil Engineering and Engineering Mechanics

Clough, R.W., and J. Penzien. (1993). Dynamics of Structures, Second edition. McGraw-Hill.

Davenport, A.G., and Steels, G.N. (1965). Dynamic behavior of massive guy-cables. J. Struct. Div., ASCE, 91(ST2), 43-70.

El-Attar, M. (1997). Nonlinear Dynamics and Seismic Response of Power Transmission Lines. PhD Thesis. McMaster University.

Eidinger, J. and Kempner, Jr., L. (2012) Risk Assessment of Transmission System under Earthquake Loading. Electrical Transmission and Substation Structures 2012: pp. 183-192.

Electric Power Research Institute – EPRI (2009). Transmission Line Reference Book: Wind-Induced Conductor Motion.

European Committee for Electrotechnical Standardization - CENELEC (2001). Overhead Transmission Line Design.

Federal Emergency Management Agency – FEMA (2003). NEHRP Recommended Provisions for Seismic Regulations for New Buildings and Other Structures (FEMA 450). Building Seismic Safety Council.

Federal Emergency Management Agency – FEMA (2006). NEHRP Recommended Provisions: Design Examples (FEMA 451). Building Seismic Safety Council. August, 2006.

Federal Emergency Management Agency – FEMA (1991). Earthquake Resistant Construction of Electric Transmission and Telecommunication Facilities Serving the Federal Government Report. Earthquake Hazard Reduction Series 56.

Filiatrault, A., Tremblay, R., Christopoulos, C., Fols, B., Pettinga, D. (2013). Elements of Earthquake Engineering and Structural Dynamics, Third edition. Presses internationales Polytechnique.

Finn, W.D.L. and Wightman, A. (2003). Ground Motion Amplification Factors for the Proposed 2005 Edition of the National Building Code of Canada. Canadian Journal of Civil Engineering (30)2:272-278.

Gani, F., Legeron, F. (2010). Dynamic response of transmission lines guyed towers under wind loading. Published on the NRC Research Press Web site at [cjce.nrc.ca](http://cjce.nrc.ca) on 5 March 2010.

Ghobarah, A. Aziz, T. S., El-Attar, M. (1995). Response of transmission lines to multiple support excitation. *Engineering Structures*, Vol. 18, n° 12, pp. 936-946. Elsevier Science.

Guevara, E. (1993). Nonlinear seismic analysis of antenna-supporting structures. M.Eng. project report, Department of Civil Engineering and Applied Mechanics, McGill University, Montreal, Quebec, Canada, 84 pp.

International Electrotechnical Commission – IEC (2003). Design Criteria of Overhead Transmission Lines. 2<sup>nd</sup> edition. October 1, 2003.

Khedr, M (1998). Seismic Analysis of Lattice Towers. PhD Thesis. Department of Civil Engineering and Applied Mechanics. McGill University. Montreal, Canada. Mohamed Abdel Halim Khedr, 1998.

Kotsubo, S., Takanishi, T., Uno, K., and Sonoda, T.(1985). 'Dynamic Tests and Seismic Analyses of High Steel Towers of Electrical Transmission Line', *Transactions of JSCE*, Vol. 15, 72-75.

Kulak, G.L.; Grodin, G.Y. Limit States Design in Structural Steel: Canadian Institute of Steel Construction. 9th Edition. 2010.

Lamontagne, M., Halchuk, S., Cassidy, J.F., and Rogers, G.C. (2008). "Significant Canadian earthquakes of the period 1600-2006." *Seismological Research Letters*, 79(2), 211-223.

Li, H., Wang, S., Lu, M., and Wang, Q. (1991). 'Seismic Calculations for Transmission Towers', *Lifeline Earthquake Engineering, Proceedings of the Third US Conference*, August 22-23, 275-284, ASCE, New York.

Li, H-N., Swarez L. E. and Singh, M. P. (1994). 'Seismic Effects on High-Voltage Transmission Tower and Cable Systems', *Proceedings of the Fifth US National Conference on Earthquake Engineering*, Earthquake Engineering Research Institute, Oakland, California, Vol. IV, 819-827.

Li, T. and Li, H. (2010) Parametric Study of Seismic Response of Transmission Tower-Line System Subjected to Multi-Component Earthquake Excitations. *Earth and Space* 2010: pp. 2925-2932.

Li, H., Shi, W., and Wang, S. (2003) Simplified Seismic Calculation Method for Coupled System of Transmission Lines and Their Supporting Tower. *Advancing Mitigation Technologies and Disaster Response for Lifeline Systems*: pp. 697-706.

Long, L.W. (1974). Analysis of Seismic Effects on Transmission Structures. IEEE Transactions on Power Apparatus and Systems, Vol. 93, N° 1, 248-254.

Madugula et. al. (2001). Dynamic response of lattice towers and guyed masts. Prepared by the Task Committee on the Dynamic Response of Lattice Towers of the Technical Committee on Special Structures and the Technical Administrative Committee on Metals of the Structural Engineering Institute of ASCE. Edited by Murty K. S. Madugula. ASCE. SEI – Structural Engineering Institute.

Mara, T. G. (2013). Capacity assessment of a transmission tower under wind loading. PhD Thesis. University of Western Ontario.

National Building Code of Canada – NBCC (2010). Volume 1. Issued by the Canadian Commission on Fire Codes. National Research Council of Canada.

National Building Code of Canada – NBCC (2010). User’s Guide. Structural Commentaries. Part 4 of Division B. Issued by the Canadian Commission on Fire Codes. National Research Council of Canada.

Natural Resources Canada (NRC). (2012). “Survey of commercial and institutional energy used buildings.” Detailed statistical report, Canada.

North American Electric Reliability Corporation – NERC (2013). Long-Term Reliability Assessment. December, 2013.

Pierre, J. R. (1995). Damage Caused by the Hanshin-Awaji (Kobe-Japan) Earthquake to the Electrical and Telecommunications Networks and its Impact on the Implementation of Emergency Measures, RE-GEN-95-40, Hydro-Québec.

Riley, M. J., L. Kempner, and W. H. Mueller. (2005). A Comparison of Seismic (Dynamic) and Static Load Cases for High-Voltage Electric Transmission Line Structures. Proceedings of the Earthquake Engineering Research Institute. San Francisco. November, 2005.

Serban, M. O. (2015). Improving the Earthquake Resilience of Existing Multi-Storey Concentrically Braced Frames Office Buildings in Moderate to High Seismic Zones. Master of Applied Sciences Thesis. Department of Building, Civil and Environmental Engineering. Concordia University. Montreal, Quebec, Canada.

Shears, M. (1968). Static and dynamic behavior of guy masts. Report N° 68-6, Structural Engineering Lab., University of California, Berkeley, 167 pp.

Simiu, E.; Scanlan, R.H. (1996). Wind Effects on Structures. Fundamentals and Applications to Design. 3<sup>rd</sup> edition. John Wiley & Sons Inc., New York.

Starossek, U. (1991). Dynamic stiffness matrix of sagging cable. *Journal of engineering mechanics*, ASCE, 117(12), 2815-2829.

Statistics Canada (2013). *Installed generating capacity, by class of electricity producer, annual*, Ottawa: Statistics Canada, retrieved 2013-01-02.

Vellozzi, J.; Cohen, E. *Dynamic Response of Tall Flexible Structures to Wind Loading*. Proceedings; Technical meeting concerning the wind loads on buildings and structures. Building Science series BSS 30. National Bureau of Standards, Washington, DC, 1970, pp. 115-128.

Yasui, H., Marukawa, H., Momomura, Y., Ohkuma, T. (1999). Analytical study of wind-induced vibration of power transmission towers. *Journal of Wind Engineering and Industrial Aerodynamics* 83 (1999) 431-441. Elsevier Sciences Ltd.

Y. H. Lei and Y. L. Chien, "Seismic analysis of transmission towers under various line configurations," *Structural Engineering and Mechanics*, vol. 31, no. 3, pp. 241–264, 2009.

**APPENDIX I**  
**EARTHQUAKE RECORDS AND RESPONSE SPECTRA**

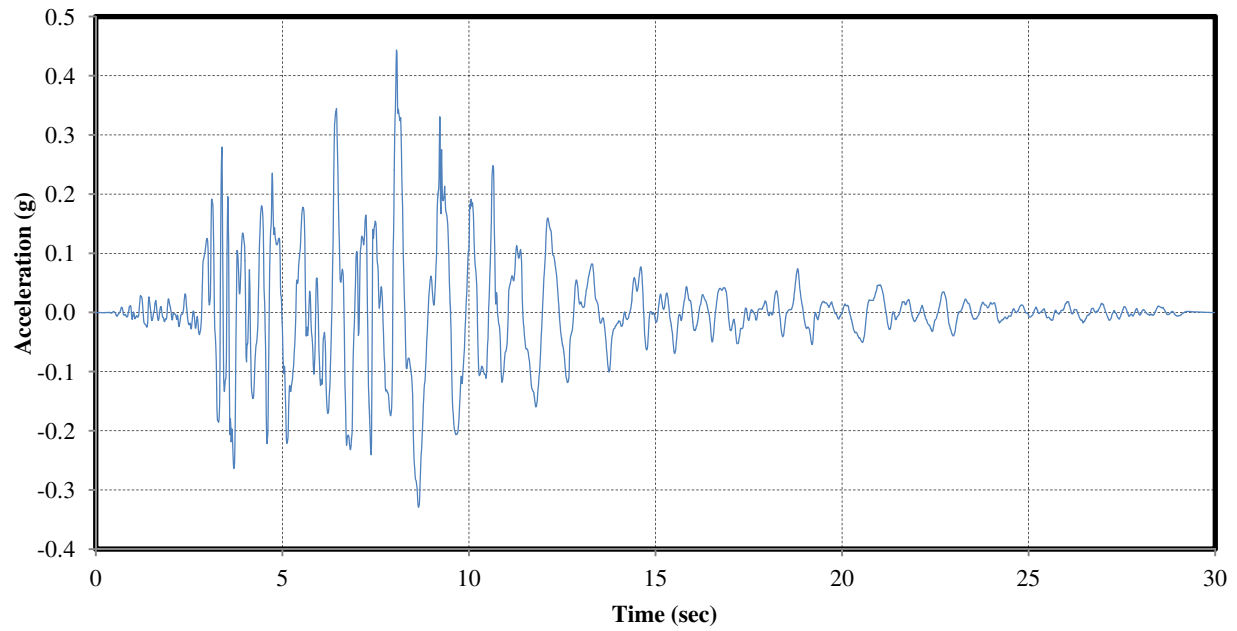


**Figure I.1 NGA n° 953. Accelerogram. Horizontal component.**

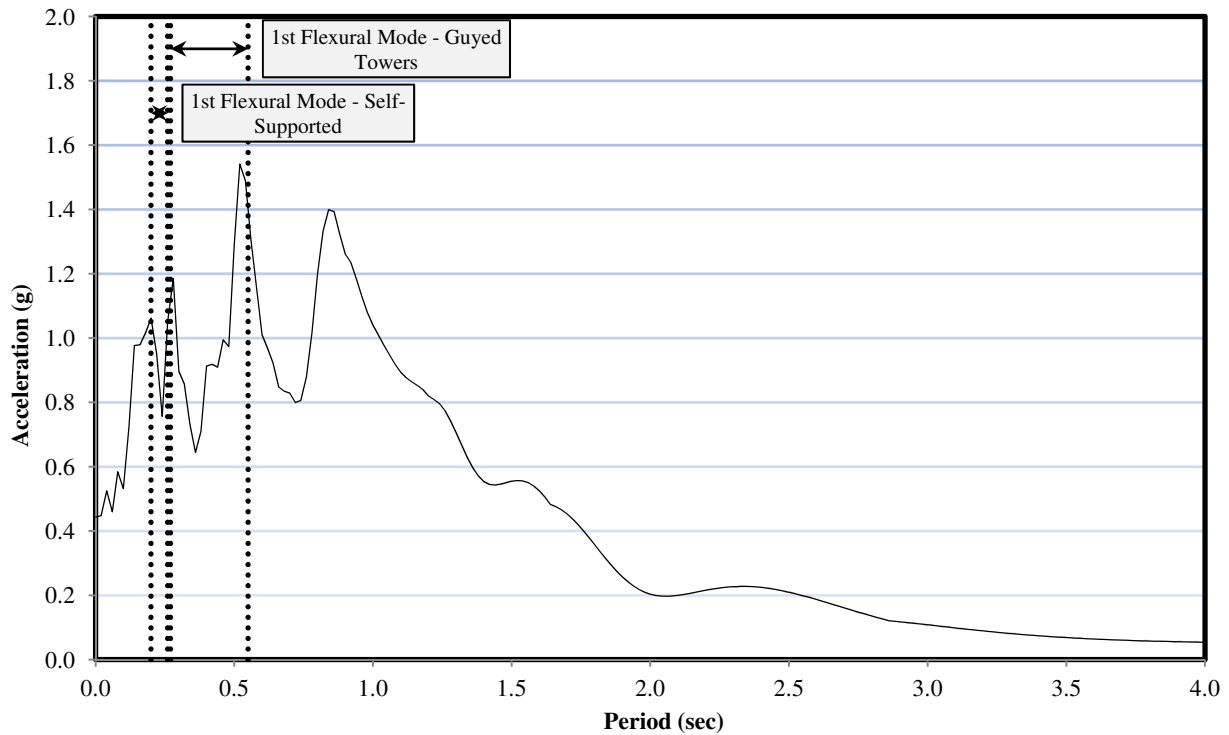


**Figure I.2 NGA n° 953. 5% damping response spectra. Horizontal component.**

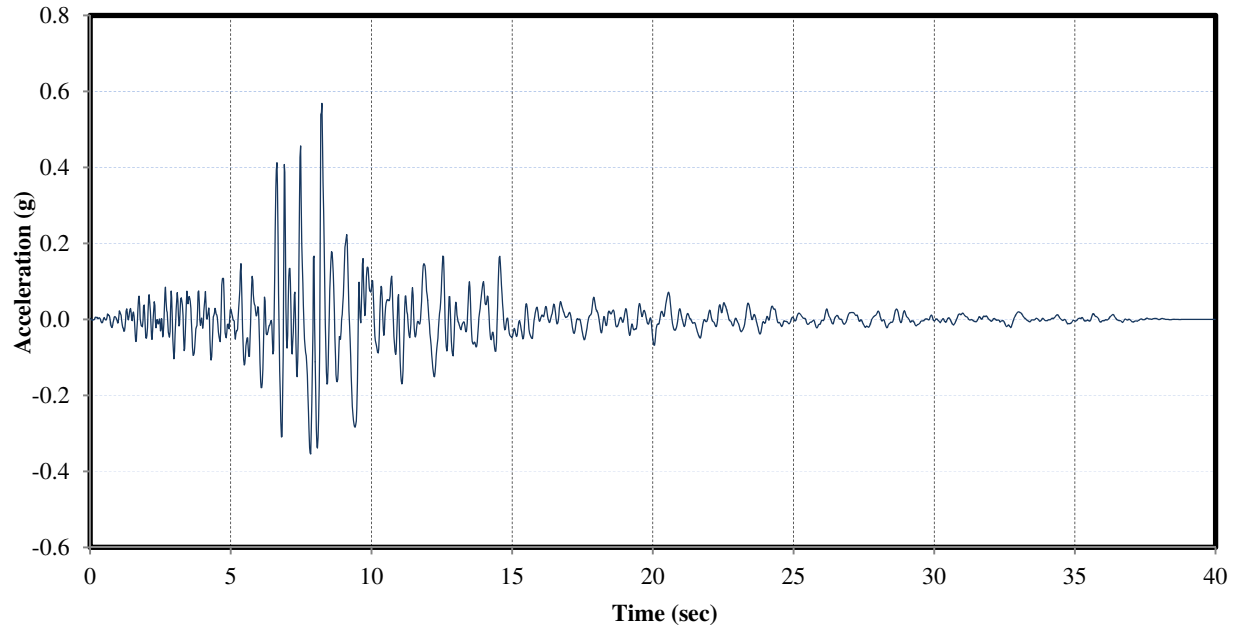


**Figure I.3 NGA n° 963. Accelerogram. Horizontal component.**

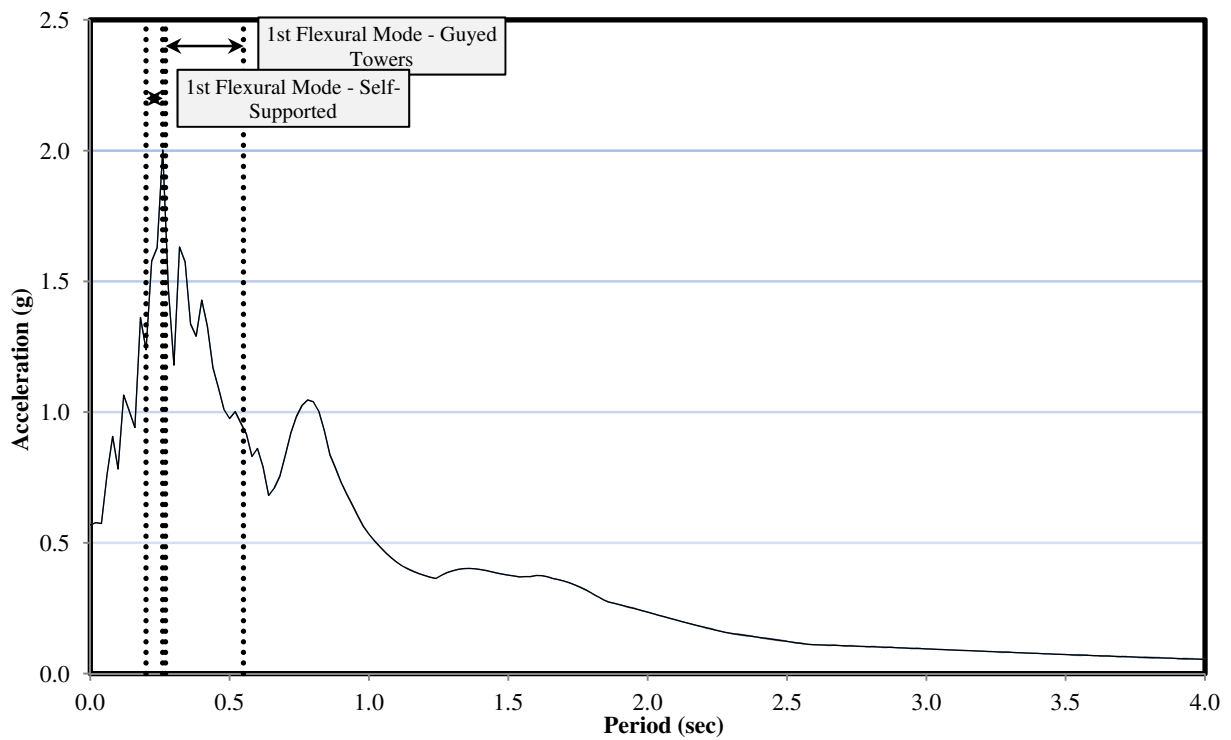


**Figure I.4 NGA n° 963. 5% damping response spectra. Horizontal component.**

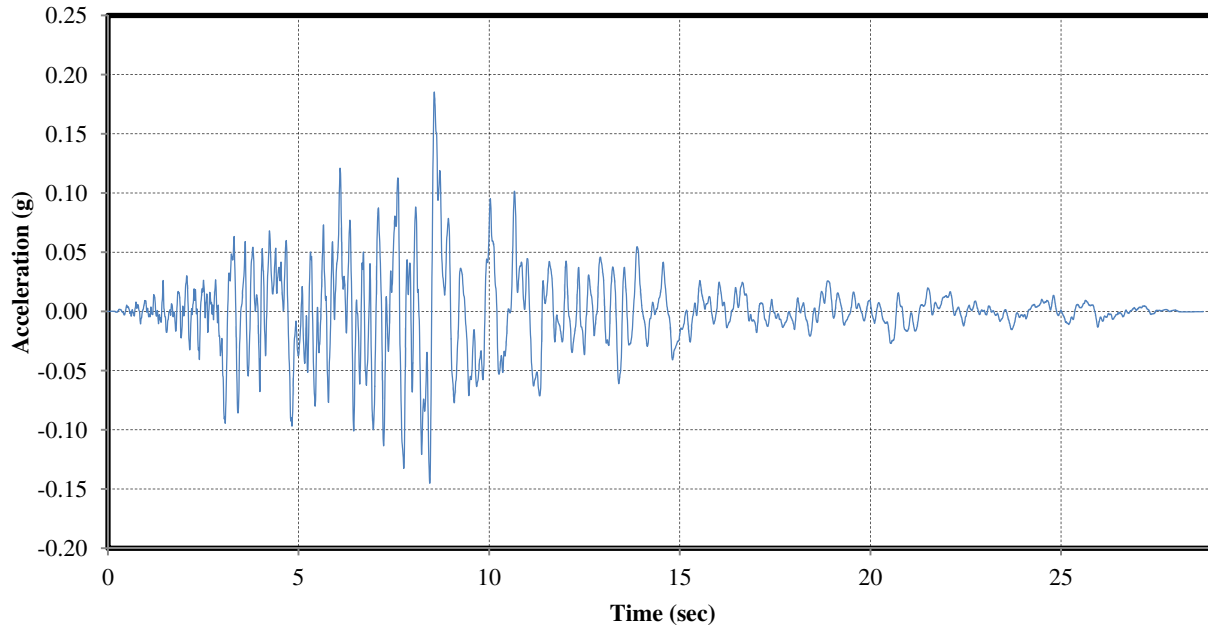


**Figure I.5 NGA n° 986. Accelerogram. Horizontal component.**

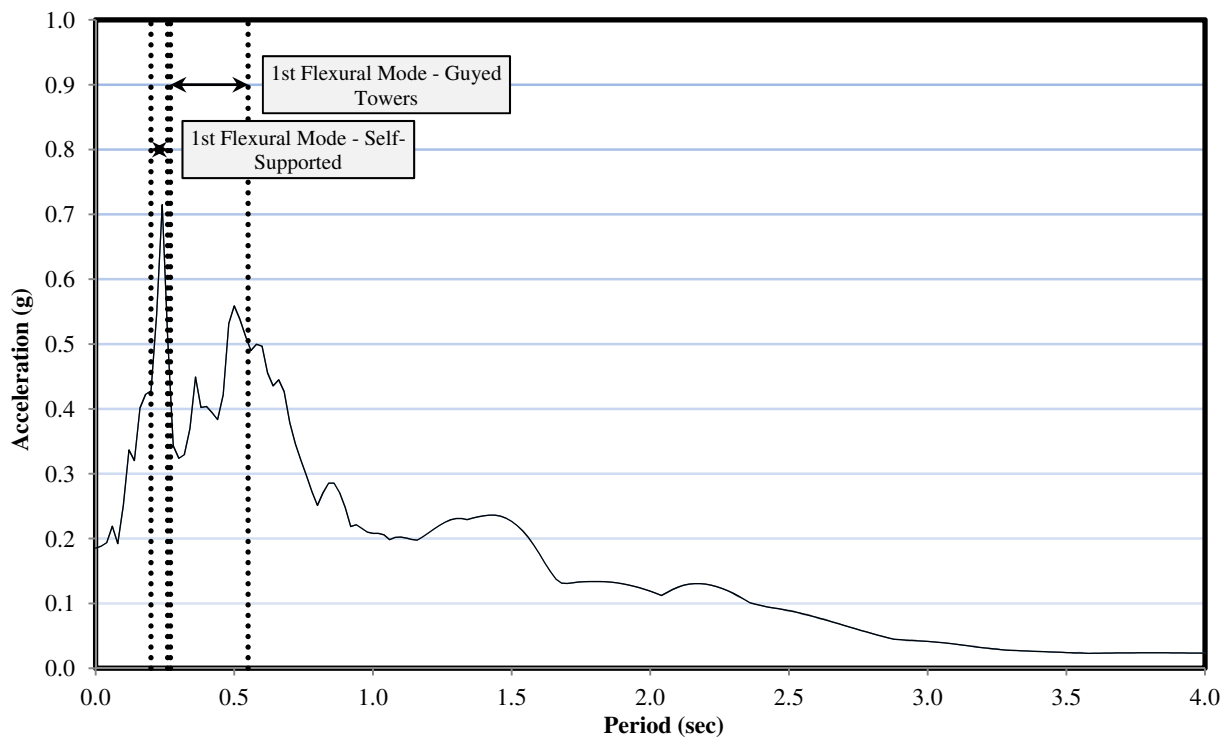


**Figure I.6 NGA n° 986. 5% damping response spectra. Horizontal component.**

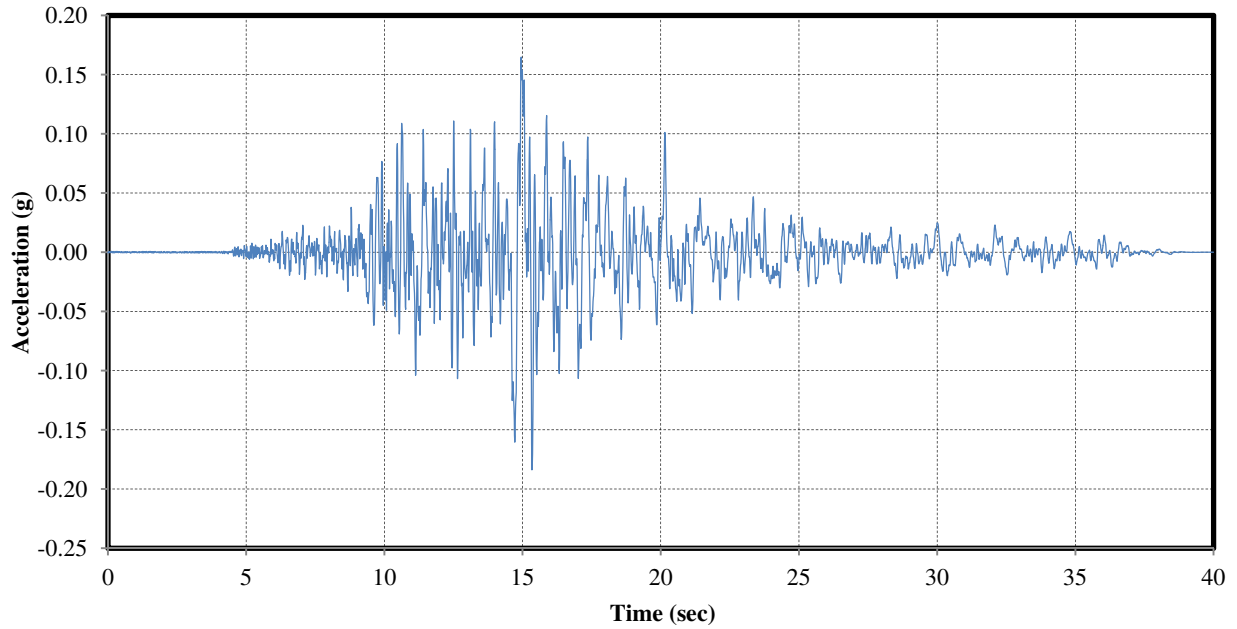


**Figure I.7 NGA n° 1005. Accelerogram. Horizontal component.**

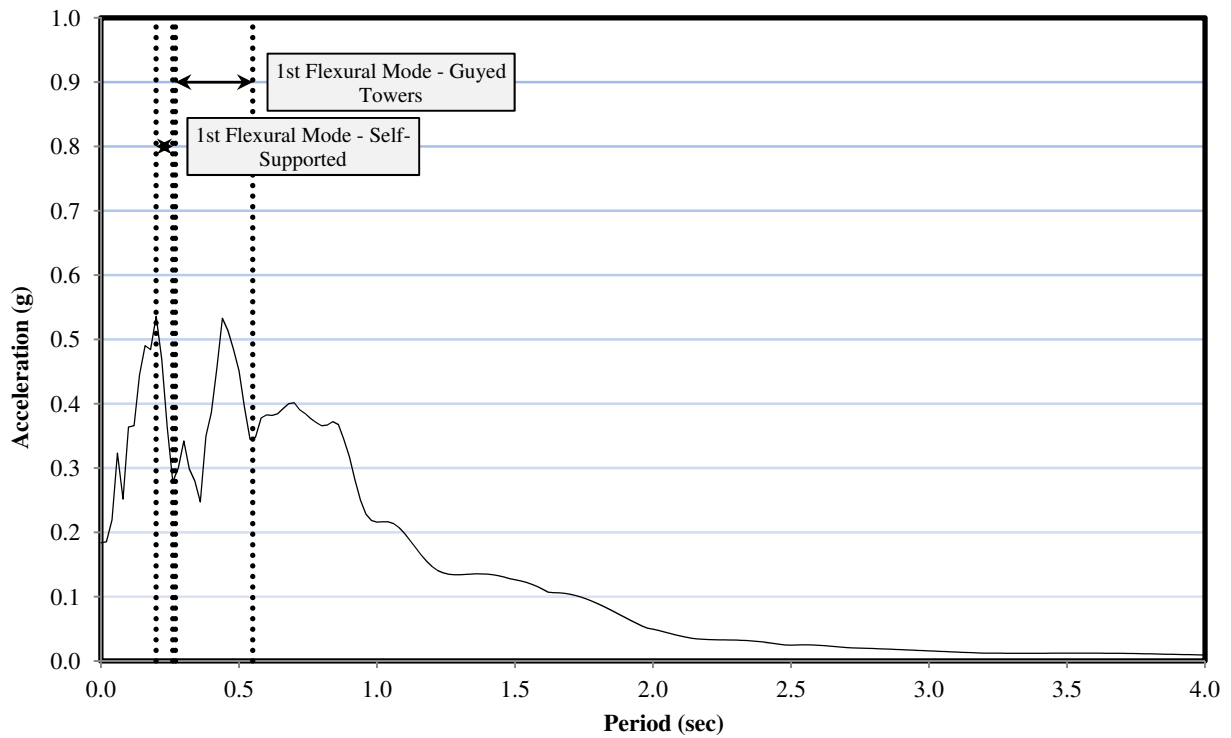


**Figure I.8 NGA n° 1005. 5% damping response spectra. Horizontal component.**

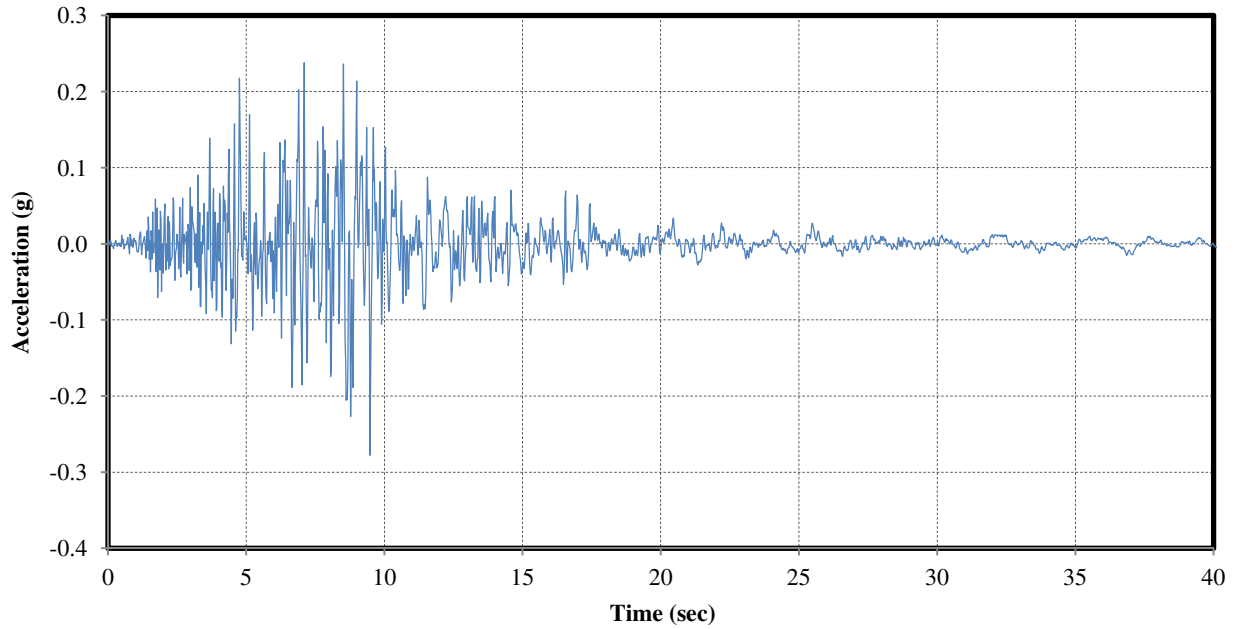


**Figure I.9 NGA n° 1006. Accelerogram. Horizontal component.**

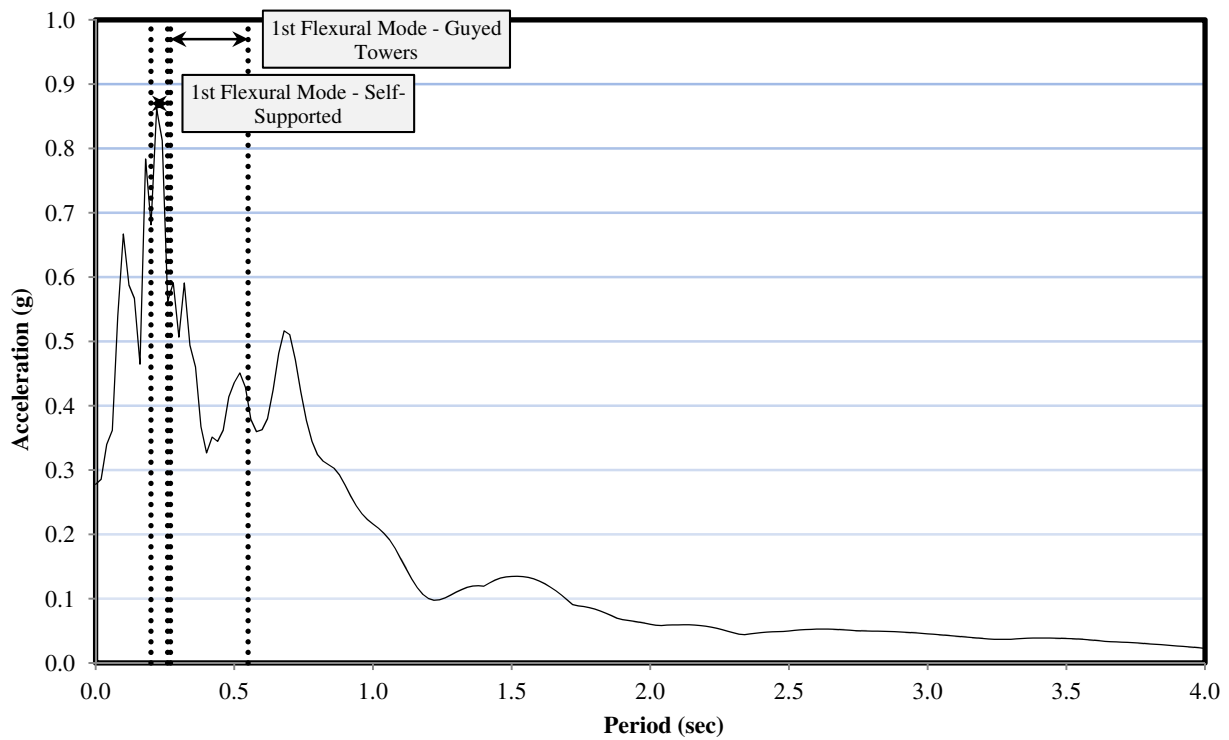


**Figure I.10 NGA n° 1006. 5% damping response spectra. Horizontal component.**

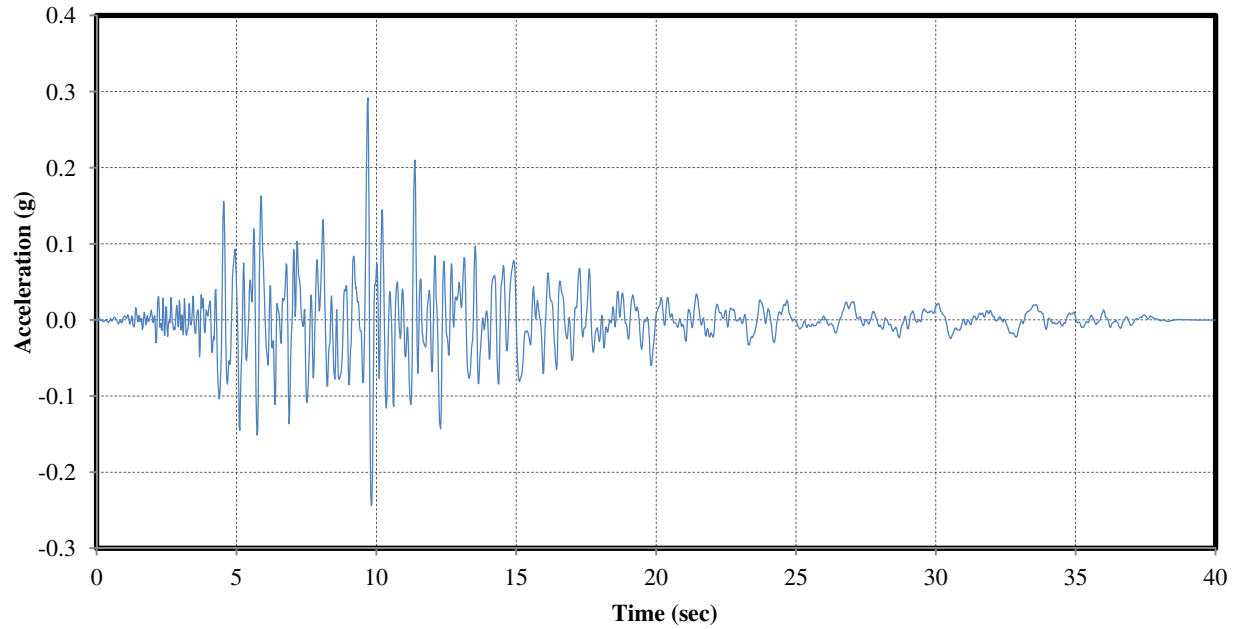


**Figure I.11 NGA n° 1039. Accelerogram. Horizontal component.**

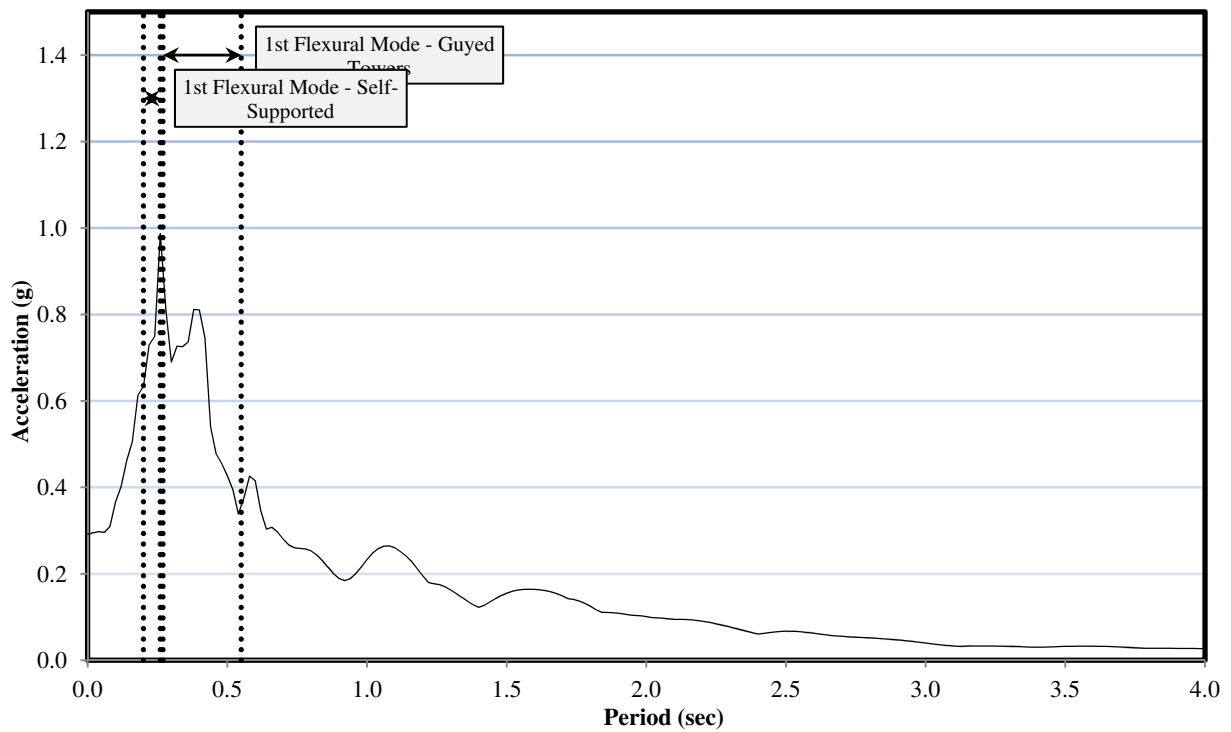


**Figure I.12 NGA n° 1039. 5% damping response spectra. Horizontal component.**

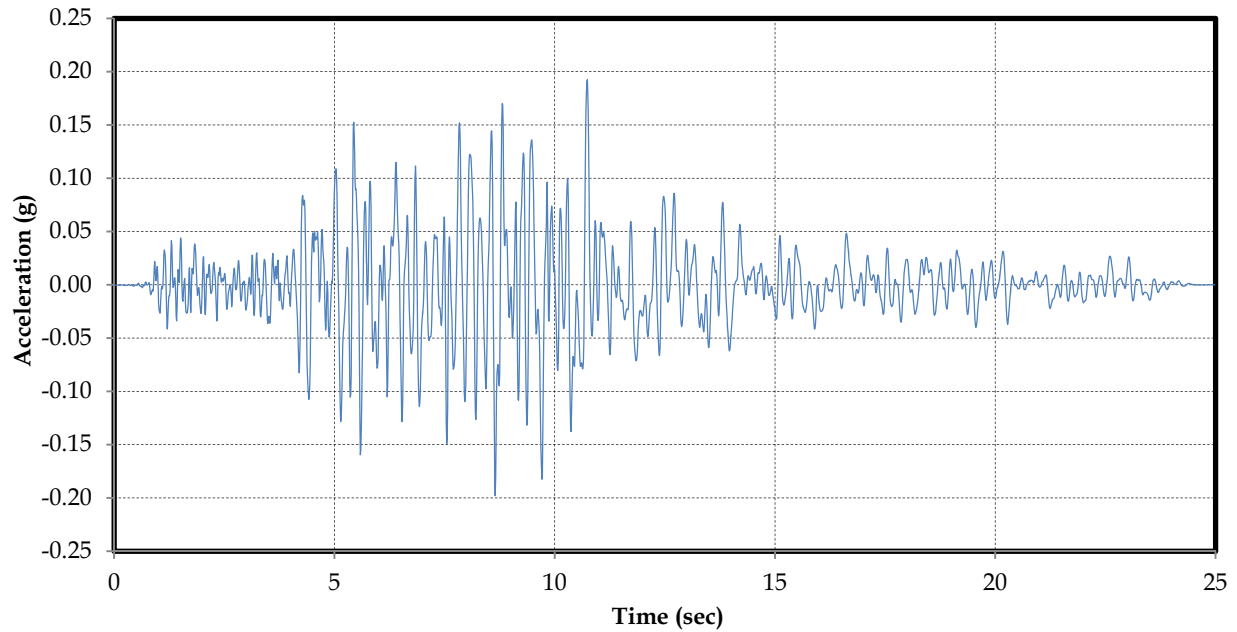


**Figure I.13 NGA n° 1049. Accelerogram. Horizontal component.**

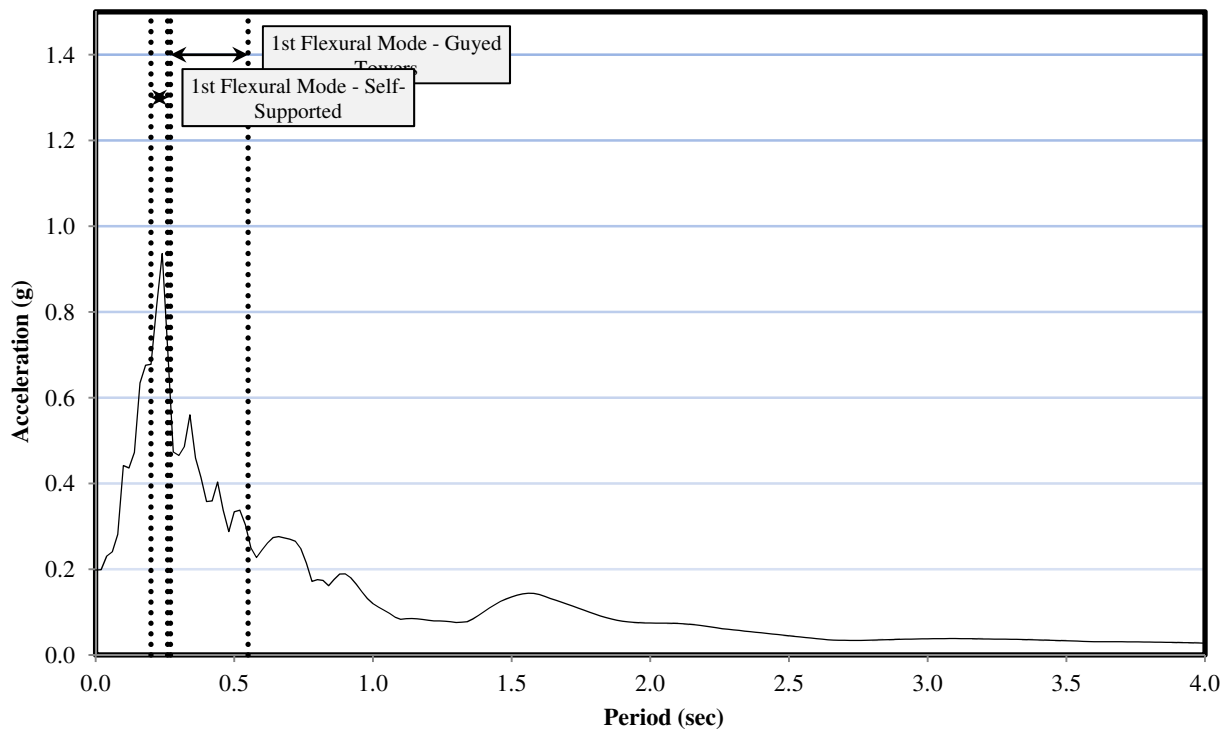


**Figure I.14 NGA n° 1049. 5% damping response spectra. Horizontal component.**

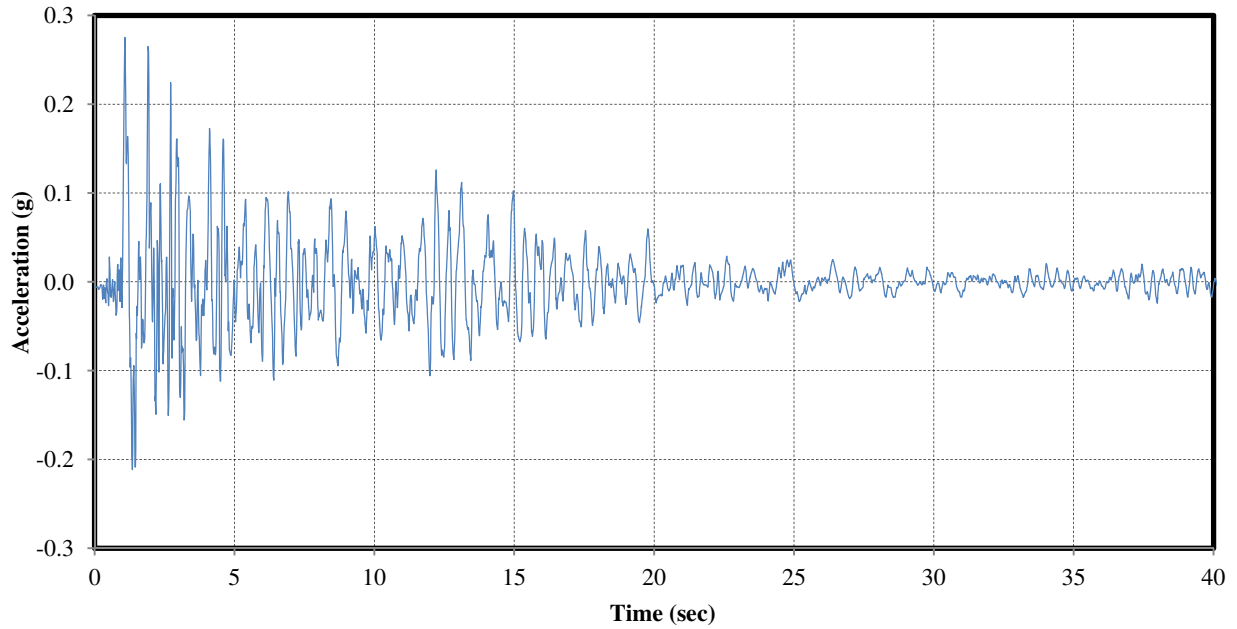


**Figure I.15 NGA n° 57. Accelerogram. Horizontal component.**

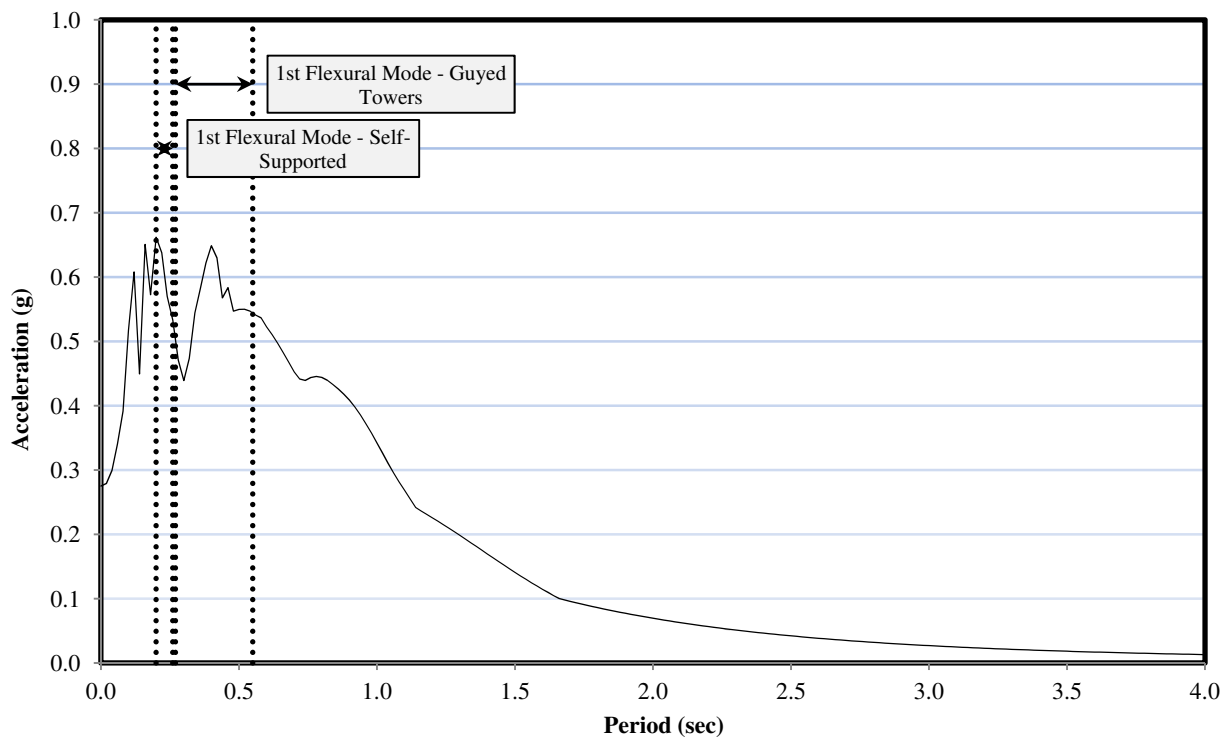


**Figure I.16 NGA n° 57. 5% damping response spectra. Horizontal component.**

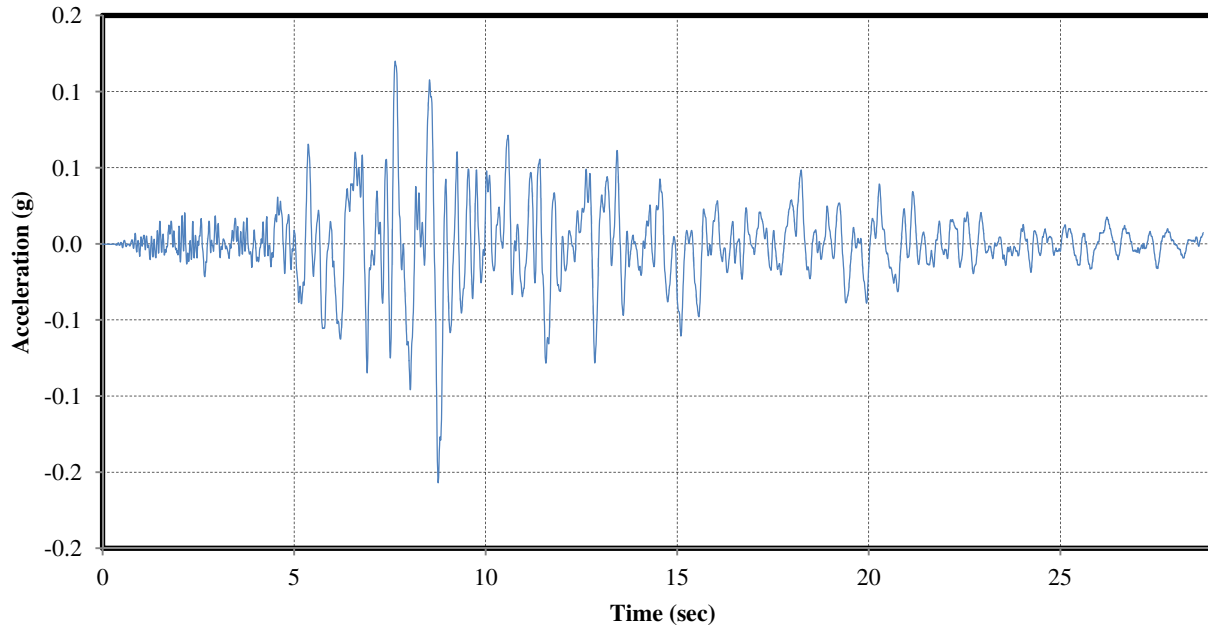


**Figure I.17 NGA n° 735. Accelerogram. Horizontal component.**

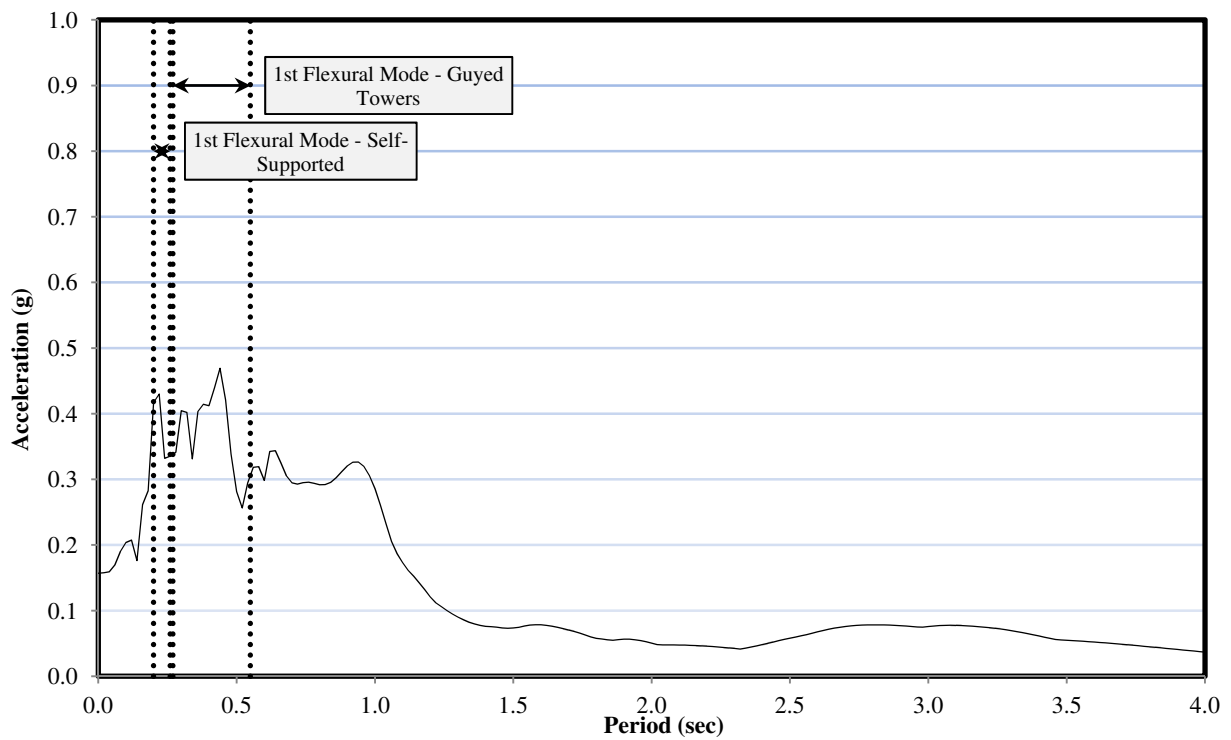


**Figure I.18 NGA n° 735. 5% damping response spectra. Horizontal component.**

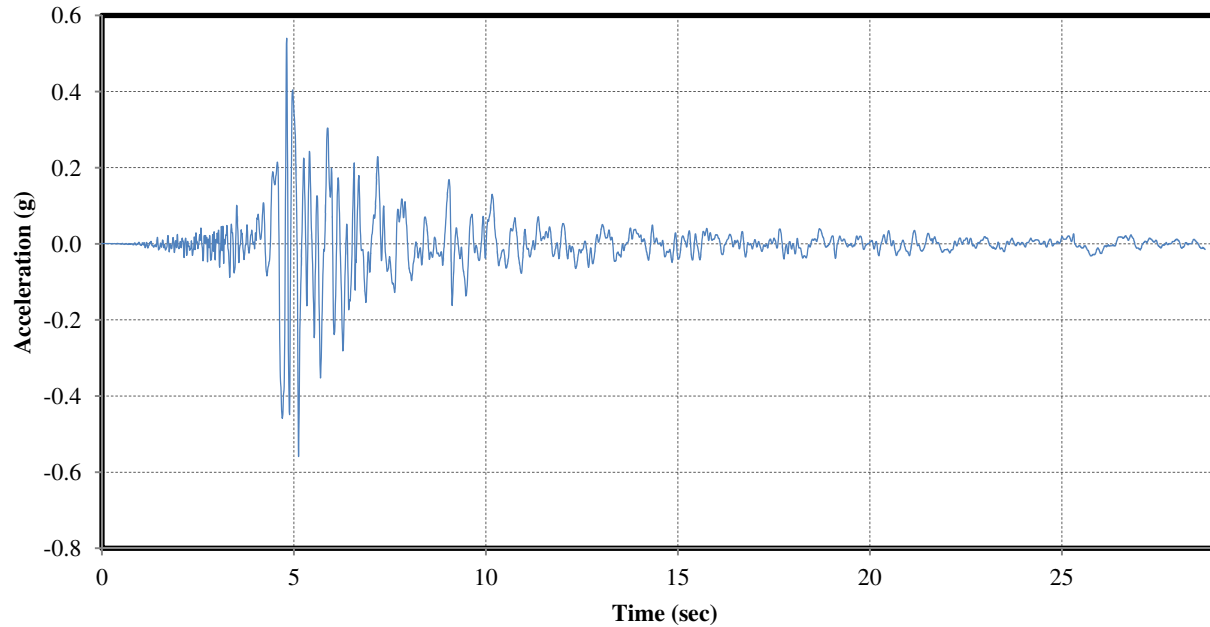


**Figure I.19 NGA n° 767. Accelerogram. Horizontal component.**

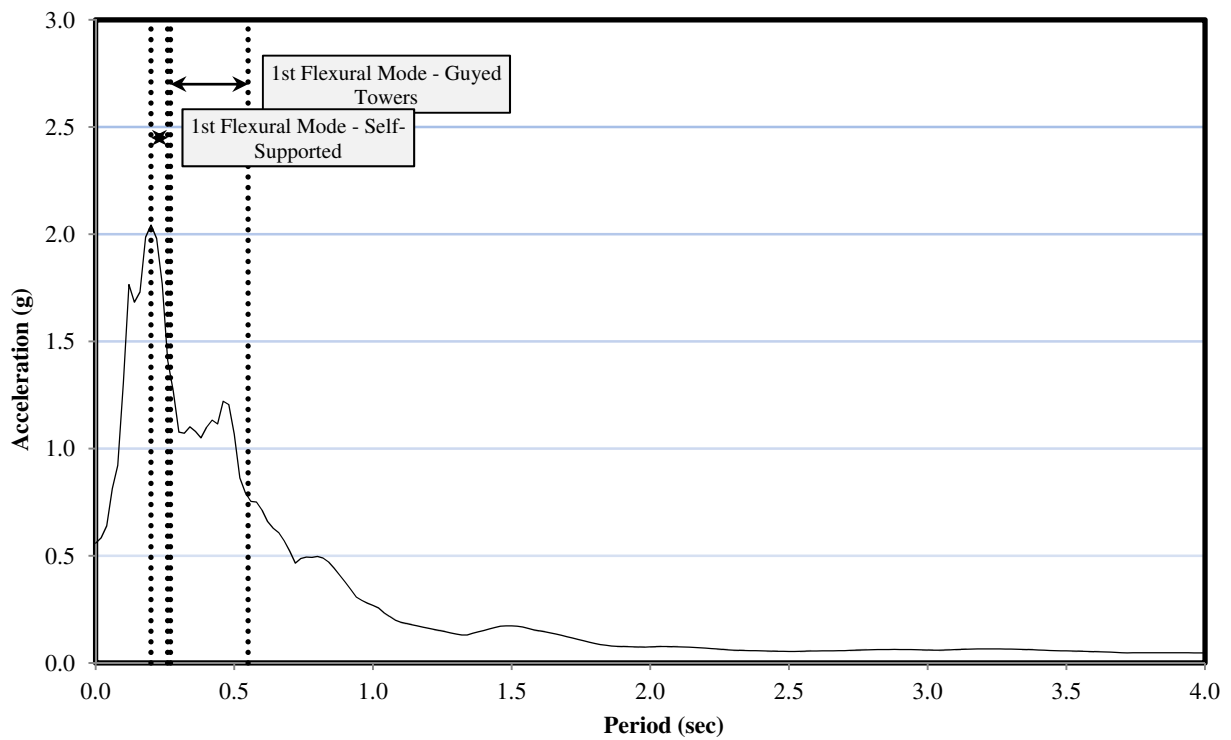


**Figure I.20 NGA n° 767. 5% damping response spectra. Horizontal component.**

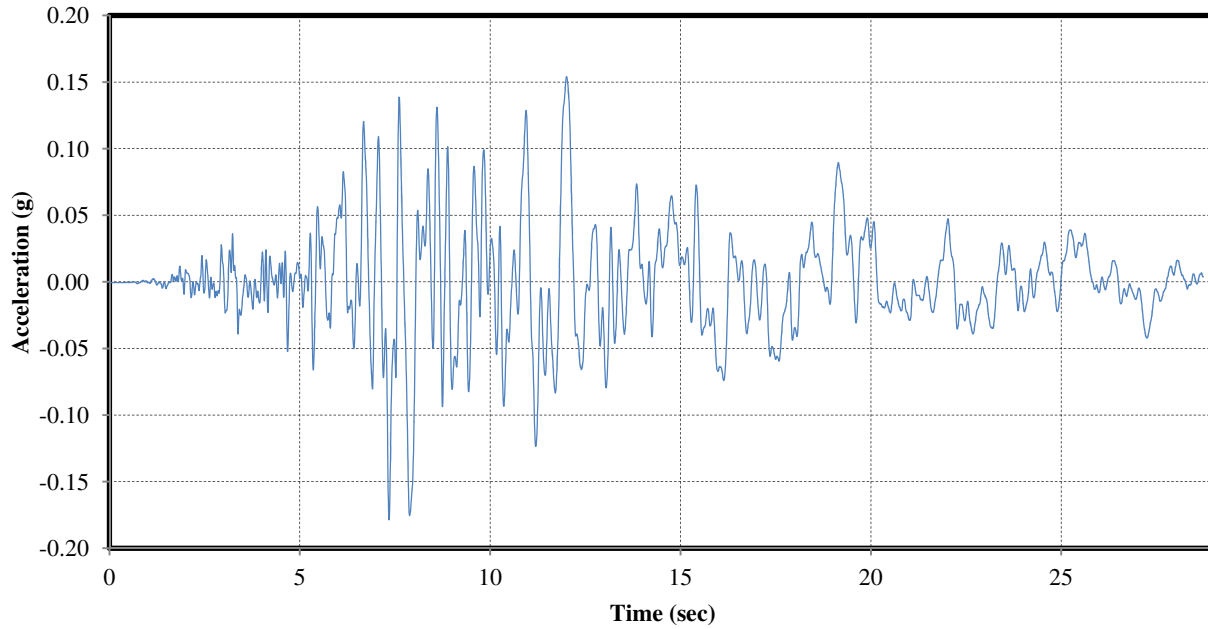


**Figure I.21 NGA n° 776. Accelerogram. Horizontal component.**

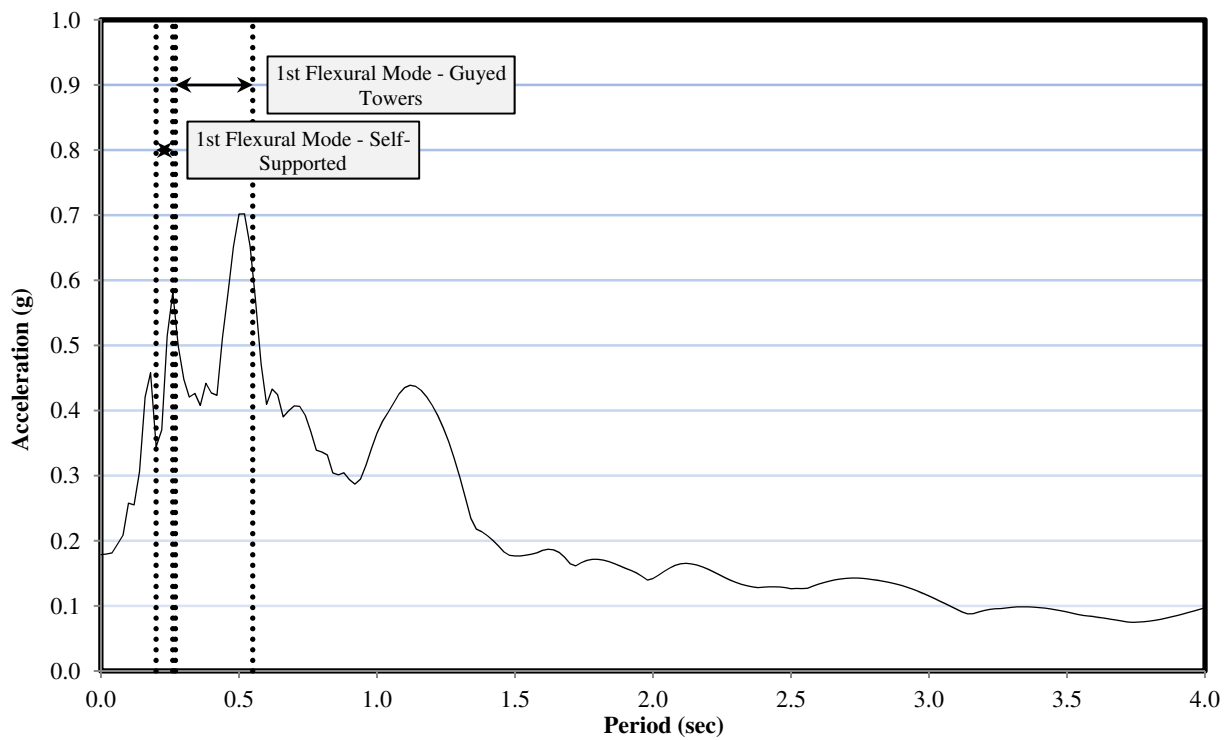


**Figure I.22 NGA n° 776. 5% damping response spectra. Horizontal component.**

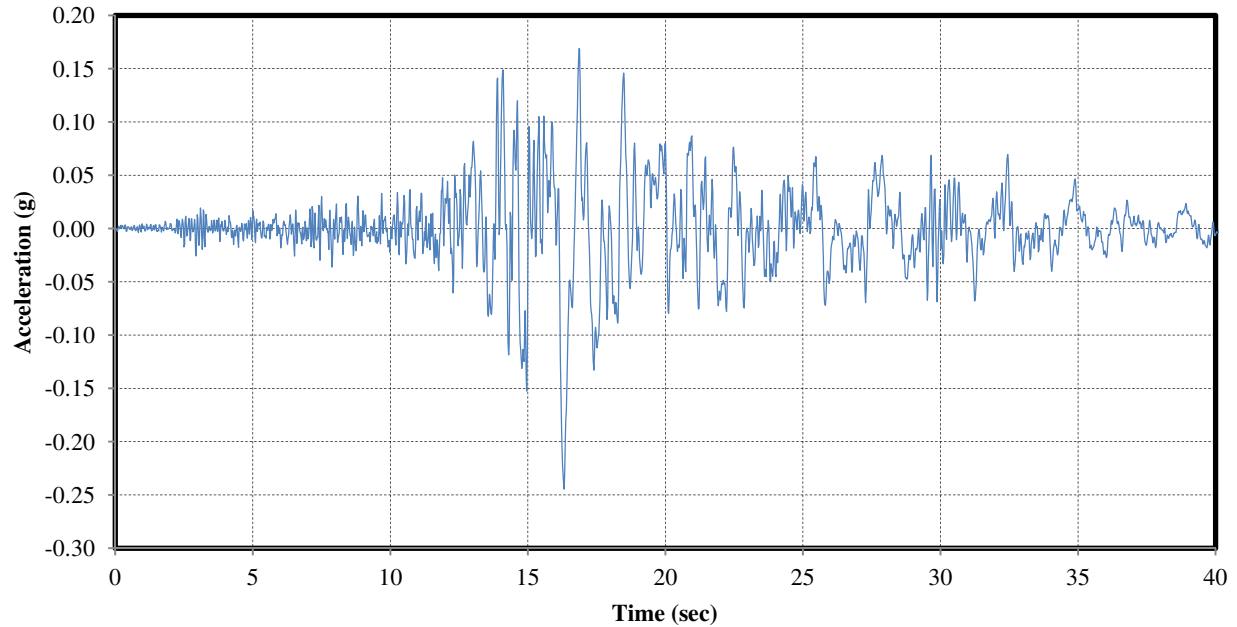


**Figure I.23 NGA n° 900. Accelerogram. Horizontal component.**

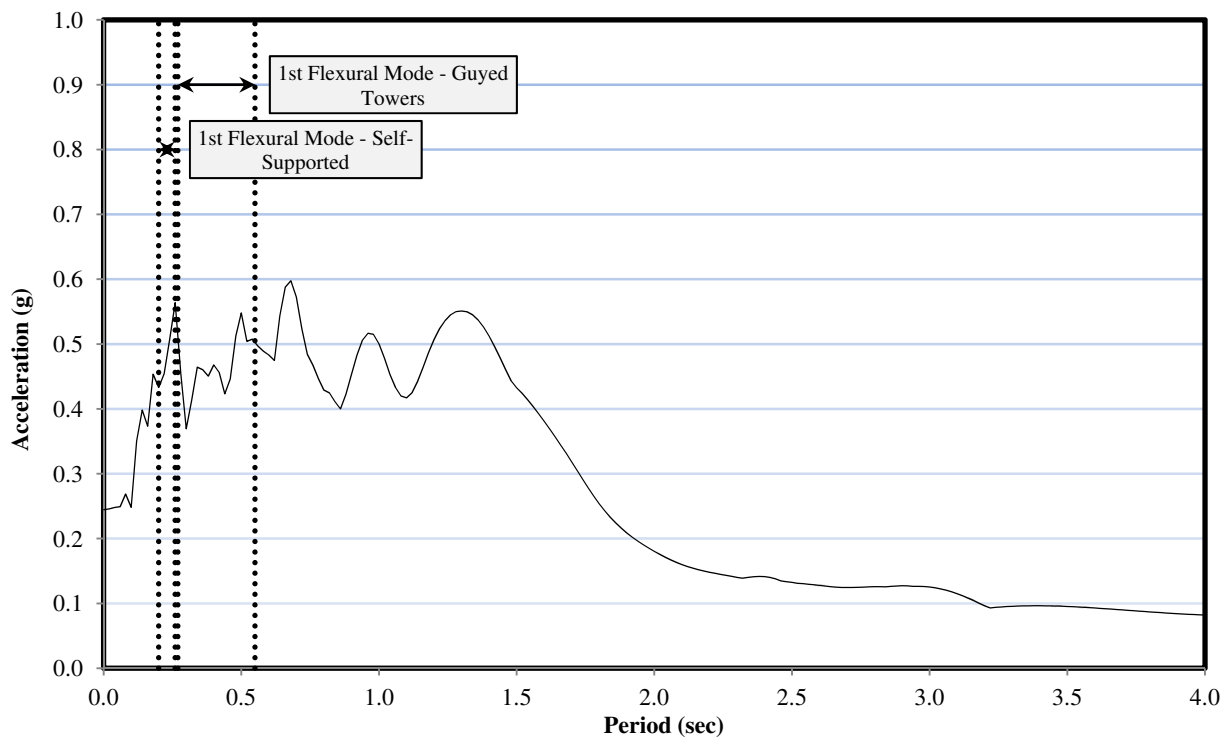


**Figure I.24 NGA n° 900. 5% damping response spectra. Horizontal component.**

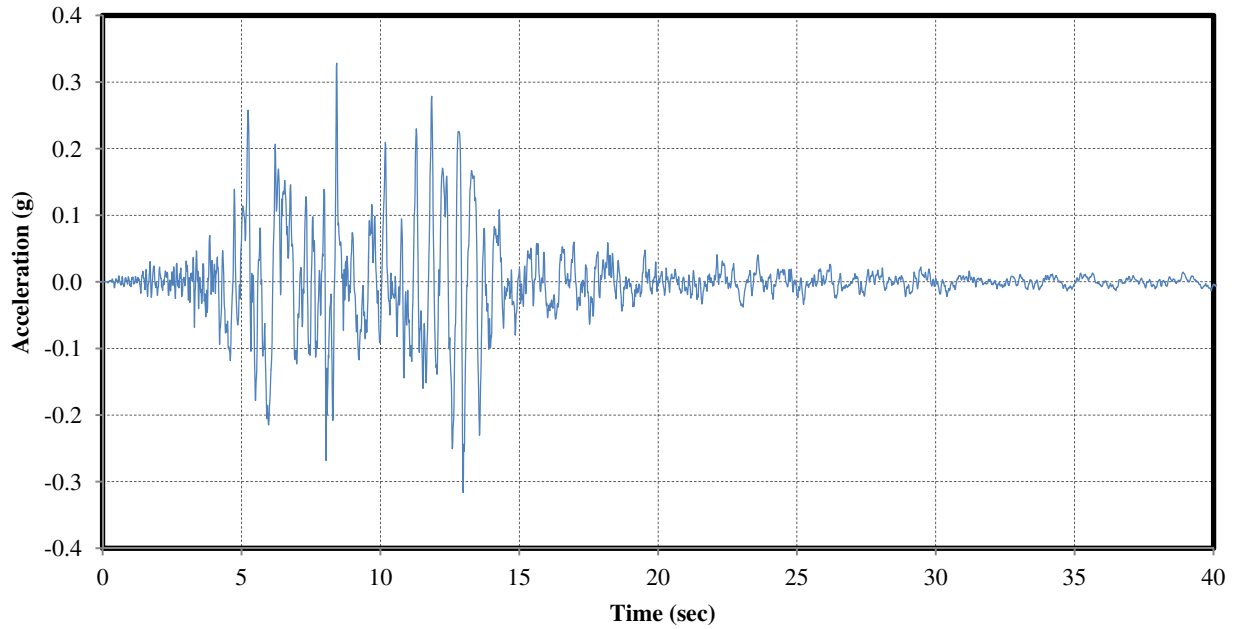


**Figure I.25 NGA n° 1787. Accelerogram. Horizontal component.**

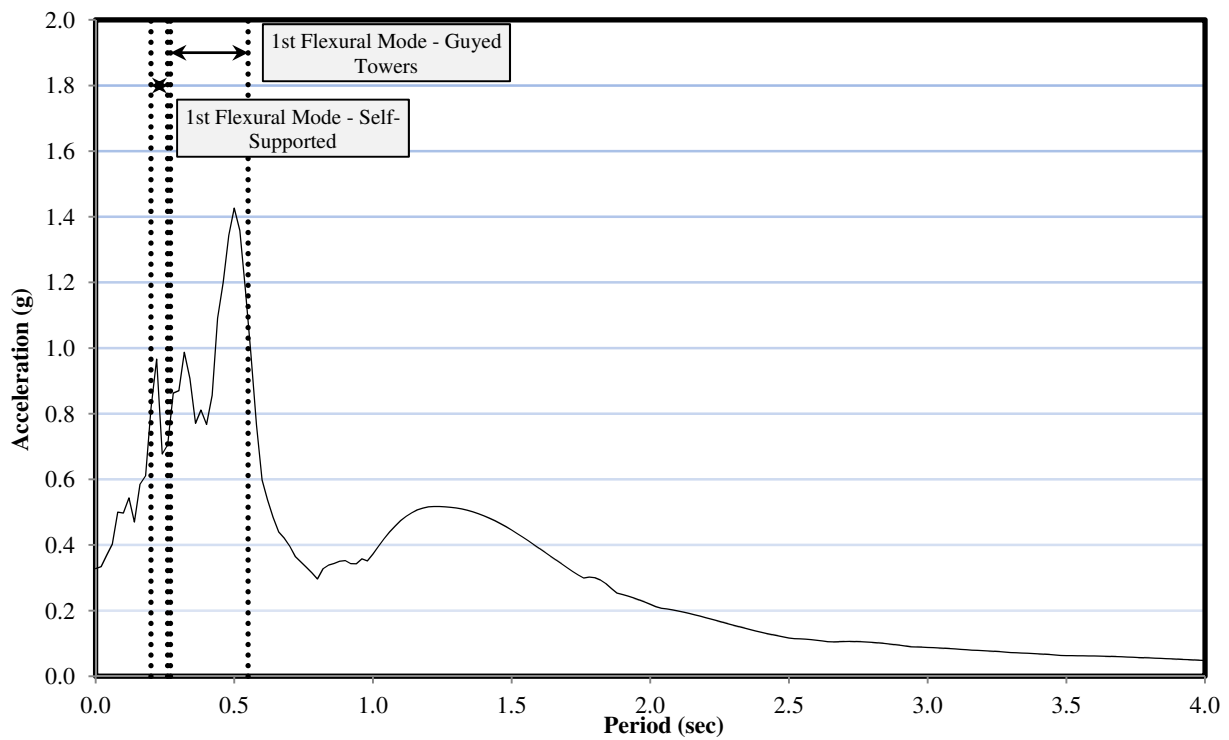


**Figure I.26 NGA n° 1787. 5% damping response spectra. Horizontal component.**

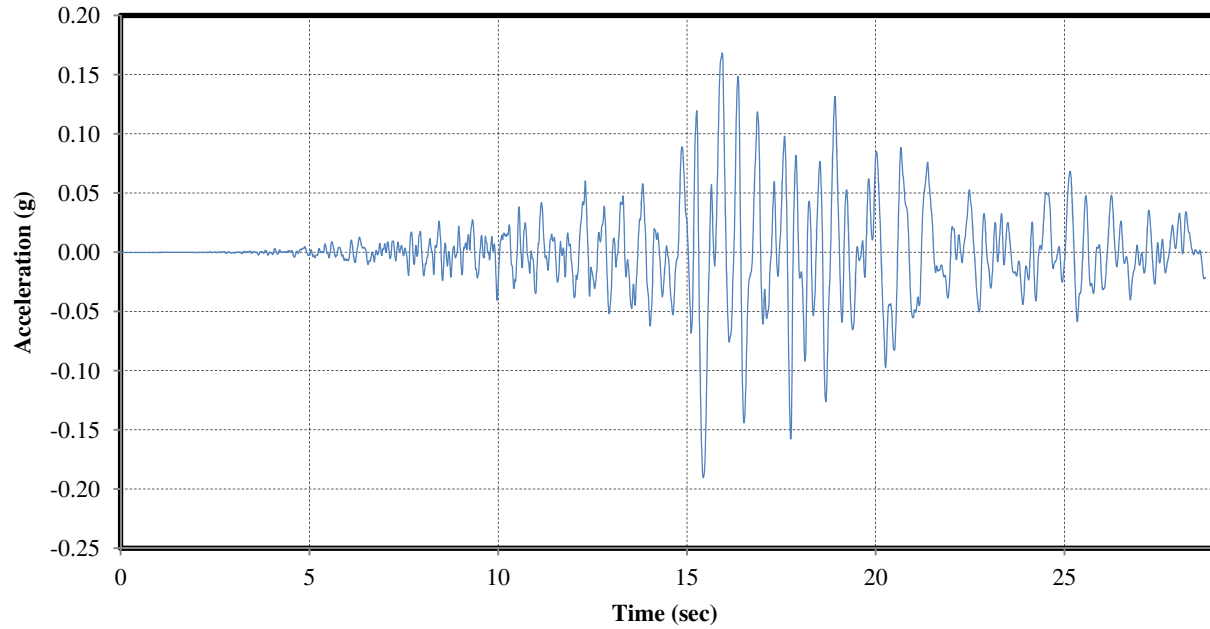


**Figure I.27 NGA n° 1794. Accelerogram. Horizontal component.**

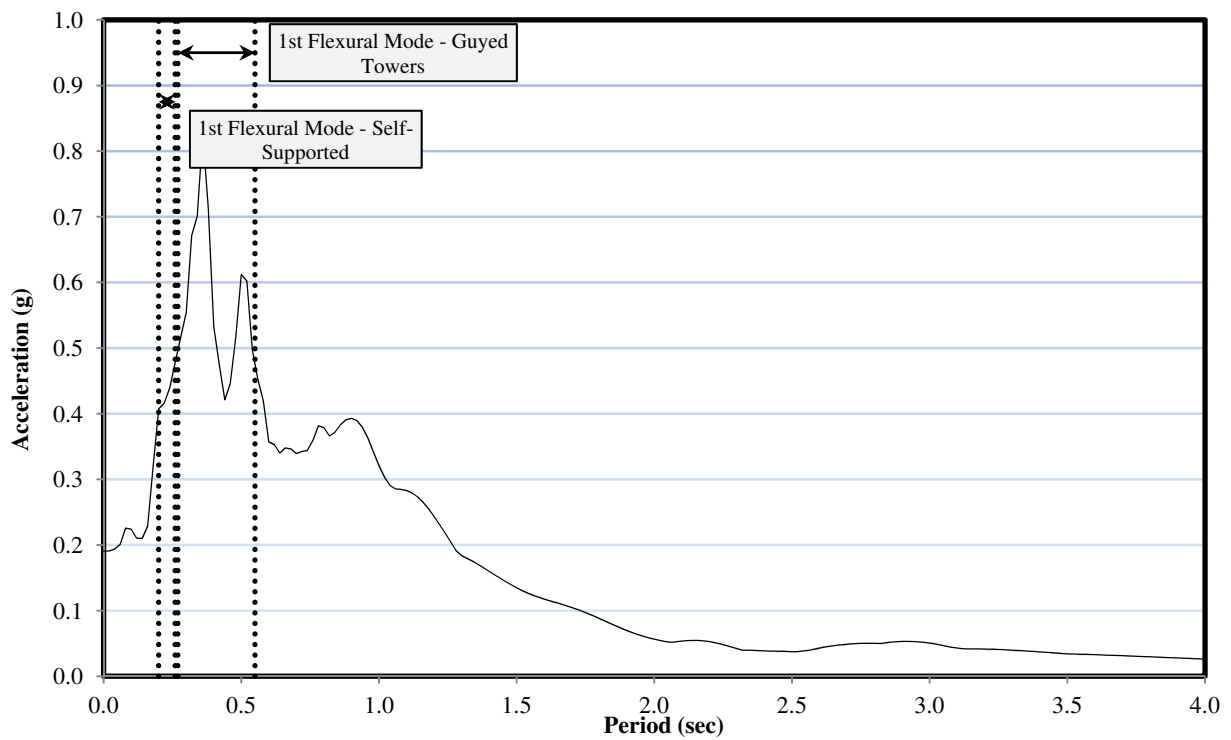


**Figure I.28 NGA n° 1794. 5% damping response spectra. Horizontal component.**

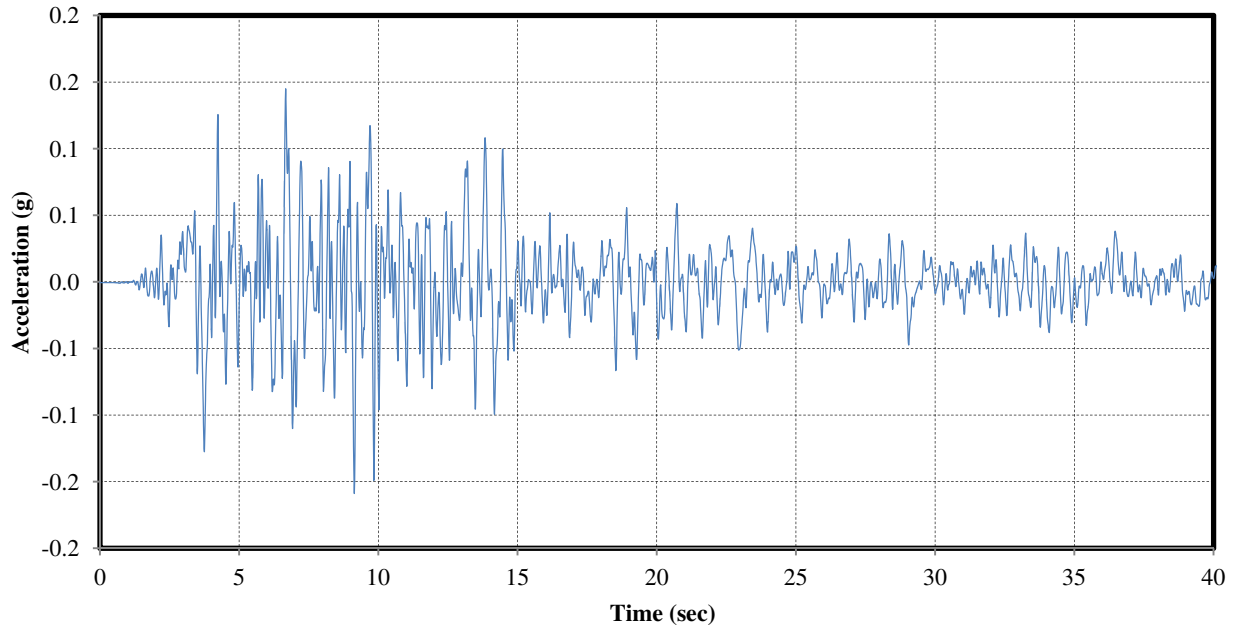


**Figure I.29 NGA n° 15. Accelerogram. Horizontal component.**

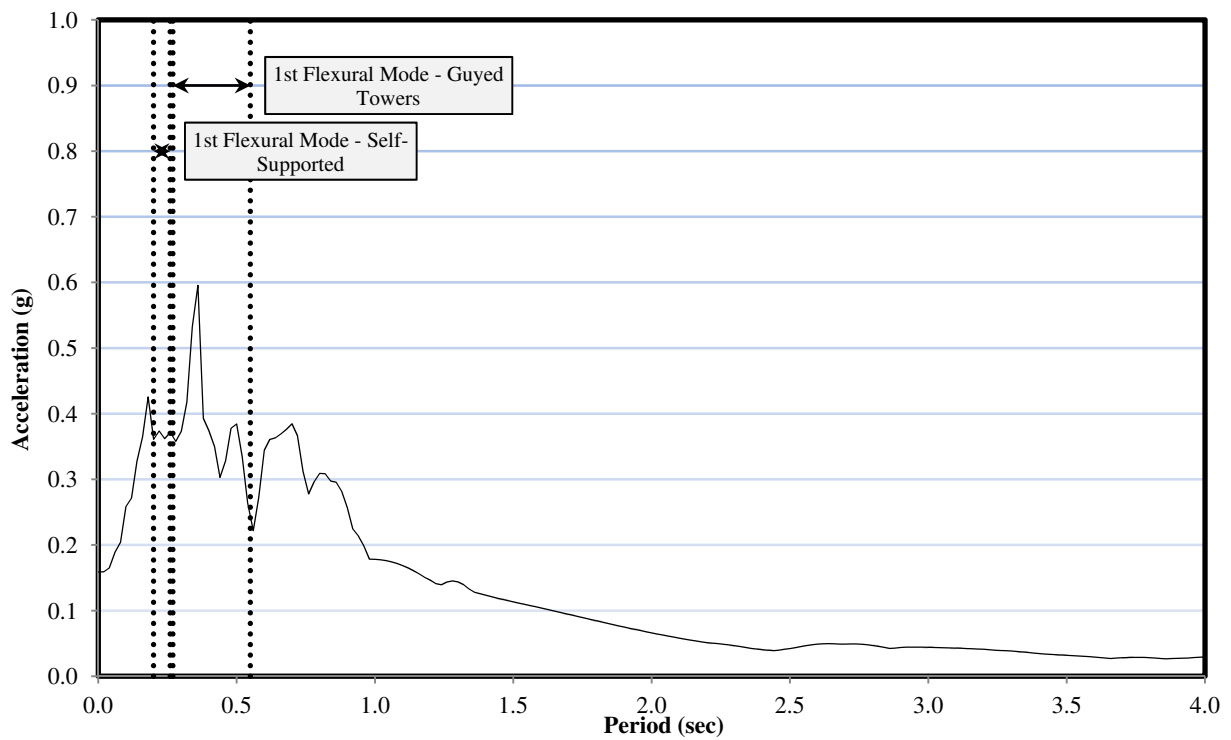


**Figure I.30 NGA n° 15. 5% damping response spectra. Horizontal component.**

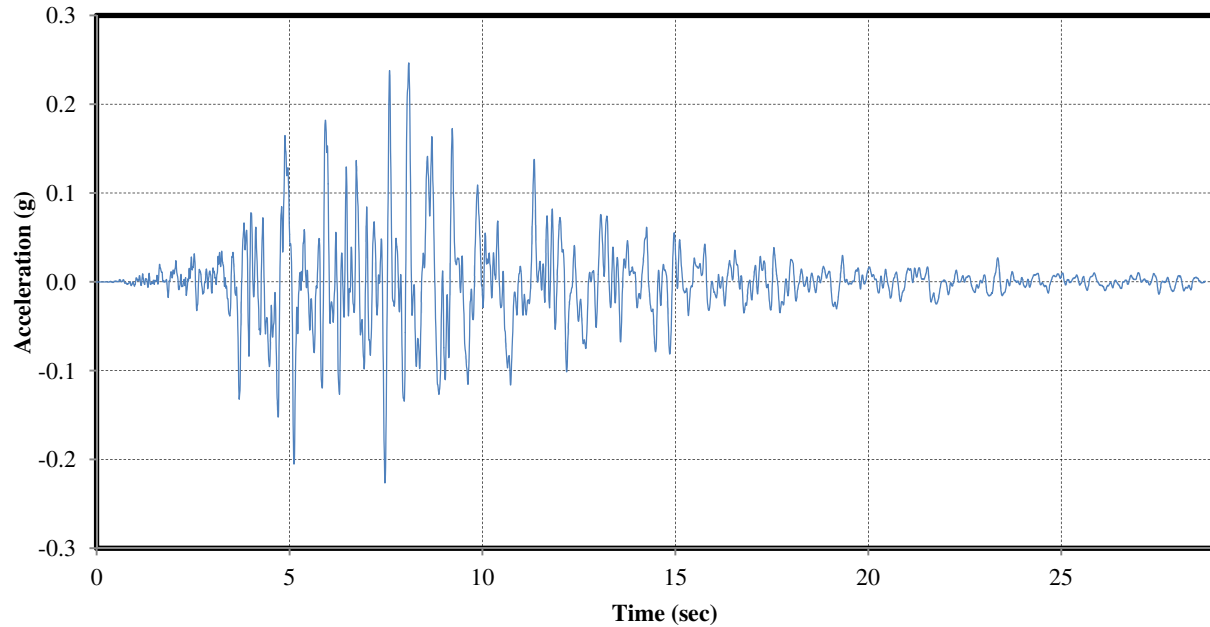


**Figure I.31 NGA n° 739. Accelerogram. Horizontal component.**

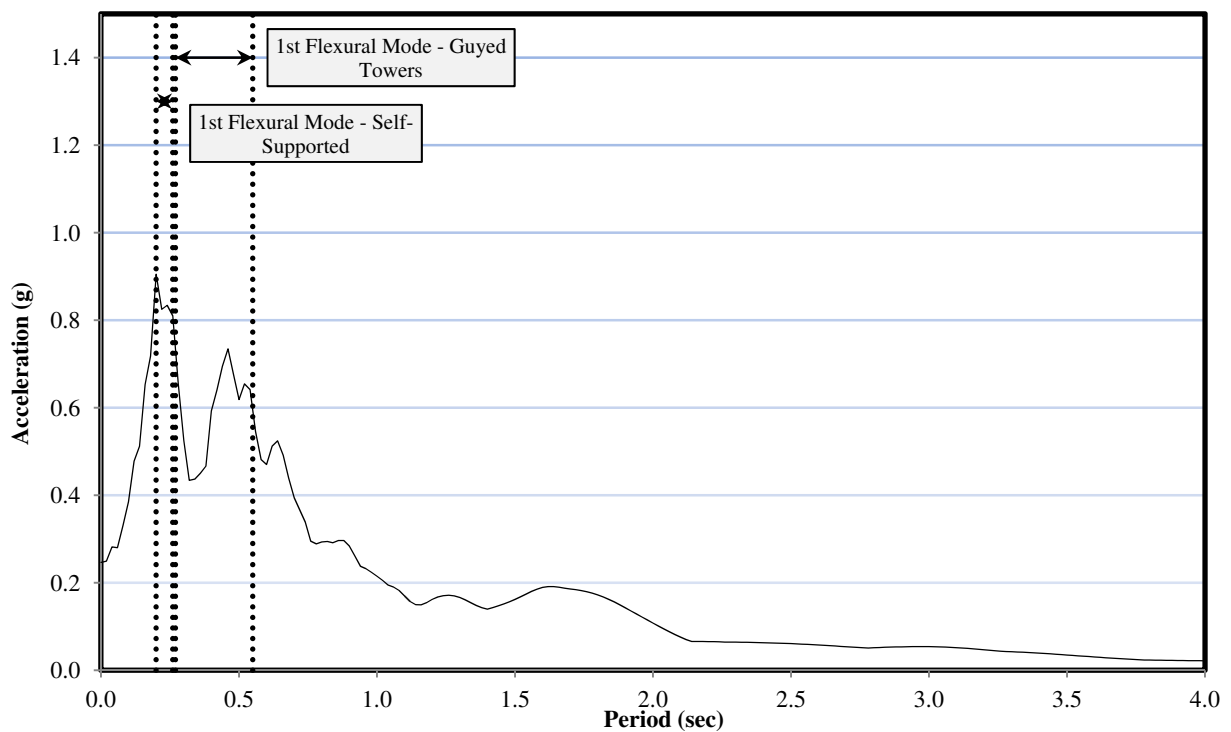


**Figure I.32 NGA n° 739. 5% damping response spectra. Horizontal component.**

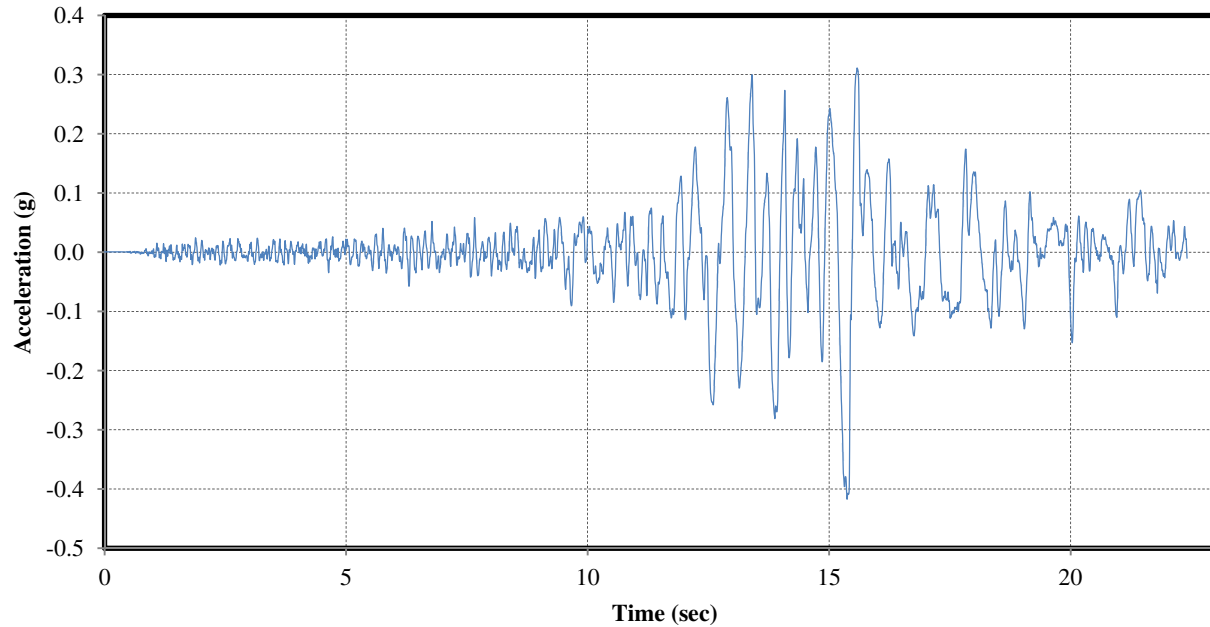


**Figure I.33 NGA n° 848. Accelerogram. Horizontal component.**

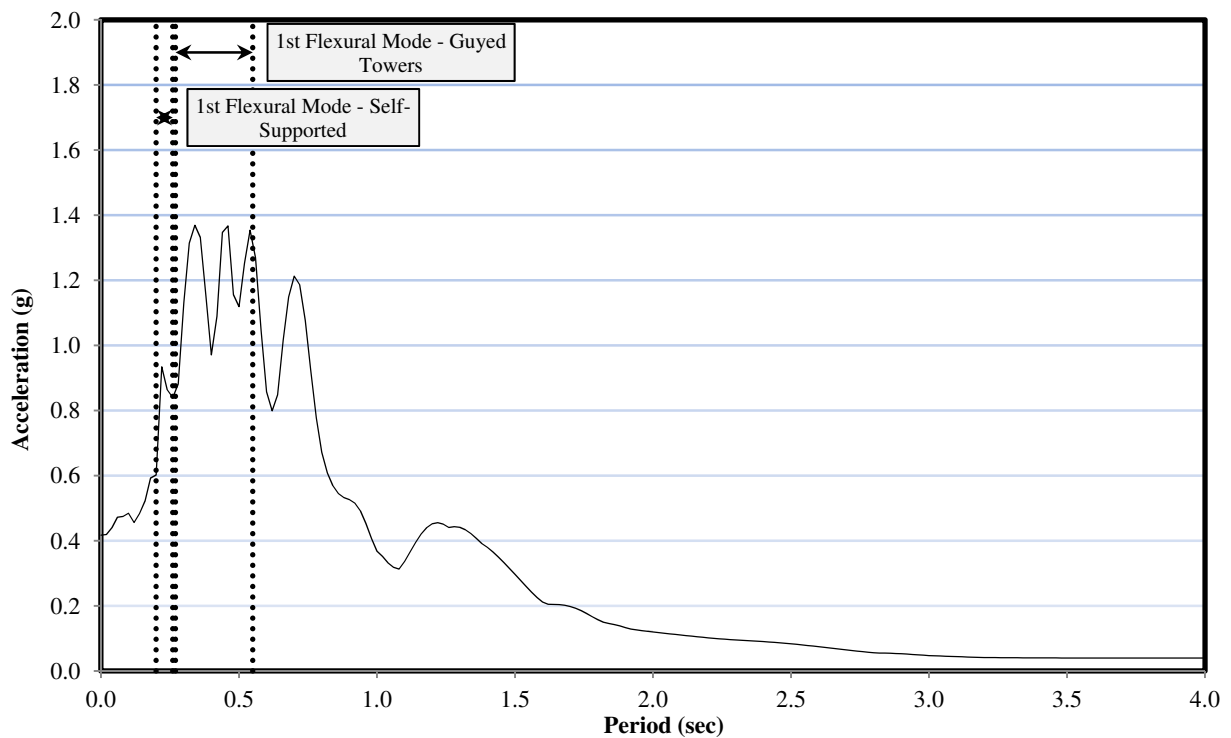


**Figure I.34 NGA n° 848. 5% damping response spectra. Horizontal component.**

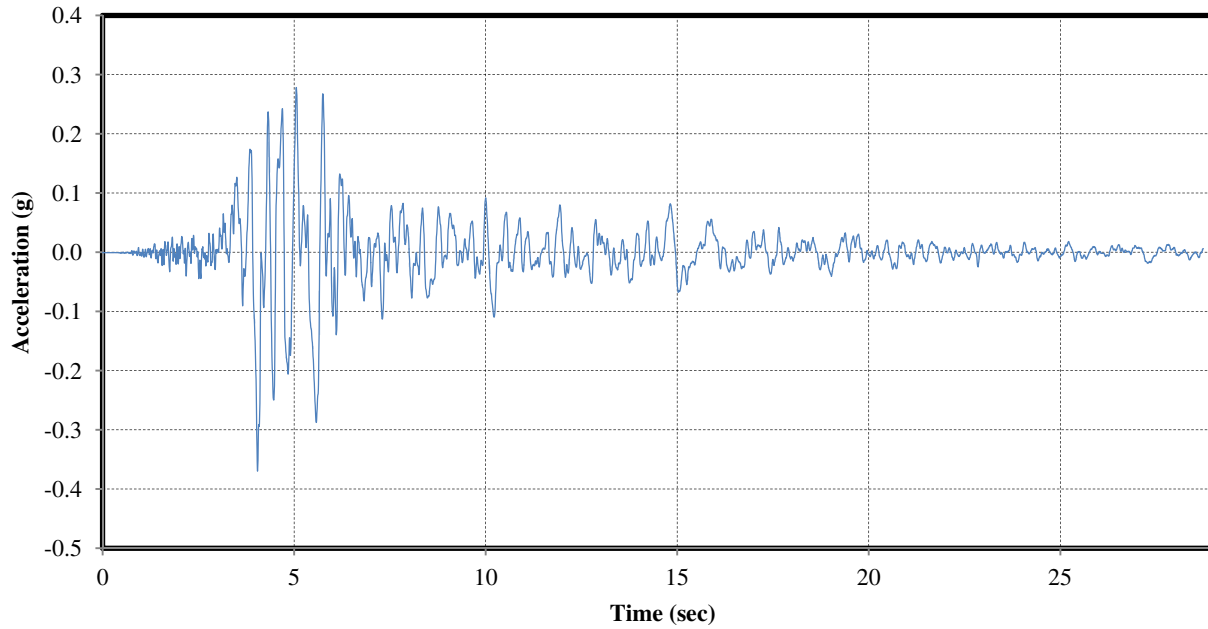


Figure I.35 NGA n° 766. Accelerogram. Horizontal component.

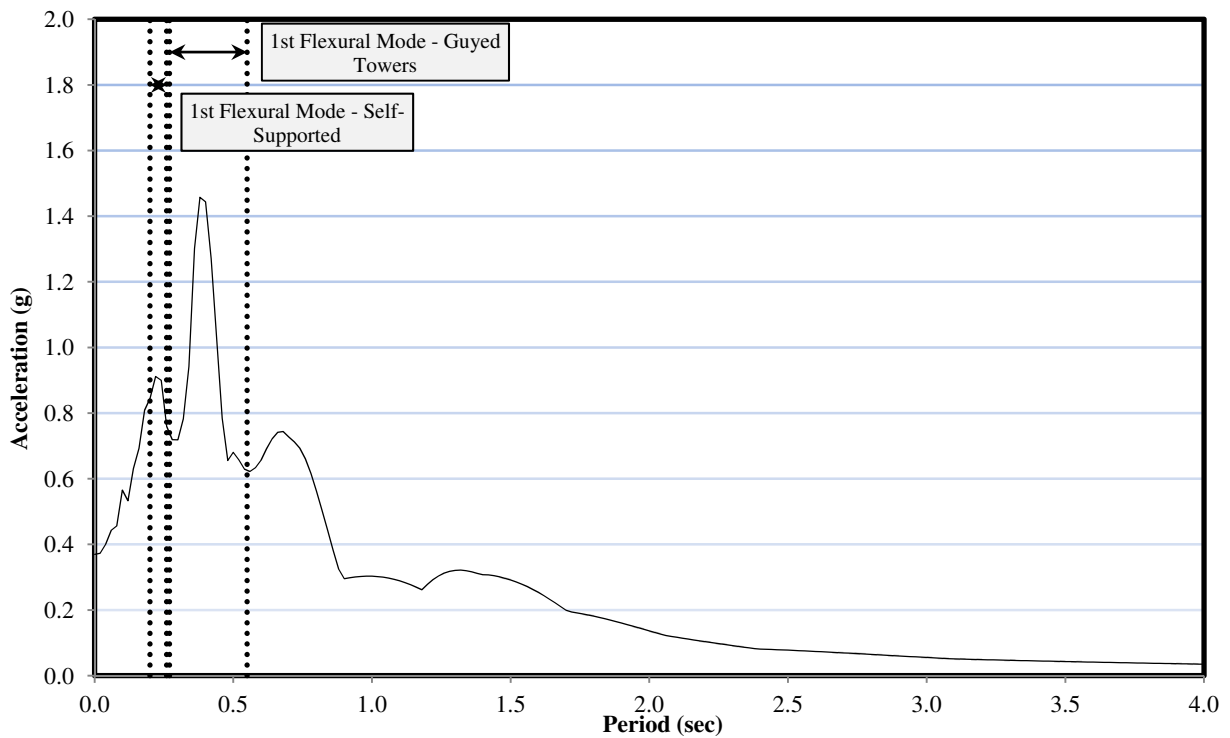
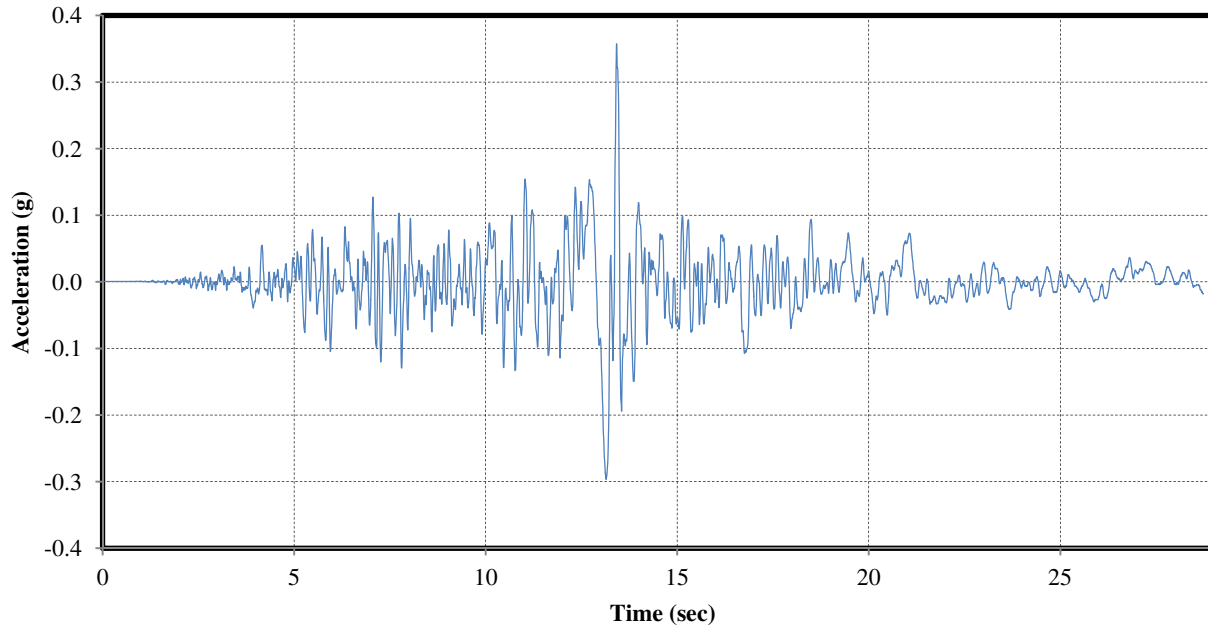
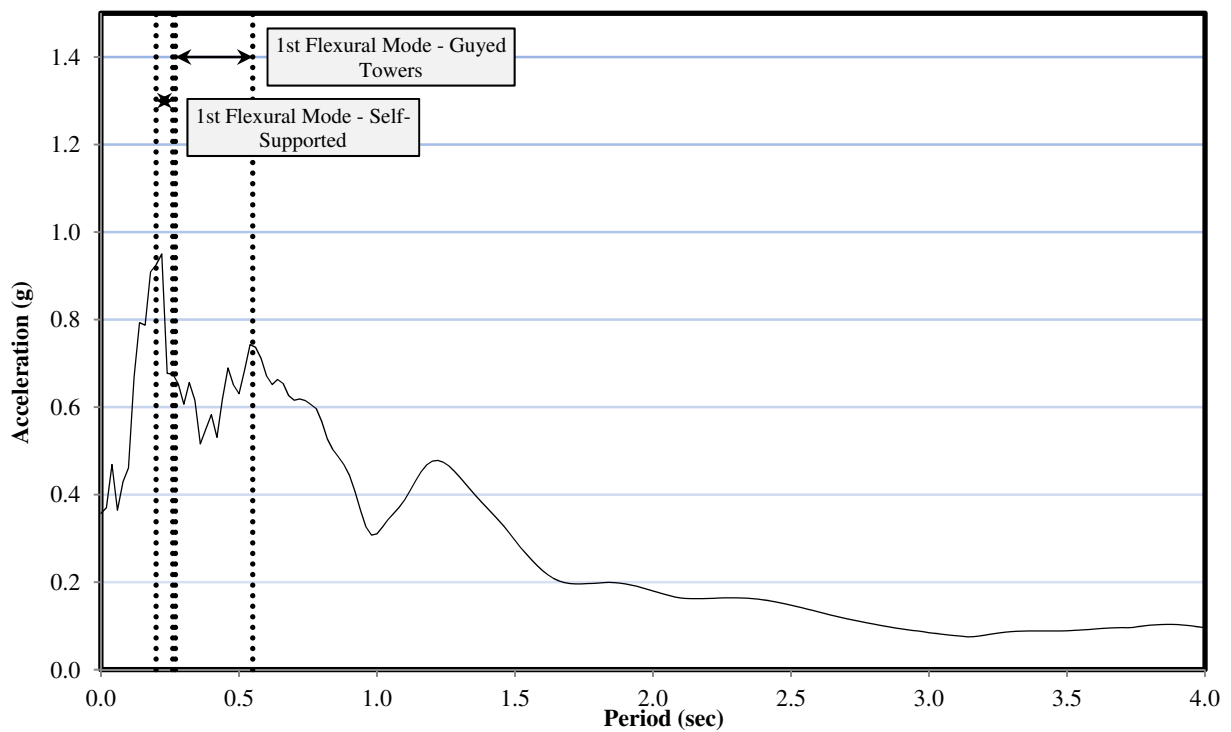


Figure I.36 NGA n° 766. 5% damping response spectra. Horizontal component.



**Figure I.37 NGA n° 721. Accelerogram. Horizontal component.**



**Figure I.38 NGA n° 721. 5% damping response spectra. Horizontal component.**

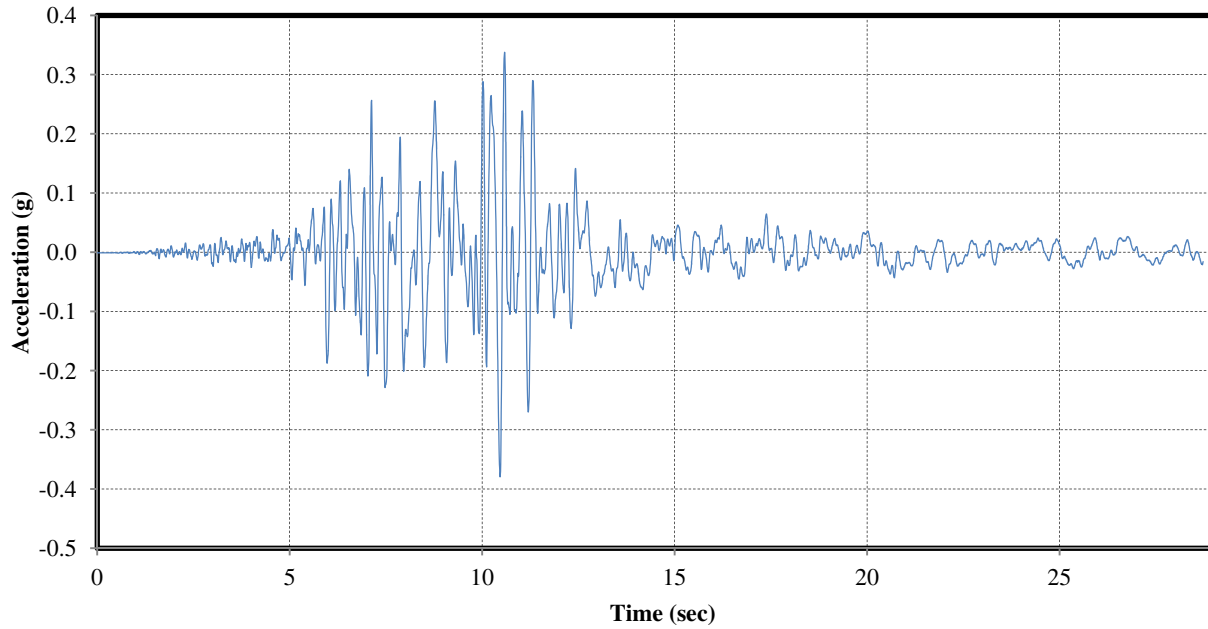


**Figure I.39 NGA n° 174. Accelerogram. Horizontal component.**

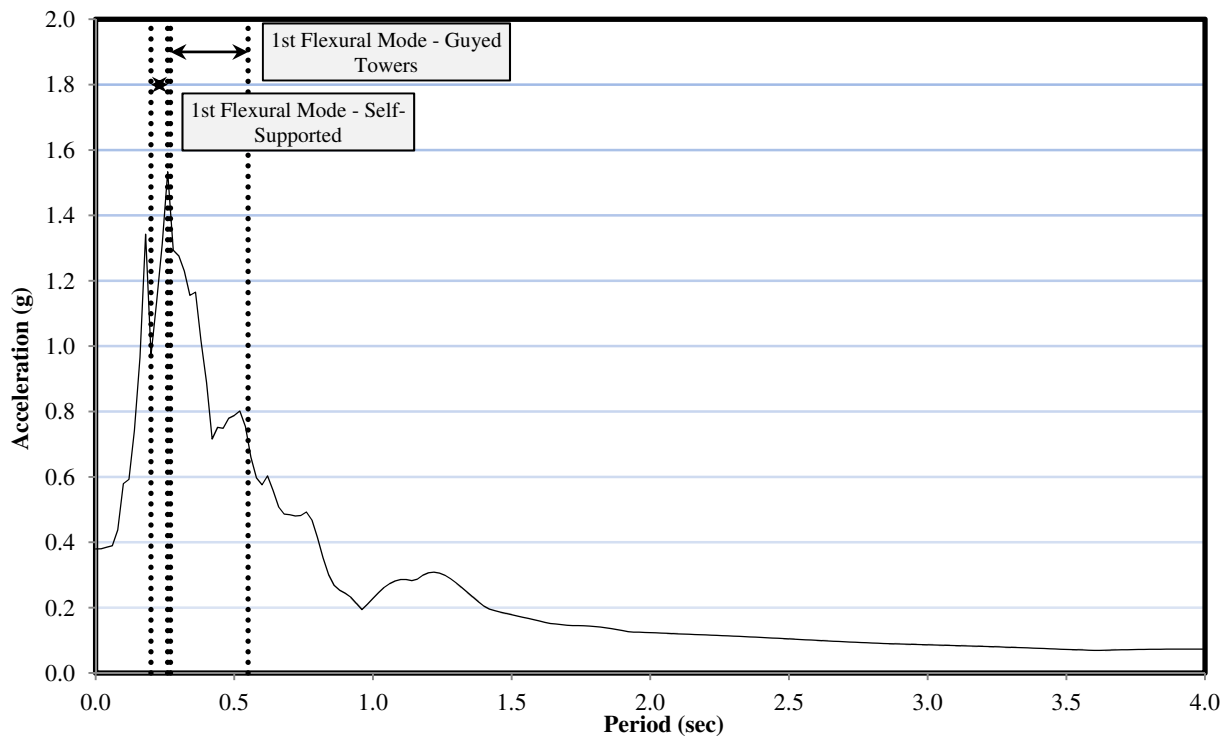


**Figure I.40 NGA n° 174. 5% damping response spectra. Horizontal component.**

**APPENDIX II**  
**RESULTS OF STATIC AND DYNAMIC ANALYSES OF TOWERS**

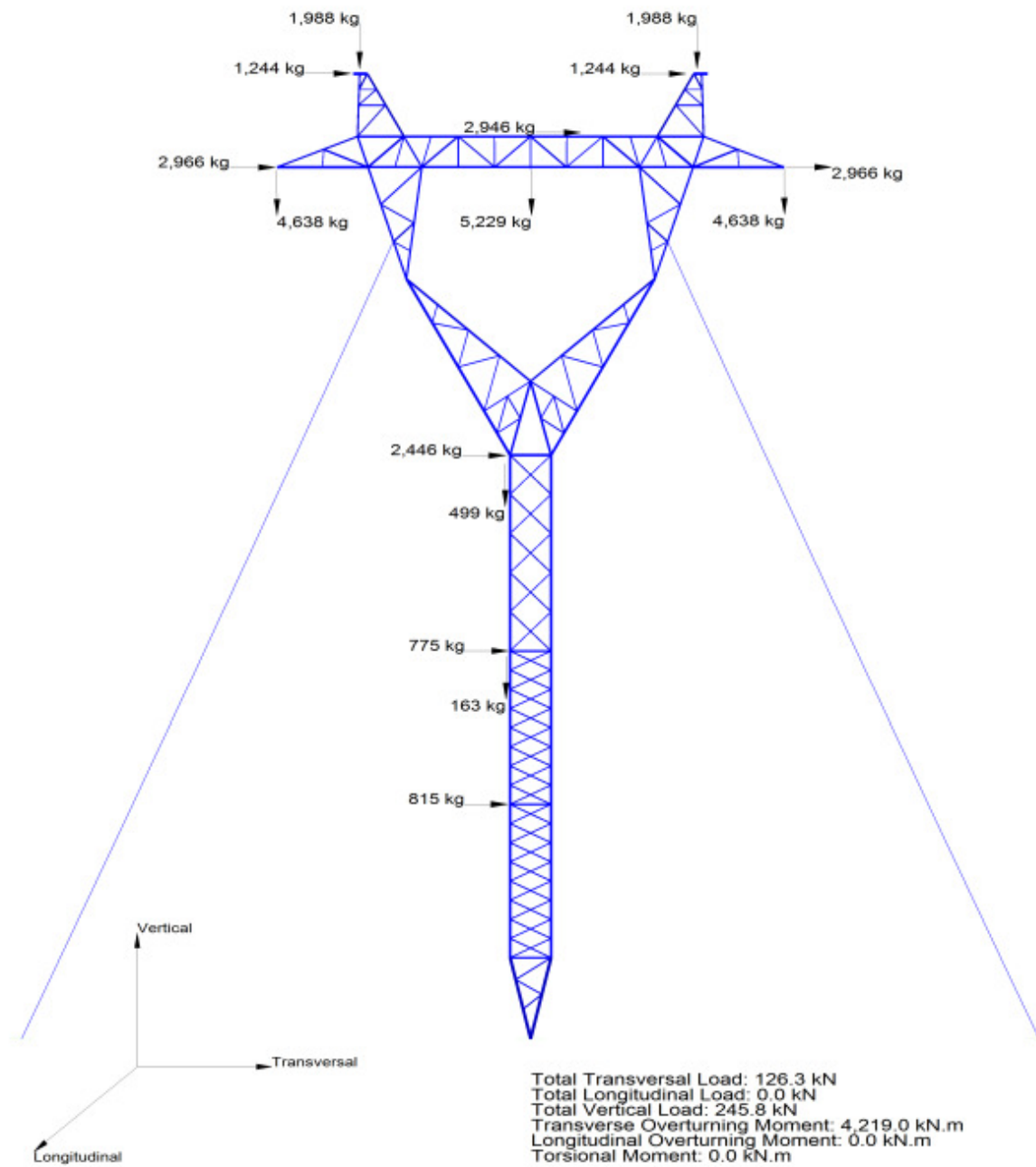


**Figure II.1. Loading tree for Test 1.**

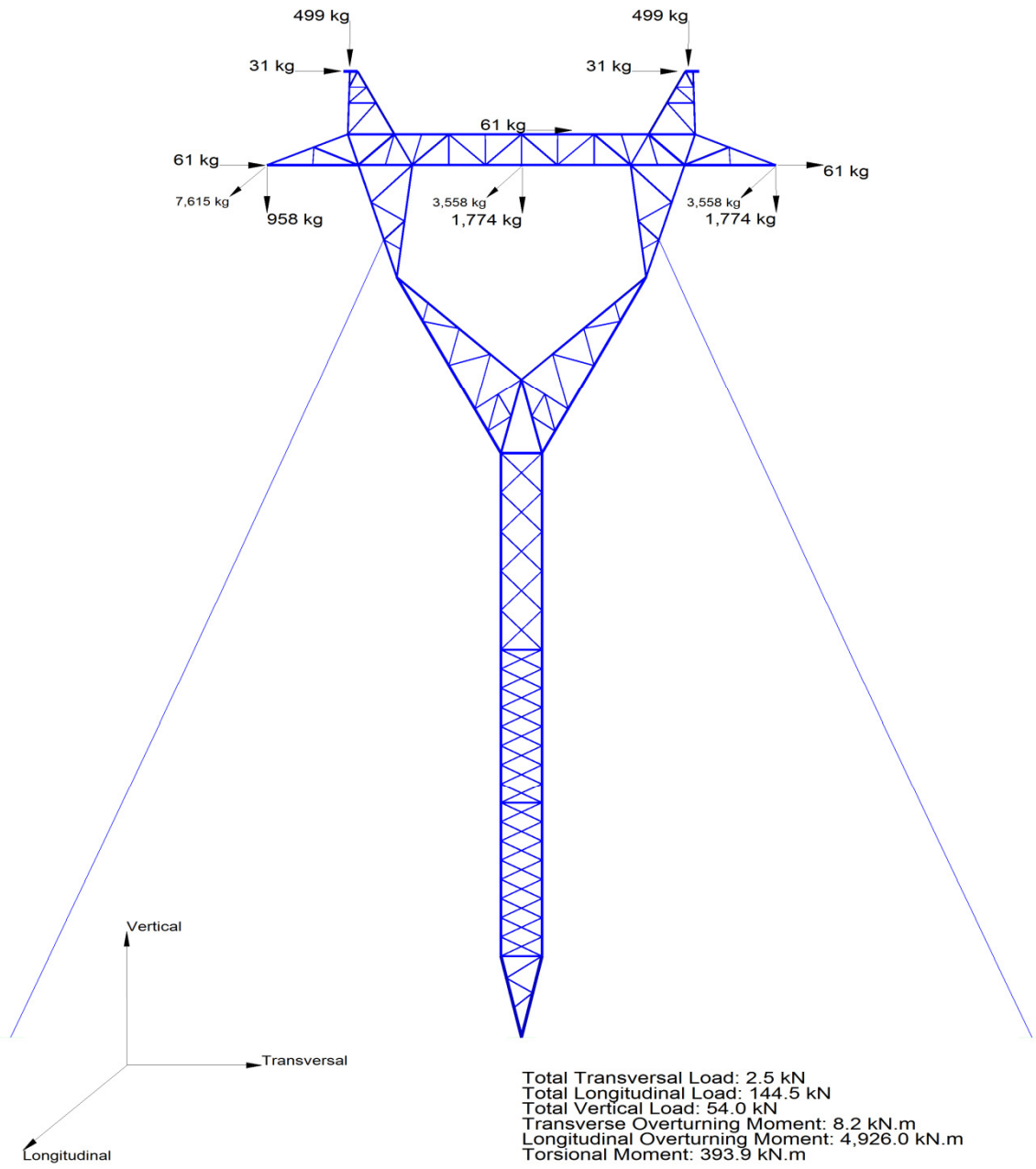


**Figure II.2. Loading tree for Test 2.**

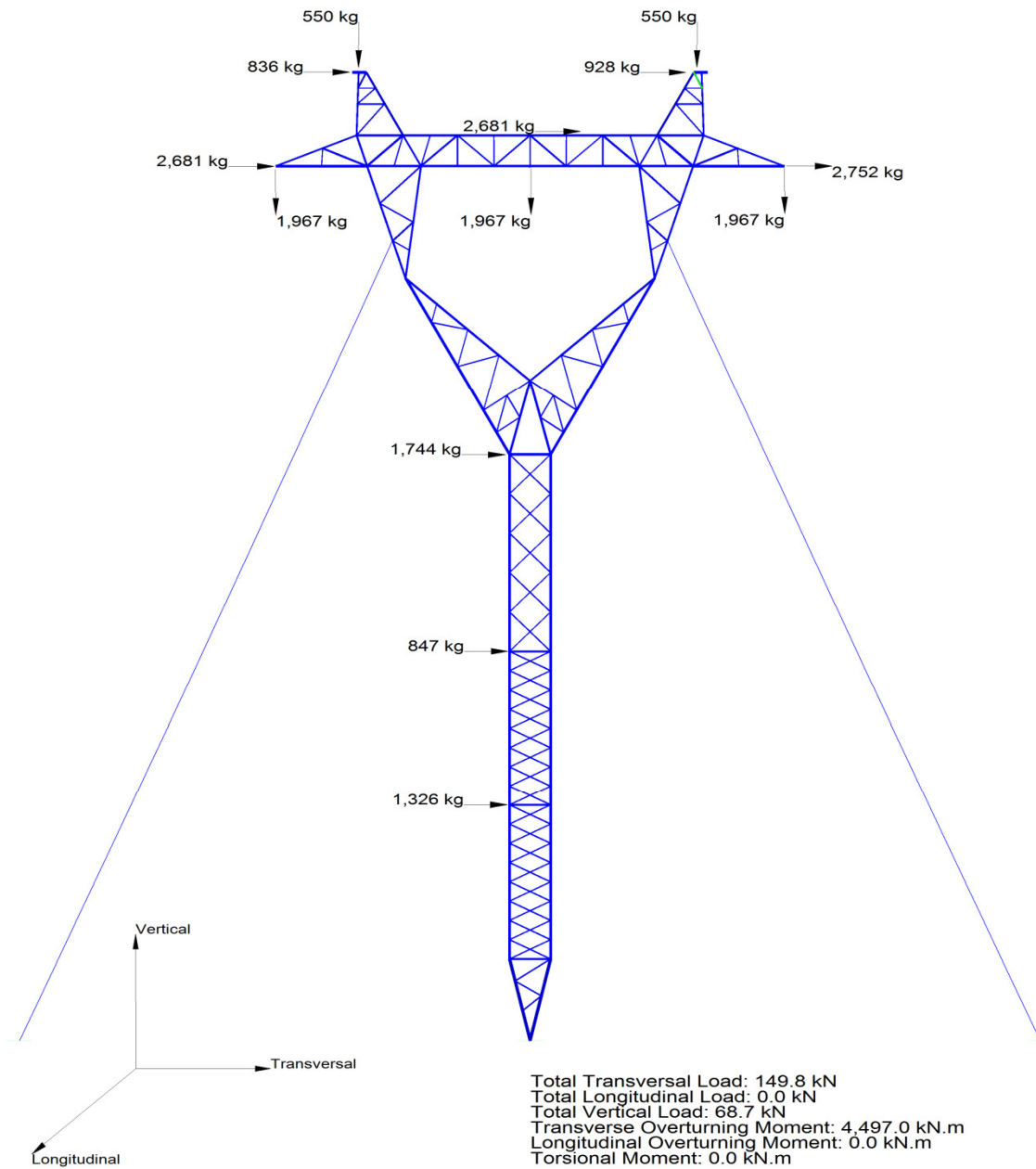


**Figure II.3. Loading tree for Test 3.**

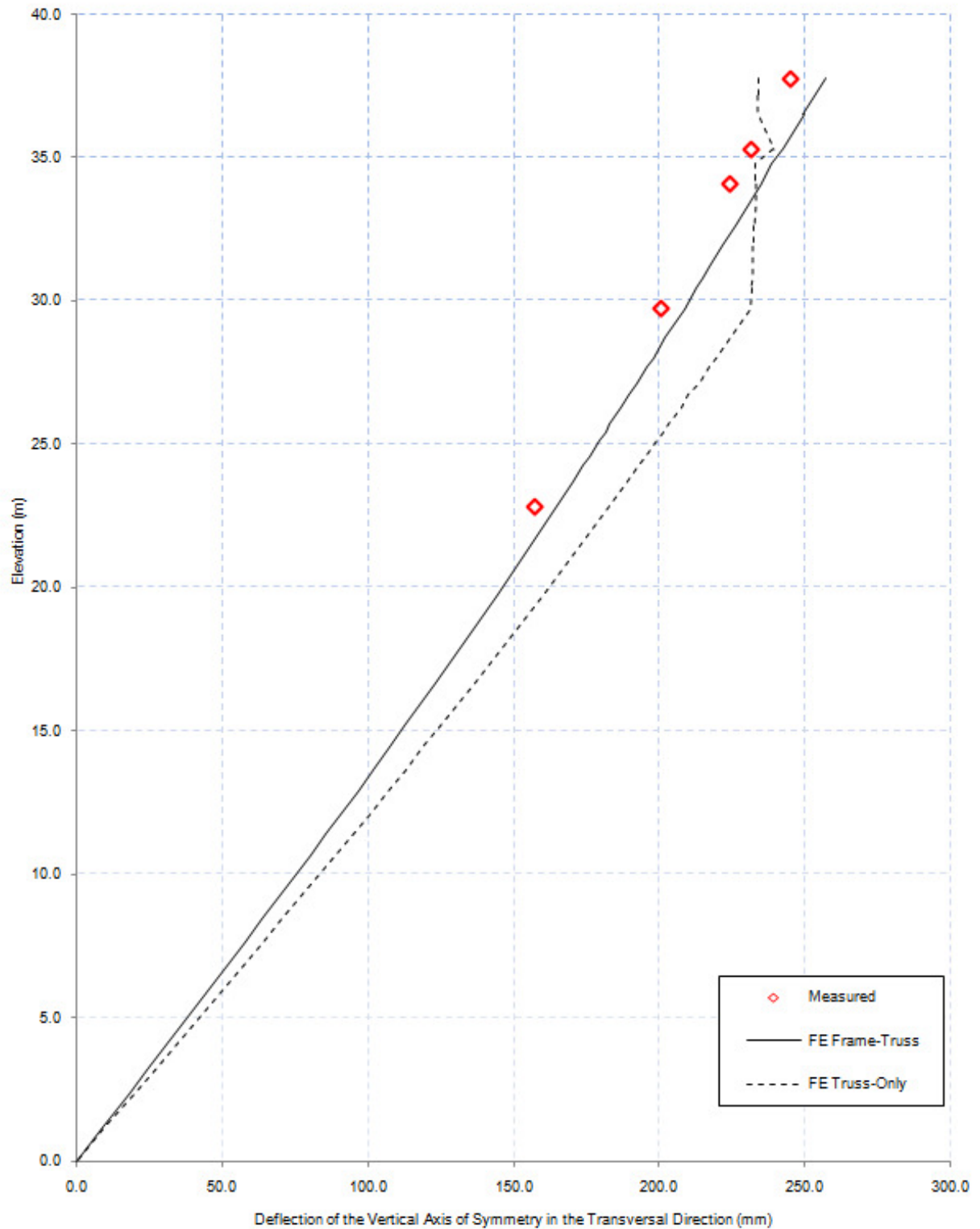


**Figure II.4. Deflection of the vertical axis of symmetry in the transversal direction for test case number 2.**

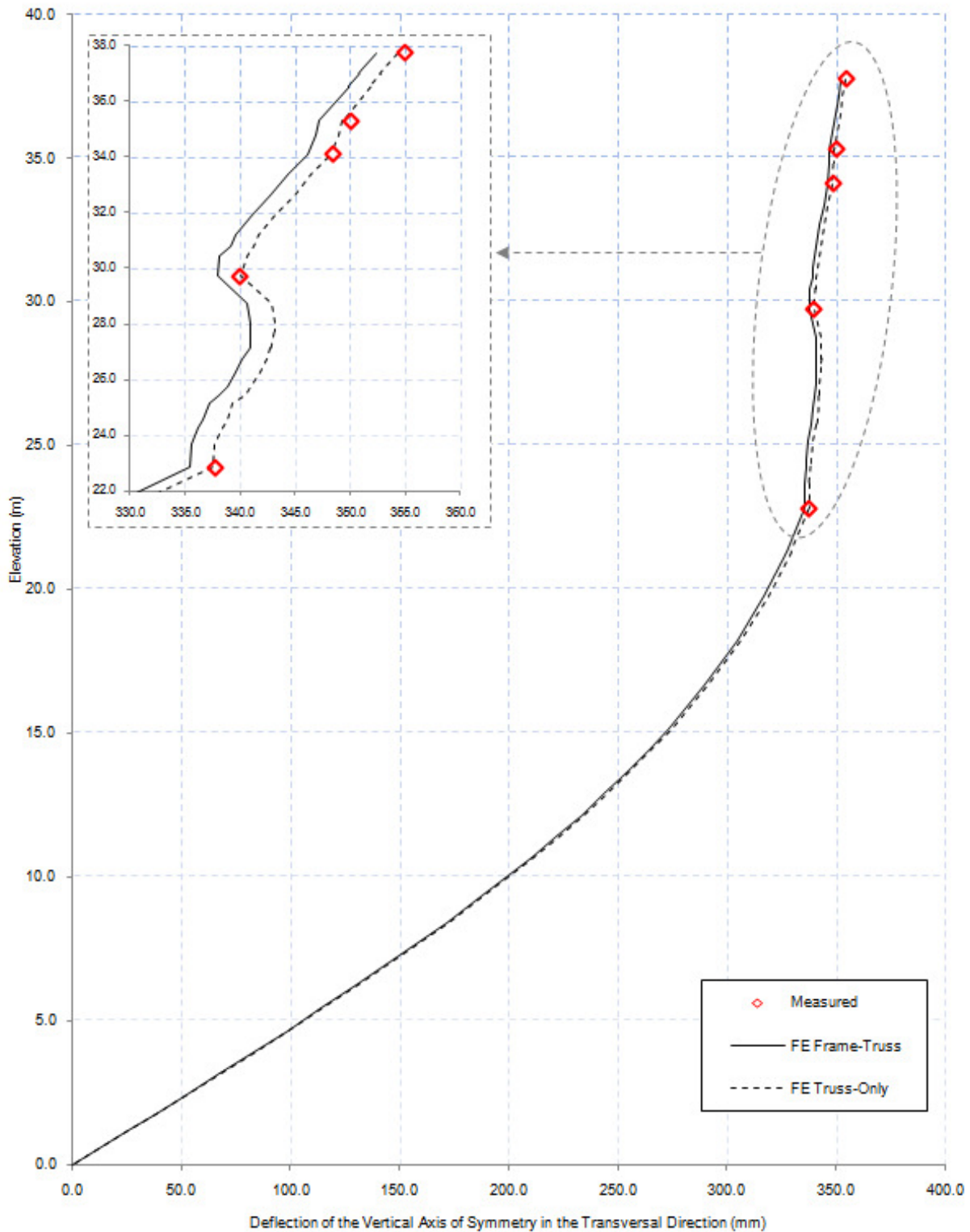


**Figure II.5. Deflection of the vertical axis of symmetry in the longitudinal direction for test case number 3 (right).**

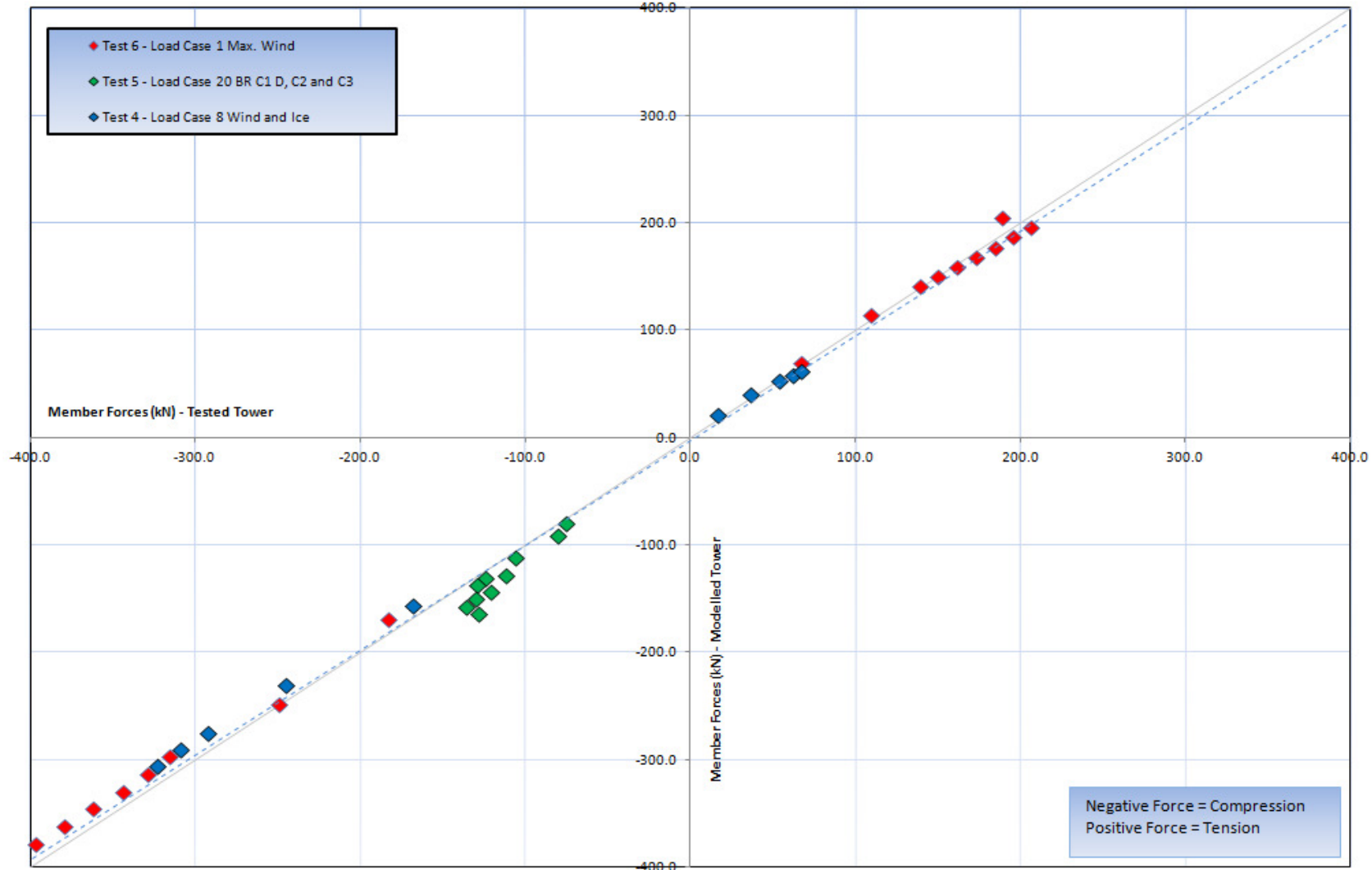


Figure II.6. Dispersion diagram – axial forces in leg members on the delta guyed tower’s mast – analytical versus full-scale prototype results.

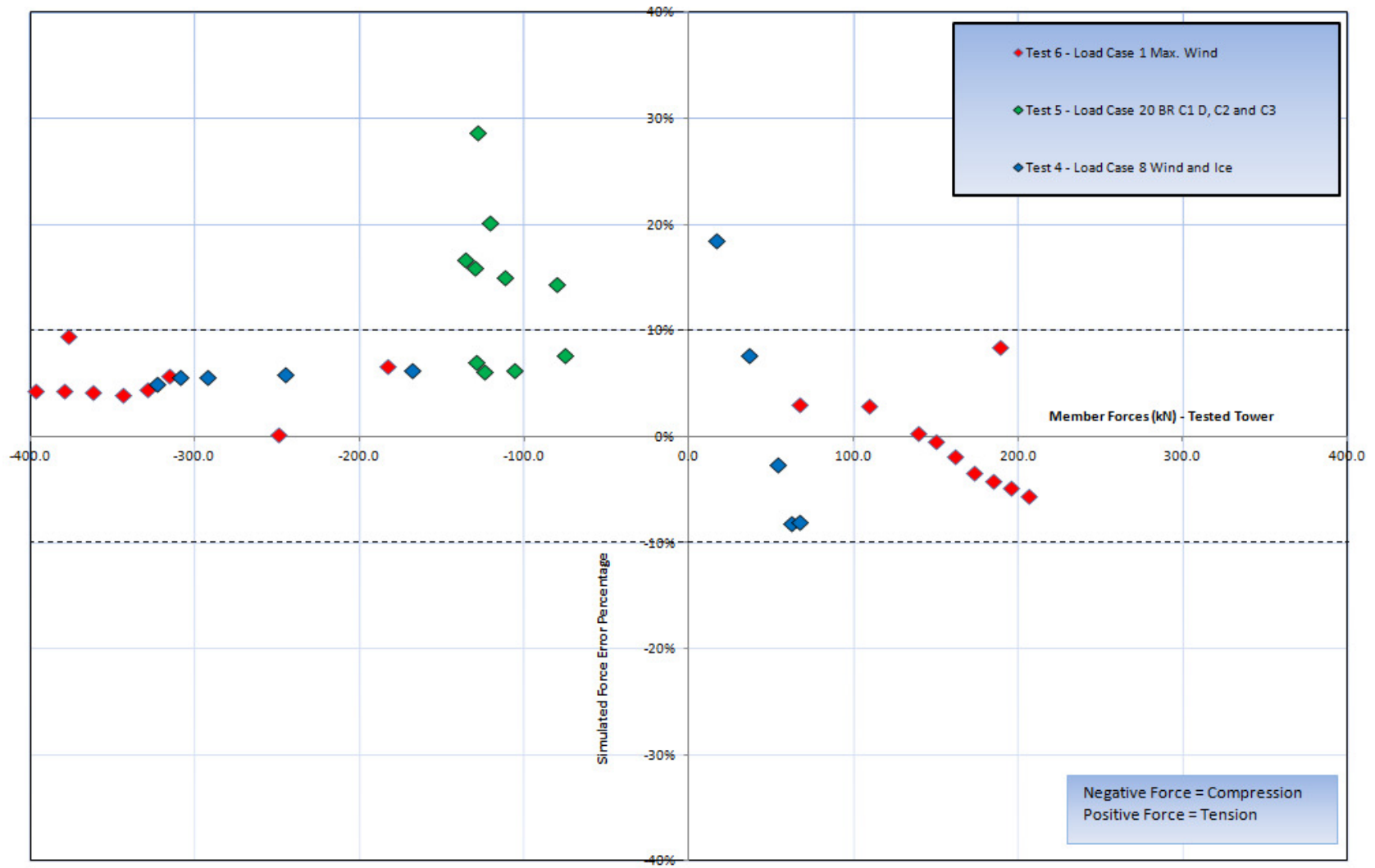
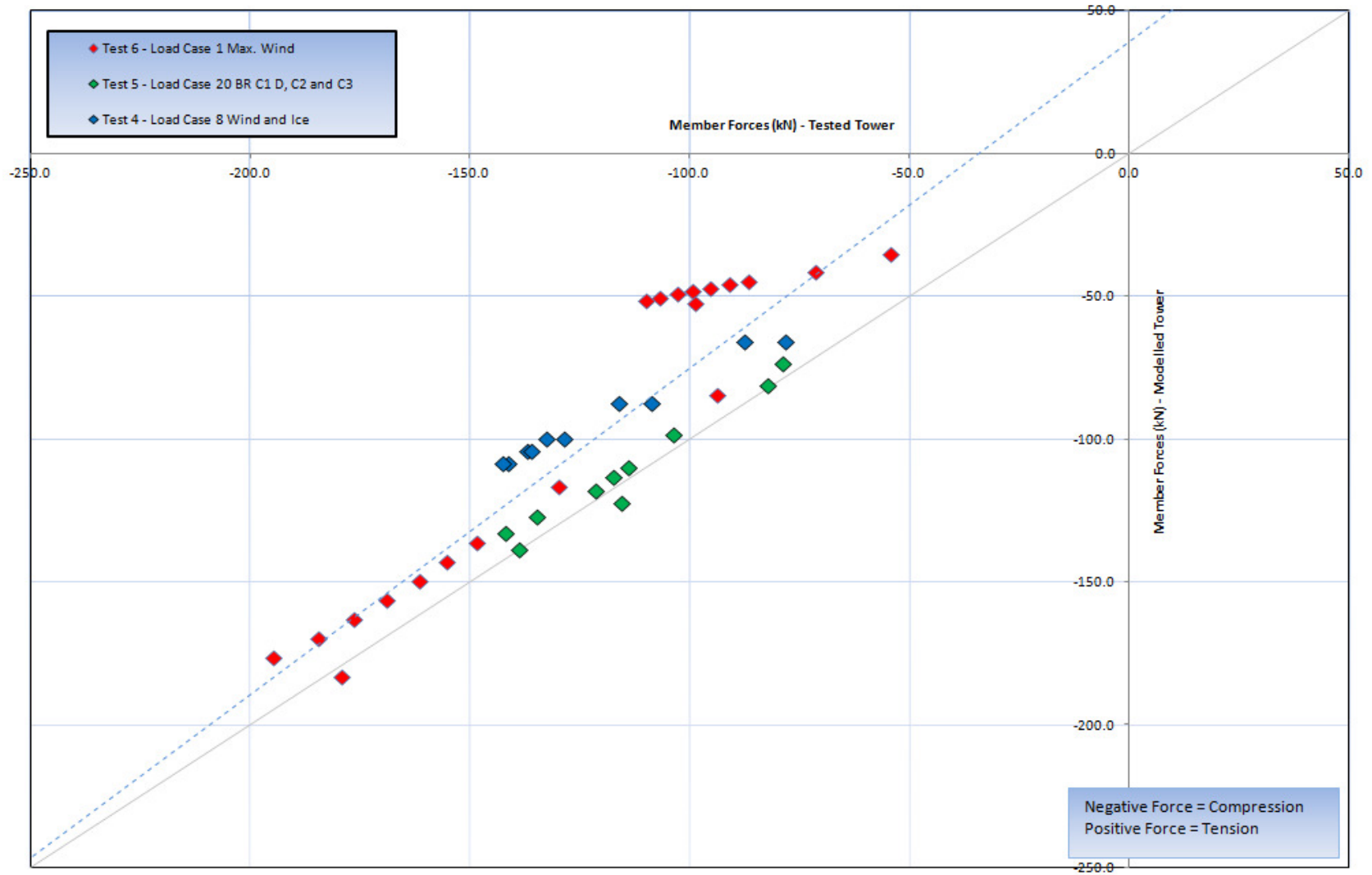


Figure II.7. Simulations' relative errors for the measured forces in the leg members on the delta guyed tower's mast.



**Figure II.8. Dispersion diagram – axial forces in members at bottom segment – analytical versus full-scale prototype results.**

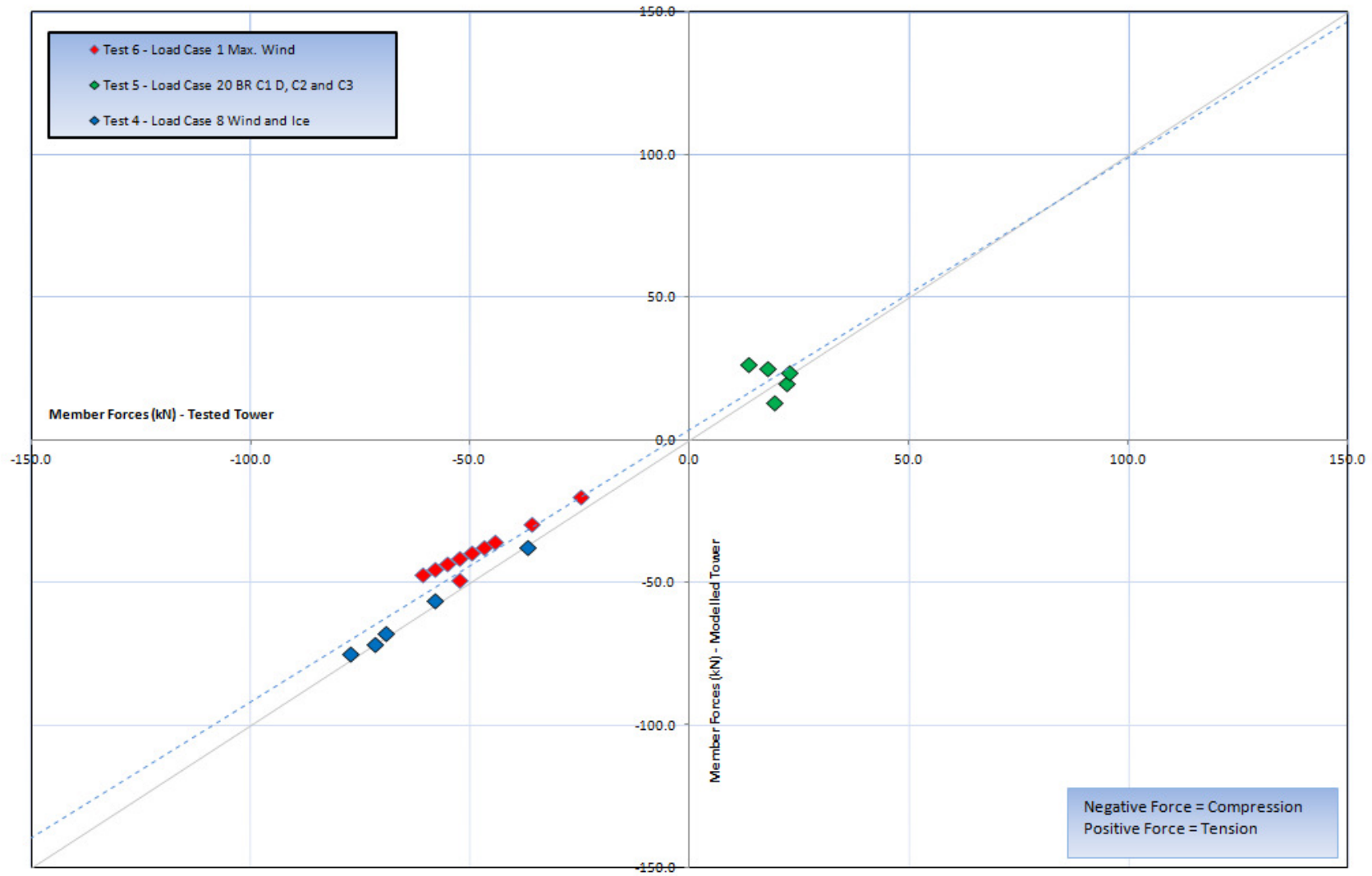
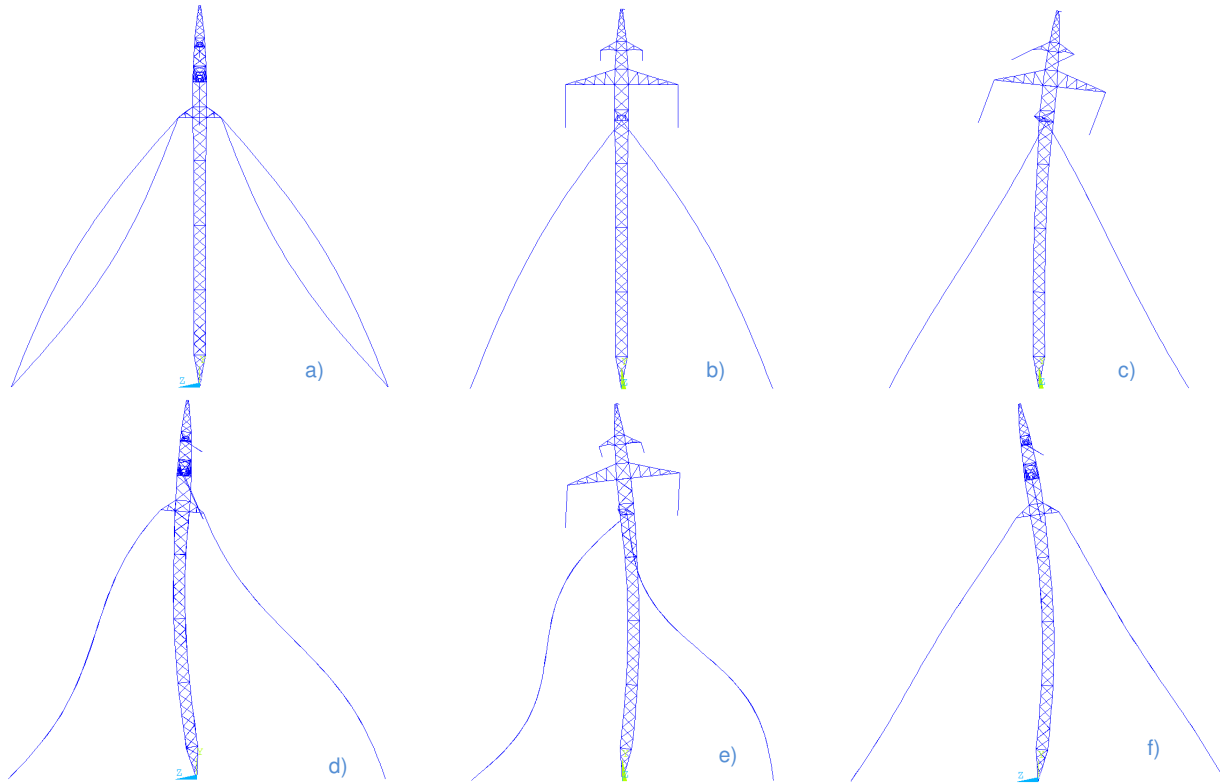


Figure II.9. Dispersion diagram – axial forces in cross-arm members – analytical versus full-scale prototype results.



**Figure II.10. Mode shapes. a) and b) cable vibration. c) 1<sup>st</sup> flexural mode of vibration in the transversal direction. d) 1<sup>st</sup> flexural mode of vibration in the longitudinal direction. e) 2<sup>nd</sup> flexural mode of vibration in the transversal direction. f) 2<sup>nd</sup> flexural mode of vibration in the longitudinal direction.**

**Table II.1. Modal properties of Mast Guyed tower.**

Mode	Period (sec)	Freq. (Hz)	Ratio of Effective Modal Mass to Total Mass			Description
			Transv.	Long.	Vertical	
1	0.75	1.33	0.05	0.03	0.00	Cable vibration
2	0.74	1.35	0.00	0.00	0.03	Cable vibration
3	0.55	1.82	0.45	0.00	0.00	1 <sup>st</sup> flexural mode - Transversal
4	0.45	2.20	0.00	0.75	0.00	1 <sup>st</sup> flexural mode - Longitudinal
5	0.38	2.63	0.05	0.00	0.00	Cable vibration
6	0.37	2.67	0.00	0.04	0.00	Cable vibration
7	0.36	2.76	0.27	0.00	0.00	2 <sup>nd</sup> flexural mode - Transversal
8	0.33	3.06	0.00	0.01	0.00	2 <sup>nd</sup> flexural mode - Longitudinal
9	0.25	4.00	0.00	0.00	0.00	Cable vibration
10	0.19	5.34	0.00	0.00	0.00	Cable vibration
11	0.16	6.21	0.00	0.00	0.00	Substructure vibration
12	0.16	6.27	0.00	0.00	0.00	Substructure vibration
13	0.16	6.38	0.00	0.00	0.00	Substructure vibration
14	0.15	6.69	0.00	0.00	0.00	Cable vibration
15	0.15	6.86	0.01	0.00	0.00	3th flexural mode - Transversal
16	0.12	8.04	0.00	0.00	0.00	Cable vibration
18	0.12	8.48	0.00	0.00	0.00	Substructure vibration
19	0.11	8.91	0.00	0.01	0.00	3th flexural mode - Longitudinal
<b>Total</b>			<b>0.85</b>	<b>0.87</b>	<b>0.09</b>	

(1) Green shading in the above table indicates the range of predominant period of vibration in the horizontal direction.

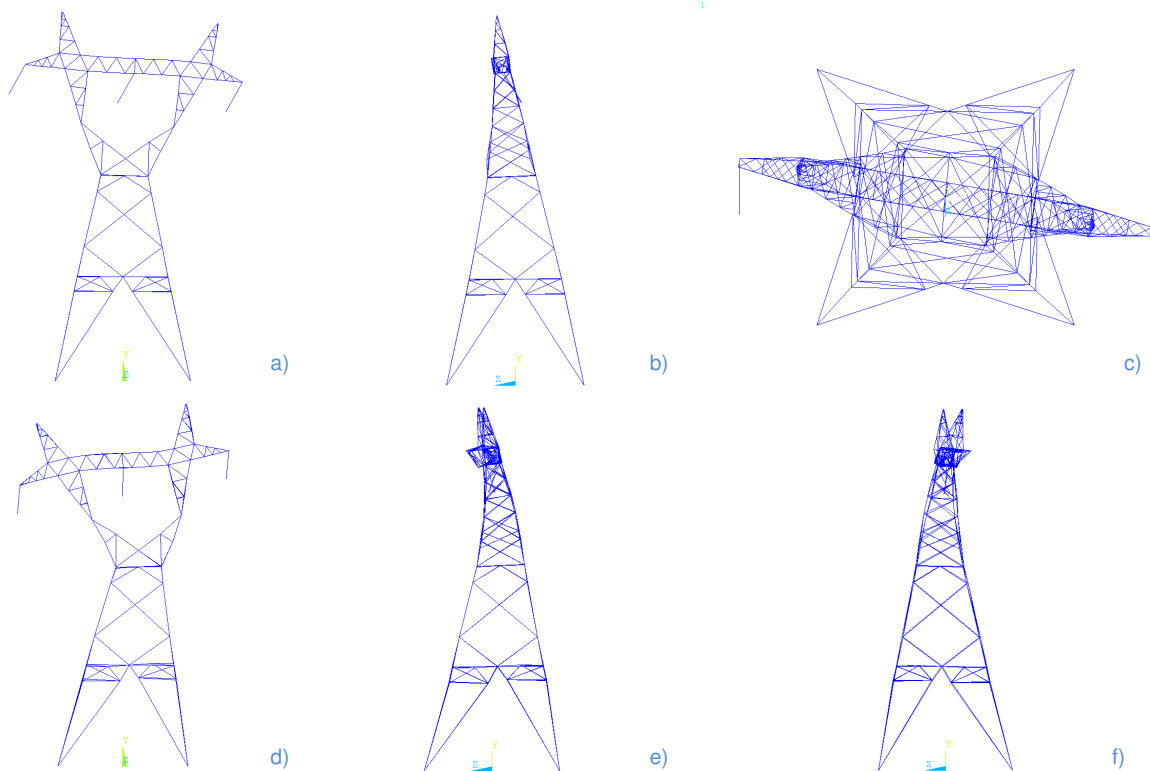


**Figure II.11. Mode shapes. a) 1<sup>st</sup> flexural mode of vibration in the transversal direction. b) 1<sup>st</sup> flexural mode of vibration in the longitudinal direction. c) tower rotation about vertical axis. d) 2<sup>nd</sup> flexural mode of vibration in the transversal direction. e) 2<sup>nd</sup> flexural mode of vibration in the longitudinal direction. f) substructure vibration – ground-wire peak and beam.**

**Table II.2. Modal properties of Delta Self-supporting Tower.**

Mode	Period (sec)	Freq. (Hz)	Ratio of Effective Modal Mass to Total Mass			Description
			Transv.	Long.	Vertical	
1	0.26	3.88	0.38	0.00	0.00	1 <sup>st</sup> flexural mode - Transversal
2	0.20	4.94	0.00	0.48	0.00	1 <sup>st</sup> flexural mode - Longitudinal
3	0.15	6.65	0.00	0.00	0.00	Tower rotation about vertical axis
4	0.08	12.16	0.44	0.00	0.00	2 <sup>nd</sup> flexural mode - Transversal
5	0.07	13.73	0.00	0.27	0.00	2 <sup>nd</sup> flexural mode - Longitudinal
6	0.07	13.86	0.00	0.05	0.00	Substructure vibration
7	0.07	15.32	0.00	0.00	0.00	Substructure vibration
8	0.06	16.11	0.00	0.11	0.00	Substructure vibration
9	0.06	16.40	0.00	0.00	0.43	
10	0.06	16.94	0.00	0.00	0.06	
11	0.06	17.65	0.14	0.00	0.00	
12	0.05	19.43	0.00	0.04	0.00	
<b>Total</b>			<b>0.96</b>	<b>0.97</b>	<b>0.49</b>	0.00

(1) Green shading in the above table indicates the range of predominant period of vibration in the horizontal direction.

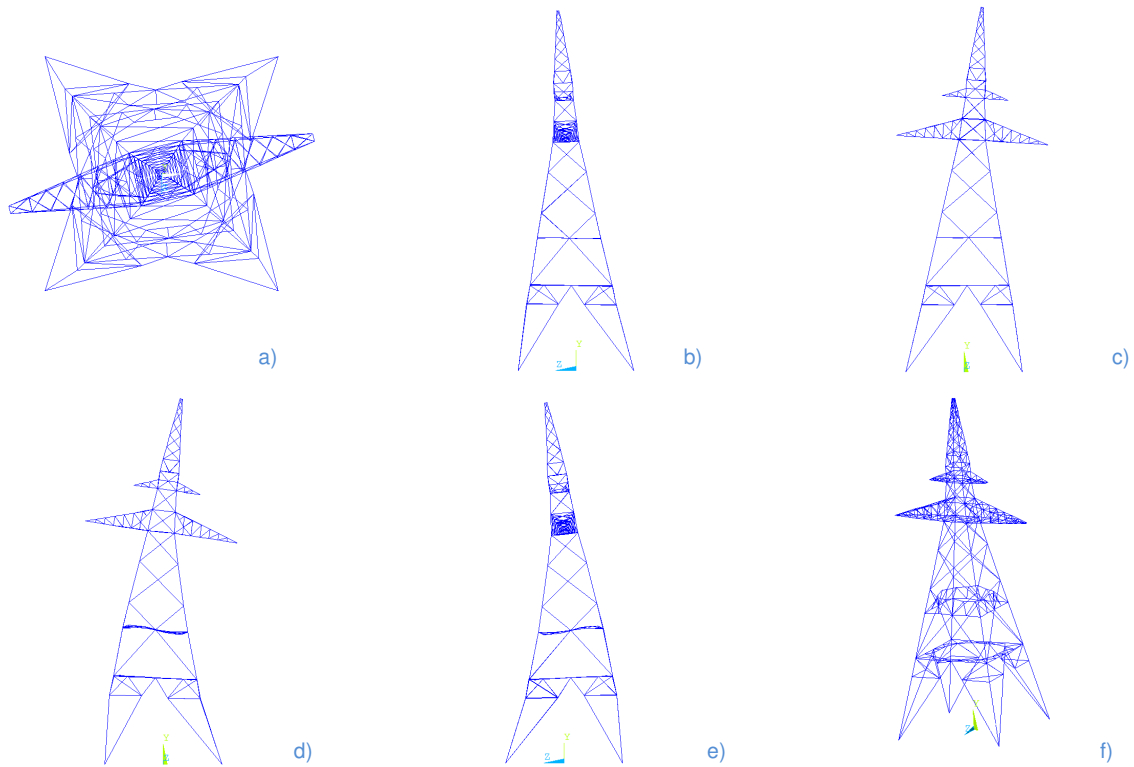


**Figure II.12. Mode shapes. a) tower rotation about vertical axis. b) 1<sup>st</sup> flexural mode of vibration in the longitudinal direction. c) 1<sup>st</sup> flexural mode of vibration in the transversal direction. d) 2<sup>nd</sup> flexural mode of vibration in the transversal direction. e) 2<sup>nd</sup> flexural mode of vibration in the longitudinal direction. f) substructure vibration.**

**Table II.3. Modal properties of Mast Self-supporting Tower.**

Mode	Period (sec)	Freq. (Hz)	Ratio of Effective Modal Mass to Total Mass			Description
			Transv.	Long.	Vertical	
1	0.25	4.02	0.00	0.00	0.00	Tower rotation about vertical axis
2	0.25	4.07	0.00	0.80	0.00	1 <sup>st</sup> flexural mode - Longitudinal
3	0.24	4.09	0.72	0.00	0.00	1 <sup>st</sup> flexural mode - Transversal
4	0.21	4.79	0.22	0.00	0.00	2 <sup>nd</sup> flexural mode - Transversal
5	0.20	4.96	0.00	0.13	0.00	2 <sup>nd</sup> flexural mode - Longitudinal
6	0.18	5.57	0.00	0.00	0.02	Substructure vibration
7	0.16	6.45	0.00	0.00	0.00	Substructure vibration
8	0.15	6.47	0.00	0.00	0.00	Substructure vibration
9	0.14	7.23	0.00	0.00	0.00	
10	0.13	7.85	0.00	0.00	0.00	
11	0.12	8.37	0.01	0.00	0.00	
12	0.12	8.55	0.00	0.01	0.00	
13	0.10	9.56	0.00	0.00	0.00	
14	0.10	9.81	0.00	0.00	0.00	
15	0.10	9.90	0.00	0.00	0.01	
16	0.10	10.04	0.00	0.00	0.00	
<b>Total</b>			<b>0.94</b>	<b>0.94</b>	<b>0.04</b>	

(1) Green shading in the above table indicates the range of predominant period of vibration in the horizontal direction.

## APPENDIX III

## RESULTS OF SEISMIC ANALYSES OF FREE-STANDING TOWERS

Table III.1. Percentage of members with seismic axial forces higher than in design load cases. Earthquake ground motions acting on longitudinal direction.

NGA	Peak Ground Accel. (g)	Pred. Period (sec)	Tower			
			Guyed Towers		Self-supporting tower	
			Delta	Mast	Delta	Mast
			<i>Tower Weight (kN)</i>			
			54.3	77.8	232.3	473.6
			<i>Tower Height (m)</i>			
			37.7	53.1	36.6	57.1
			Percentage of members with seismic axial forces higher than in design load cases			
1787	0.36	0.50	20%	20%	11%	1%
735	0.36	0.44	7%	8%	1%	1%
15	0.37	0.36	11%	5%	11%	2%
776	0.38	0.52	11%	5%	3%	4%
986	0.41	0.24	21%	4%	6%	11%
900	0.42	0.68	8%	7%	14%	5%
1005	0.42	0.20	29%	17%	11%	5%
1794	0.44	0.36	22%	4%	2%	1%
1049	0.47	0.24	25%	6%	19%	22%
766	0.55	0.38	24%	8%	6%	1%
739	0.57	0.20	34%	22%	9%	4%
174	0.57	0.26	21%	15%	8%	20%
848	0.58	0.34	32%	19%	6%	3%
767	0.62	0.20	25%	19%	8%	8%
963	0.63	0.26	24%	7%	13%	2%
57	0.63	0.20	62%	21%	14%	7%
1006	0.64	0.22	17%	7%	23%	13%
1039	0.67	0.26	21%	19%	17%	18%
721	0.68	0.22	20%	15%	7%	9%
953	0.84	0.52	60%	20%	18%	9%
		<b>Min.</b>	<b>7%</b>	<b>4%</b>	<b>1%</b>	<b>1%</b>
		<b>Max.</b>	<b>62%</b>	<b>22%</b>	<b>23%</b>	<b>22%</b>
		<b>Mean</b>	<b>25%</b>	<b>12%</b>	<b>10%</b>	<b>7%</b>

**Table III.2. Percentage of members with seismic axial forces higher than in design load cases. Earthquake ground motions acting on vertical direction.**

NGA	Peak Ground Accel. (g)	Pred. Period (sec)	Tower			
			Guyed Towers		Self-supporting tower	
			Delta	Mast	Delta	Mast
			<i>Tower Weight (kN)</i>			
			54.3	77.8	232.3	473.6
			<i>Tower Height (m)</i>			
			37.7	53.1	36.6	57.1
Percentage of members with seismic axial forces higher than in design load cases						
1787	0.36	0.50	1%	2%	9%	1%
735	0.36	0.44	1%	1%	8%	1%
15	0.37	0.36	1%	2%	10%	2%
776	0.38	0.52	1%	4%	11%	1%
986	0.41	0.24	1%	4%	12%	3%
900	0.42	0.68	1%	3%	10%	4%
1005	0.42	0.20	1%	2%	10%	2%
1794	0.44	0.36	31%	3%	12%	2%
1049	0.47	0.24	1%	4%	13%	7%
766	0.55	0.38	1%	4%	10%	2%
739	0.57	0.20	1%	4%	10%	3%
174	0.57	0.26	1%	3%	11%	4%
848	0.58	0.34	1%	3%	12%	3%
767	0.62	0.20	1%	4%	11%	3%
963	0.63	0.26	1%	1%	10%	2%
57	0.63	0.20	1%	3%	12%	2%
1006	0.64	0.22	1%	3%	12%	7%
1039	0.67	0.26	1%	3%	11%	8%
721	0.68	0.22	1%	4%	12%	1%
953	0.84	0.52	1%	4%	16%	3%
		<b>Min.</b>	<b>1%</b>	<b>1%</b>	<b>8%</b>	<b>1%</b>
		<b>Max.</b>	<b>31%</b>	<b>4%</b>	<b>16%</b>	<b>8%</b>
		<b>Mean</b>	<b>2%</b>	<b>3%</b>	<b>11%</b>	<b>3%</b>

**Table III.3. Number of members with capacity exceeded and maximum capacity usage of guy cables. Earthquake ground motions applied in longitudinal direction.**

NGA	Peak Ground Acceleration (g)	Predominant Period (sec)	Tower					
			Guyed tower				Self-supporting tower	
			Delta		Mast		Delta	Mast
			Number of Members	Guy Max. Usage	Number of Members	Guy Max. Usage	Number of Members	Number of Members
1787	0.36	0.50	-	22%	-	41%	-	-
735	0.36	0.44	-	16%	-	33%	-	-
15	0.37	0.36	-	18%	-	28%	-	-
776	0.38	0.52	-	16%	-	30%	-	-
986	0.41	0.24	-	23%	-	24%	-	-
900	0.42	0.68	-	20%	-	26%	-	-
1005	0.42	0.20	4	33%	-	40%	-	-
1794	0.44	0.36	-	23%	-	25%	-	-
1049	0.47	0.24	4	25%	-	29%	-	25
766	0.55	0.38	2	25%	-	33%	-	-
739	0.57	0.20	5	32%	-	46%	-	-
174	0.57	0.26	-	21%	-	37%	-	20
848	0.58	0.34	4	27%	-	39%	-	-
767	0.62	0.20	2	25%	-	40%	-	-
963	0.63	0.26	-	23%	-	29%	-	-
57	0.63	0.20	17	54%	-	47%	-	-
1006	0.64	0.22	-	19%	-	26%	-	-
1039	0.67	0.26	1	22%	-	40%	-	4
721	0.68	0.22	-	21%	-	37%	-	-
953	0.84	0.52	9	40%	-	41%	-	-
		<b>Min.</b>	-	<b>16%</b>	-	<b>24%</b>	-	<b>4</b>
		<b>Max.</b>	<b>17</b>	<b>54%</b>	-	<b>47%</b>	-	<b>25</b>

**Table III.4. Number of members with capacity exceeded and maximum capacity usage of guy cables. Earthquake ground motions applied in vertical direction.**

NGA	Peak Ground Acceleration (g)	Predominant Period (sec)	Tower					
			Guyed tower				Self-supporting tower	
			Delta		Mast		Delta	Mast
			Number of Members	Guy Max. Usage	Number of Members	Guy Max. Usage	Number of Members	Number of Members
1787	0.36	0.50	-	7%	-	16%	-	-
735	0.36	0.44	-	8%	-	18%	-	-
15	0.37	0.36	-	8%	-	18%	-	-
776	0.38	0.52	-	7%	-	17%	6	-
986	0.41	0.24	-	8%	-	18%	-	-
900	0.42	0.68	-	8%	-	18%	-	-
1005	0.42	0.20	-	7%	-	18%	-	-
1794	0.44	0.36	21	8%	-	16%	-	-
1049	0.47	0.24	-	8%	-	18%	2	-
766	0.55	0.38	-	8%	-	18%	-	-
739	0.57	0.20	-	10%	-	16%	-	-
174	0.57	0.26	-	8%	-	16%	-	-
848	0.58	0.34	-	8%	-	16%	-	-
767	0.62	0.20	-	8%	-	18%	-	4
963	0.63	0.26	-	7%	-	18%	-	-
57	0.63	0.20	-	8%	-	16%	2	-
1006	0.64	0.22	-	7%	-	18%	-	1
1039	0.67	0.26	-	7%	-	18%	-	-
721	0.68	0.22	-	8%	-	17%	-	-
953	0.84	0.52	-	8%	-	17%	-	4
		<b>Min.</b>	-	<b>7%</b>	-	<b>16%</b>	<b>2</b>	<b>1</b>
		<b>Max.</b>	<b>21</b>	<b>8%</b>	-	<b>18%</b>	<b>6</b>	<b>4</b>

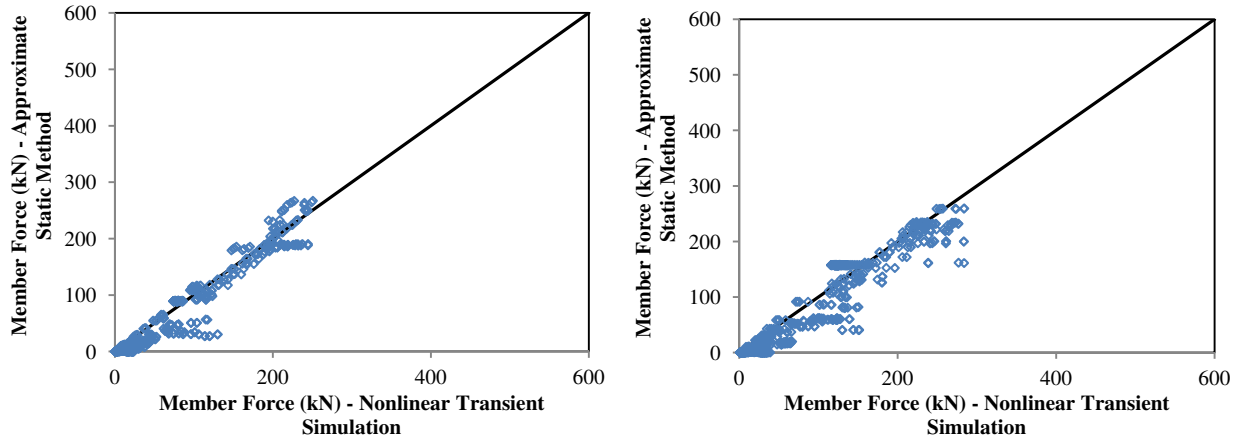


**Figure III.1. Dispersion diagrams comparing member axial forces of delta guyed tower obtained from nonlinear transient analysis and from the proposed approximate static method under NGA 57 record applied in transversal direction (left) and longitudinal direction (right).**

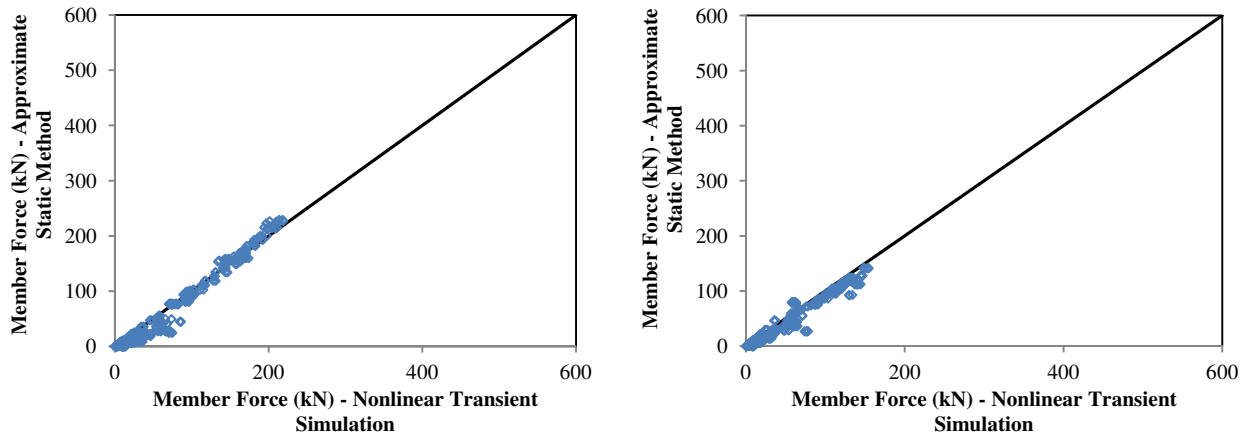


**Figure III.2. Dispersion diagrams comparing member axial forces of delta guyed tower obtained from nonlinear transient analysis and from the proposed approximate static method Under NGA 174 record applied in transversal direction (left) and longitudinal direction (right).**

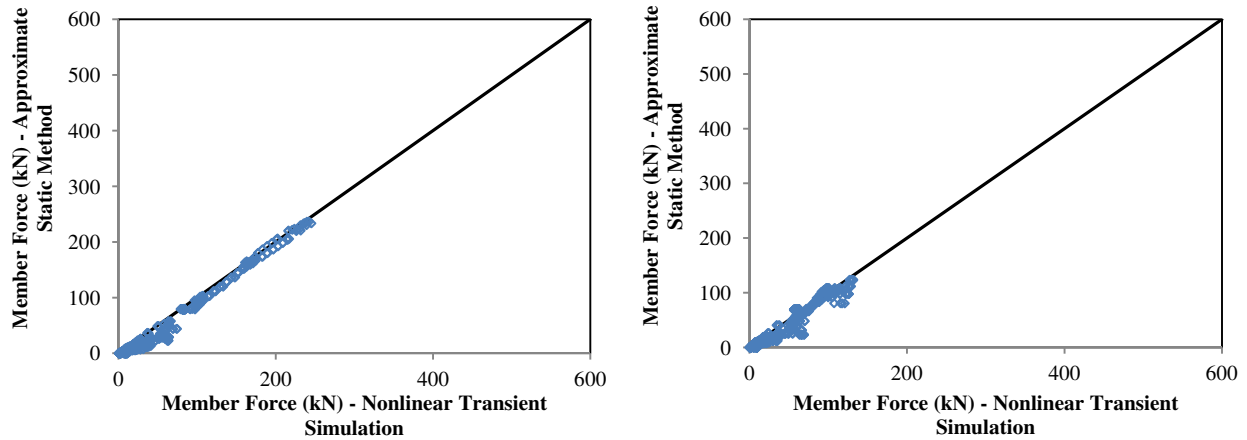


**Figure III.3. Dispersion diagrams comparing member axial forces of delta guyed tower obtained from nonlinear transient analysis and from the proposed approximate static method under NGA 721 record applied in transversal direction (left) and longitudinal direction (right).**

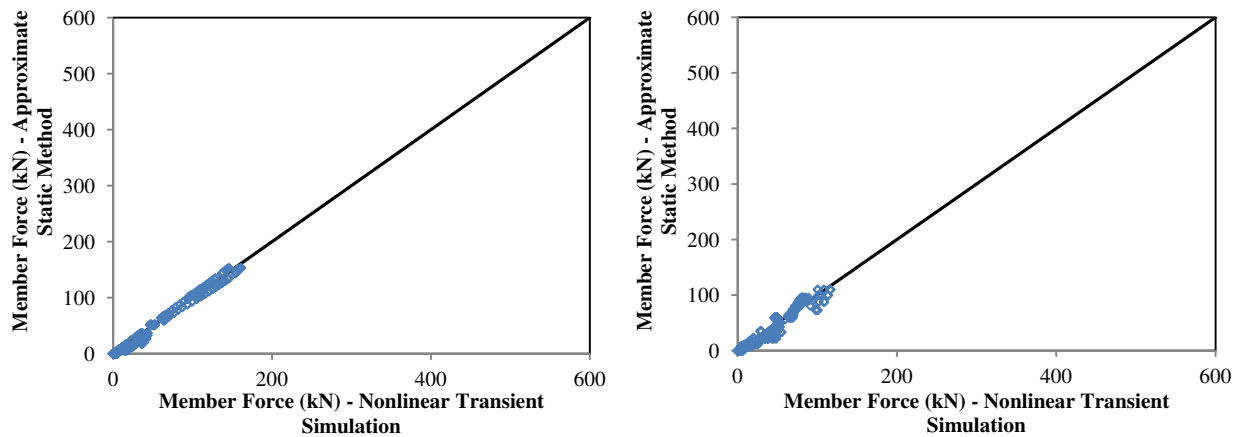


**Figure III.4. Dispersion diagrams comparing member axial forces of delta guyed tower obtained from nonlinear transient analysis and from the proposed approximate static method under NGA 766 record applied in transversal direction (left) and longitudinal direction (right).**

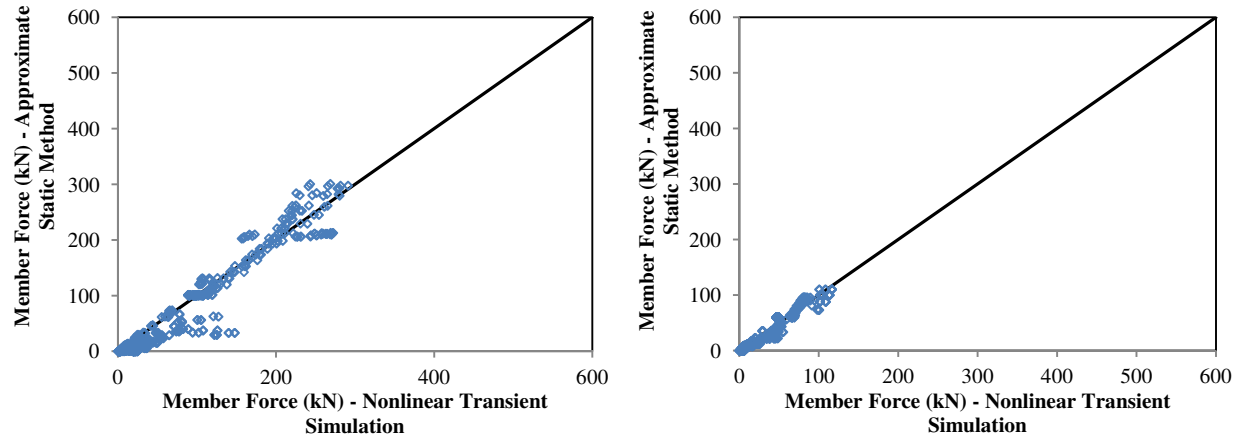


**Figure III.5. Dispersion diagrams comparing member axial forces of delta guyed tower obtained from nonlinear transient analysis and from the proposed approximate static method under NGA 776 record applied in transversal direction (left) and longitudinal direction (right).**

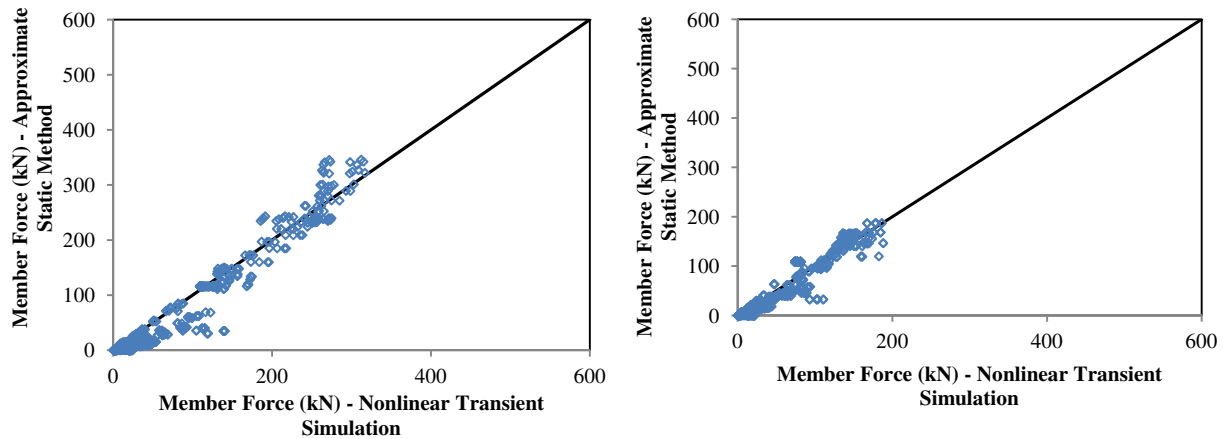


**Figure III.6. Dispersion diagrams comparing member axial forces of delta guyed tower obtained from nonlinear transient analysis and from the proposed approximate static method under NGA 848 record applied in transversal direction (left) and longitudinal direction (right).**

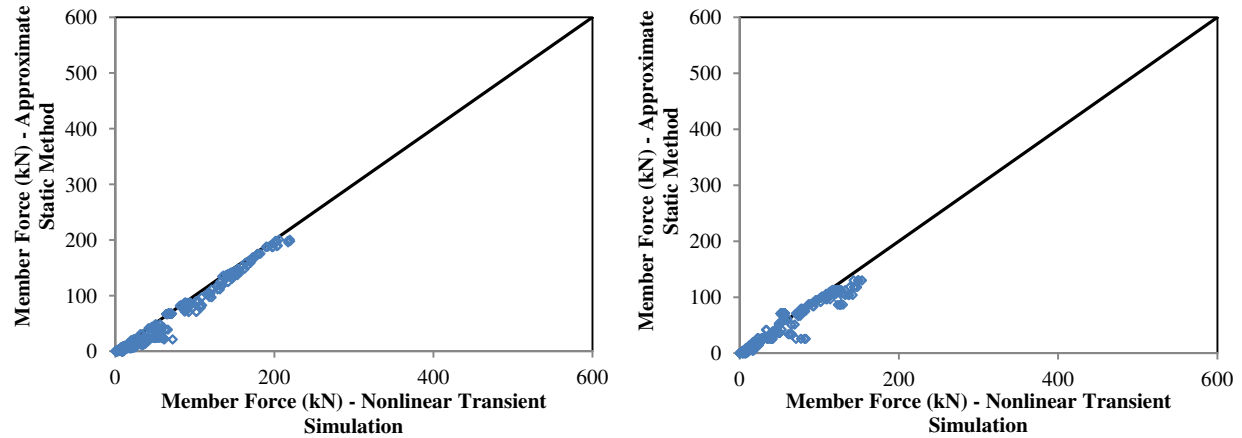


**Figure III.7.** Dispersion diagrams comparing member axial forces of delta guyed tower obtained from nonlinear transient analysis and from the proposed approximate static method under NGA 1006 record applied in transversal direction (left) and longitudinal direction (right).

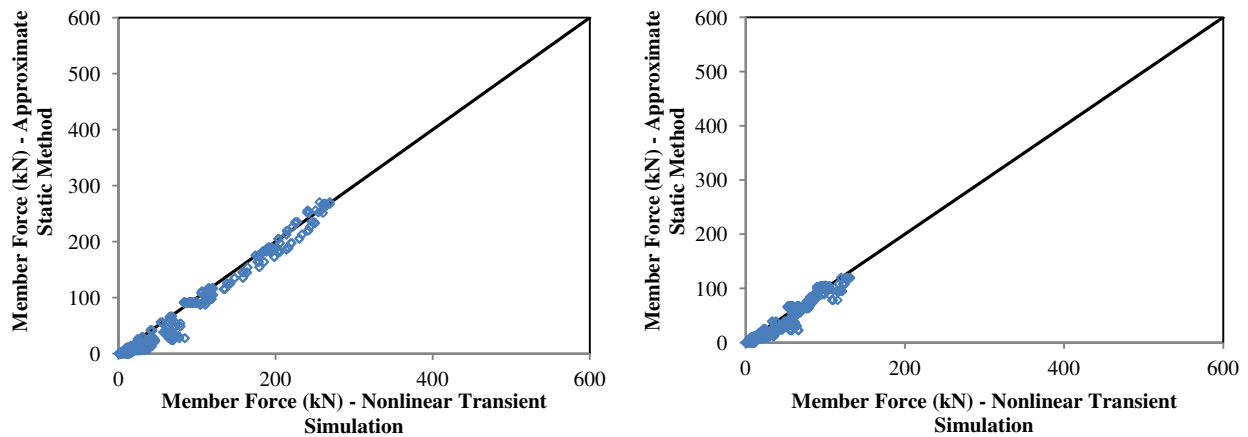


**Figure III.8.** Dispersion diagrams comparing member axial forces of delta guyed tower obtained from nonlinear transient analysis and from the proposed approximate static method under NGA 1787 record applied in transversal direction (left) and longitudinal direction (right).

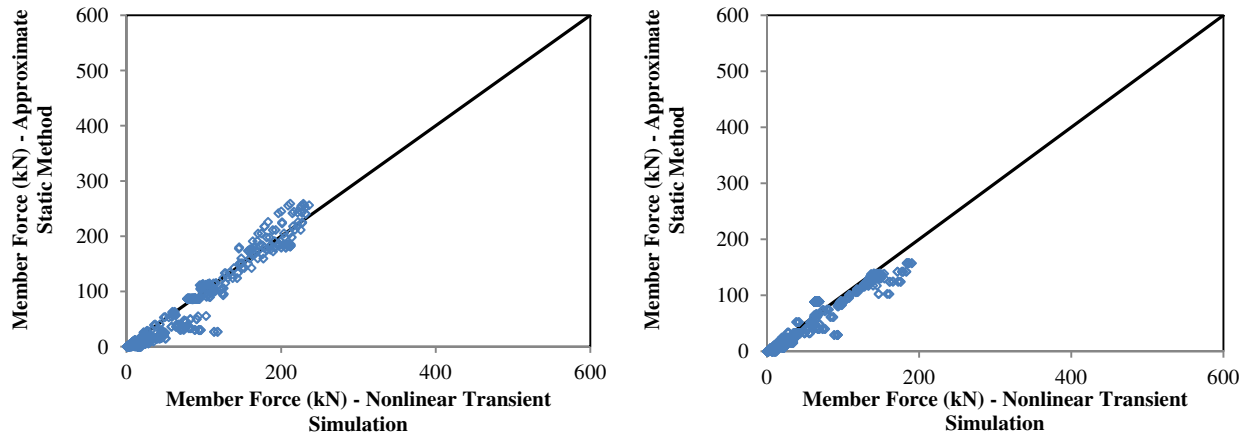


**Figure III.9.** Dispersion diagrams comparing member axial forces of delta guyed tower obtained from nonlinear transient analysis and from the proposed approximate static method under NGA 1794 applied in transversal direction (left) and longitudinal direction (right).

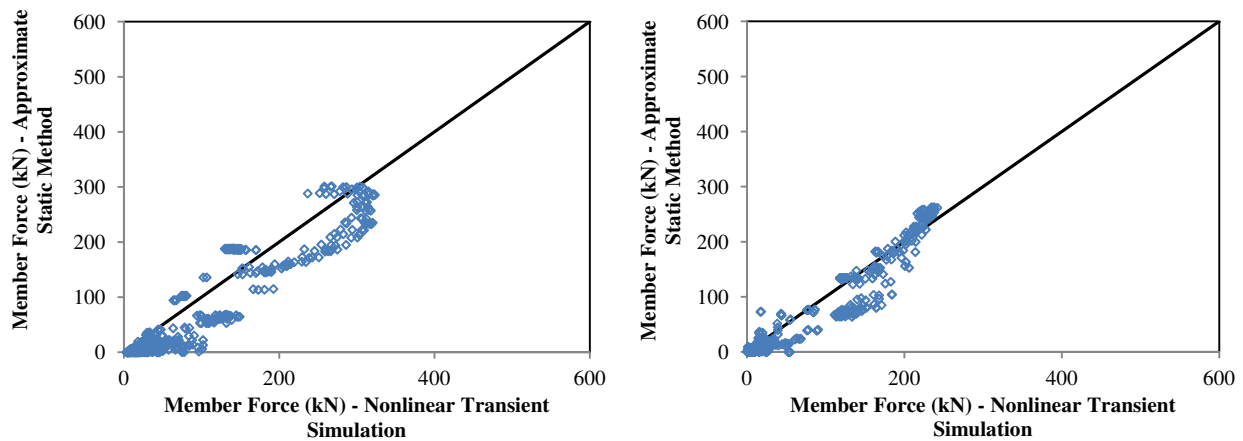


**Figure III.10.** Dispersion diagrams comparing member axial forces of mast guyed tower obtained from nonlinear transient analysis and from the proposed approximate static method under NGA 57 applied in transversal direction (left) and longitudinal direction (right).

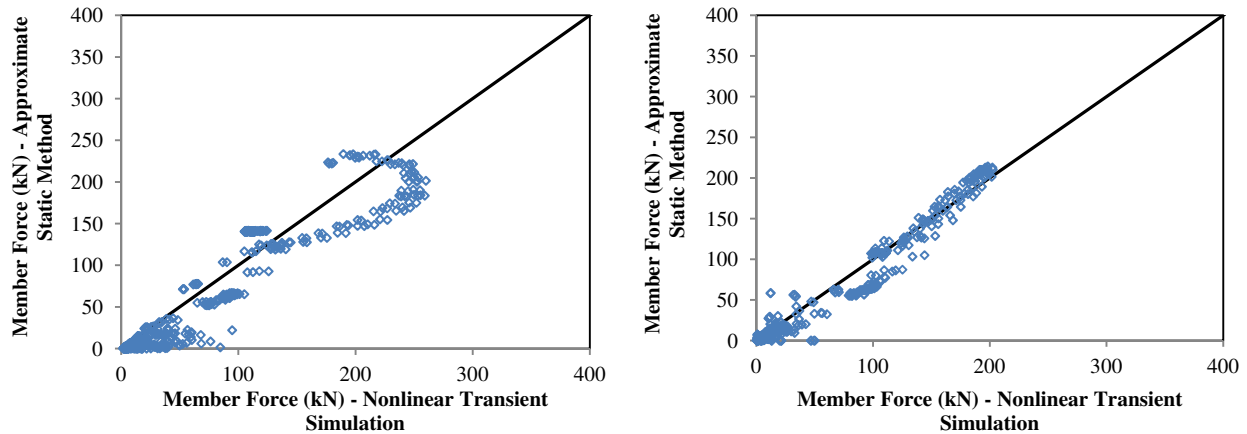


**Figure III.11.** Dispersion diagrams comparing member axial forces of mast guyed tower obtained from nonlinear transient analysis and from the proposed approximate static method under NGA 174 record applied in transversal direction (left) and longitudinal direction (right).

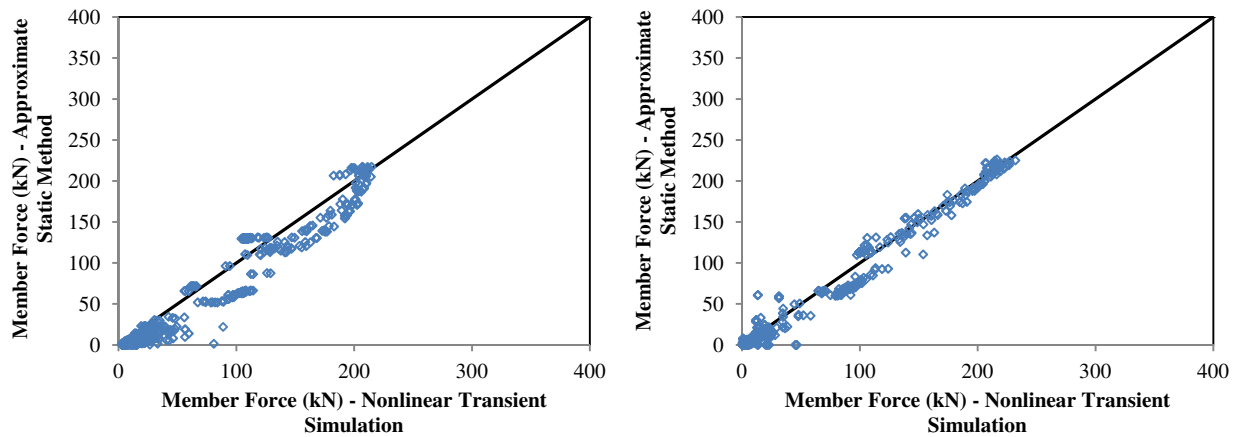


**Figure III.12.** Dispersion diagrams comparing member axial forces of mast guyed tower obtained from nonlinear transient analysis and from the proposed approximate static method under NGA 721 record applied in transversal direction (left) and longitudinal direction (right).

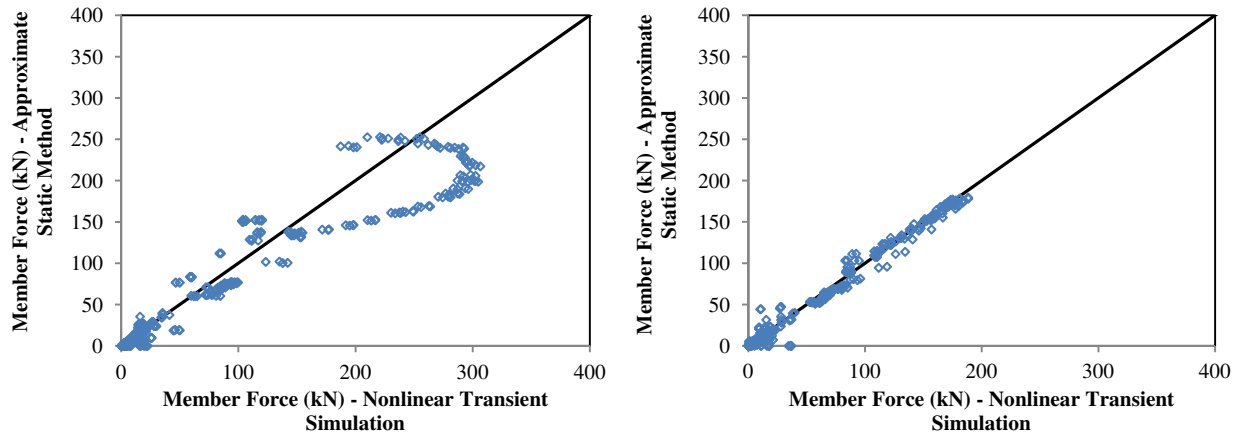


**Figure III.13.** Dispersion diagrams comparing member axial forces of mast guyed tower obtained from nonlinear transient analysis and from the proposed approximate static method under NGA 766 record applied in transversal direction (left) and longitudinal direction (right).

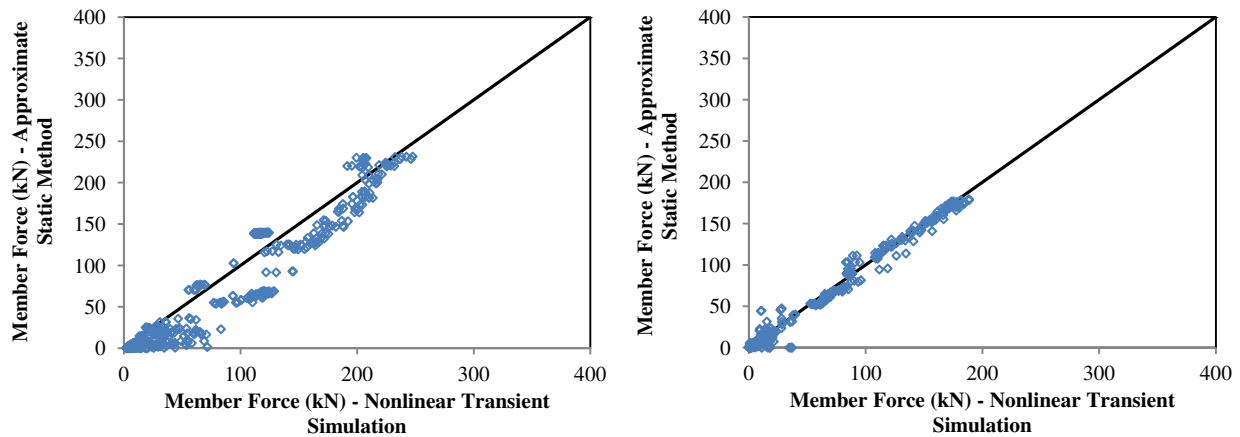


**Figure III.14.** Dispersion diagrams comparing member axial forces of mast guyed tower obtained from nonlinear transient analysis and from the proposed approximate static method under NGA 776 record applied in transversal direction (left) and longitudinal direction (right).

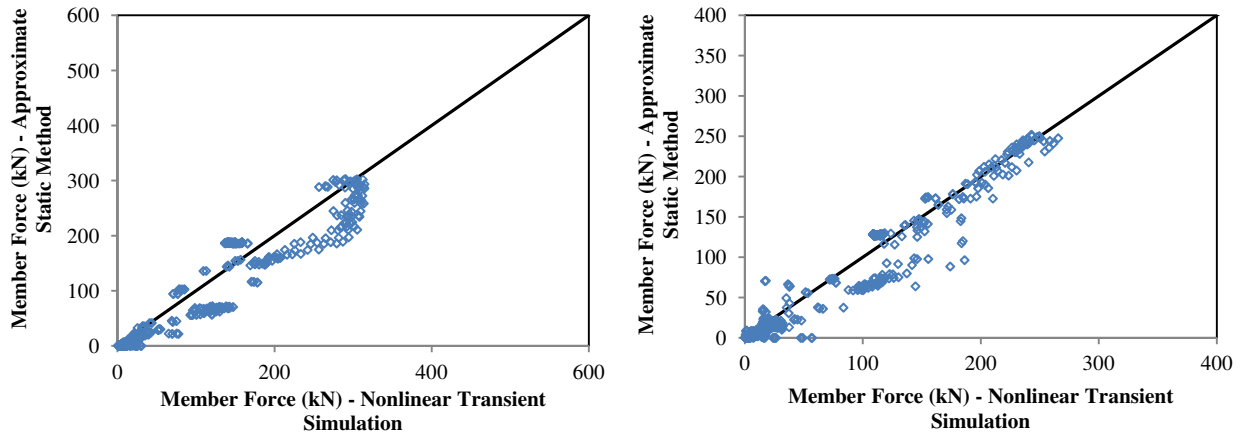


**Figure III.15.** Dispersion diagrams comparing member axial forces of mast guyed tower obtained from nonlinear transient analysis and from the proposed approximate static method under NGA 848 record applied in transversal direction (left) and longitudinal direction (right).

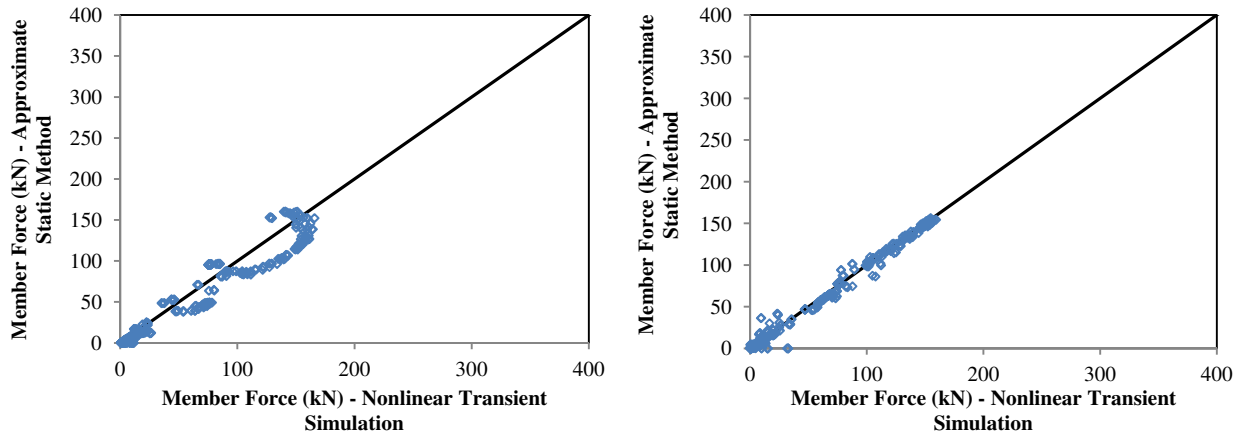


**Figure III.16.** Dispersion diagrams comparing member axial forces of mast guyed tower obtained from nonlinear transient analysis and from the proposed approximate static method under NGA 1006 record applied in transversal direction (left) and longitudinal direction (right).

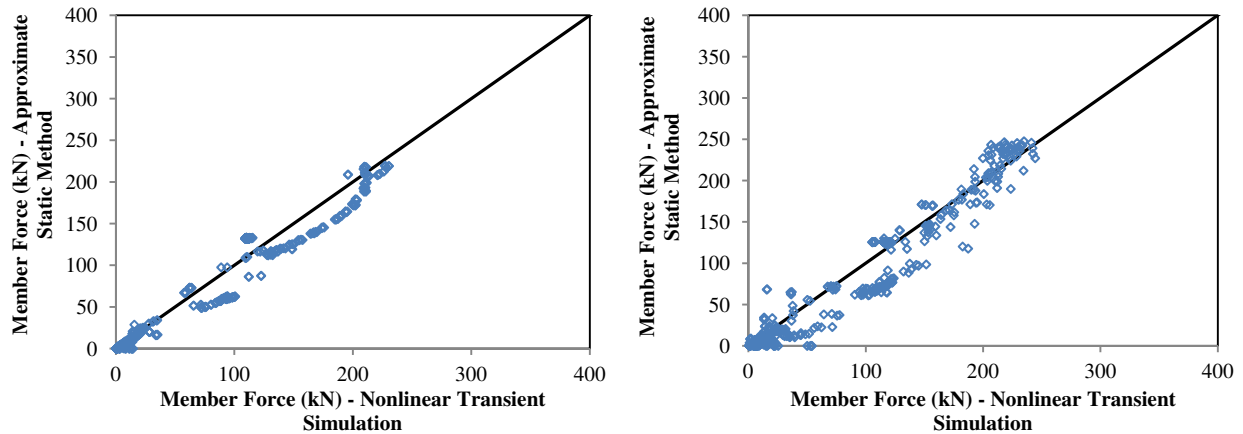


**Figure III.17.** Dispersion diagrams comparing member axial forces of mast guyed tower obtained from nonlinear transient analysis and from the proposed approximate static method under NGA 1787 record applied in transversal direction (left) and longitudinal direction (right).

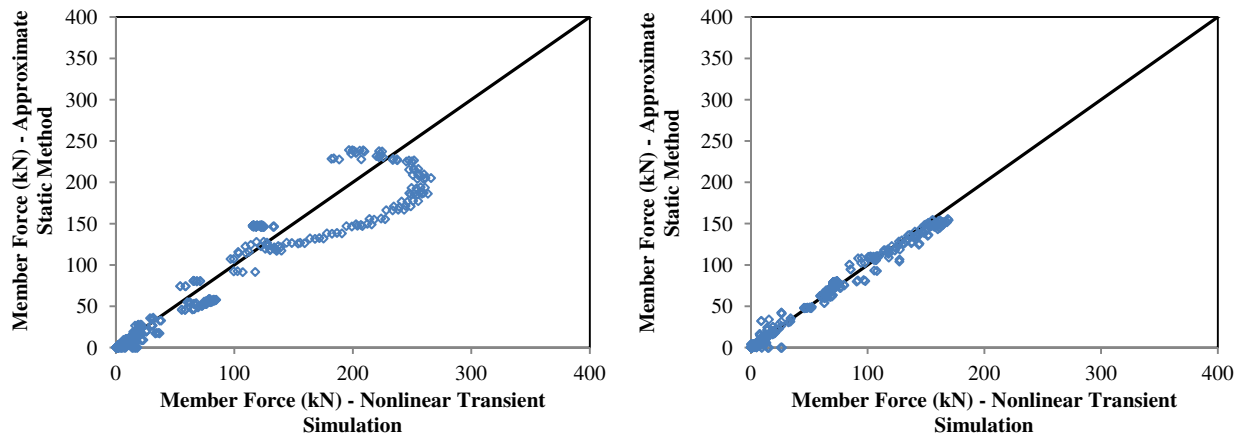


**Figure III.18.** Dispersion diagrams comparing member axial forces of mast guyed tower obtained from nonlinear transient analysis and from the proposed approximate static method under NGA 1794 record applied in transversal direction (left) and longitudinal direction (right).

## APPENDIX IV

## RESULTS OF SEISMIC ANALYSES OF COUPLED TOWER-CONDUCTOR SYSTEM

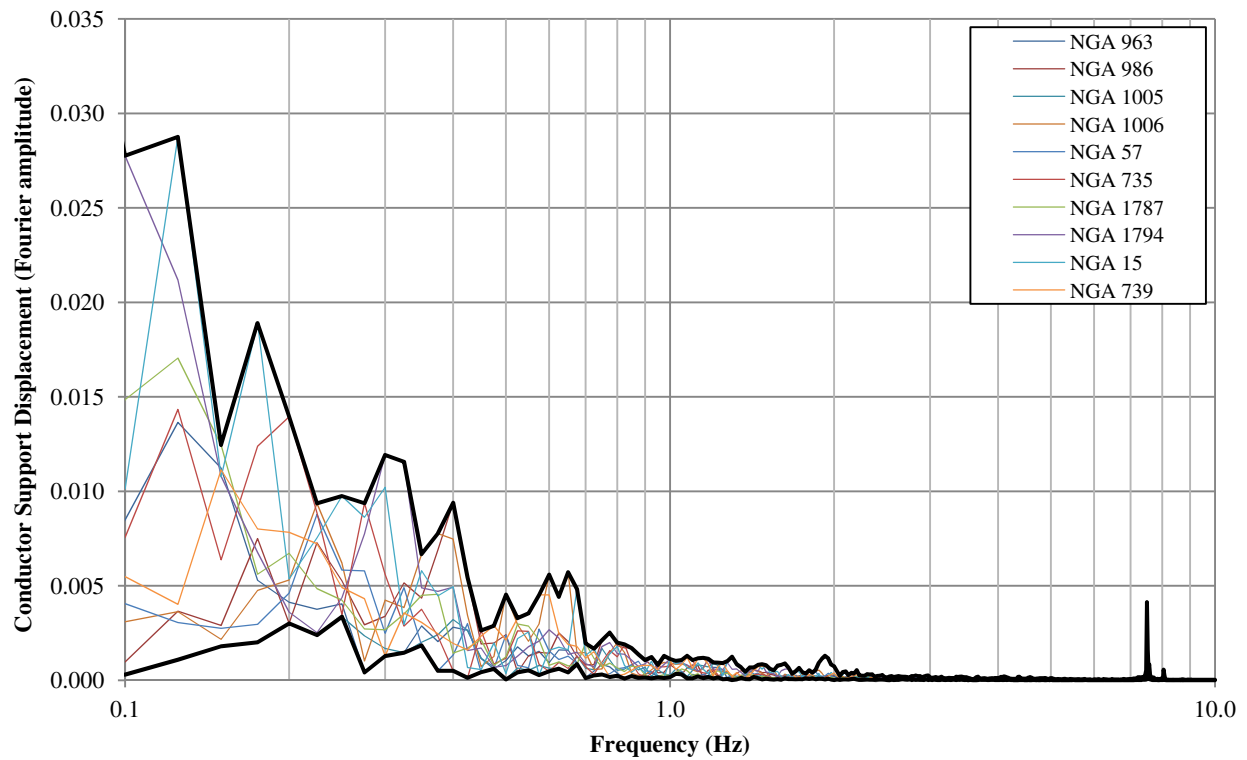


**Figure IV.1. Fourier response spectra of conductor support displacement in the vertical direction for all studied earthquake ground motions. Delta Self-supporting tower.**

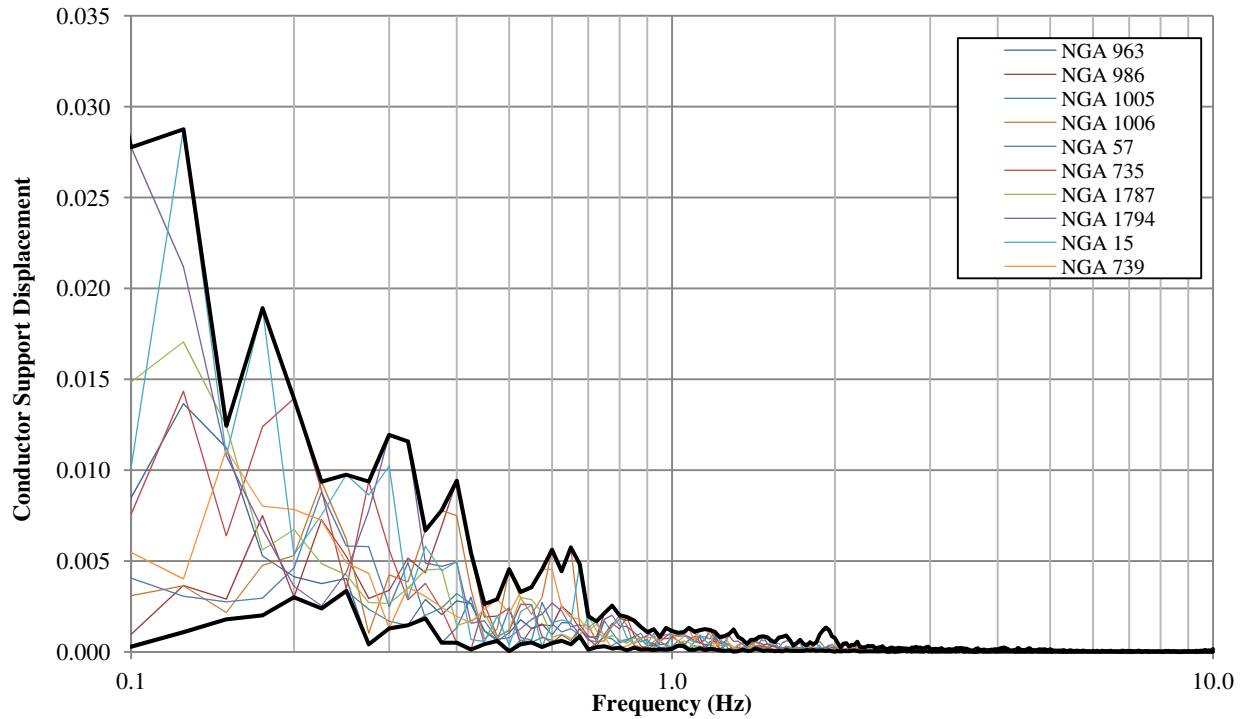


**Figure IV.2.** Fourier response spectra of conductor support displacement in the vertical direction for all studied earthquake ground motions. Delta guyed tower.

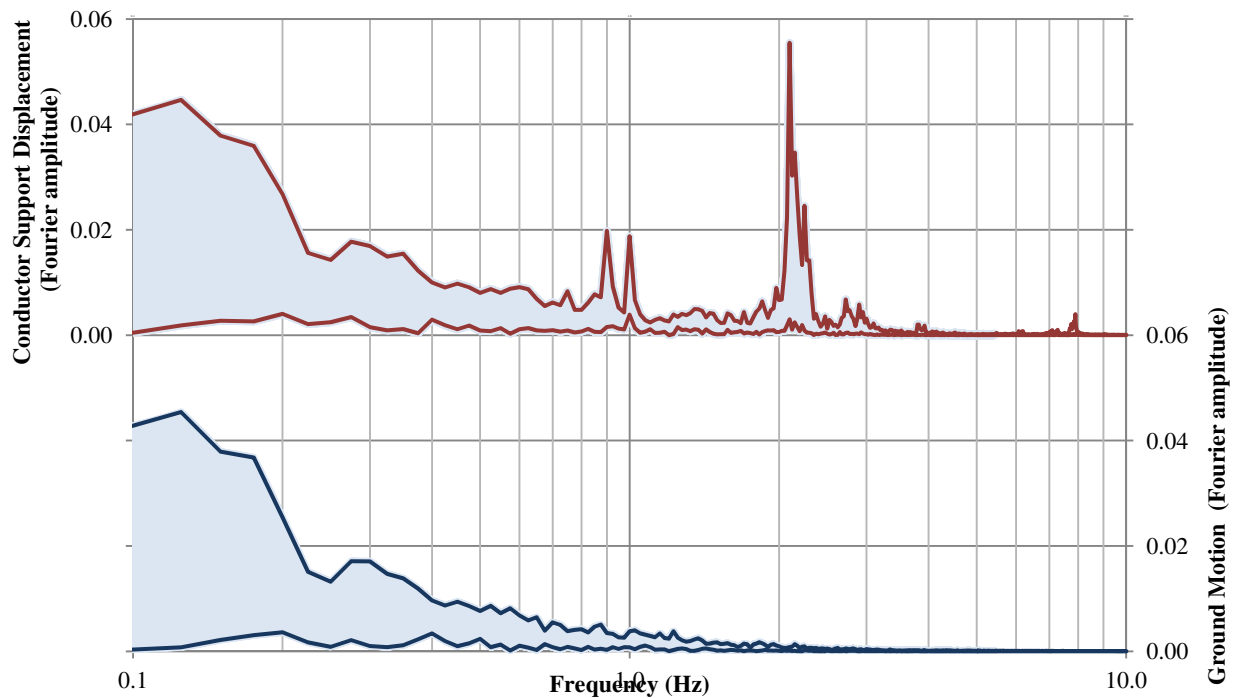


**Figure IV.3.** Envelope curves of Fourier response spectra of conductor support displacement (top) and earthquake ground motion base displacement (bottom). Mast guyed tower.

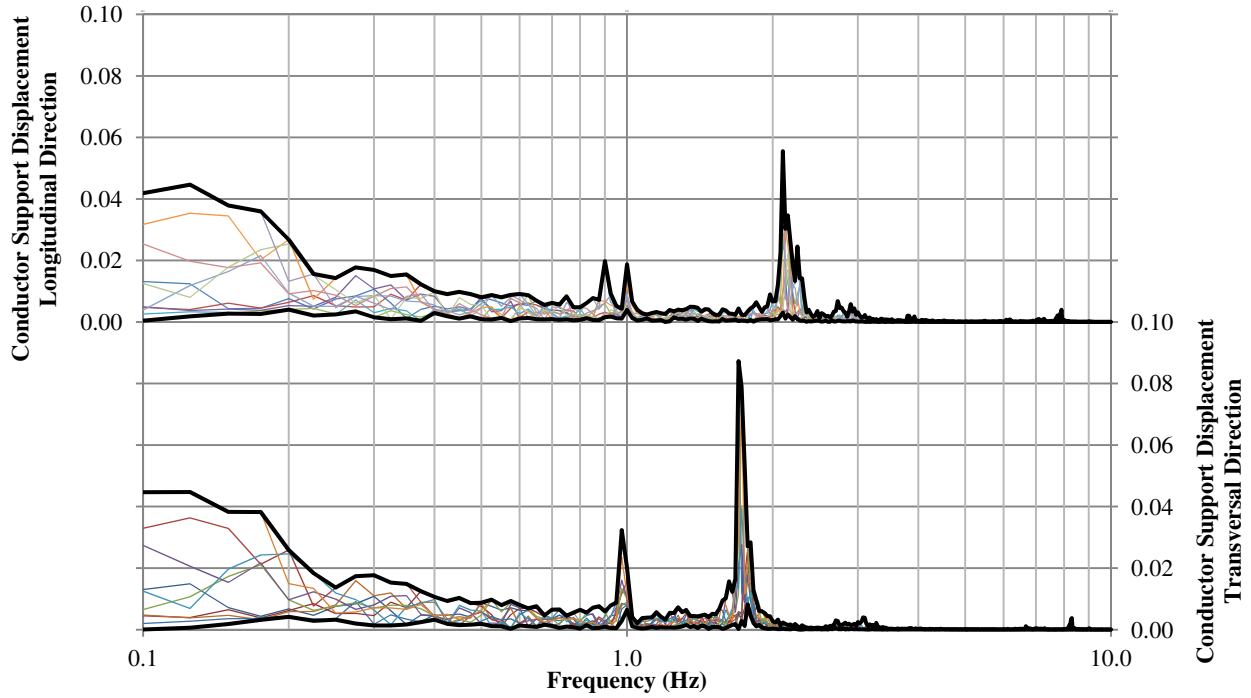


**Figure IV.4. Fourier response spectra of conductor support displacement in the longitudinal direction (top) and in the transversal direction (bottom) for all studied earthquake ground motions. Mast guyed tower.**

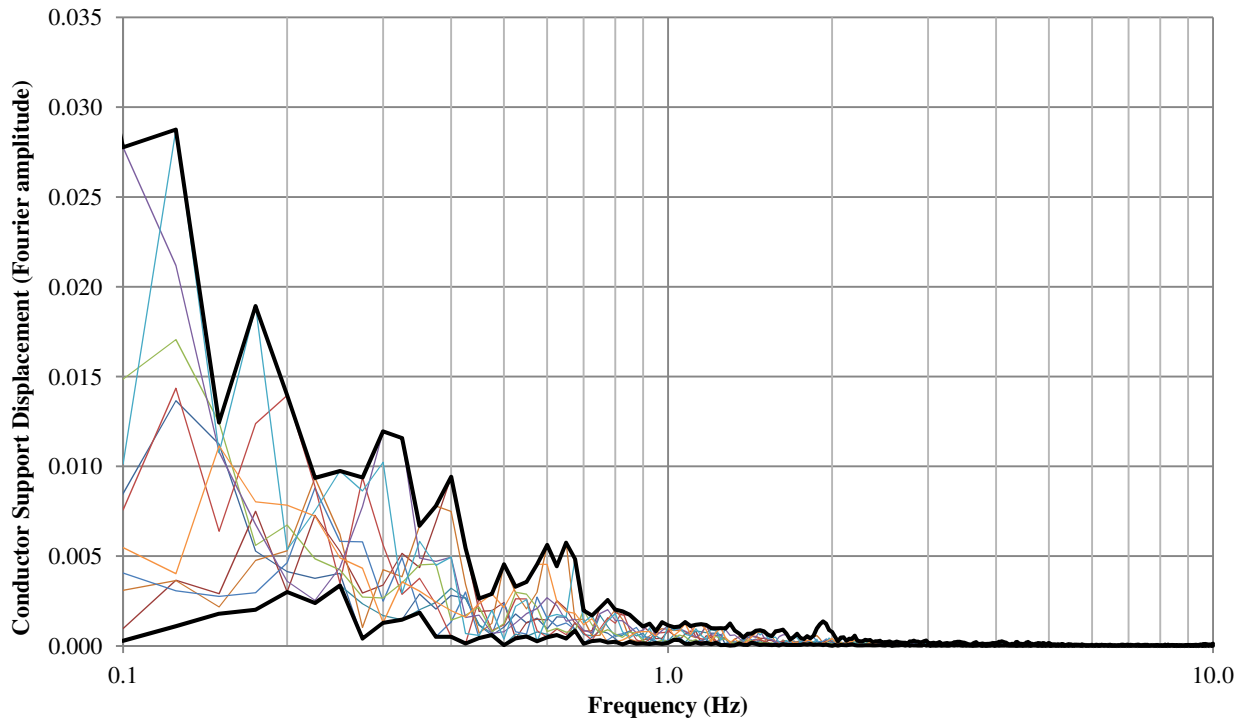


**Figure IV.5. FOURIER response spectra of conductor support displacement in the vertical direction for all studied earthquake ground motions. Mast guyed tower.**

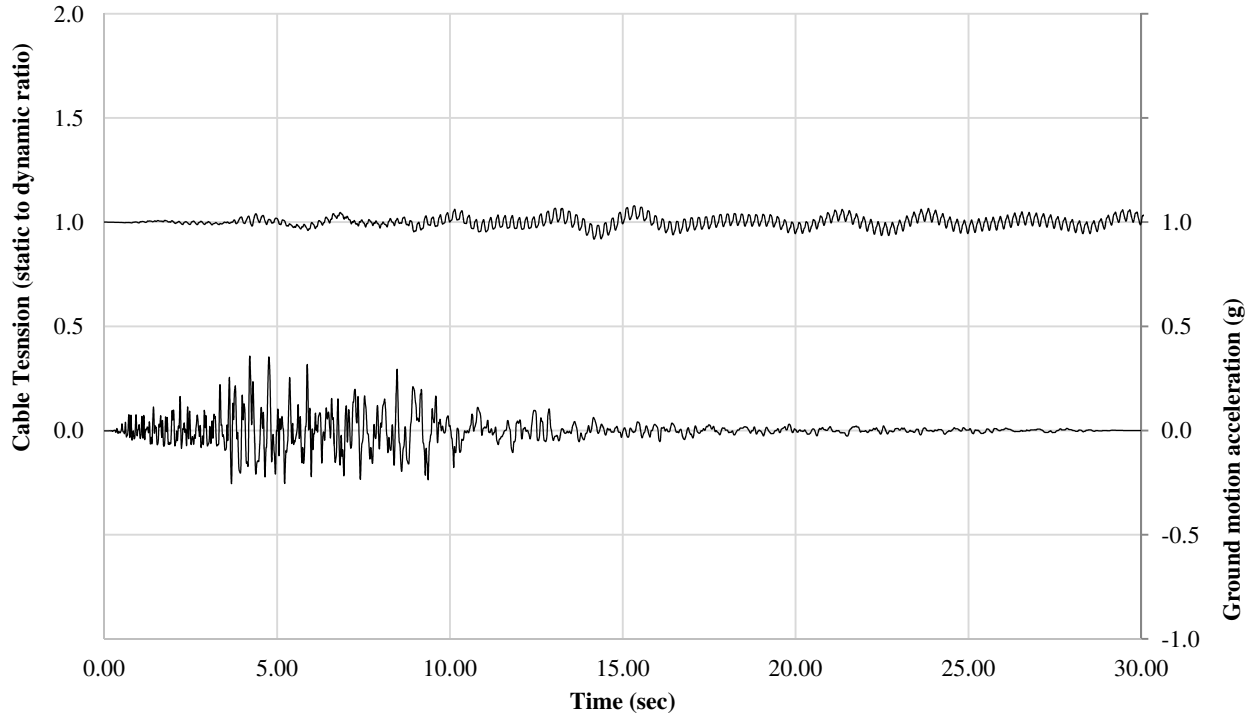


**Figure IV.6. Time-history of conductor cable tension ratio under NGA 953 applied in vertical direction. Scenario “A”: seismic motion at one of the supporting nodes.**

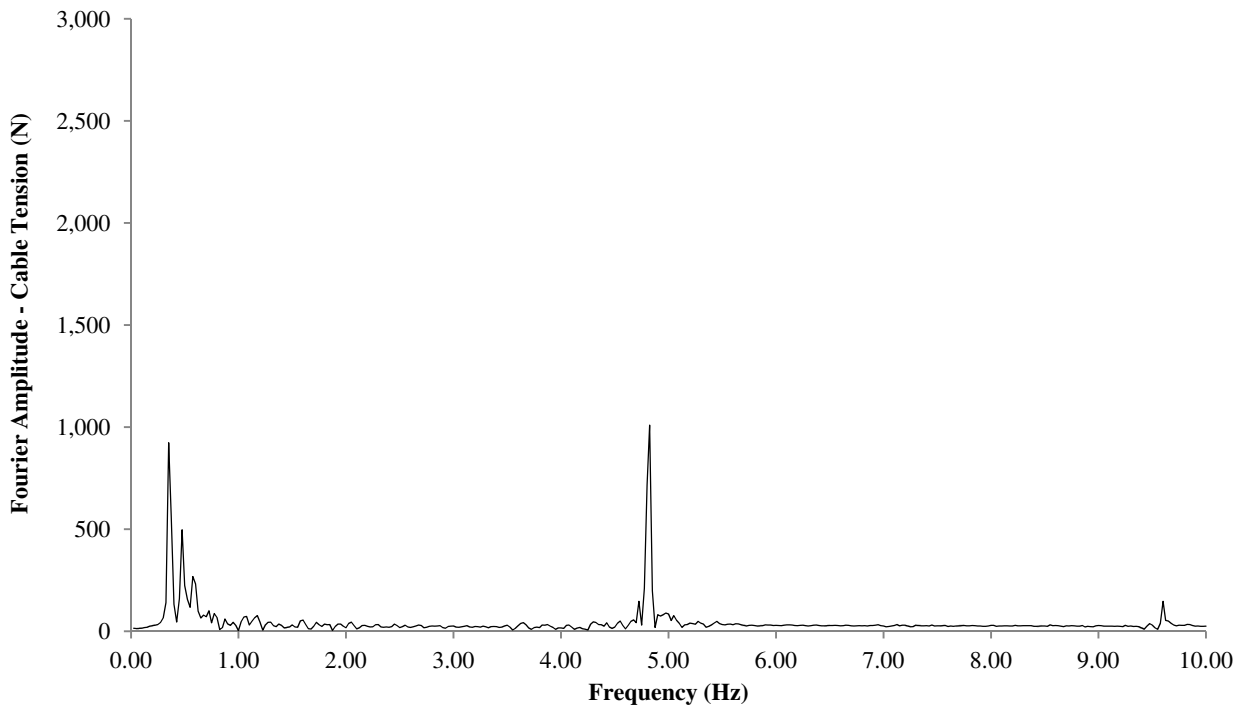


**Figure IV.7. Fourier response spectra of conductor cable tension under NGA 953 applied in vertical direction. Scenario “A”: seismic motion at one of the supporting nodes.**

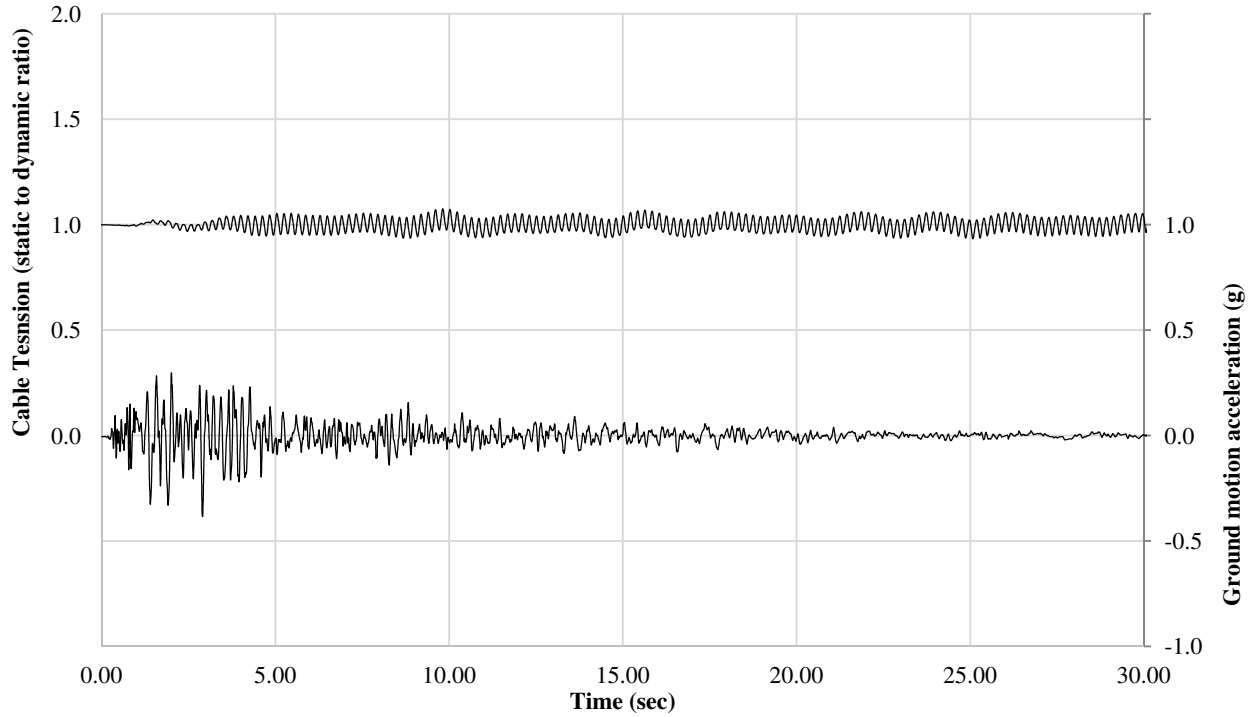


**Figure IV.8. Time-history of conductor cable tension ratio under NGA 57 applied in vertical direction. Scenario “A”:** seismic motion at one of the supporting nodes.

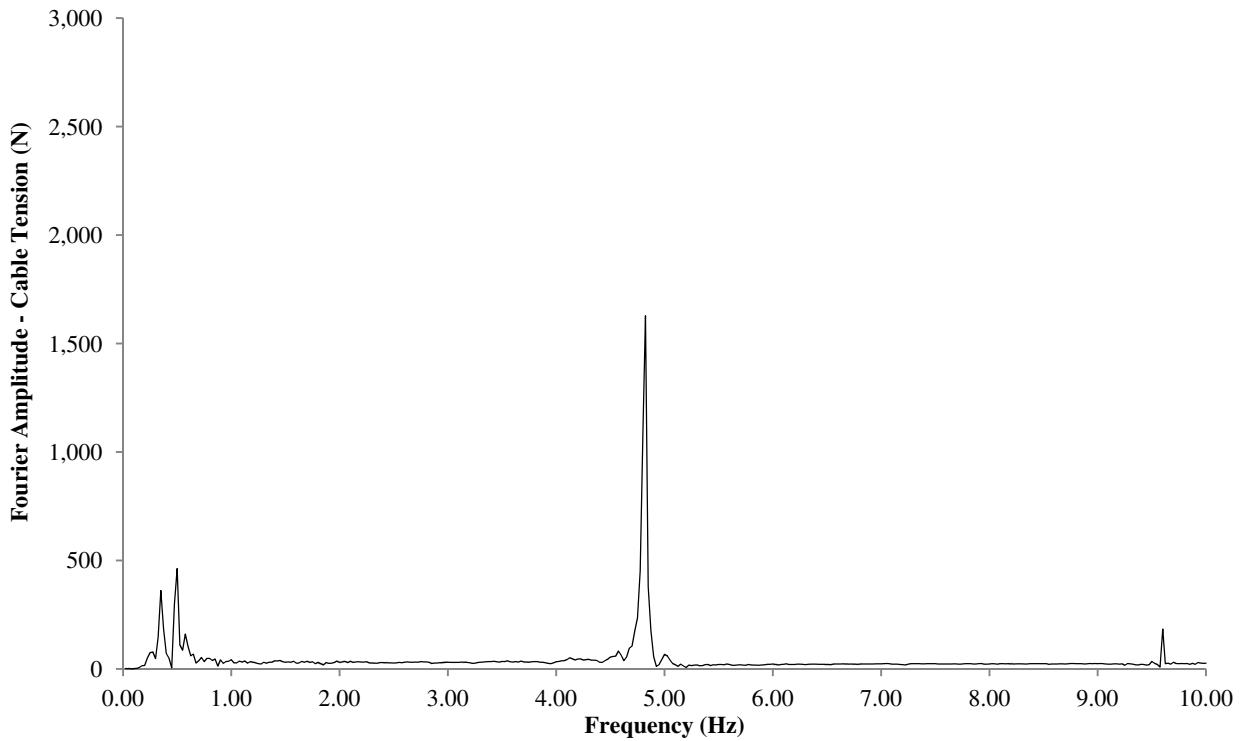


**Figure IV.9. Fourier response spectra of conductor cable tension under NGA 57 applied in vertical direction. Scenario “A”:** seismic motion at one of the supporting nodes.

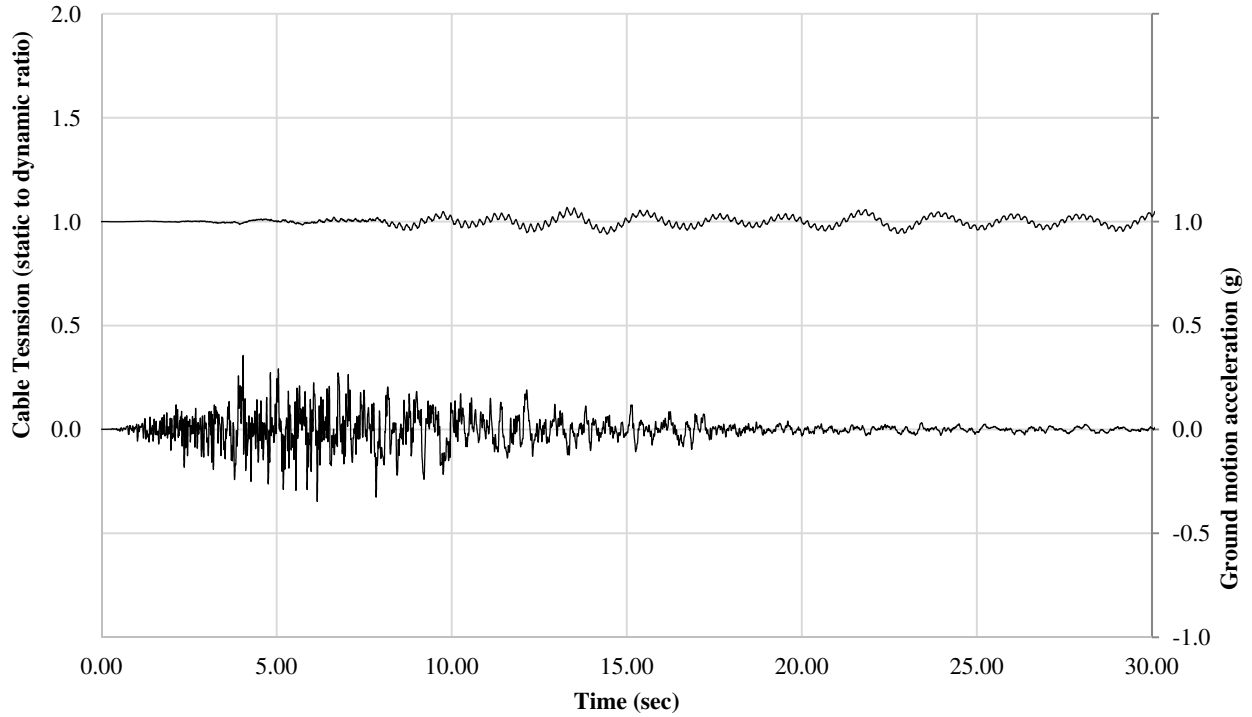


**Figure IV.10. Time-history of conductor cable tension ratio under NGA 739 applied in vertical direction. Scenario “A”: seismic motion at one of the supporting nodes.**

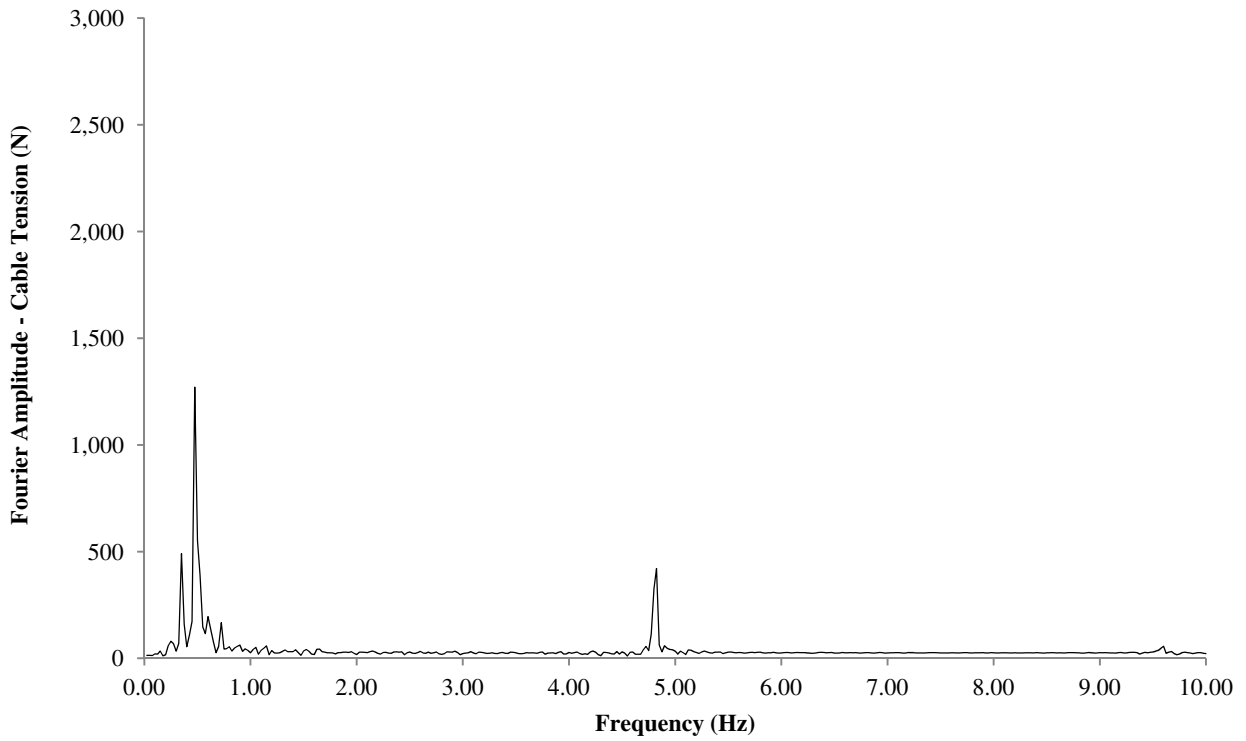


**Figure IV.11. Fourier response spectra of conductor cable tension under NGA 739 applied in vertical direction. Scenario “A”: seismic motion at one of the supporting nodes.**

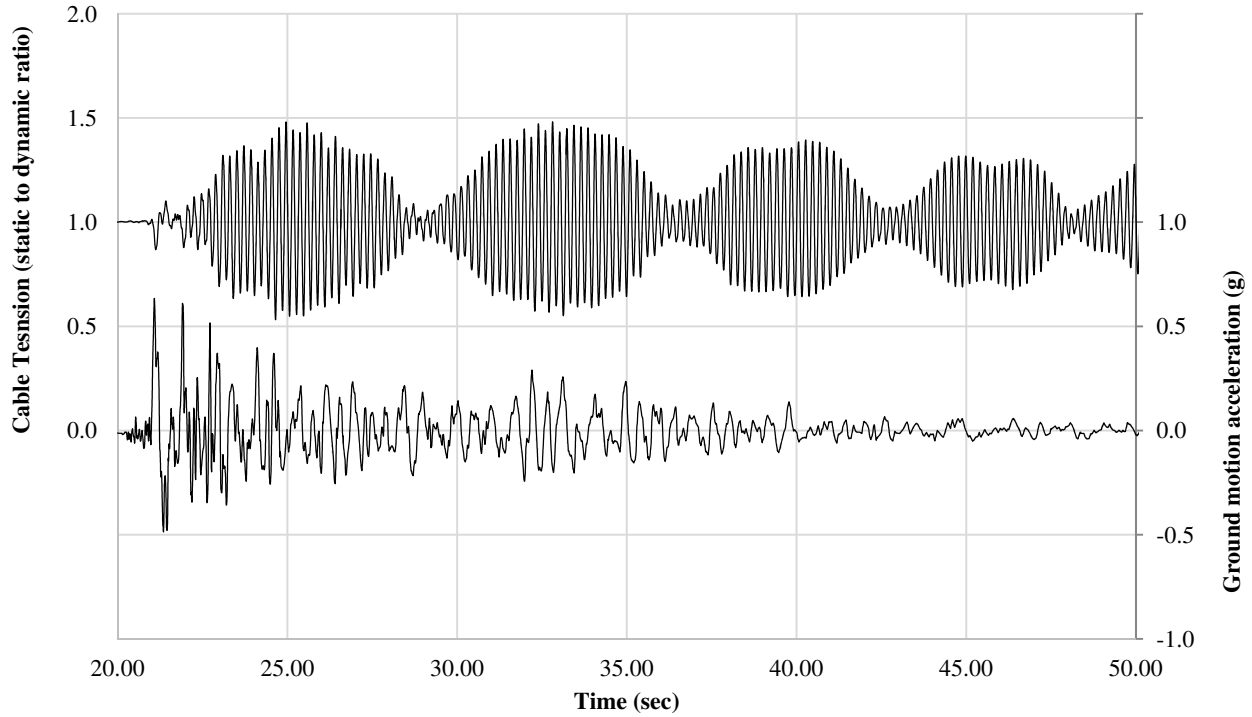


**Figure IV.12. Time-history of conductor cable tension ratio and NGA 57 record accelerogram in longitudinal direction. Scenario “B”: synchronous seismic motion on both supporting end nodes.**

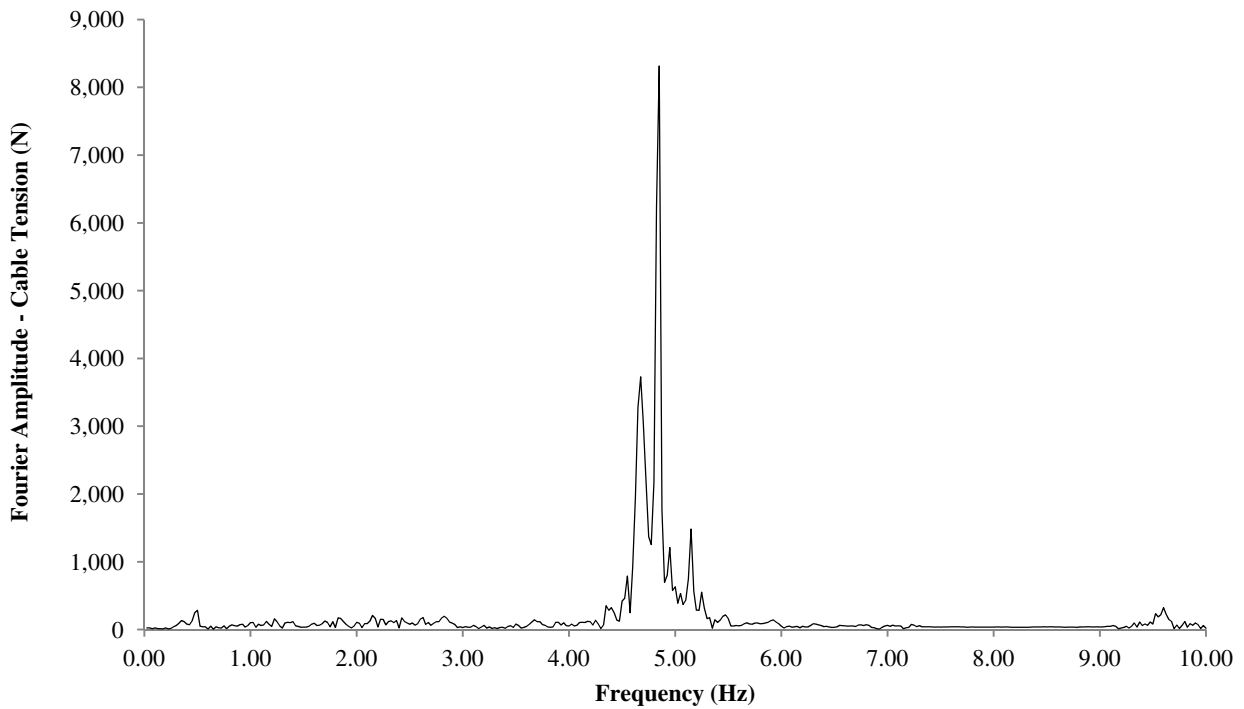


**Figure IV.13. Fourier response spectra of conductor cable tension under NGA 57 applied in longitudinal direction. Scenario “B”: synchronous seismic motion on both supporting end nodes.**

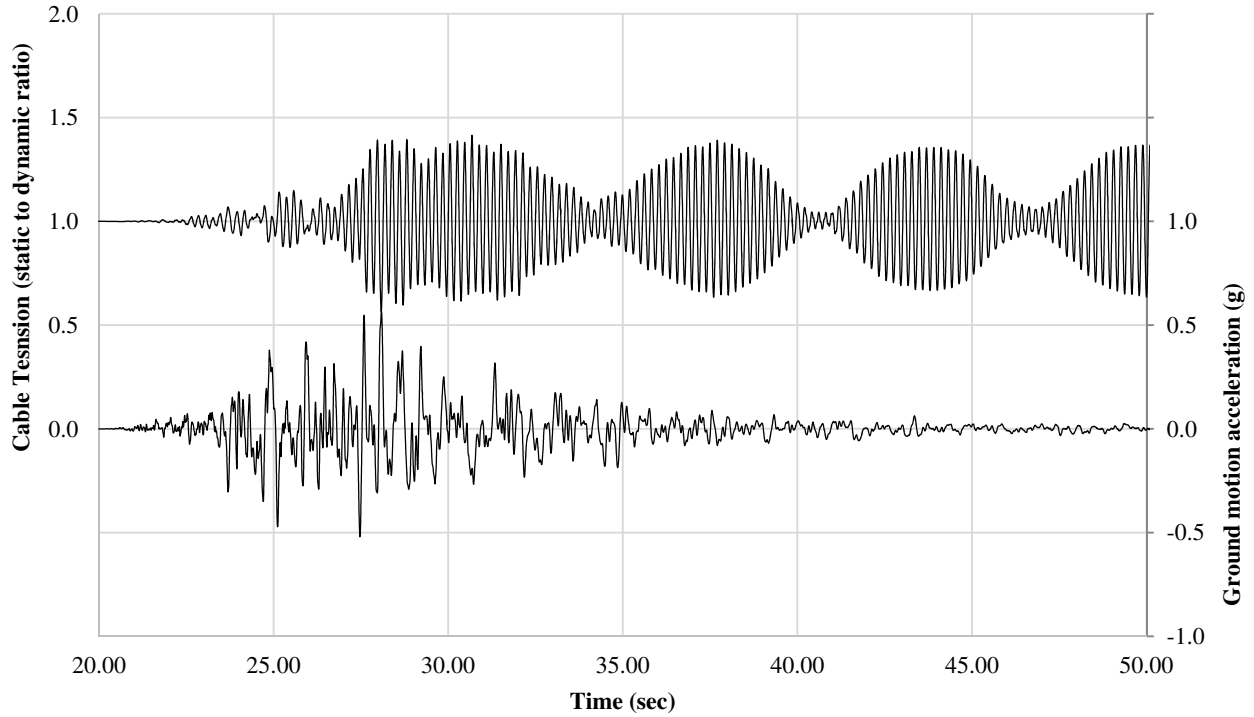


**Figure IV.14. Time-history of conductor cable tension ratio and NGA 739 record accelerogram in longitudinal direction. Scenario “B”:** synchronous seismic motion on both supporting end nodes.

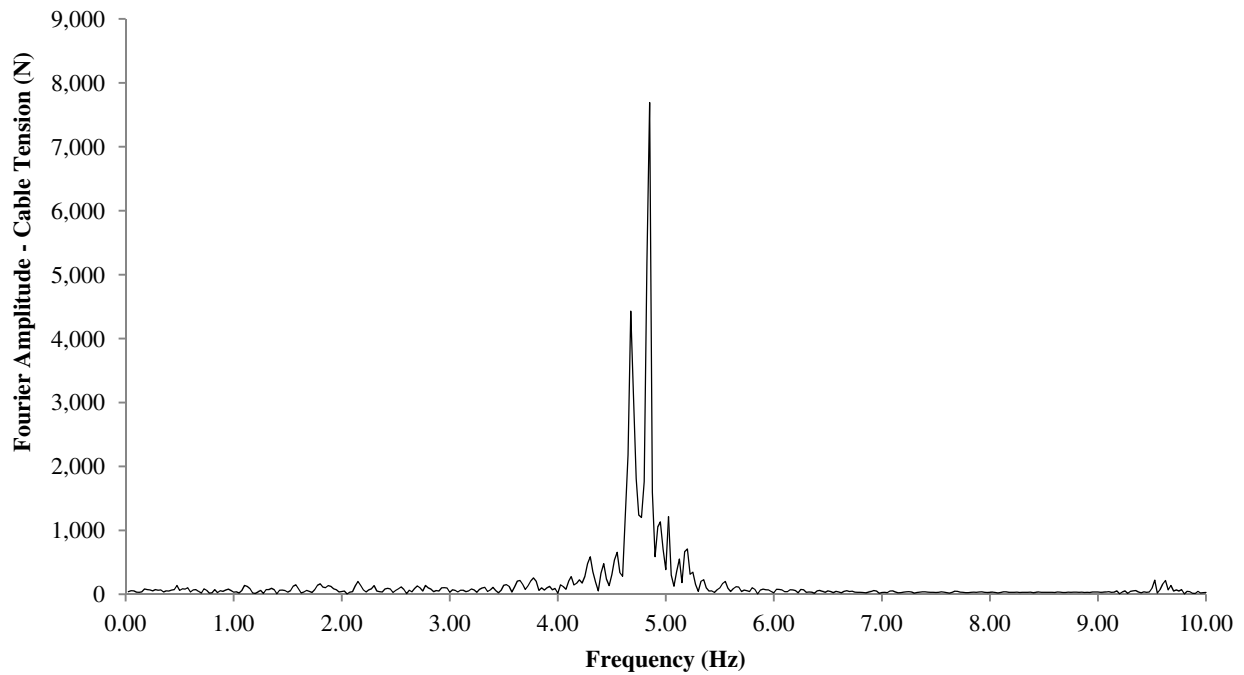


**Figure IV.15. Fourier response spectra of conductor cable tension under NGA 739 applied in longitudinal direction. Scenario “B”:** synchronous seismic motion on both supporting end nodes.

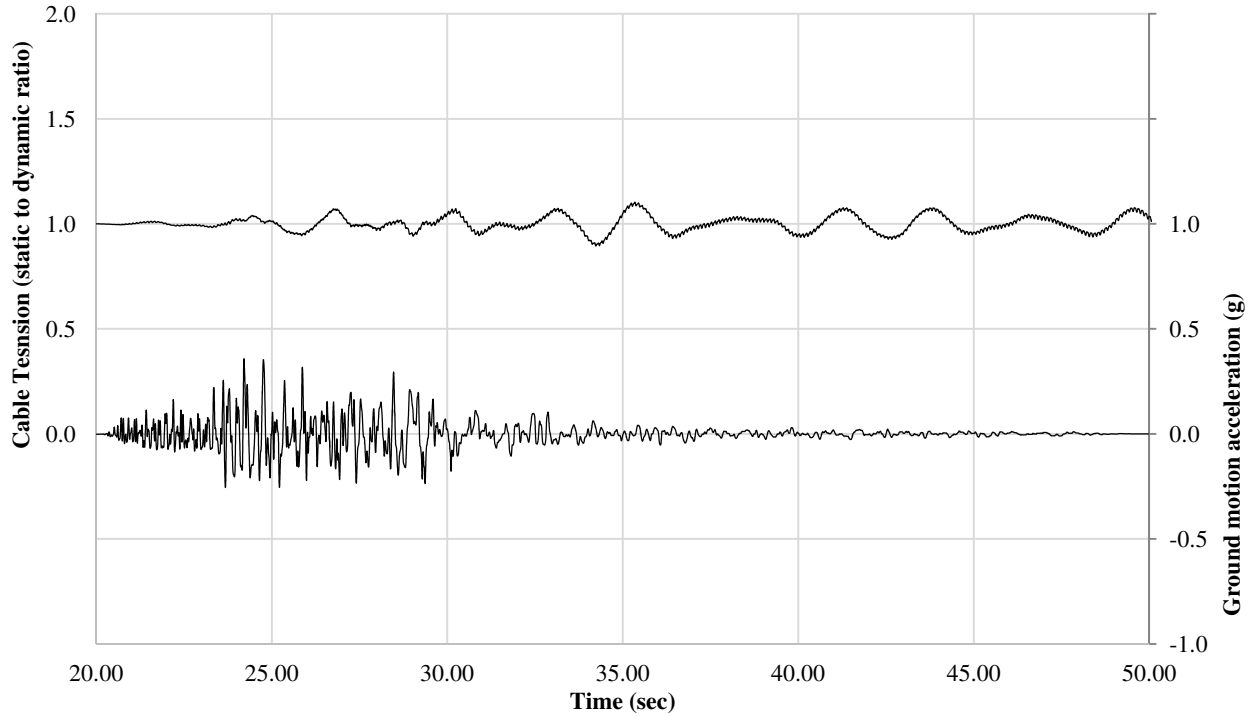


**Figure IV.16. Time-history of conductor cable tension ratio under NGA 953 record applied in vertical direction. Scenario “B”: synchronous seismic motion on both supporting end nodes.**

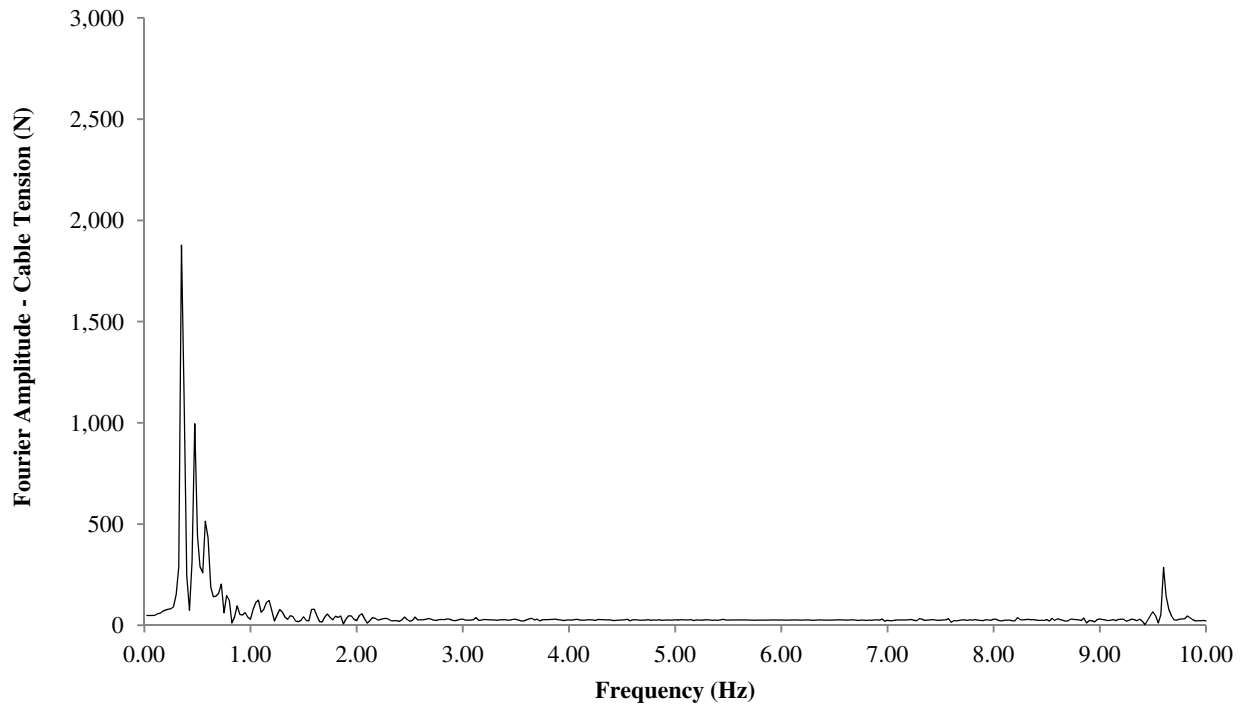


**Figure IV.17. Fourier response spectra of conductor cable tension under NGA 953 applied in vertical direction. Scenario “B”: synchronous seismic motion on both supporting end nodes.**

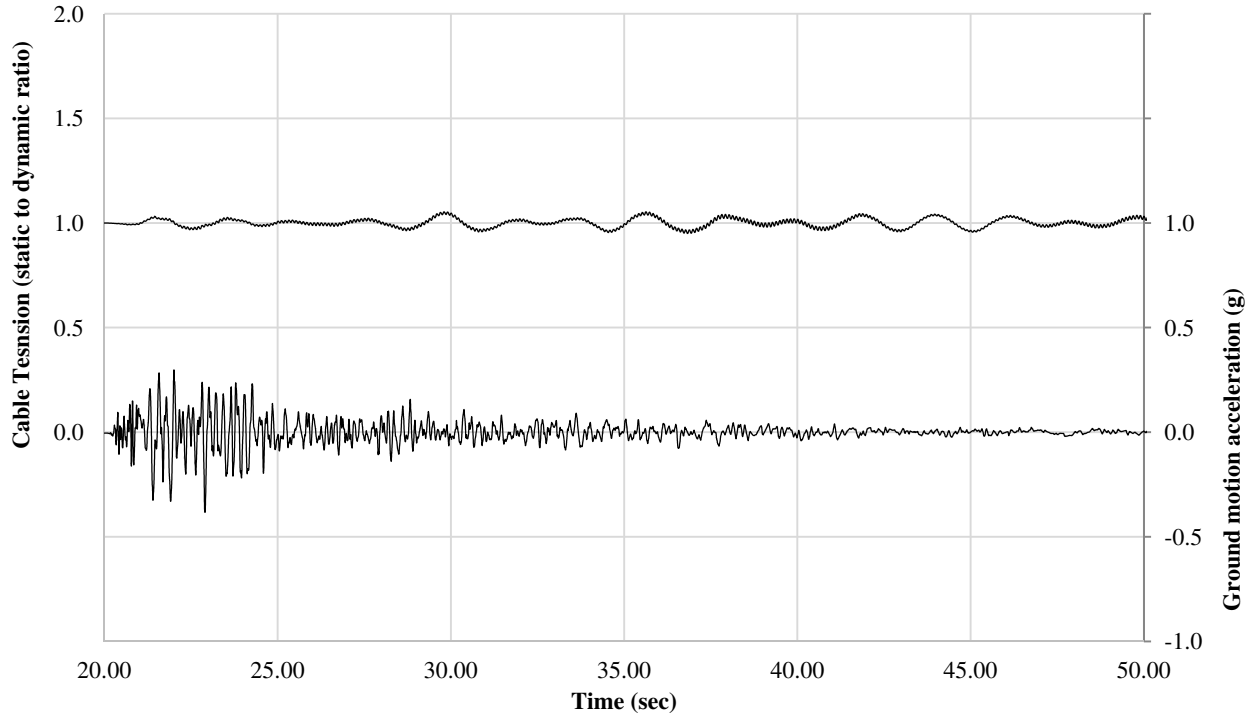


**Figure IV.18. Time-history of conductor cable tension ratio under NGA 57 applied in vertical direction. Scenario “B”: synchronous seismic motion on both supporting end nodes.**

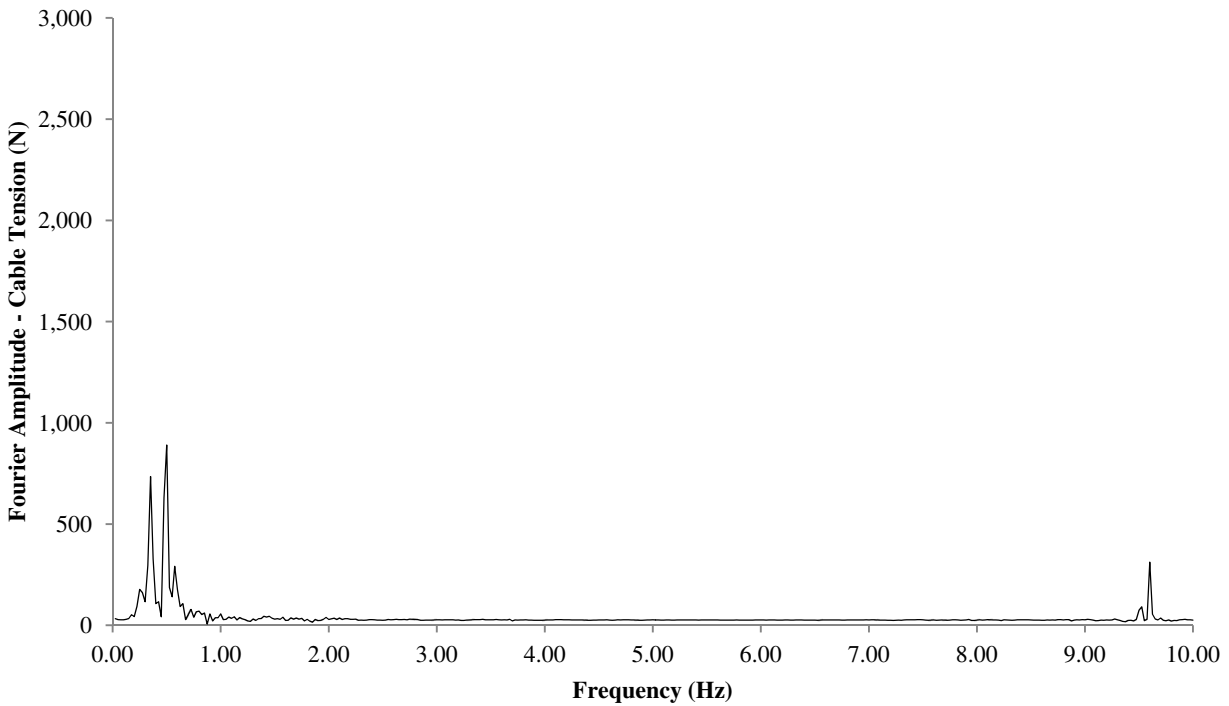


**Figure IV.19. Fourier response spectra of conductor cable tension under NGA 57 applied in vertical direction. Scenario “B”: synchronous seismic motion on both supporting end nodes.**

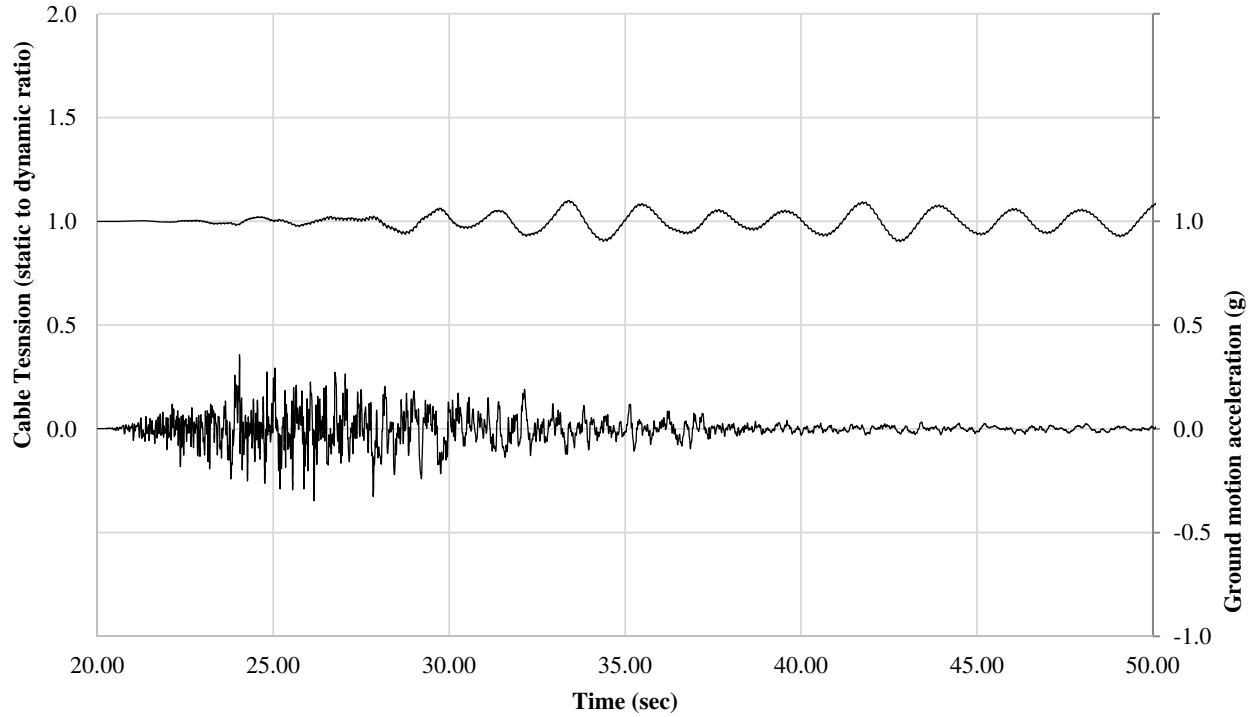


**Figure IV.20. Time-history of conductor cable tension ratio under NGA 739 applied in the vertical direction. Scenario “B”: synchronous seismic motion on both supporting end nodes.**

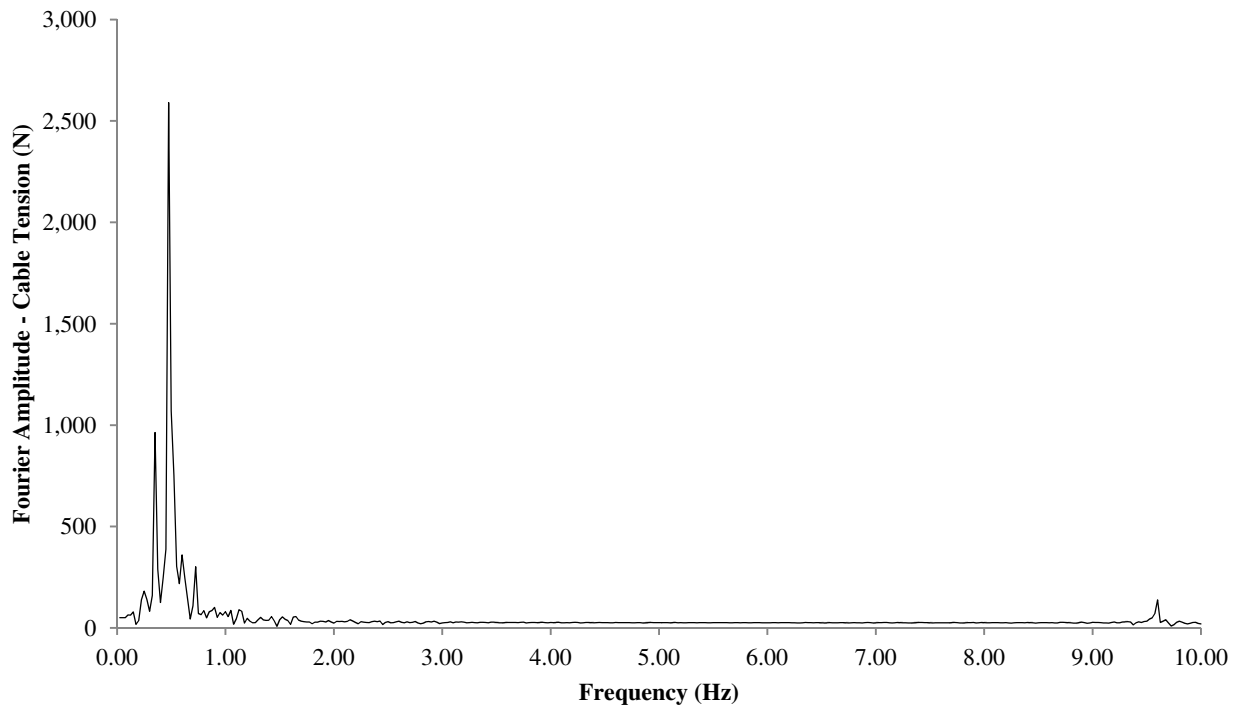


**Figure IV.21. Fourier response spectra of conductor cable tension under NGA 739 applied in the vertical direction. Scenario “B”: synchronous seismic motion on both supporting end nodes.**

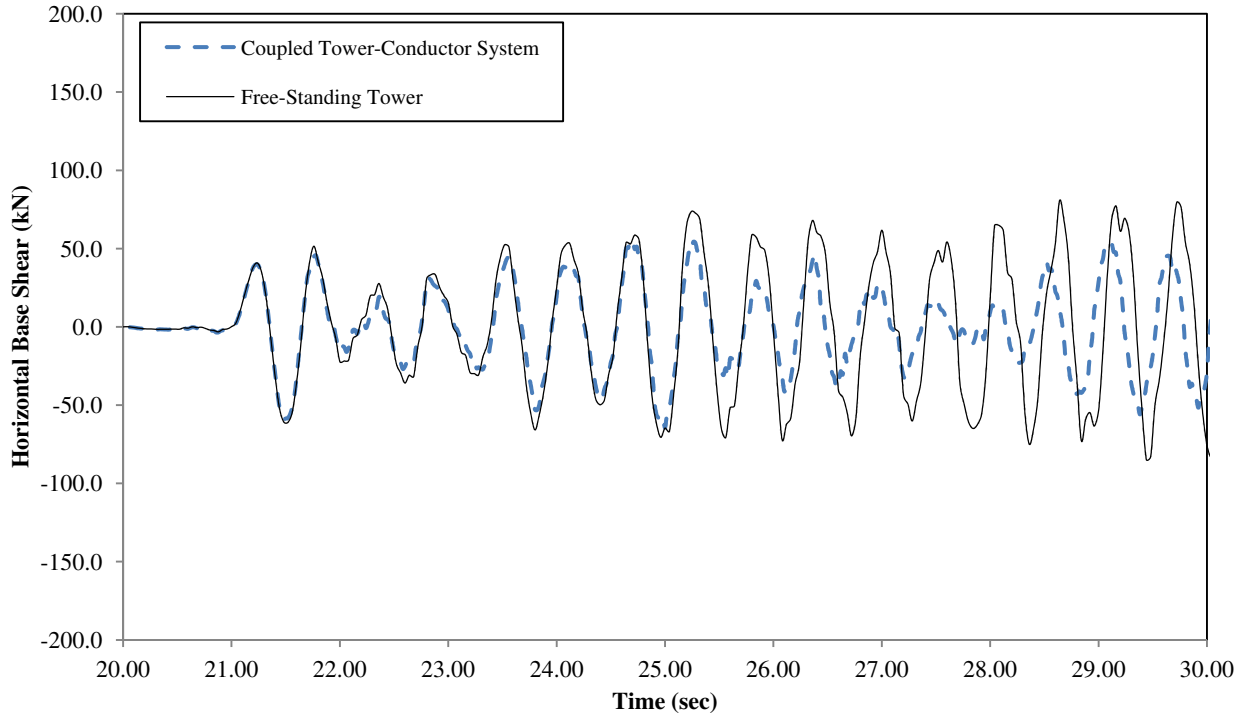


**Figure IV.22. Time-history of horizontal base shear of Free-Standing Delta Guyed Tower and Coupled Delta Guyed Tower-Conductor System. under NGA 57 applied in the transversal direction.**

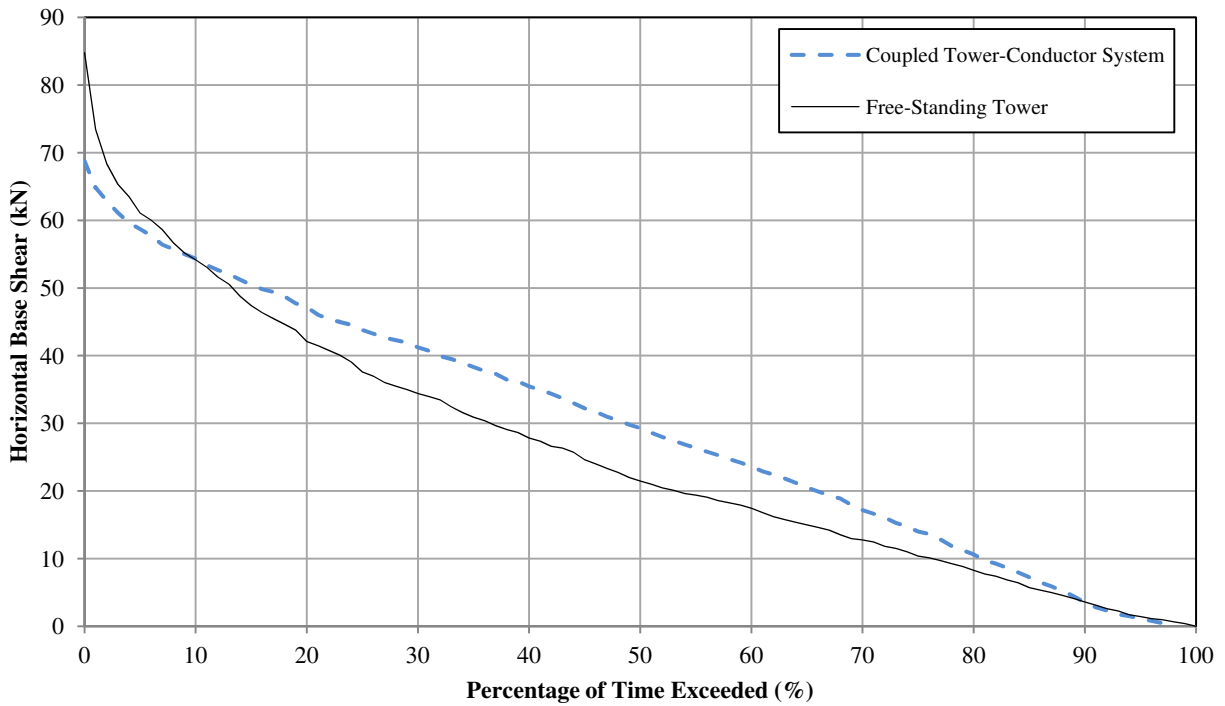


**Figure IV.23. Persistence curve of horizontal base shear time-history of Free-Standing Delta Guyed Tower and Coupled Delta Guyed Tower-Conductor System under NGA 57 applied in transversal direction.**

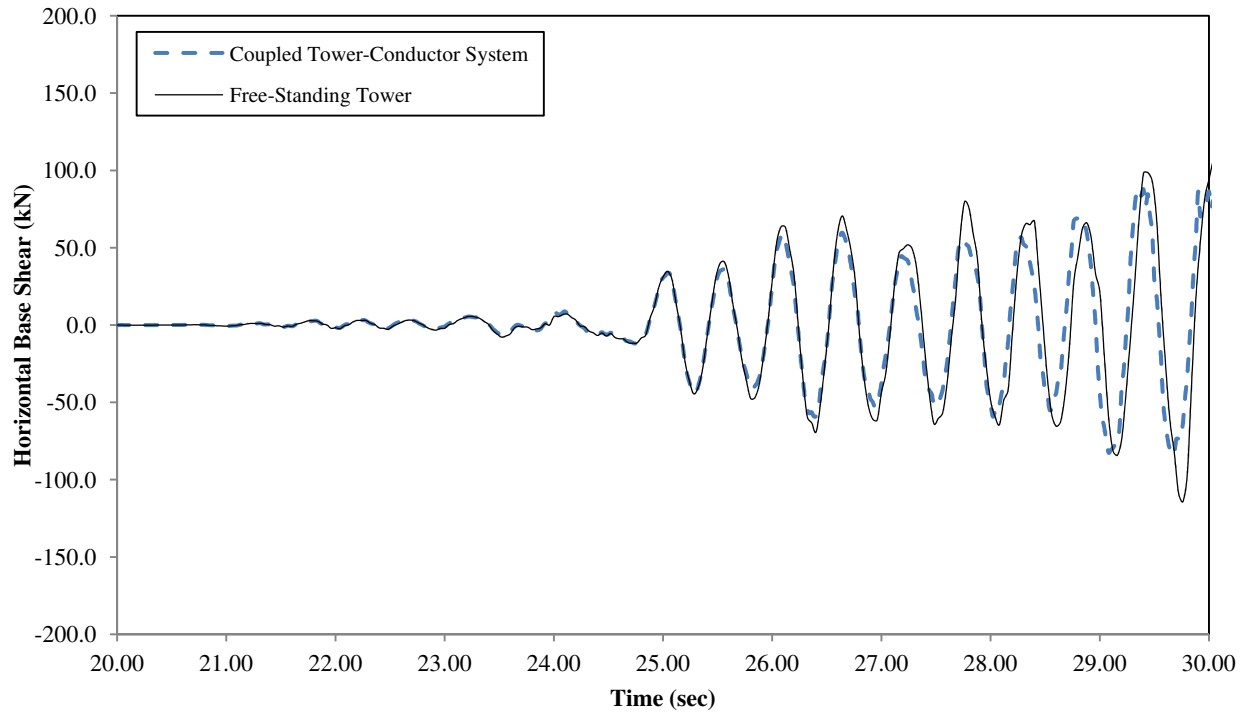


**Figure IV.24. Time-history of horizontal base shear of Free-Standing Delta Guyed Tower and Coupled Delta Guyed Tower-Conductor System under NGA 739 applied in transversal direction.**

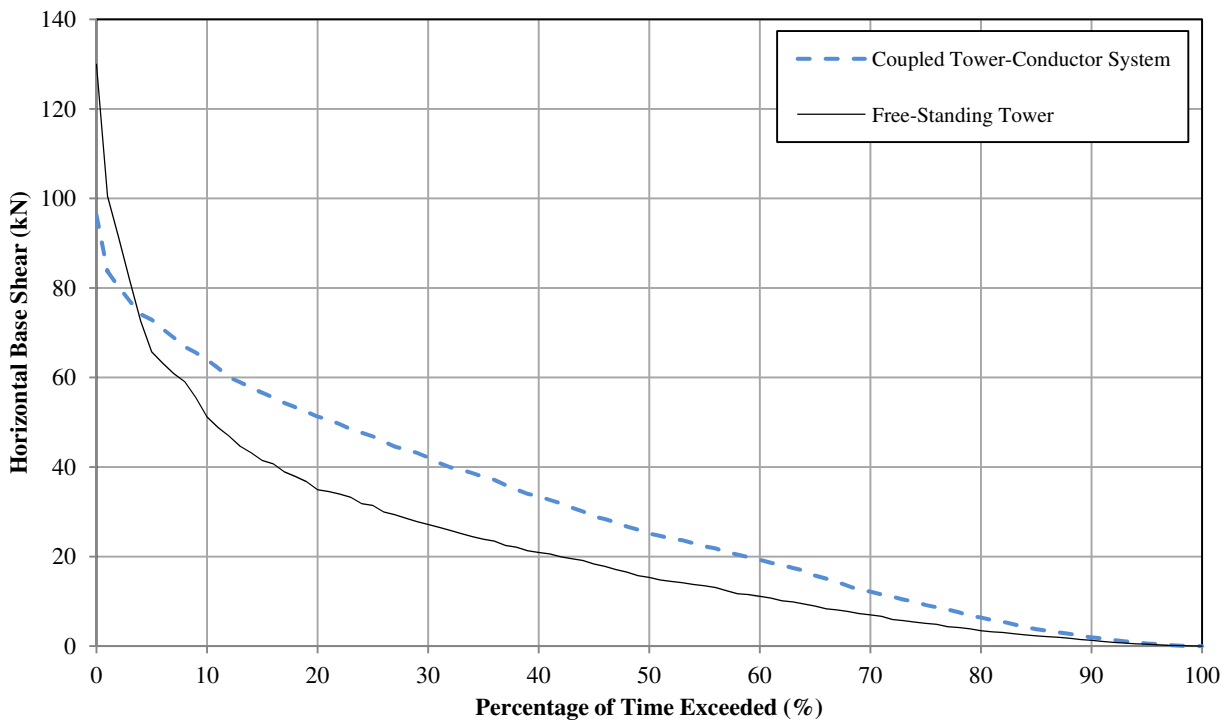


**Figure IV.25. Persistence curve of horizontal base shear time-history of Free-Standing Delta Guyed Tower and Coupled Delta Guyed Tower-Conductor System under NGA 739 applied in transversal direction.**

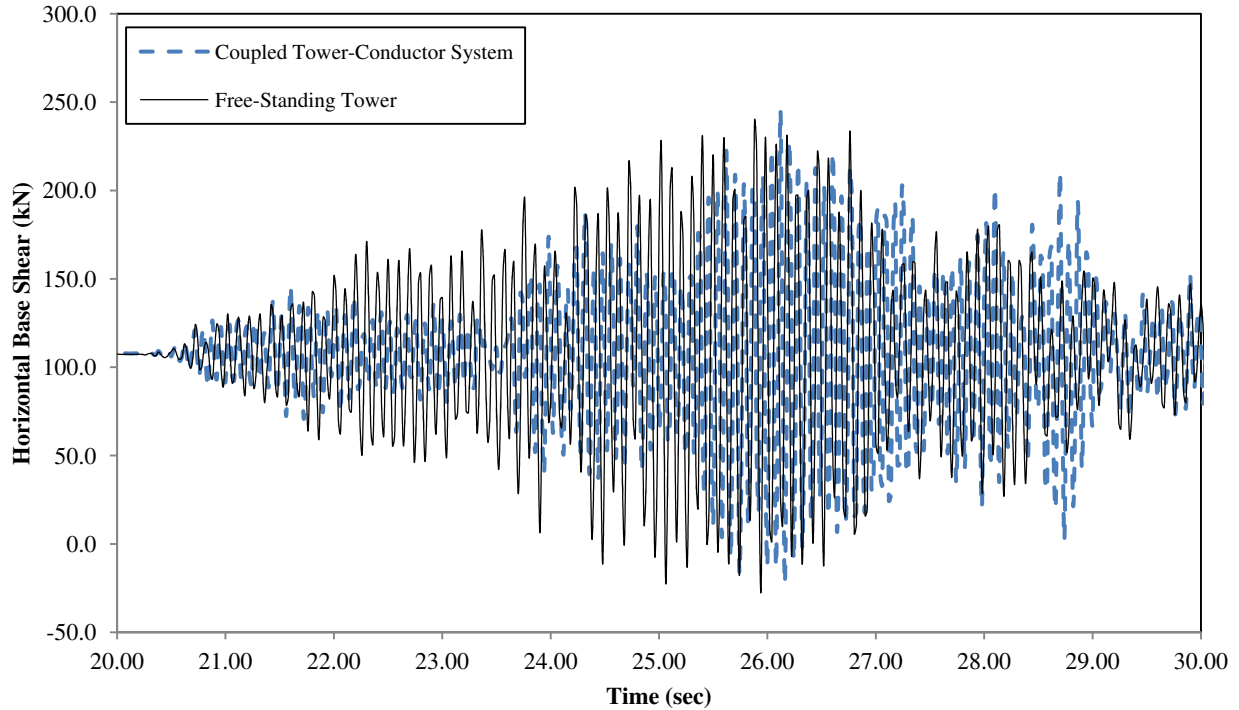


**Figure IV.26. Time-history of horizontal base shear of Free-Standing Delta Guyed Tower and Coupled Delta Guyed Tower-Conductor System under NGA 953 applied in vertical direction.**

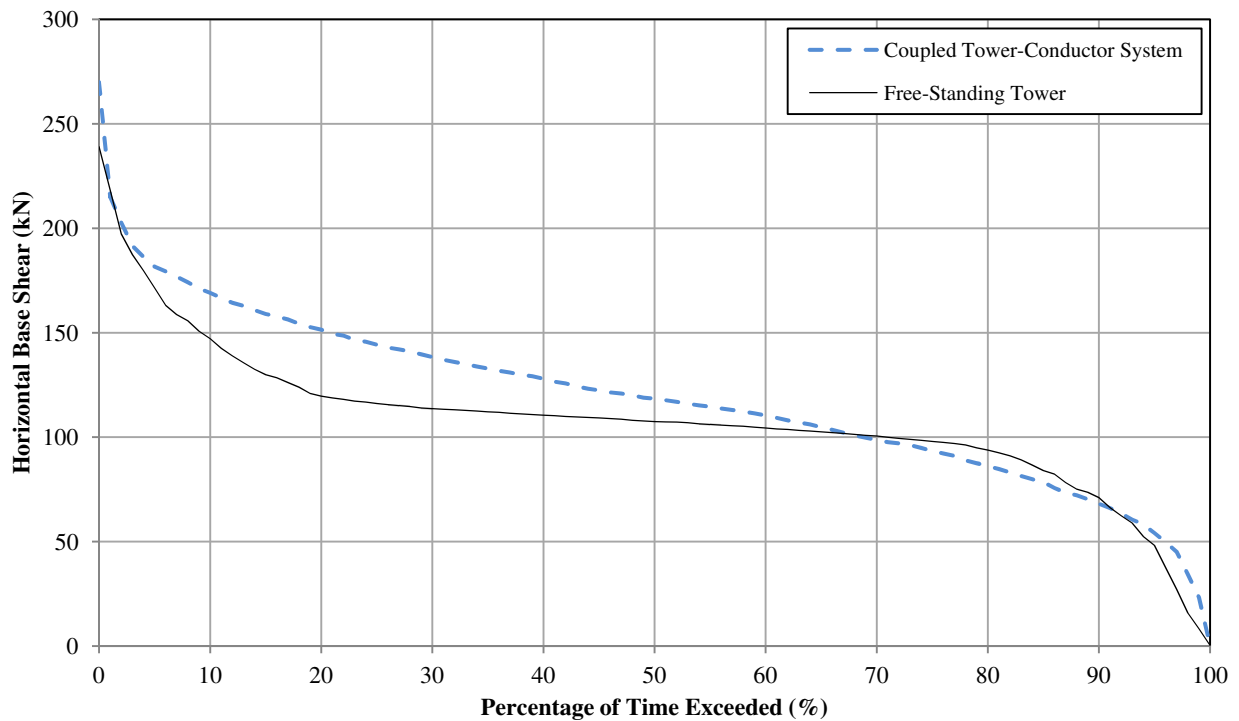


**Figure IV.27. Persistence curve of horizontal base shear time-history of Free-Standing Delta Guyed Tower and Coupled Delta Guyed Tower-Conductor System under NGA 953 applied in transversal direction.**

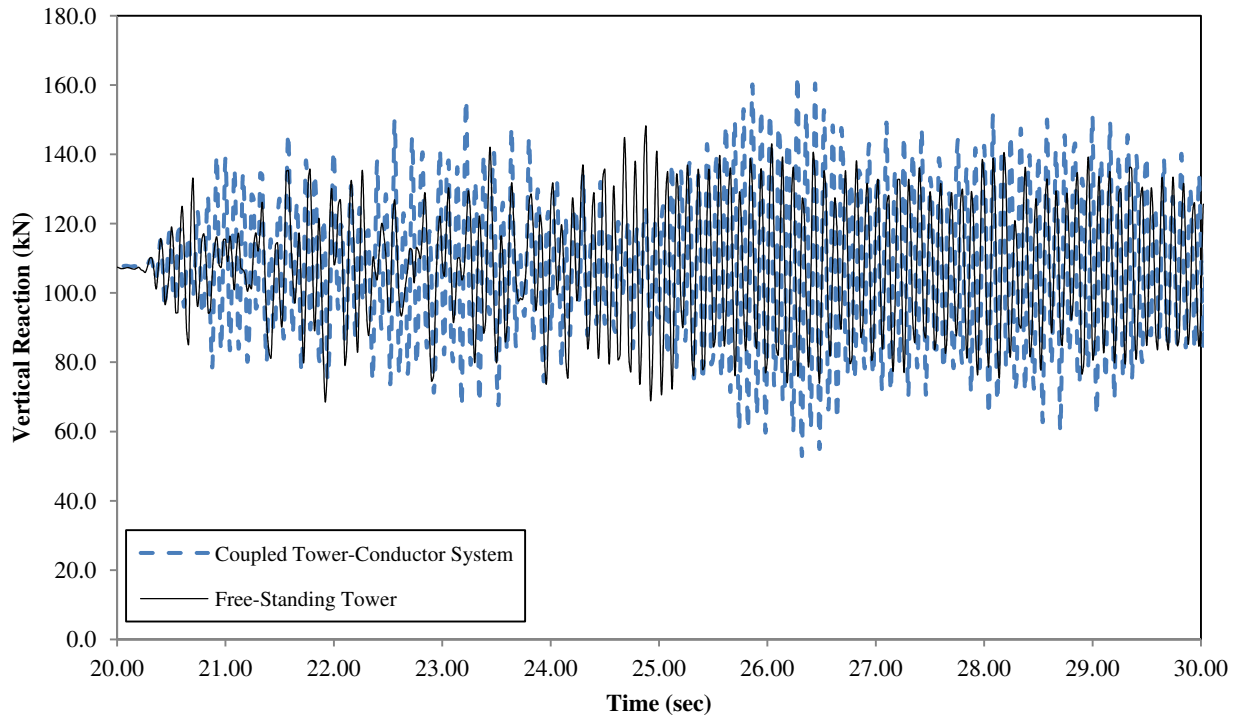


**Figure IV.28. Time-history of horizontal base shear of Free-Standing Delta Guyed Tower and Coupled Delta Guyed Tower-Conductor System under NGA 57 applied in vertical direction.**

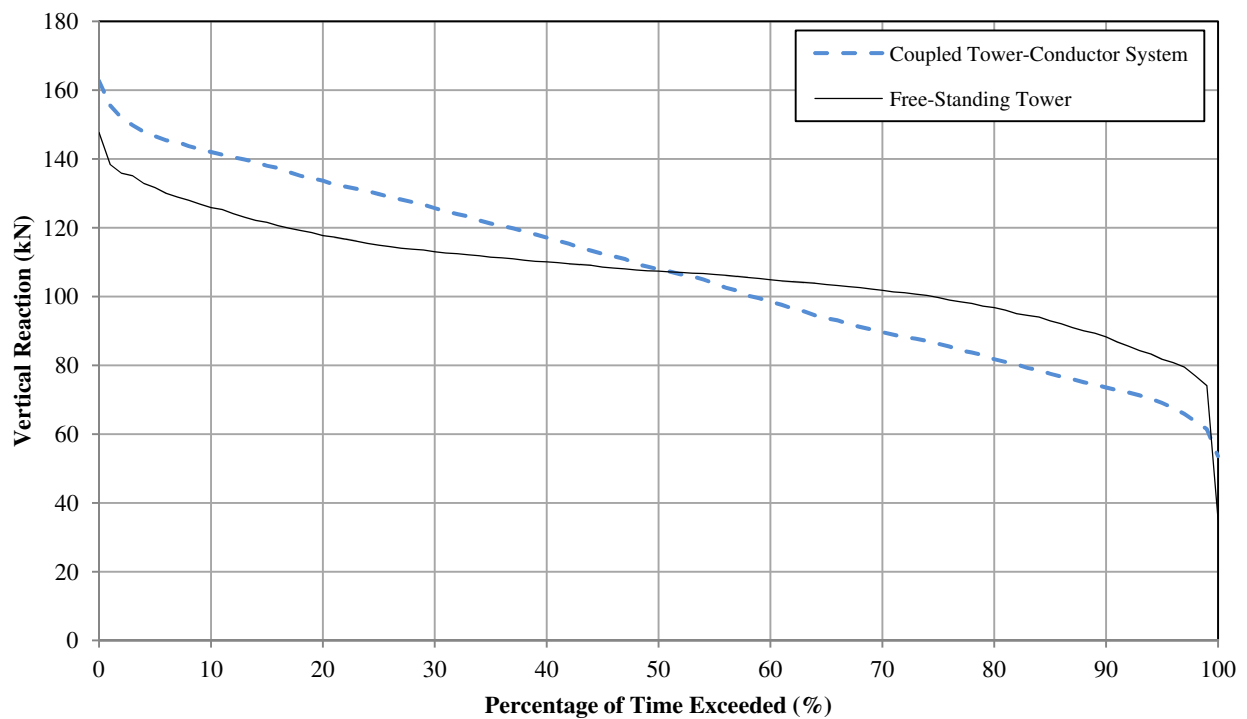


**Figure IV.29. Persistence curve of horizontal base shear time-history of Free-Standing Delta Guyed Tower and Coupled Delta Guyed Tower-Conductor System under NGA 57 applied in transversal direction.**